

Medical University of South Carolina

MEDICA

MUSC Theses and Dissertations

2015

Design of Novel Histone Demethylase Inhibitors as Drug Candidates to Prevent Cardiac Ischemia-Reperfusion Injury

Craig Jerome Kutz

Medical University of South Carolina

Follow this and additional works at: <https://medica-musc.researchcommons.org/theses>

Recommended Citation

Kutz, Craig Jerome, "Design of Novel Histone Demethylase Inhibitors as Drug Candidates to Prevent Cardiac Ischemia-Reperfusion Injury" (2015). *MUSC Theses and Dissertations*. 463.

<https://medica-musc.researchcommons.org/theses/463>

This Dissertation is brought to you for free and open access by MEDICA. It has been accepted for inclusion in MUSC Theses and Dissertations by an authorized administrator of MEDICA. For more information, please contact medica@musc.edu.

Design of Novel Histone Demethylase Inhibitors as Drug Candidates to Prevent Cardiac Ischemia-Reperfusion Injury

by

Craig Jerome Kutz

A dissertation submitted to the faculty of the Medical University of South Carolina in partial fulfillment of the requirements for the degree of Doctor of Philosophy in the College of Graduate Studies

Department of Drug Discovery and Biomedical Sciences

2015

Approved by:

Co-Chairman, Advisory Committee

Patrick Woster

Co-Chairman, Advisory Committee

Donald Menick

Advisory Committee

Steven Kubalak

Craig Beeson

Zhi Zhong

Campbell McInnes

ABSTRACT

CRAIG JEROME KUTZ. Design of Novel Histone Demethylase Inhibitors as Drug Candidates to Prevent Cardiac Ischemia-Reperfusion Injury. (Under the direction of PATRICK WOSTER and DONALD MENICK)

Current therapies to assist short- and long-term outcomes after acute myocardial infarction (AMI) depend on primary percutaneous coronary intervention shortly after ischemic insult. Upon reperfusion, localized influx of oxidative stressors overwhelms the endogenous antioxidant systems and lead to contractile dysfunction and arrhythmias. The extent of irreversible myocyte damage during ischemia-reperfusion (IR) injury is a key determinant in patient outcomes and therefore, strategies to reduce oxidative damage are essential. In recent years, increasing evidence indicates that epigenetic enzymes such as the histone demethylases and deacetylases play crucial roles during cardiovascular disease (CVD). One such enzyme, lysine specific demethylase-1 (LSD1), is hypoxia-inducible and regulates oxidative balance through epigenetic silencing of oxidative scavenging enzymes and production of hydrogen peroxide. Our predominant goal in this dissertation was to develop an LSD1 inhibitor with enhanced drug-like properties that is well tolerated by cardiac tissue and cardioprotective during IR. We identified a novel 3,5-diamino-1,2,4-triazoles scaffold that can be used to design potent, reversible, competitive LSD1 inhibitors that produce little or no overt cytotoxicity. Thus, *the central hypothesis of this dissertation is that novel LSD1 inhibitors with enhanced drug-like*

properties can be used to mitigate cardiac ischemia-reperfusion structural damage and contractile dysfunction with minimal toxicity to myocytes.

Our approach is innovative in that 1) we will design the first reported series of potent, reversible competitive inhibitors of LSD1 that display limited cytotoxicity, and 2) we will identify LSD1 as a new therapeutic target to mitigate myocardial IR injury. To accomplish this, we will focus on three aims. **Specific Aim 1** - Perform hit-to-lead optimization through structural modification of a new small molecule scaffold to discover reversible LSD1 inhibitors with suitable efficacy, negligible toxicity and enhanced drug-like properties. **Specific Aim 2** - Determine the LSD1 target selectivity, cellular cytotoxicity, and cellular phenotypic changes in histone methylation of lead compounds. **Specific Aim 3** – evaluate the pharmacodynamic efficacy of a lead 3,5-diamino-1,2,4-triazole derivative to mitigate post-IR contractile dysfunction and infarction using two murine models of IR.

TABLE OF CONTENTS

1. Abstract	ii
2. List of Figures	vi
3. List of Tables	xi
4. List of Schemes and General Structures	xi
5. List of Abbreviations	xii
6. Chapter 1 – Background and Significance	1
I. Cardiovascular Disease and Economic Burden	2
II. Acute Myocardial Infarction and Clinical Treatment	3
a. Heart Failure and Left Ventricular Remodeling in AMI	4
III. Ischemia-Reperfusion Injury	8
a. General Pathophysiology/Mechanism of Ischemia-Reperfusion	9
b. Apoptosis in Ischemia-Reperfusion	12
c. Autophagy in Ischemia-Reperfusion	13
d. Necrosis in Ischemia-Reperfusion	14
e. Protection Strategies - Preconditioning	14
IV. Epigenetics – Dynamic Regulation of the Genome	17
a. Epigenetics in Cardiovascular Disease	21
V. Epigenetic Enzymes – Erasers and Writers	22
a. Lysine Specific Demethylase-1 (LSD1/KDM1A)	22
b. Histone Deacetylases (HDACs)	27
c. Histone Methyltransferases and Acetyltransferases	28
VI. Other Flavin-Dependent Amine Oxidases	29
a. Spermine Oxidase and Polyamine Metabolism	30
b. Monoamine Oxidases	34
VII. Synthetic Amine Oxidase Inhibitors	35
a. Lysine Specific Demethylase-1 Inhibitors	35
b. Spermine Oxidase Inhibitors	39
VII. Specific Aims	40
a. Central Hypothesis	41

VII. Significance	43
7. Chapter 2 – Materials and Experimental Methods	45
I. Chemistry Reagents and Reactions	45
II. In Vitro Drug Characterization and Enzyme Assays	53
III. Preclinical Testing – Ex Vivo and In Vivo IR Models	59
IV. Data Analysis and Statistics	63
V. Ethical Aspects of Research and Animal Care	63
8. Chapter 3 – Structure-Based Discovery of Small Molecule LSD1 Inhibitors	65
I. Introduction	66
II. Results	69
a. Virtual Screen for Novel LSD1 Inhibitors	69
b. In Silico Molecular Docking and Predicted Catalytic Binding Affinity	71
c. In Vitro Activity Against Recombinant LSD1/CoREST	73
d. Synthesis of 3,5-diaminotriazole analogues	74
e. Compound 9 is a reversible, competitive inhibitor of LSD1	80
III. Discussion	83
IV. Limitations and Future Directions	85
9. Chapter 4 – Assessment of selectivity, toxicity, and target validation of 3,5-diamino-1,2,4-triazoles	87
I. Introduction	88
II. Results	91
a. Selectivity of 3,5-diaminotriazoles – Monoamine Oxidase	91
b. Selectivity of 3,5-diaminotriazoles – Spermine Oxidase	94
c. SMO inhibitor MDL72527 does not Inhibit LSD1	96
d. LSD2 inhibitor GSK-LSD1 does not inhibit SMO	96
e. Differential inhibitors of LSD1, SMO, and MAO	99
f. 3,5-diaminotriazoles show limited cytotoxicity	101
g. Cellular phenotype and histone methylation changes of 3,5-diaminotriazoles	107
h. Disruption of epigenetic complexes in primary	

cardiomyocytes	109
i. Toxicology screen of compound 9 in CD1 mice.....	111
III. Discussion	116
IV. Limitations and Future Directions	119
10. Chapter 5 – LSD1 as a novel therapeutic target to mitigate post-IR contractile dysfunction and infarction	122
I. Introduction	123
II. Results	128
a. LSD1 protein is increased within infarcted tissue following IR injury and levels of protein expression correlate to severity of cardiac contractile dysfunction	128
b. Pilot study – Verlindamycin sustains cardiac function and reduces infarct area following IR injury:.....	131
c. Pilot study – Verlindamycin treatment preconditioning of the heart was not achieved via the canonical RISK signaling pathway.....	135
d. Pilot study – Pretreatment with verlindamycin increased endogenous antioxidants:.....	138
e. Pilot study – Evaluate histone methylation changes by verlindamycin.....	138
f. Pilot study – in vivo analysis of long-term cardiac function with verlindamycin treatment.....	140
g. Pilot Study – VLM facilitates cardioprotection by early-onset acute mechanisms.....	142
h. Novel 3,5-diamino-1,2,4-triazole compound 9 improves acute cardiac function.....	144
i. Dual inhibition of LSD1 and SMOx show cardioprotection from IR injury	149
j. LSD1 inhibition attenuates heart failure remodeling with reduced ejection fraction	154
III. Discussion	158
IV. Limitations and Future Directions	162
11. Chapter 6 – Overall Summary and Discussion	166
12. List of References	174

LIST OF FIGURES

CHAPTER ONE

- Figure 1.1.** Coronary artery anatomy; pg.3
- Figure 1.2.** Heart failure with preserved ejection Fraction; pg. 5
- Figure 1.3.** Frank-Starling relationship in heart failure; pg. 6
- Figure 1.4.** Cohort study of HFrEF vs HFpEF patients over 11-year follow up; pg. 8
- Figure 1.5.** Reactive oxygen species (ROS) and tissue damage; pg. 11
- Figure 1.6.** Cardiac ischemia-reperfusion injury and pharmacologic preconditioning; pg. 15
- Figure 1.7.** Epigenetic regulation of gene Expression; pg. 18
- Figure 1.8.** Lysine Specific Demethylase-1; pg. 25
- Figure 1.9.** Homology between amine oxidase family: Lysine Specific Demethylase-1 and Spermine Oxidase; pg. 30
- Figure 1.10.** Diagram polyamine metabolism; pg. 31
- Figure 1.11.** Monoamine oxidase activity on mitochondrial membrane creates oxidative damage during IR; pg. 34
- Figure 1.12.** Structures of amine oxidase inhibitors; pg.36

CHAPTER TWO

- Figure 2.1.** Langendorff *ex vivo* isolated heart retrograde perfusion apparatus; pg. 61

CHAPTER THREE

- Figure 3.1.** Workflow chart and structure-based drug design of novel LSD1 inhibitors; pg. 68
- Figure 3.2.** Virtual screen of Maybridge HitFinder library against LSD1/CoREST; pg. 70
- Figure 3.3.** Molecular docking of Compound **9**; pg. 72
- Figure 3.4.** Initial LSD1 inhibition assay; pg. 78
- Figure 3.5.** LSD1 inhibition assay of synthesized Compounds; pg. 79
- Figure 3.6.** LSD1 enzyme kinetics shows **9** as a competitive inhibitor; pg. 81
- Figure 3.7.** Thermal biomolecular binding of compound **9** to LSD1; pg. 82
- Figure 3.8.** Lead optimization of compound **9** derivatives unveil novel compounds with improved potency; pg. 86

CHAPTER FOUR

- Figure 4.1.** Workflow chart and structure-based drug design of novel LSD1 inhibitors; pg. 90
- Figure 4.2.** Monoamine oxidase A and B activity; pg. 93
- Figure 4.3.** LSD1 inhibitors exhibit potency against SMO; pg. 95
- Figure 4.4.** SMO inhibitor MDL72527 selectivity; pg. 97
- Figure 4.5.** LSD1 inhibitor GSK-LSD1 selectivity; Pg. 98
- Figure 4.6.** Cell viability and compound cytotoxicity

		in Calu-6 cells; pg. 104
Figure 4.7.	Cell viability in MCF-10a, MDA-MB-231, and CA46; pg. 105
Figure 4.8.	Cell viability and compound cytotoxicity in PC3 and PANC1; 106
Figure 4.9.	Global methylation changes; pg. 108
Figure 4.10.	Primary rat cardiomyocytes provide preliminary data on 3,5-diamino-1,2,4 triazoles efficacy <i>in vitro</i> to disrupt co-repressor complexes; pg. 110
Figure 4.11.	Histology of compound 9 treated CD1 male mice – kidney, heart, liver; pgs. 113-115
CHAPTER FIVE		
Figure 5.1.	Workflow chart and preclinical testing of compound 9 ; pg. 126
Figure 5.2.	LSD1 increases within the infarction following IR; pg. 130
Figure 5.3.	Verlindamycin; contractile recovery upon reperfusion in isolated male rat hearts after 30mins ischemia; pg. 133
Figure 5.4.	Infarct area in isolated rat hearts treated with LSD1 inhibitors; pg. 134
Figure 5.5.	RISK survival signaling during IR injury; Pg. 136
Figure 5.6.	Isoform-specific roles of p38 during IR injury; pg. 137
Figure 5.7.	Antioxidant quantity and global histone methylation; pg. 139
Figure 5.8.	Verlindamycin (VLM) in chronic <i>in vivo</i> IR injury; pg. 141

Figure 5.9.	Verlindamycin (VLM) treatments at 1-hr are comparable to 18hr/1hr treatments; pg. 143
Figure 5.10.	Compound 9 , contractile recovery upon reperfusion in isolated male rat hearts after 30mins ischemia; pg. 146
Figure 5.11.	Compound 9 , hypoxia-induced rigor contracture; pg. 147
Figure 5.12.	Infarct area in isolated rat hearts treated with LSD1 inhibitors; pg. 148
Figure 5.13.	GSK-LSD1 (3), contractile recovery upon reperfusion in isolated male rat hearts after 30mins ischemia; pg. 150
Figure 5.14.	MDL72527 (11), contractile recovery upon reperfusion in isolated male rat hearts after 30mins ischemia; pg. 151
Figure 5.15.	Left ventricle pressures of ischemic hearts following 60-minutes reperfusion; pg. 153
Figure 5.16.	Transthoracic echocardiographs of 7 day IR study; pg. 155
Figure 5.17.	Compound 9 and GSK-LSD1 reduction of chronic <i>in vivo</i> IR injury and cardiac remodeling; pg. 156
Figure 5.18.	Compound 9 pretreated 4-hours prior to heart removal, contractile recovery upon reperfusion in isolated male rat hearts after 30mins ischemia; pg. 164

LIST OF TABLES

Table 1.1.	List of histone modifications, enzymes and their epigenetic phenotype; pg. 20
Table 3.1.	Structures, cLogP and LSD1 inhibitory activity for 3,5-diaminotriazoles 9-25 ; pgs. 76-77
Table 3.2.	Structures and LSD1 activity of compounds from Scheme 1 ; pg. 79
Table 4.1.	Amine oxidase inhibitor classes and selectivity for LSD1, MAOs, and SMO; pg. 100
Table 4.2.	Human immortalized cell lines and descriptions; pg. 103
Table 4.3.	Clinical laboratory values for toxicology study; pg. 112
Table 5.1.	Absolute values 7days post-IR (mean \pm SEM) of in vivo LAD ligation-reperfusion with LSD1 inhibitors; pg. 157

LIST OF SCHEMES AND GENERAL STRUCTURES

Scheme 1.	Structures of amine oxidase inhibitors; pg. 75
Scheme 2.	Click chemistry of 10 derivatives; pg. 86
General Structure 1.	3,5-diamino-1,2,4-triazole scaffold; pg. 75

LIST OF ABBREVIATIONS

ALP	Alkaline Phosphatase
ALT	Alanine Aminotransferase
AMI	Acute Myocardial Infarction
AST	Aspartate Aminotransferase
BA	Basophils (in blood)
BUN	Blood Urea Nitrogen
CO	Cardiac Output
CVD	Cardiovascular Disease
DNMT	DNA Methyltransferase
DP or LVDP	Left Ventricular Developed Pressure
EDP or LVEDP	Left Ventricular End Diastolic Pressure
EF	Ejection Fraction (%)
EO	Eosinophils (in blood)
FS	Fractional Shortening (%)
GLU	Glucose
H3K4me1	Histone 3 Lysine 4 dimethylation
H3K4me2	Histone 3 Lysine 4 monomethylation
Hb	Hemoglobin (in blood)
HCT	Hematocrit (of blood)
HDAC	Histone Deacetylase
HFpEF	Heart Failure Preserved Ejection Fraction
HFrEF	Heart Failure Reduced Ejection Fraction
IR	Ischemia-Reperfusion
LAD	Left Anterior Descending Coronary Artery
LSD1	Lysine Specific Demethylase-1
LV	Left Ventricle
LVdD	Left Ventricular Diameter at Diastole
LVDP or DP	Left Ventricular Developed Pressure
LVDs	Left Ventricular Diameter at Systole
LVEDP or EDP	Left Ventricular End Diastolic Pressure
LVEDV	Left Ventricular End Diastolic Volume
LY	Lymphocytes (in blood)
MAO	Monoamine Oxidase
MCH	Mean Cell Hemoglobin (in blood)
MCHC	Mean Cell Hemoglobin Concentration
MCV	Mean Cell Volume (in blood)
MO	Monocytes (in blood)
MPV	Mean Platelet Volume (in blood)
NE	Neutrophils (in blood)
ODC	Ornithine Decarboxylase
PAO	Polyamine Oxidase
PLT	Platelets (in blood)
QD	per day (drug dosing)

RBC	Red Blood Cells (in blood)
RDW	Red Blood Cell Width (in blood)
RISK	Reperfusion Injury Survival Kinases
ROS	Reactive Oxygen Species
SAHA	Suberoylanilide Hydroxamic Acid (HDAC inhib.)
SMO or SMOx	Spermine Oxidase
SSAT	Spermine/Spermidine N-1 Acetyl Transferase
SV	Stroke Volume
TCP	Tranylcypromine (Compound 2)
TTC	2,3,5-Triphenyltetrazolium Chloride
VLM	Verlindamycin (Compound 5)
WBC	White Blood Cells (in blood)

CHAPTER 1: Background and Significance

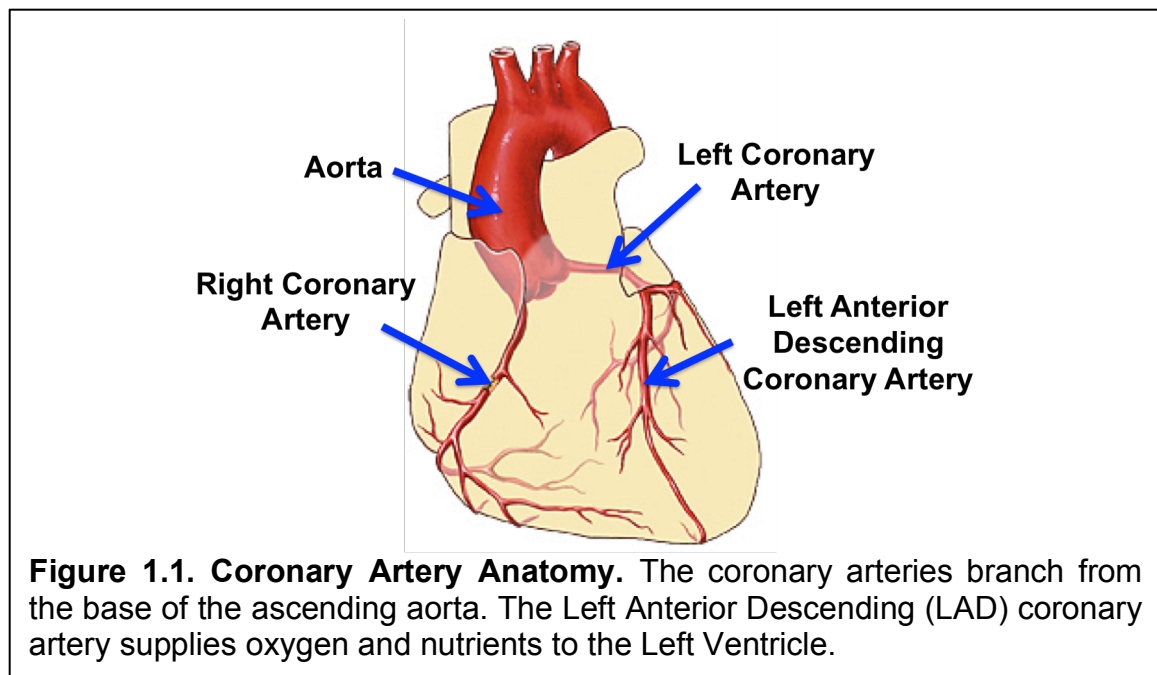
I. CARDIOVASCULAR DISEASE AND ECONOMIC BURDEN

Cardiovascular disease (CVD) remains one of the leading causes of death in the United States, contributing to approximately 1 of every 3 mortalities.¹ More than 83 million adults in the United States alone live with CVD, which causes more than 2,100 deaths *per day*.² According to the American Heart Association, an American experiences a new or recurrent coronary attack (defined as hospitalized from a myocardial infarction or coronary heart disease attack) every 34 seconds.¹ Other than high blood pressure, coronary heart disease has the highest prevalence rate (6.2%; >20 years old, both sexes) of all CVD. This includes an overall 2.8% prevalence of an acute myocardial infarction (AMI).³ Although the rates of CVD in recent years have declined slightly, the economic burden on the health care system still exceeds \$300 billion in direct costs annually.⁴ The Center for Disease Control (CDC) reports that for every \$6 spent in the U.S. on health care, \$1 accounts for the treatment of CVD.² This is astonishing in light of data that indicates these numbers will continue to rise with the ever-growing geriatric population. The demographic shift alone is estimated to triple the cost of CVD treatment by 2030.⁵ To combat this trend, there is a significant investment in cardiac drug development and prevention of heart failure, hypertension, lipid disorders and stroke, which has had a profound effect. For instance, in a study in *Health Affairs*, medications for blood pressure and cholesterol alone reduce costs of emergency room visits and inpatient hospitalizations by \$10 per patient according to the CDC.² Continued research in cardiac drug development remains a prominent focus of pharmaceutical

companies, as indicated by the high volume of clinical phase trials for new therapeutic compounds for CVD.⁶⁻⁷

II. ACUTE MYOCARDIAL INFARCTION AND CLINICAL TREATMENT

The heart is a highly oxidative organ, demanding large amounts of oxygen consumption to maintain tissue energy demands during contraction. The myocardium is supplied by O₂ and nutrients through an external vasculature, the coronary arteries. The coronary arteries branch from the base of the ascending thoracic aorta and provide energy supply to the cardiac muscle (**Figure 1.1**). When functioning normally, the myocardial oxygen consumption (MVO₂) can range from 8-70 ml O₂/min per 100g depending on the tissue demand.⁸ In comparison, the brain only requires 3 ml O₂/min per 100g. However, an inadequate supply of O₂ to the myocardium resulting from occlusion of blood flow



through a coronary artery can result in tissue hypoxia, often characterized clinically as angina, or chest pain. If this O₂ insufficiency is prolonged, irreversible myocyte damage occurs distal to the region supplied by the occluded coronary artery, and an AMI results. Depending on the location of anoxia, a multitude of clinical sequelae can occur, ranging from no visible distress to sudden death.⁹

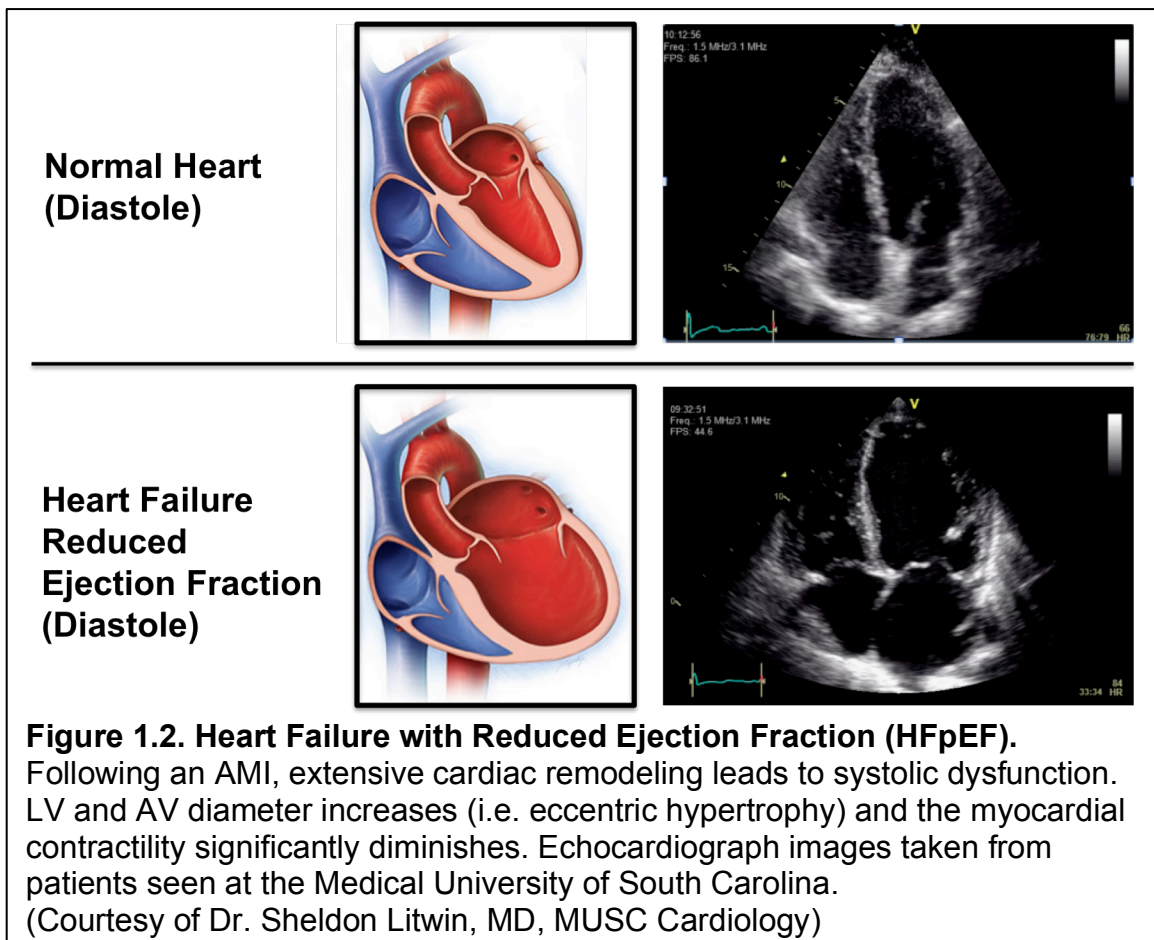
Since the 1980's, a large number of clinical trials demonstrated that restoration of flow to an occluded coronary artery improved patient morbidity and mortality following an AMI.¹⁰ In particular, reperfusion therapy reduced infarct damage and sustained left ventricular function if performed within the first 24-hrs. This was a monumental finding in treatment of AMI because the magnitude of myocardial infarct damage correlates with a patient's prognosis and outcome.¹⁰ The current standard of care for patients with severe transmural infarctions is immediate re-establishment of blood flow to the ischemic myocardium, usually performed by cardiac catheterization.⁹ This includes treatment by 1) primary percutaneous transluminal coronary angioplasty and/or 2) thrombolytic therapy.⁹⁻

10

Heart Failure and Left Ventricular (LV) Remodeling in AMI:

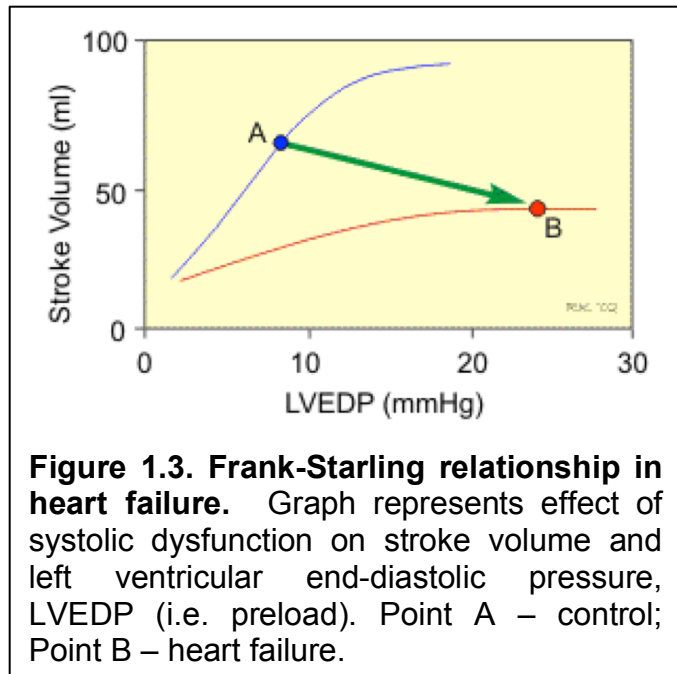
Recovery from an AMI leads to extensive remodeling of the LV chamber and architecture, which when left unabated leads to heart failure. In particular, pathological changes in LV volume and shape are driven by substantial myocyte hypertrophy, cell death and fibrotic repair.¹¹⁻¹² This adaptive process in cardiac remodeling is an elaborate response to the severity of infarction caused by an

AMI. In a clinical trial spanning 35 medical centers across the United States, Solomon *et al.* demonstrated that patients with larger infarctions developed larger LV end diastolic dilation with a loss of systolic ejection fraction, indicating significant LV remodeling.¹³ **Figure 1.2** shows an example of a clinical presentation of LV end diastolic dilation.



The first stage of LV remodeling takes place within the infarcted tissue. The necrotic debris and fibrotic scar tissue formed distal to the occluded coronary artery begins to thin and expand.¹² This places an increased demand on remote

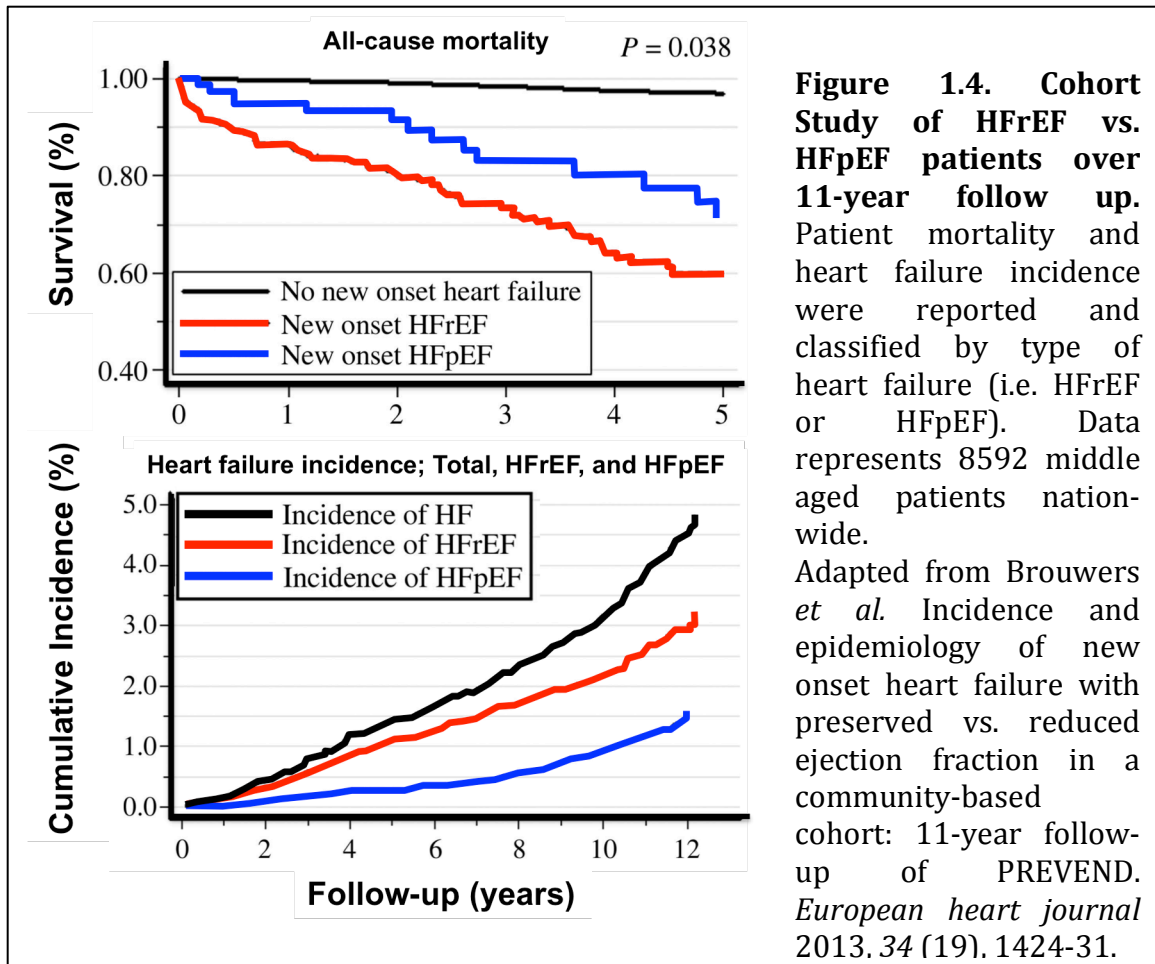
myocardium outside of the infarct zone, leading to the next phase of remodeling – eccentric hypertrophy and LV expansion.^{8, 11, 14} Ventricular dilation is caused by new sarcomeres formed in-series with existing myofilaments to improve cardiovascular compliance, an adaptive



mechanism to increase stroke volume (SV) and sustain cardiac output (CO). According to the Frank-Starling relationship between SV and preload (aka LV end diastolic pressure, LVEDP), this increased SV creates a higher pressure on the LV (**Figure 1.3**).⁸ This is fundamental because wall stress is directly proportional to LVEDP, which in turn means a higher tissue oxygen demand, and thus, a lower mechanical efficiency.⁸

The clinical manifestation of pathological cardiac remodeling is heart failure. In the benchmark echocardiograph clinical study VALIANT (Valsartan in Acute Myocardial Infarction), patients with evident LV remodeling following an AMI had a significantly worse prognosis.¹⁵ The earliest understood form of heart failure following an AMI is defined as left ventricular (LV) systolic dysfunction by loss of ejection fraction (EF) <0.35 (i.e. heart failure with reduced ejection fraction, HFrEF).¹⁴ Ejection fraction is a measurement of systolic efficiency and is

calculated by the ratio of SV to LV end diastolic volume (LVEDV). In HFrEF patients, SV is maintained due to the increased compliance of the myocardium, but EF is reduced because of increased LVEDV.^{8, 14} In fact, the loss of cardiac inotropy, or contractility, is often indicative of systolic dysfunction. However, clinical studies with inotropic agents alone produced poor patient improvements in HFrEF, indicating that systolic dysfunction associated with LVEDV dilation is a multifactorial pathology.¹⁶ Thus, current clinical standard for HFrEF aim to reduce the load placed on the heart, and thus, ablate LV dilation (e.g. beta blockers, ACE Inhibitors, angiotensin-receptor blockers).¹⁴ Interestingly, more and more clinical studies indicate that over half of heart failures actually demonstrate *preserved* ejection fraction (HFpEF).¹⁴ In cohort study of 8,592 middle-aged patients with heart failure, HFrEF had a higher incidence than HFpEF and lead to increased mortality (**Figure 1.4**).¹⁷ The pathophysiology and nuances between HFrEF and HFpEF will not be covered as it is outside the scope of this project.



III. ISCHEMIA-REPERFUSION INJURY

Despite the advancements in reperfusion therapy with percutaneous coronary intervention and thrombolytics, treatment of AMI continues to be palliative. Paradoxically, recannulation of occluded vessels, either spontaneously or by therapeutic intervention, causes a secondary wave of damage to the myocardium, resulting in arrhythmias, mechanical dysfunction, and myocyte death.¹⁸⁻¹⁹ In other words, cell death and cardiac dysfunction occurs as a result of the initial tissue ischemia that takes place during an AMI, but also

due to the subsequent reflow of the vascular bed. This detrimental phenomenon is known as ischemia-reperfusion (IR) injury and can account for up to 50% of tissue death during an infarction.²⁰ Myocardial death after IR injury can be attributed to cell apoptosis, necrosis, and autophagy. However, it is still unclear how much impact on the myocardium each process has individually.

General Pathophysiology/Mechanism of Ischemia-Reperfusion:

Depletion of oxygen supply to cells reduces energy production significantly by shifting the focus from aerobic respiration (net ~36 ATP) to anaerobic glycolysis (net 2 ATP). Within minutes, the reduced ATP production causes a nearly complete abolishment of myocardial contractile force. If sustained, a gradual rise in diastolic tension takes place, as myocardial phosphocreatine stores deplete and Ca^{2+} -mediated crossbridging of myofibrils creates a state of rigor, or contracture²¹, and leads to diastolic insufficiency. In addition, the increased glycolytic dependency during anoxia causes an accumulation of acidic byproducts (i.e. lactic acid, H^+), lowering the intracellular pH.²⁰ Loss of ATP is aggravated by a drop in mitochondrial membrane potential, leading to reversal of the F_1F_0 -ATPase and up to nearly 50% further ATP hydrolysis.²²

Upon reperfusion of the previously hypoxic tissue, a complicated cascade of detrimental ion cycling, mitochondrial dysfunction, oxidative damage and inflammatory signaling occurs. Through a series of membrane transporters, the myocardium attempts to normalize the intracellular acidity. The extrusion of a H^+ is accompanied by an antiport of Na^+ into the cell, creating a transient rise in

intracellular Na^+ . This results in reversal of the sarcolemmal Na/Ca Exchanger (NCX). The significance of this event is the non-stoichiometric counter transport of a 3 Na^+ out of the cell for 1 Ca^{2+} into the cell, leading to a calcium overload within the myocyte.²⁰

Calcium overload within the myocyte is a hallmark insult during IR injury. The abundant Ca^+ (along with pH homeostasis and ATP insufficiency) leads to dysregulation of the mitochondrial permeability transition pore (PTP), a key regulator of mitochondrial membrane potential and mitochondrial integrity. Mitochondrial damage, along with the sudden influx of O_2 to the previously anoxic tissue, causes a harmful wave of reactive oxygen species (ROS) formation.

Another hallmark of reperfusion injury is the huge influx of ROS. ROS are highly reactive molecules that produce lipid peroxidation and sulfhydryl oxidation, resulting in membrane leak, intracellular protein changes, and transcriptional reprogramming.²³ ROS radicals include hydrogen peroxide (H_2O_2), superoxide ($\bullet\text{O}_2^-$), hydroxyl radical ($\bullet\text{OH}$), peroxynitrate (ONOO^-), and hydroxyl ion (OH^-). Free radicals contain unpaired electrons in their outermost shells, an unstable arrangement that react uncontrollably with proteins, lipids, and DNA to establish an outer stable shell of electrons. Because of their highly reactive nature, the influx of ROS during IR injury is considered a huge contributor to the damage caused by reperfusion (**Figure 1.5**). In addition, oxidative stress in cardiomyocytes and vascular smooth muscle causes

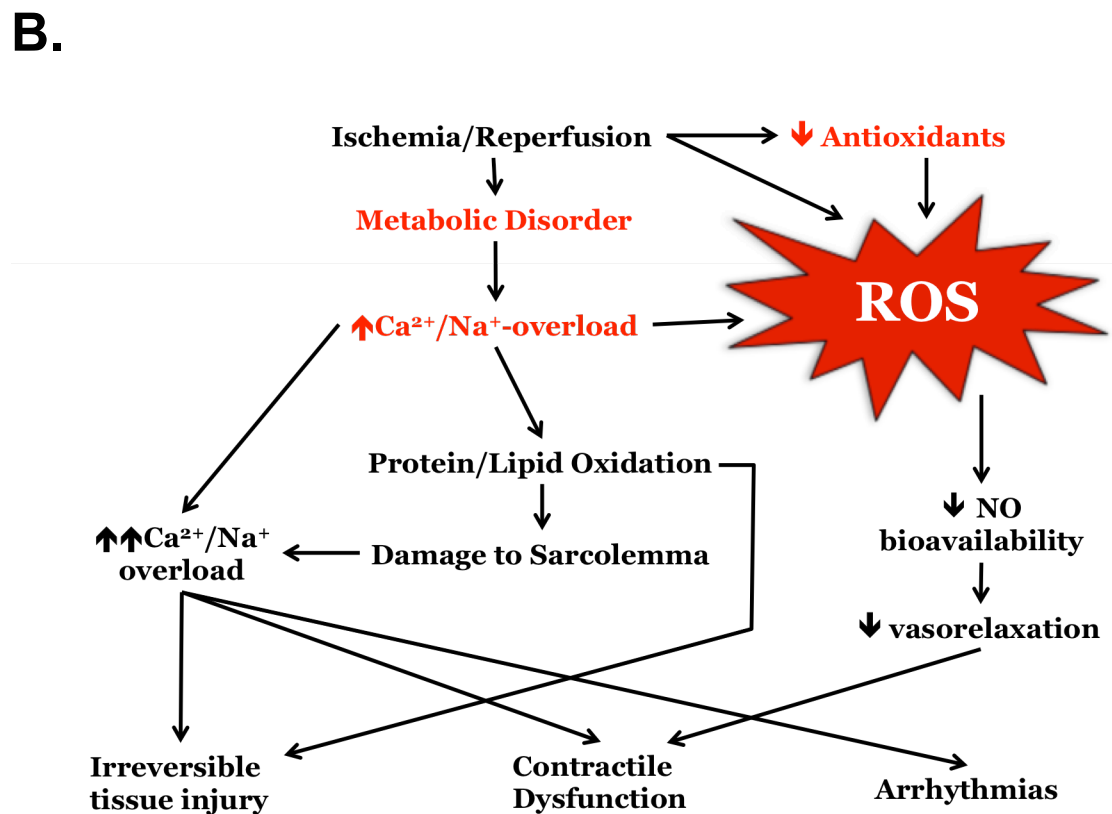
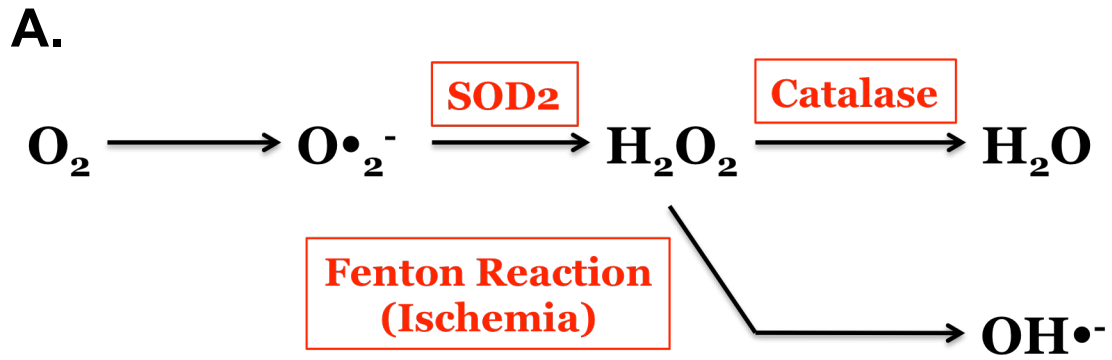


Figure 1.5. Reactive oxygen species (ROS) and tissue damage. (A) ROS radicals include hydrogen peroxide (H_2O_2), superoxide ($\text{O}_2^{\cdot-}$), hydroxyl radical ($\text{OH}\cdot$), peroxynitrate (ONOO^-), and hydroxyl ion (OH^-). (B) Tissue damage and dysfunction caused by ischemia-reperfusion and the influx of ROS. Metabolic disorder caused by low oxygen leading to increased intracellular acidosis.

decreased efflux of Ca^{2+} and sequestration of the sarcoplasmic reticulum Ca^{2+} -ATPase pump, thus causing additional Ca^{+} -homeostasis dysfunction.

Oxidative damage caused by ROS also creates a non-specific inflammatory response in the myocardium. The pro-inflammatory cytokine tumor necrosis factor alpha ($\text{TNF}\alpha$) is released, leading to structural and functional damage of the tissue. Within the first 24-hours, the innate immunity infiltration of the tissue (i.e. neutrophils and macrophages) leads to further localized tissue damage.²⁰ Granulocytes, such as neutrophils, and macrophages are phagocytes that employ a respiratory burst of ROS to remove necrotic waste. However, these “internal garbage cleaners” indirectly contribute to the oxidizing agent milieu within cardiomyocytes during IR.

Apoptosis in Ischemia-Reperfusion Injury:

Programmed cell death is a highly organized series of internal and external cascades that result in a non-inflammatory cell removal. Apoptosis was first described in 1972 by Kerr *et al.* and has since been widely characterized.²⁴ Membrane blebbing, cellular shrinking, nuclear fragmentation, and chromosomal condensation all take place to form apoptotic bodies that are eventually removed by the body’s intrinsic immune system.²⁴ In short, downstream signaling of pro-apoptotic proteins (i.e. caspases, *Bad*, *Bax*, *Bak*, *Bid*, etc.) leads to the release of the electron carrier cytochrome c into the cytoplasm and facilitates DNA damage.²⁵

Many studies have shown that ablation of apoptosis can lead to reduction of infarction. For instance, transgenic knockout studies with a pro-apoptotic protein Bax show a significant reduction of IR injury in the heart.²⁶ Conversely, overexpression of the antiapoptotic protein *Bcl-2* renders the heart more resistant to IR insult.²⁷ However, complete ablation of apoptosis is not sufficient for complete survival from IR, indicating a contributory role of other cell death mechanisms.

Autophagy in Ischemia-Reperfusion Injury:

An intriguing strategy to limit reperfusion damage and replenish energy stores within a tissue is conducted through modulation of autophagy. Autophagy is a dynamic intracellular process used as a quality control by cells to sequester and recycle damaged cellular components. This is accomplished by isolating damaged organelles and protein aggregates into lysosomes for degradation and efflux of macromolecules.²⁵ The up-regulation of lysosomal pathways during ischemia has been widely characterized.²⁸ Yet, depending on the framework of activation, it is still unclear whether manipulation of autophagy-related proteins are beneficial or detrimental during I/R injury.

Many studies indicate that an increase in autophagy is cardioprotective.²⁸⁻
²⁹ The depletion of ATP during ischemia induces AMPK-mTOR signaling and indirectly increases scavenging of high-energy fatty acids and amino acids, thus recouping critical biosynthetic molecules.³⁰ However, Valentim et al demonstrated that inhibition of ischemia-induced autophagy leads to improved

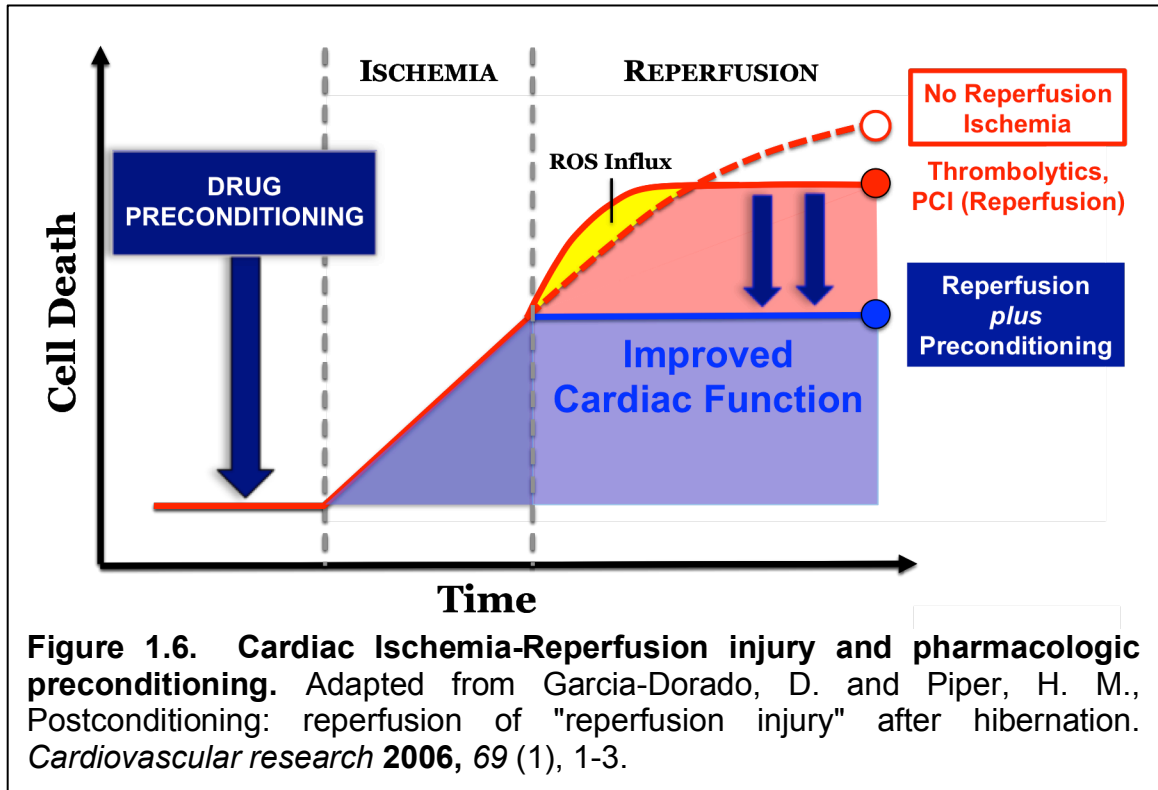
cardiomyocyte survival.³¹ Similar results were found in ischemic brain injury.³² This may be in part due to prevention of hyperactive autophagy during reperfusion when ATP/O₂ are sufficient. The debate about whether autophagy is cytoprotective or cytotoxic is still under investigation.

Necrosis in Ischemia-Reperfusion Injury:

Necrosis is another form of cell death, but is considered “uncontrolled” or external cell injury because of the significant inflammatory response associated with it. Contrary to apoptosis, necrosis is often caused by an external insult (i.e. toxins, infections, or trauma). Initially, the cells begin to swell and the nucleus degrades. Soon after, membrane disruption and rupture lead to a release of localized inflammatory cytokines and as a result, cause immune system infiltration.²⁵ Because of the associated membrane rupturing, biochemical markers of an AMI typically measured in the clinical, such as troponin or creatine kinases, are thought to be due to myocyte necrosis. Although IR pathophysiology is considered a more orchestrated cell death by apoptosis, an extent of irreversible necrosis still occurs and leads to a localized inflammatory reaction.

Protection Strategies – Preconditioning:

An effective method to reduce the damage caused by IR is by the phenomenon of ischemic preconditioning.³³⁻³⁴ In short, this method of protection for IR damage entails mechanical exposure of tissue to short, nonlethal periods



of ischemia that attenuate damage of further IR insults. Although studies in rodents show substantial benefits in mechanical preconditioning, the positive effect has not successfully translated to the clinic.³⁵ For decades, researchers have tried to mimic mechanical preconditioning by pharmacologic manipulation of protective survival signaling. However, new insight into pathways that governs preconditioning provides new strategies to develop successful therapeutic targets for pharmacological intervention (**Figure 1.6**).

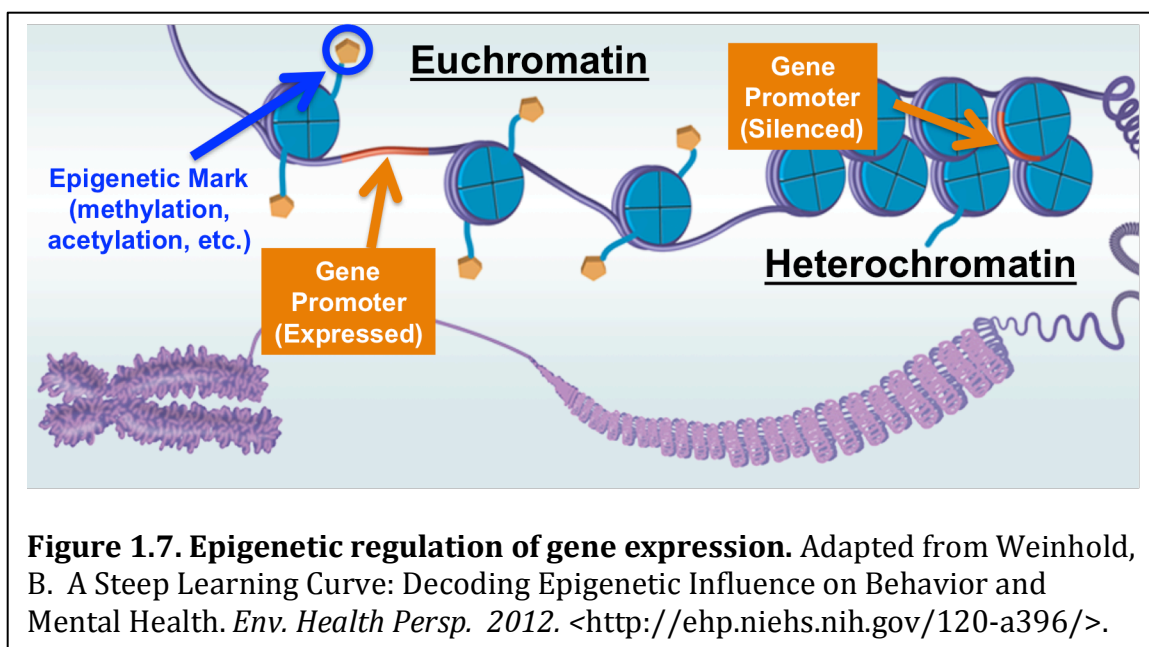
The protection provided by preconditioning is biphasic – an early phase of preconditioning and a more chronic phase. The early window occurs within 1-hour of preconditioning and does not appear to depend on protein synthesis.³⁶ Thus, “early preconditioning” is contingent on manipulation of post-translational modification of cell signaling molecules that act against programmed cell death or

activate endogenous cell survival maintenance programs. These include phosphorylation, methylation, and acetylation of effector molecules. Post-translational modifications influence a protein's conformation, dictate their location within the cell, alter interactions with other proteins, and adjust activity of signaling. Because early preconditioning is exhausted quickly, research has focused on the fluidity of signaling cascades to induce protection.³⁷ For example, activation of PI3K and its downstream targets Akt, p70S6K, and ERK1/2 have been deemed the Reperfusion Injury Survival Kinase (RISK) pathway.³⁸ Other cell signaling effector molecules shown to induce preconditioning include mTOR³⁷, eNOS/NO³⁹, inhibition of PKC- ϵ , and inhibition of GSK⁴⁰. Cell survival signaling stabilizes the endoplasmic reticulum⁴¹, ablates cell death programs (i.e. Bax/Bad/Bcl2)⁴², increases antioxidants (i.e. SOD2 and Catalase)^{23, 43}, and activates repair factors (i.e. HIF-1 α).⁴⁴ Late phase preconditioning, on the other hand, conveys protection from IR up to a few days.⁴⁵ Although many of the same pathways in early preconditioning are also affected in late phase, the longevity of late phase indicates de novo synthesis of cardioprotective proteins.

Preconditioning provides the greatest potential for therapy by reprogramming the myocardium into a “defensive phenotype” from IR damage. In recent years, research in the field of epigenetics has linked the biphasic nature of preconditioning. Epigenetics is a unique regulatory network of enzymes for genome and non-genome protein regulation and will be discussed in further detail later.

IV. EPIGENETICS: DYNAMIC REGULATION OF THE GENOME

In the late 1980's and early 1990's, the human genome project was an enormous undertaking that was predicted to revolutionize the way the medical field conducted patient-oriented healthcare. However, certain recent nuances in the complexity of gene regulation made this mission exceedingly difficult. Until recently, a dichotomy existed as to why genetically identical, monozygotic-twins exhibited different susceptibility to diseases. One widely accepted explanation for these genotype-independent changes in phenotype is that the environment plays a key role in disease susceptibility – the age-old debate of “nature versus nurture”. In the past two decades, the rapidly expanding field of epigenetics demonstrated that the human genome is extremely dynamic in its ability to change gene expression and not confined to the sequence of base pairs within the DNA. Epigenetic regulation of gene expression focuses on dynamic modifications of histones, DNA, and microRNAs that are flexible enough to respond to internal and exogenous environmental stimuli and change the genetic landscape independent of the genome.⁴⁶ Put simply, the field of epigenetics reminds researchers that a simple arrangement of sugar-containing base pairs is just the tip of the iceberg in understanding the human genome.



Human DNA is composed of over 3 billion nucleotide pairs, making it nearly 5 feet long. Storage of such a vast amount of genetic data in a micrometer-sized cell is accomplished by a series of structural packaging strategies involving histones (**Figure 1.7**). Histone proteins occur as heterooctamers that consist of one H3-H4 tetramer and two H2A-H2B dimers. These proteins interact with double stranded DNA in such a way that approximately 146 base pairs of DNA are wrapped around the histone octamer to form nucleosomes. The lysine-containing tails of histones, consisting of up to 40 amino acid residues, protrude through the DNA strand, and act as a site for post-translational modification of chromatin. The affinity of DNA for each histone independently governs the ability of transcriptional machinery to read the genetic code. This higher order of transcriptional regulation creates physical limitations

through the winding and unwinding of DNA within nucleosomes. Euchromatin is chromatin loosely packed around histones, and thus, is spatially oriented in a transcriptionally active conformation. On the contrary, heterochromatin is tightly packaged, creating a steric hindrance for *trans*-acting transcription factors and effectively silencing genes in the region.

The dynamic interplay between histones and chromatin conformation is critical for selective control of gene expression, and chromatin-remodeling enzymes have now become attractive therapeutic targets for multiple diseases with an epigenetic basis. Epigenetic histone enzymes are capable of manipulating nucleosomes between states of heterochromatin and euchromatin, and thus, effectively controlling gene transcription. For instance, a number of post-translational histone residue modifications are known to control gene expression, including methylation, acetylation, ubiquitination, sumoylation, ADP-ribosylation and phosphorylation.⁴⁷ **Table 1** demonstrates how post-translational methyllysines and acetyllysines on different histone residues can influence gene transcription.

Table 1. List of histone modifications, enzymes and their epigenetic phenotype.

Histone H3 Modifications

Histone Mark	Genetic Regulation	Histone Methyltransferases	Histone Demethylases
H3-Lysine 4 (H3-K4)			
<i>H3K4me</i>	Activation	MLL1, MLL2, MLL3, MLL4, MLL5, hSET1A, hSET1B, ASH1	LSD1 , JARID1A, JARID1B, JARID1C, JARID1D, FBXL10
<i>H3K4me2</i>	Activation		
<i>H3K4me3</i>	Activation		
H3-Lysine 9 (H3-K9)			
<i>H3K9me</i>	Activation	SUV39H1, SUV39H2, G9a, EuHMTase, SETDB1	LSD1 , JMJD1A, JMJD1B, JMJD2A, JMJD2B, JMJD2C, JMJD2D
<i>H3K9me2</i>	Repression		
<i>H3K9me3</i>	Repression		
<i>H3K9acetyl</i>	Repression	Histone Deacetylases (HDACs)	
H3-Lysine 27 (H3-K27)			
<i>H3K27me</i>	Activation	EZH2	UTX, JMJD3
<i>H3K27me2</i>	Repression		
<i>H3K27me3</i>	Repression		
H3-Lysine 36 (H3-K36)			
<i>H3K36me</i>	Elongation	SET2, NSD1, SMYD2	FBXL10, FBXL11, JMJD2A, JMJD2B, JMJD2C
<i>H3K36me2</i>	Elongation		
<i>H3K36me3</i>	Elongation		

Other Modifications Not Listed: *H3K79me1-3*, *H3K14acetyl*, *H4K20me*, *H2BK5me1/3*, *H3R2/17/26me*, *H4R3me*, *H3S10*

me = monomethyl; me2 = dimethyl; me3 = trimethyl; acetyl = acetylation

Epigenetics in Cardiovascular Disease:

Various types of CVD have long been described as familial diseases. Yet, studies of monozygotic twins suggest that the genome is not an all-or-none determinant of disease incidence.⁴⁸⁻⁴⁹ In recent years, increasing evidence indicates that epigenetic factors may be driving CVD and therapeutically targeting these enzymes can limit the pathogenesis of atherosclerosis, angiogenesis, IR-injury, cardiac hypertrophy and heart failure, just to name a few.⁵⁰

Epigenetic control of genes by histone manipulation can be used to reverse detrimental transcriptional changes during CVD. One example to prevent the damaging increases in H_2O_2 and O^{2-} during IR injury is by enhancing the endogenous antioxidant enzymes catalase and SOD2.^{43, 51} In particular, these promoters can be modulated through epigenetic enzymes.⁵¹⁻⁵² Yet, another example of epigenetic control is the endothelial response to hypoxia and sheer stress during angiogenesis and AMI. The NOS3 promoter encodes eNOS, which catalyzes the formation of the potent vasodilator nitric oxide (NO).⁵³ NO can react with ROS species to form reactive nitrogen species, another toxic metabolite that causes cellular damage.⁵³

Extensive research has demonstrated the therapeutic potential of targeting epigenetic enzymes in CVD.⁵⁴ The specific epigenetic modifiers and their individual roles in CVD will be discussed in further detail in the next section.

V. EPIGENETIC ENZYMES – ERASERS AND WRITERS

Lysine Specific Demethylase-1 (LSD1/KDM1A)

Until 2004, methylation of histones was considered an irreversible event, much akin to DNA methylation of CpG islands.⁵⁵ Shi *et al.* challenged this notion with their discovery of the flavin-dependent amine oxidase lysine specific demethylase 1 (LSD1, also known as KDM1A or BHC110).⁵⁵ For the first time, an enzyme was shown to remove methyl groups from the ϵ -amino group of lysine residues in the histone tail. Several histone residues contain mono-, di-, and tri-methylation of lysine residues (H3K4, H3K9, H3K27, H3K36, H3K79, H4K20). Notably, the landscape of various methylation marks dictate chromatin packaging and cellular phenotype. LSD1 preferentially catalyzes the removal of mono- and dimethylated forms of the activating mark H3K4 (H3K4me1, H3K4me2) to repress gene transcription (**Figure 1.8B**).⁵⁵⁻⁵⁶ However, LSD1 demethylation of the deactivating marks H3K9me1/2 have also been reported in an androgen receptor-mediated event, resulting in up-regulation of a gene.⁵⁷ Thus, LSD1 activity can play multiple roles in gene regulation.

Recently, a noncanonical function of LSD1 in demethylation of non-histone proteins has been described. For instance, the tumor suppressor protein p53 is post-translationally modified at lysine 370 (K370).⁵⁸ Monomethylation at this residue stabilizes p53 and prevents its ubiquitination. Also, dimethyl-K370 (K370me2) facilitates binding of p53 to 53BP1, a cofactor used to shuttle and activate p53. LSD1 demethylates K370me2 to K370me and promotes degradation of p53.⁵⁹ Therefore, LSD1 can repress pro-apoptotic functions of

downstream p53 signaling. LSD1 also has been shown to stabilize DNA methyltransferase (DNMT1) through manipulation of lysine residue methylation.⁶⁰ Clearly, LSD1 can play a huge role in protein regulation outside of its traditional histone function.

LSD1, as well as all flavin-containing amine oxidases, catalyze the oxidation of an amine-containing lysine residue using molecular oxygen as the electron acceptor (**Figure 1.8B**).⁶¹ During the initial removal of the histone tail methyllysine substrate, the α -CH is oxidized by the FAD prosthetic group to form an imine intermediate. Reduced FAD, in turn, is oxidized by molecular oxygen to produce a hydrogen peroxide byproduct. The resulting imine intermediate is then non-enzymatically hydrolyzed to form the demethylated substrate and formaldehyde. Regeneration of the oxidized form of FAD then produces hydrogen peroxide.^{56, 61-62}

LSD1 is a very large, asymmetrical protein (~110kDa) that contains three structural domains – an amine oxidase catalytic domain, a SWIRM domain, and a long helical tower domain (**Figure 1.8A**).⁶³ The C-terminus amine oxidase domain contains the cofactor FAD and is the site of demethylation. In close proximity, the N-terminus SWIRM domain is a highly conserved DNA binding domain.⁶⁴ Extending from these is the tower domain, a long helix-turn-helix motif used primarily for the extensive protein binding interactions of LSD1. In particular, extensive crystal structures demonstrate the close intermolecular relationship between LSD1 and the multidomain corepressor protein, CoREST.⁶³ CoREST contains long α -helical motifs that bind with high affinity to the structural

tower domain of LSD1, rendering LSD1 more resistant to proteosomal degradation.⁶²⁻⁶³ In addition, this interaction facilitates an LSD1 conformation that favors the H3K4 substrate.⁶²

LSD1 and CoREST also associate with HDAC1/2 and BHC80 in this large co-repressor complex (**Figure 1.8C**). Interestingly, the close interaction and crosstalk between binding partners within this LSD1:CoREST:HDAC1/2 complex influence individual catalytic activity. For instance, LSD1 is more active against hypoacetylated nucleosomes and acetylation of H3K9 causes a nearly 6-fold increase in K_m value for an N-terminal histone tail.⁶⁵ In other words, deacetylation of acetyl H3K9 by HDAC1/2 facilitates LSD1-catalyzed demethylation.⁶⁵ Similarly, Zhang *et al.* showed that hyperacetylation of lysine tails caused a concurrent increase in methylation of histones.⁶⁶ In recent years, this interdependency between epigenetic enzymes has been a focus of therapeutic targets and continues to be an intriguing, yet fairly unexplored, method to treat disease.⁶⁷

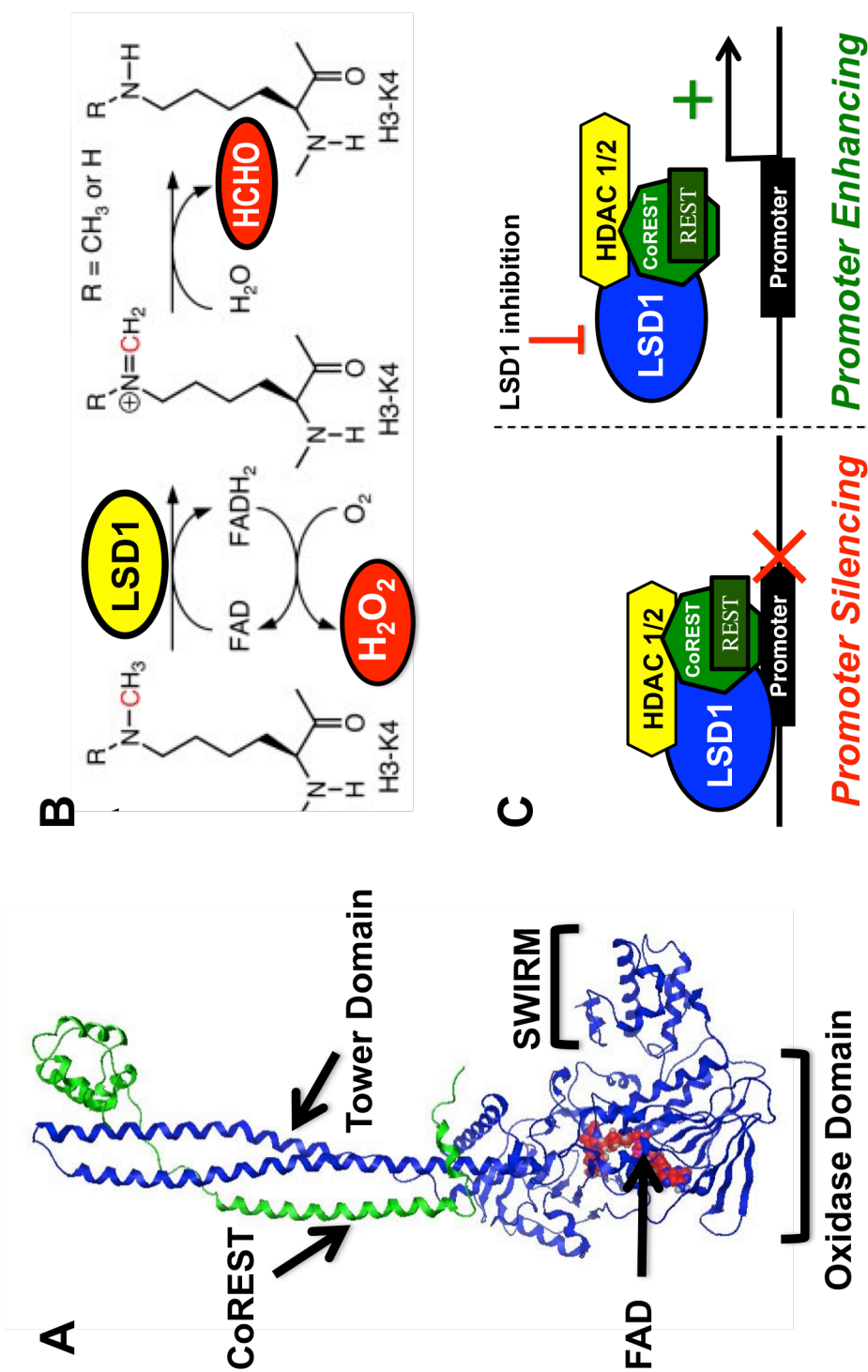


Figure 1.8. Lysine Specific Demethylase-1. A.) LSD1-CoREST crystal structure (PDB: 2V1D) showing the tower domain interaction, DNA-binding domain SWIRM, and the amine oxidase domain. B.) LSD1 catalytic mechanism using cofactor FAD and production of byproduct H_2O_2 and formaldehyde. C.) LSD1:CoREST:HDAC1 corepressor complex regulates gene transcription.

Because LSD1 is overexpressed in a number of human cancers (e.g. acute myeloid leukemia, neuroblastoma, retinoblastoma, prostate cancer, breast cancer, lung cancer and bladder cancer),⁶⁸⁻⁷¹ the protein is traditionally an important target for antitumor agents.⁷² However, new emerging roles for LSD1 in disease pathogenesis other than cancer are being reported.⁷³⁻⁷⁷ Of particular interest to IR injury, LSD1 was shown to play a direct role in the DNA damage response and is recruited to sites of DNA damage through the interaction with E3 ubiquitin ligase RNF168.⁷⁸ In addition, LSD1 can generate a local burst of H₂O₂ and formaldehyde that induce oxidative damage of nearby DNA residues.⁷⁹ In the past half-decade, histone demethylases have been implicated in CVD only a handful of times. In 2011, Zhang *et al.* became the first to identify a histone demethylase as the key regulator in the reprogramming of gene expression associated with cardiac hypertrophy.⁸⁰ Subsequently, LSD1 itself was shown to regulate vascular function and blood pressure during salt sensitive hypertension.⁸¹ Since these findings were reported, little additional work has been done in this area.

The close functional and structural epigenetic binding partner (i.e. Class I HDACs) has been extensively studied in CVD and IR injury (Discussed in more detail under “Histone Deacetylases”).⁵¹ Therefore, since HDAC inhibitors have shown preclinical efficacy for limiting cardiac IR damage, *we proposed that targeting their close counterpart, LSD1, might also provide efficacy for IR Injury.* To date, this hypothesis has not been tested, but increasing evidence indicates that LSD1 may play a role in IR damage. For instance, LSD1 appears to be

inducible and responsive to hypoxia.⁸²⁻⁸³ During ischemic brain injury, LSD1 expression was induced in a region and cell specific fashion after cerebral IR that coincided directly with changes in H3K4 methylation.⁸² Likewise, hypoxia-induced silencing of BRCA1 promoter in breast cancer is mediated by LSD1.⁸³ Evidence also suggests that LSD1 may contribute to the oxidative environment through direct production of ROS and silencing of antioxidant enzymes.⁵² It is recruited to the superoxide dismutase (SOD2) promoter in diabetic retinopathy to suppress SOD2 expression through modulation of H3K4 methylation.⁵² Therefore, we hypothesize that LSD1 may be a novel target that plays an important role in cardiac IR injury.

Histone Deacetylases (HDACs)

Histone deacetylases represent a large class of histone erasers responsible for the post-translational removal of an ϵ -N -acetyl moiety from specific lysine residues on the histone tail, thus preventing recruitment of *trans*-acting transcription factors. As a result, HDACs repress gene transcription.⁸⁴ In addition, a large number of non-histone substrates are known.⁸⁵ These well characterized epigenetic enzymes have been considered to play a role in CVD pathology for years. Most importantly, ischemia induces HDAC activity in the heart.¹⁹ Therefore, many studies have shown the efficacy of HDAC inhibition to attenuate cardiac IR injury.^{19, 29, 51}

In brief, the 18 isoforms of HDACs are divided into four classes. Class I, II, and IV are the zinc dependent metalloproteins and class III comprise the

NAD⁺-dependent sirtuins.⁸⁴ Of particular interest, the class I HDACS (1, 2, 3, and 8) are small nuclear histone erasers that cooperate in discrete co-repressor complexes, one of which (i.e. CoREST/REST) incorporates LSD1.⁸⁶ The crosstalk between LSD1 and HDACs has been discussed above (see “Lysine Specific Demethylase-1”). Only recently has the significance of a class-specific HDAC inhibitor been applied to cardiac IR.⁵¹ In fact, class I specific HDAC inhibitors sustained cardiac function and ablated infarction following IR injury in an *ex vivo* isolated rat heart model.⁵¹ However, isoform-specific (as opposed to class-specific) HDAC inhibitors do not exist, although many have been developed that show a preference for a given HDAC isoform. Therefore, the propensity for off-target effects mediated by inhibition of multiple isoforms can complicate mechanistic studies.

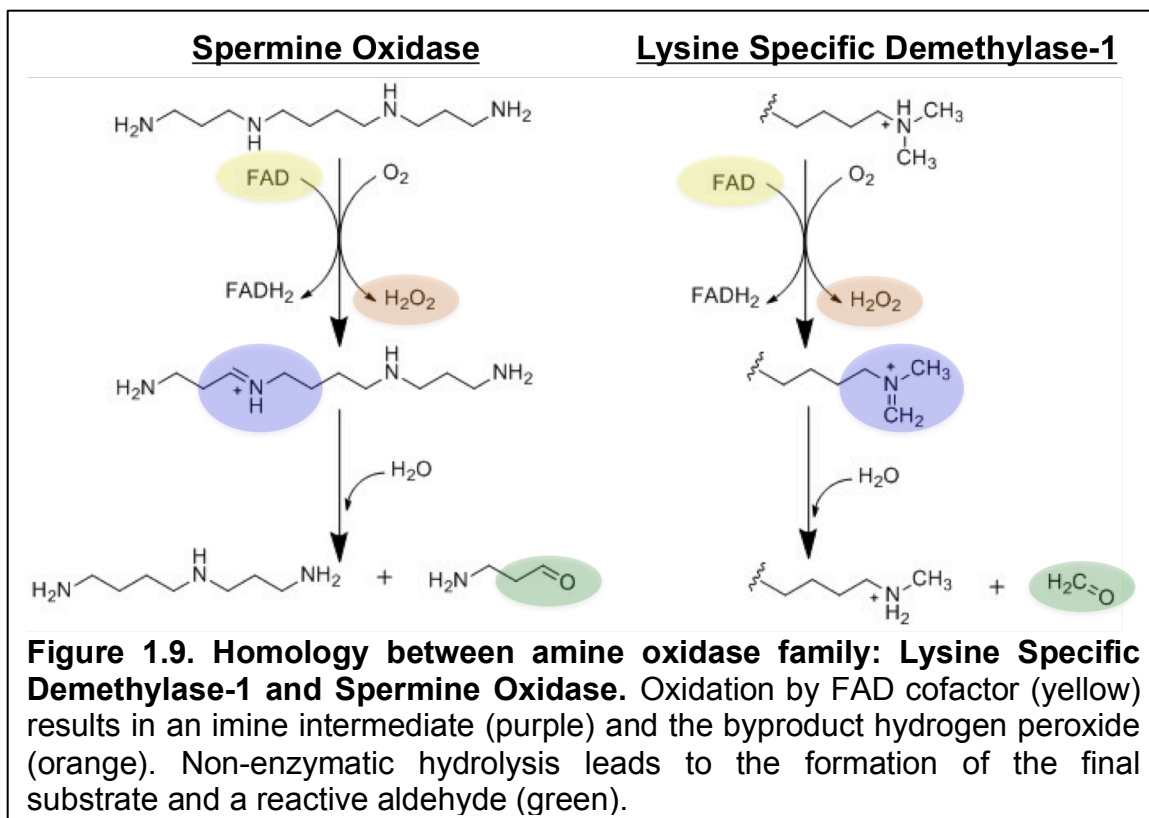
Histone Methyltransferases and Acetyltransferases

The early dogma for gene regulation was that post-translational acetylation and methylation of histones and DNA was irreversible. However, the discovery of epigenetic erasers (i.e. HDACs, histone demethylases, etc.) revolutionized our understanding of transcriptional regulation.⁸⁷ In fact, the epigenetic landscape is a vastly dynamic environment, and gene expression is modulated through freely reversible enzymatic processes. It is worth noting that large families of histone methyltransferases (HMTs) and histone acetyltransferases (HATs) are also crucial in regulating gene transcription. For instance, both HMTs and HATs transfer a methyl or acetyl residue, respectively,

onto the ϵ -nitrogen of a specific lysine residue.⁸⁸ Importantly, activities of HMTs and/or HATs have been implicated in CVD.⁸⁹⁻⁹⁰ These enzymatic transformations confer reversibility to post-translational modifications of histones and the mechanisms discussed for LSD1 and HDACs. However, these epigenetic writers will not be discussed in any further detail.

VI. OTHER FLAVIN-DEPENDENT AMINE OXIDASES

The amine oxidase enzymes all contain evolutionarily conserved FAD-dependent catalytic pockets. Each enzyme oxidizes biogenic amines (primary, secondary, and tertiary) into imine intermediates and produces H₂O₂ and aldehyde byproducts, as described earlier. Each amine oxidase adapted specialized motifs and cellular localization, giving them different biological functions. The amino acid sequences within the active sites demonstrate similar architecture, with the FAD prosthetic cofactor in close proximity of a lysine-containing residue. LSD1 uniquely adapted a SWIRM and tower domain to facilitate its interaction with chromatin.⁹¹ **Figure 1.9** demonstrates the close homology between catalytic mechanisms of LSD1 and another amine oxidase, spermine oxidase (discussed further below).



VI.a. Spermine Oxidase and Polyamine Metabolism

The origin of LSD1 discovery (previously known as KIAA0601) can be traced back to work by Shi *et al.* and their observation of sequence homology with common amine oxidases.⁵⁵ In particular, the prior perception of KIAA0601 was as a polyamine oxidase that reflected an additional role in lysine demethylation. Since then, the characterization of LSD1's biochemical mechanism has diverged significantly from the polyamine oxidases. However, significant off-target implications of current synthetic LSD1 inhibitors fail to consider polyamine oxidases in their screens. Clearly, the close homology of LSD1 to the polyamine oxidases, such as spermine oxidase, merits further consideration as a potential off-target enzymes.

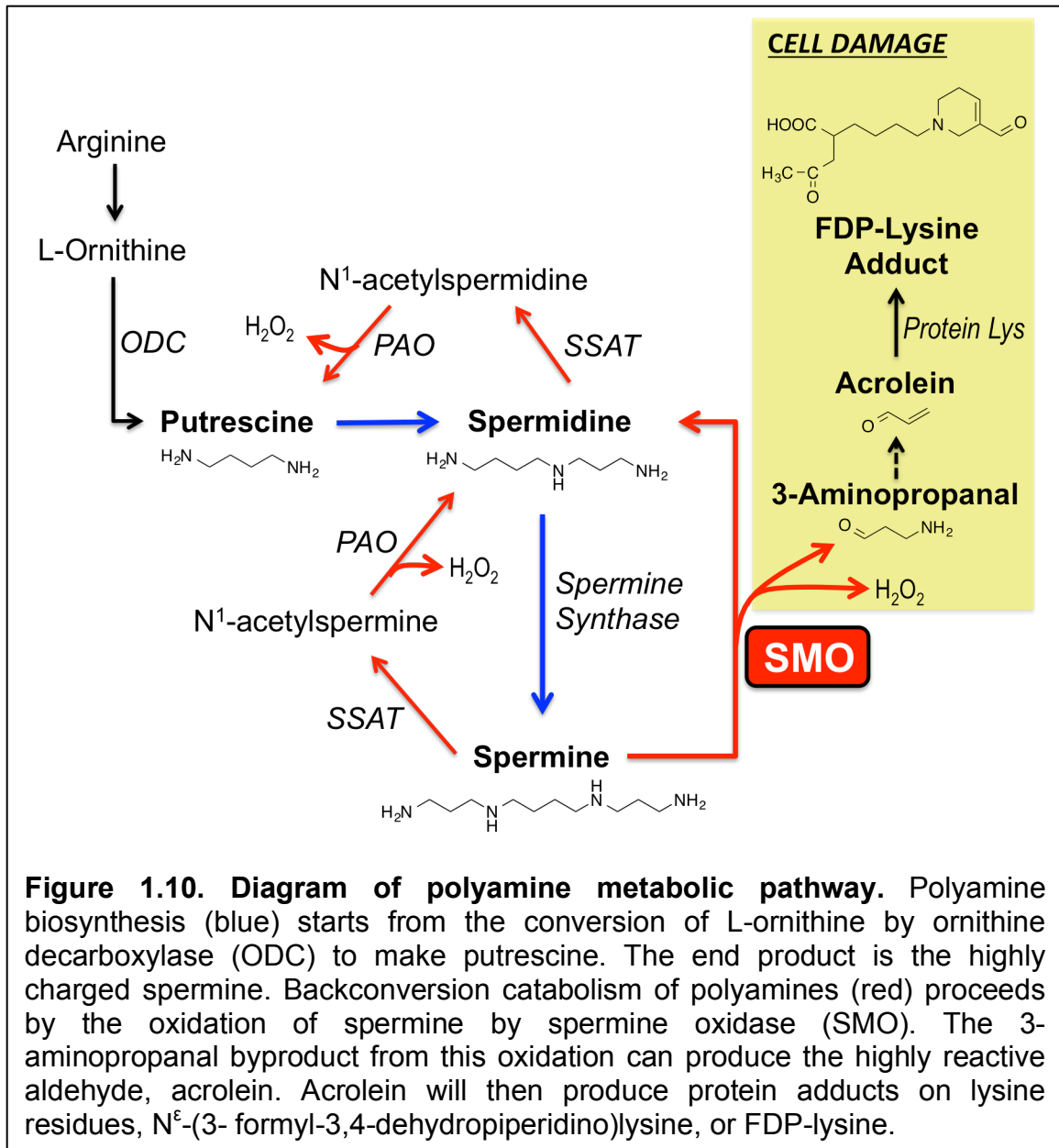


Figure 1.10. Diagram of polyamine metabolic pathway. Polyamine biosynthesis (blue) starts from the conversion of L-ornithine by ornithine decarboxylase (ODC) to make putrescine. The end product is the highly charged spermine. Backconversion catabolism of polyamines (red) proceeds by the oxidation of spermine by spermine oxidase (SMO). The 3-aminopropanal byproduct from this oxidation can produce the highly reactive aldehyde, acrolein. Acrolein will then produce protein adducts on lysine residues, N^ε-(3-formyl-3,4-dehydropiperidino)lysine, or FDP-lysine.

Polyamines are ubiquitous, highly charged species and are essential in homeostatic cell growth, differentiation, and death.⁹² They include putrescine, spermidine, and spermine (**Figure 1.10**). For several decades, manipulation of the intracellular level of polyamines has been a key strategy to modulate cell growth. For instance, it is well characterized that higher polyamine

concentrations contribute to actively growing cells, whereas depletion are typical of quiescent cells.⁹³ Polyamines contain highly protonated amines at physiologic pH, and thus, bind profusely to negatively charged species within the cell, including DNA, membrane bound lipids, and negatively charge proteins.⁹⁴ As such, they often facilitate protein:protein and protein:nucleic acid interactions (e.g. transcription factor binding to DNA). In addition, polyamines can stabilize membranes against lysis⁹⁵, prevention of mitochondrial damage by sustaining respiratory control⁹⁶, and have anti-inflammatory action through suppression of vascular permeability.⁹⁷ In fact, the end product in the polyamine synthetic pathway (i.e. Spermine) prevents generation of reactive hydroxyl radicals and acts as a potent antioxidant.⁹⁴

Fundamental polyamine biosynthesis is initiated by ornithine decarboxylase (ODC), which catalyzes arginine and L-ornithine decarboxylation to form putrescine.⁹⁸ Sequential addition of an aminopropyl group to putrescine and spermidine are performed to produce spermidine and spermine, respectively. This reaction is catalyzed by their respective synthases and decarboxylated S-adenosyl-L-methionine (dcSAM) to complete the synthetic portion of the polyamine pathway.⁹⁹

Polyamine catabolism is also a highly regulated process. Spermine and spermidine are each acetylated by spermine/spermidine-N¹-acetyltransferase (SSAT) and then oxidized by polyamine oxidase (PAO) to produce putrescine.⁹⁹ Similar to other amine oxidases, this process yields hydrogen peroxide and a reactive aldehyde. Most importantly, the backconversion of spermine to

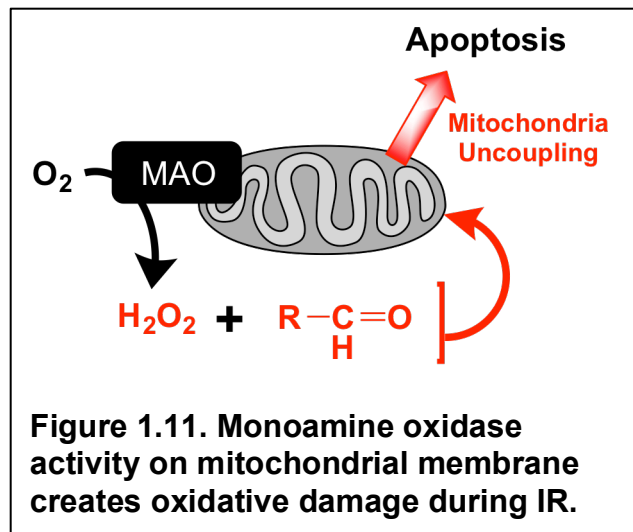
spermidine is facilitated by the recently characterized amine oxidase, spermine oxidase (SMO).⁹⁸

Of particular interest, accumulating evidence in polyamine metabolism implicates a role during ischemia-reperfusion injury. SMO and SSAT are up-regulated during kidney and hepatic IR injury, leading to depletion of spermine and spermidine with a dramatic increase in the backconversion end product, putrescine.¹⁰⁰ In the heart, Han *et al.* demonstrated that within myocardial infarcted tissue, there was temporal depletion of spermine and spermidine, which they found were due to overexpress SSAT and ODC.¹⁰¹ This is key in itself because spermine is a natural antioxidant and anti-inflammatory agent.⁹⁴ In fact, exogenous spermine given to an isolated rat heart after 40-min of global ischemia caused in improvement in cardiac hemodynamic parameters (i.e. LVDP, LVEDP, and +/-dP/dt) when reperfused for 30-minutes.¹⁰²

Consequently, during IR injury, the enhanced polyamine backconversion increases the pool of putrescine and generates toxic byproducts H₂O₂ and 3-aminopropanal (**Figure 1.10**).^{98, 100} 3-aminopropanal is in itself cytotoxic, but can be metabolized into other highly reactive aldehydes, including acrolein.¹⁰³ The unsaturated aldehyde readily generates protein adducts on lysine residues, N^ε-(3-formyl-3,4-dehydropiperidino)lysine, or FDP-lysine, and can lead to irreversible membrane disruption, mitochondrial damage, oxidative stress and cell death.¹⁰³

VI.b. Monoamine Oxidases

Among the most highly characterized members of the amine oxidase family are the monoamine oxidases A and B (MAO-A, MAO-B). MAO-A is highly abundant in cardiomyocytes.¹⁰⁴ The mitochondrial membrane bound MAOs play an important role in catecholamine and serotonin metabolism. In addition, the heart is sensitive to chronic neurohormonal stimulation and peripheral hemodynamic stress, both processes that produce extensive epinephrine, norepinephrine, and dopamine.¹⁰⁵ Like other amine oxidases, oxidation of these substrates creates H_2O_2 production, which can facilitate cell apoptosis.¹⁰⁶ During hemodynamic or hypertrophic stress, circulating/tissue levels of catecholamines increase, subsequently causing MAO-derived H_2O_2 overproduction.¹⁰⁷ As a result, multiple studies have used MAO-inhibitors to decrease oxidative damage and improve cardiac function during CVD.¹⁰⁸⁻¹⁰⁹ Oxidative stress caused by MAO-A on the outer mitochondrial membrane results in mitochondrial uncoupling and further ROS release, leading to tissue damage and contractile dysfunction (**Figure 1.11**).¹⁰⁵



Although the scope of this dissertation does not include a discussion of the role of MAO inhibition in cardioprotection, LSD1 inhibitors have the potential to produce significant off-target effects involving MAO.⁵⁶ The therapeutic risk and

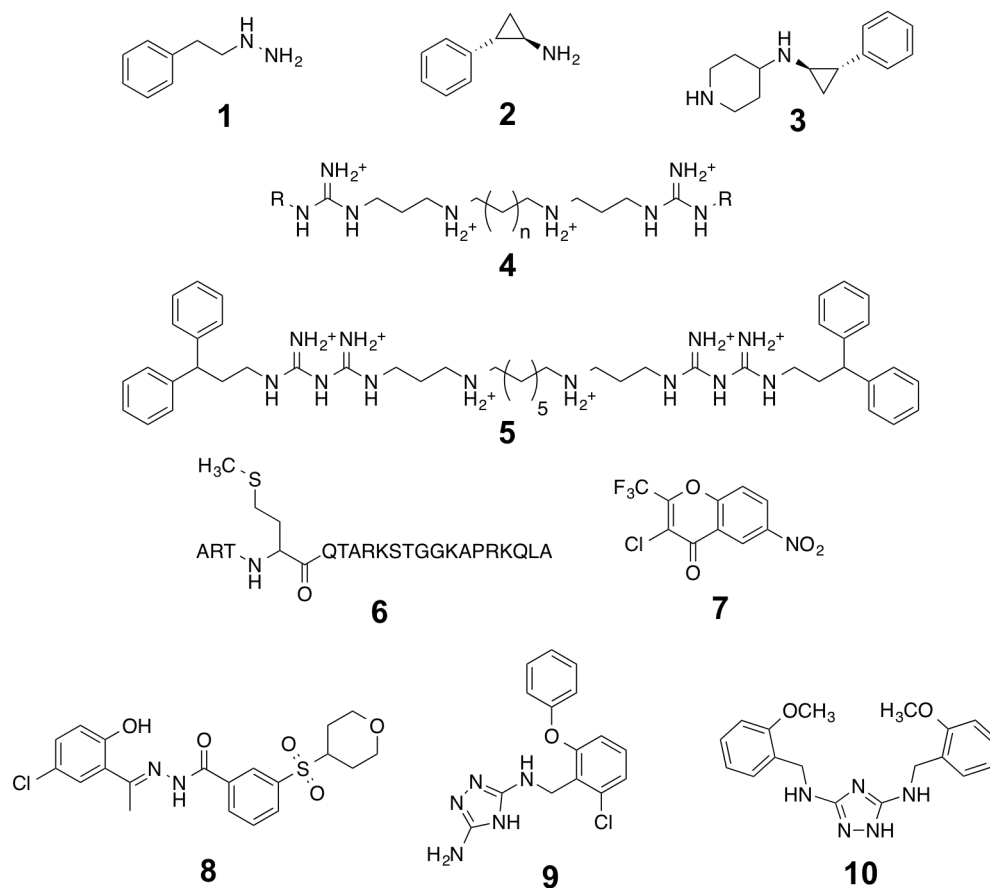
adverse side effects of MAO inhibition (e.g. nausea, drowsiness, lightheaded, malignant hypertension, sleep disturbances, etc.) caused by their large involvement in the neuroendocrine system make them undesirable targets.

VII. SYNTHETIC AMINE OXIDASE INHIBITORS

VII.a. Lysine Specific Demethylase-1 Inhibitors

To date, a number of small molecule inhibitors of LSD1 have been described, as shown in **Figure 1.12**. Because the FAD/amine-oxidase domain of LSD1 shows considerable sequence and structural homology to MAO-A and B, the earliest inhibitors of LSD1 focused on scaffolds similar to traditional MAO inhibitors. Lee *et al.* demonstrated the ability of several MAO inhibitors to reduce nucleosome demethylation by recombinant LSD1/CoREST.¹¹⁰ Although selective MAO inhibitors (i.e. pargyline, clorgyline) showed limited ability to reduce LSD1 activity, nonselective MAO inhibitors demonstrated substantial efficacy. Both phenelzine (**1**) and tranylcypromine (**2**) successfully inhibited LSD1/CoREST.¹¹⁰ In fact, tranylcypromine revealed an enzymatic $IC_{50} < 2\mu M$ and effectively increased *in vitro* global H3K4me2 in P19 embryonic carcinoma and de-repression of LSD1 target genes Erg1 and Oct4.¹¹⁰ Tranylcypromine is an irreversible, mechanism-based inhibitor that covalently binds FAD, either through a modification of FAD to form cinnamaldehyde-FAD and/or atropaldehyde-FAD¹¹¹, an FAD-heterocyclic pyrrolidine adduct¹¹², or N(5) intermediate FAD adduct.¹¹³ LSD1 inhibitors based on the tranylcypromine

Lysine Specific Demethylase-1 Inhibitors



Spermine Oxidase Inhibitors

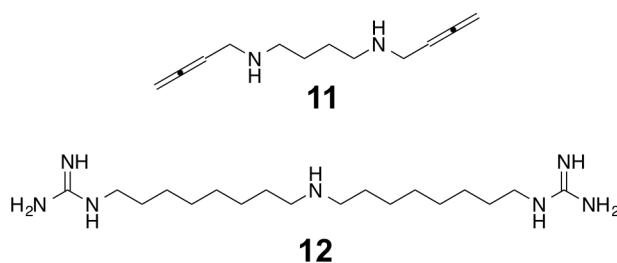


Figure 1.12. Structures of amine oxidase inhibitors. **1**, phenelzine; **2**, tranylcypromine; **3**, GSK-LSD1; **4**, (bis)guanidines; **5**, (bis)biguanides; **6**, [K⁴-Met]-21mer peptide; **7**, γ -pyrone Namoline; **8**, N'-(1-phenylethylidene)-benzohydrazides; **9**, N³-(2-chloro-6-phenoxybenzyl)-4H-1,2,4-triazole-3,5-diamine; **10**, N³,N⁵-bis(2-methoxybenzyl)-1H-1,2,4-triazole-3,5-diamine; **11**, MDL-72527; **12**, guazatine.

scaffold have been produced and characterized, and in March 2015, the first phase-I clinical trial of an LSD1 inhibitor (ORY-1001) was started for the treatment of acute myeloid leukemia.¹¹⁴ Shortly thereafter, a second clinical trial was begun involving the tranylcypromine-based inhibitor, GSK-LSD1/GSK2879552 (**3**), which is a highly specific and potent LSD1 inhibitor with an IC₅₀ of 16 nM and >1000 fold selectivity over LSD2, MAO-A, and MAO-B.¹¹⁴

A small number of effective LSD1 inhibitor classes have been discovered that are based on scaffolds other than the tranylcypromine backbone. For instance, our lab hypothesized that due to the structural similarity of LSD1 to the polyamine oxidases SMO and APAO, long chain oligoamine homologues could also act as LSD1 inhibitors. A series of (bis)guanidine (**4**) and (bis)biguanide (**5**) analogues originally designed as anti-trypanosomal agents acted as non-competitive LSD1 inhibitors at concentrations <2 μM.¹¹⁵⁻¹¹⁷ Most importantly, these polyamine mimics were the first compounds that were shown to increase H3K4 methylation, and to re-express epigenetically silenced tumor suppressors (i.e. SFRP1, SFRP4, SFRP5, and GATA5).¹¹⁸ Additional functionalized isosteric (bis)ureidopropyl and (bis)thioureidopropyldiamine derivatives with 3-5-3 and 3-6-3 carbon backbones also demonstrated relative potency.¹¹⁹ Similar functional moieties were reported by Dulla *et al.* using functionalized phenyl oxazole derivatives, although they exhibited only moderate potency.¹²⁰

Although inhibitors based on a linear peptide backbone are susceptible to hydrolysis and difficult to deliver, many highly potent compounds have been reported.¹²¹⁻¹²² Forneris *et al.* described a 21-mer peptide (**6**) that is analogous to

the H3K4 substrate region of LSD1, wherein Lys4 was replaced by a methionine. This linear peptide was a potent inhibitor of recombinant LSD1 with a K_i value of 0.04 μM , and of LSD1 bound to CoREST with a K_i value of 0.05 μM .¹²¹ More recently, cyclic peptide analogues with lactam bridges between Lys5 and Glu10 of the 21-mer were developed, and these compounds were significantly more stable to hydrolysis in rat plasma and revealed competitive inhibition of LSD1 ($K_i = 385 \mu\text{M}$).¹²³

Despite the recent flurry of LSD1 inhibitor discovery efforts, most utilize latent electrophilic scaffolds that produce irreversible, mechanism-based inactivation of LSD1,⁵⁶ and very few reversible inhibitors have been reported. Irreversible, or suicide inhibitors, typically bind covalently to proteins and generally have extended half-lives. Thus, they are more likely to produce off-target effects mediated through other enzymes. By contrast, if a reversible inhibitor produces off-target toxicity, it can be alleviated by administration of high concentrations of the natural substrate. Therefore, in epigenetically driven disorders where cytotoxicity is not a desired endpoint, such as CVD, reversible inhibitors are preferable.

Willmann *et al.* utilized a virtual screen of a natural product-inspired library to identify the γ -pyrone namoline (**7**), which acts as a competitive, reversible inhibitor of LSD1 ($\text{IC}_{50} = 50 \mu\text{M}$).¹²⁴ In addition, small molecule peptidomimetics have been published as reversible compounds, but only show *in vitro* phenotype changes in substrate at 1 mM.¹²⁵ Recently, a novel class of N'-(1-phenylethylidene)-benzohydrazides was characterized as highly selective,

reversible LSD1 inhibitors.¹²⁶ These highly potent ($K_i = 31$ nM) compounds typified by **8** produced significant anti-proliferative ability in several cancer cell lines, albeit within the low micromolar range. This suggests that the *in vitro* activity in cancer cells may be a substantial off-target effect. In addition, the core N'-(2-hydroxybenzylidene)hydrazide motif has previously been characterized as a frequent hitter in many biochemical assays.¹²⁷ Enzyme kinetic studies revealed that these analogues produce non-competitive inhibition, meaning the inhibitor may not prevent the enzyme from binding to its substrate by occupying the active site.

VIII.b. Spermine Oxidase Inhibitors

Because polyamines play significant roles in mammalian cells, it is not surprising that disruption of one polyamine metabolic enzyme can have countless cellular effects. Several groups have identified amines, guanidines or similar analogues that act as selective inhibitors of APAO and SMO. The most widely used polyamine modulator was designed in 1985 as a butadienyl putrescine derivative.¹²⁸ N,N-bis(2,3-butadienyl)-1,4-butanediamine, also known as MDL 72,527 (**11**), is a potent inhibitor of murine PAO,¹²⁹ as well as human APAO and SMO, but does not inhibit MAO.¹³⁰⁻¹³¹ Cona *et al.* demonstrated that guazatine (**12**) is a non-competitive inhibitor of maize PAO and can selectively inhibit human recombinant APAO and SMO.¹³² Other guanidines, such as the (bis)guanidines and (bis)biguanides described earlier (“Lysine Specific Demethylase-1 Inhibitors”), produced significant inhibition of SMO (42% at 10

μM) and APAO (92% at 10 μM).¹¹⁷ To date, a limited number of SMO inhibitors have been identified and MDL 72,527 continues to be used as a standard in research.

VIII. SPECIFIC AIMS

To date, no standard therapy exists that can mitigate the injury caused by reperfusing an occluded coronary artery after an AMI. In fact, up to 50% of total infarct damage is attributed to IR injury. Upon reperfusion, a secondary wave of damage leads to contractile dysfunction and arrhythmias. The extent of irreversible myocyte damage is a key determinant in patient short- and long-term outcomes and therefore, the need for therapies to reduce IR injury are apparent. However, pharmaceutical strategies to reduce IR damage have yet to translate successfully into the clinics.

In recent years, increasing evidence indicates that epigenetic enzymes such as the histone demethylases and deacetylases play crucial roles during CVD. One such enzyme, LSD1, is hypoxia-inducible and regulates oxidative balance through epigenetic silencing of oxidative scavenging enzymes and production of H_2O_2 . Yet, the role LSD1 and other demethylase enzymes play in cardiac IR has yet to be explored. Our overall goal is to validate LSD1 as a novel therapeutic target, and to discover a new series of potent, reversible inhibitors that are well tolerated by cardiac tissue.

The CENTRAL HYPOTHESIS of this dissertation is that novel LSD1 inhibitors with enhanced drug-like properties can be used to mitigate cardiac ischemia-reperfusion structural damage and contractile dysfunction with minimal toxicity to myocytes.

In order to test this hypothesis, we pursued the following Specific Aims:

Specific Aim 1. Perform hit-to-lead optimization through structural modification of a new small molecule scaffold to discover reversible LSD1 inhibitors with suitable efficacy, negligible toxicity and enhanced drug-like properties. A virtual screen using recombinant LSD1/CoREST crystal structure (PDB 2D1V) was used to identify two hit compounds, (**9** and **10**), that were shown to act as potent, selective and nontoxic LSD1 inhibitors in vitro.¹³³ We will use a structure-based drug design approach to produce a focused library of 3,5-diamino-1,2,4-triazole analogs that will be screened as LSD1 inhibitors. Compounds will be synthesized by heterocyclization of appropriately functionalized N-substituted N'-cyano-S-methylisothiurea and hydrazine. Screening for in vitro activity against recombinant LSD1/CoREST will be performed using an HRP-coupled fluorometric assay. For selected compounds, kinetic constants (K_i and V_{max}) and binding affinity values will be measured by isothermal titration calorimetry.

Specific Aim 2. Determine the LSD1 target selectivity, cellular cytotoxicity, and cellular phenotypic changes in histone methylation of lead compounds. Many known LSD1 inhibitors are based on the irreversible pan-

amine oxidase inhibitor tranylcypromine, a clinical MAO inhibitor. It is challenging to design a TCP-based LSD1 inhibitor for clinical use that is specific, has low toxicity, and is devoid of the many biological responses as TCP itself. Therefore, the purpose of this aim will be to identify LSD1-specific inhibitors from compounds produced in Specific Aim 1. LSD1 inhibitory activity will be compared to inhibition of MAO-A and MAO-B using a commercial kit to determine a selectivity index and cytotoxicity will be evaluated using a standard MTS reduction assay. Inhibitors meeting pre-determined criteria (50-fold LSD1 selectivity, $IC_{50} < 5\mu M$, $cLogP < 5$, cell viability $IC_{50} > 50\mu M$) will be evaluated for phenotypic effects (increases in H3K4me2) by immunofluorescent staining and western blotting. Co-immunoprecipitation will also be performed to determine whether the test compound promotes disruption of LSD1:CoREST:HDAC1/2. Finally, we will evaluate *in vivo* toxicology of a 3,5-diamino-1,2,4-triazole derivative using CD1 mice.

Specific Aim 3. Evaluate the pharmacodynamic efficacy of a lead 3,5-diamino-1,2,4-triazole derivative to mitigate post-IR contractile dysfunction and infarction using two murine models of IR. The purpose of this aim will be to A) ascertain the protective effects of selected lead compounds identified in Specific Aim 2 in reducing infarct and in improving contractile function, and B) to establish LSD1 as an effective therapeutic target to abrogate IR damage. We will use both an *ex vivo* isolated heart and an *in vivo* left anterior descending coronary artery ligation-reperfusion model. Sprague-Dawley rats will be

pretreated with each compound and their hearts will be isolated by Langendorff preparation. After inducing transient global IR, left ventricular (LV) contractile function and myocardial infarction will be observed. In addition, CD1 mice will be evaluated 7-days post-IR surgery by echocardiography for functional analysis.

IX. SIGNIFICANCE

Treatment strategies for AMI continue to be palliative and methods for reducing infarction following reperfusion have proven insufficient. Successful completion of these aims will provide the first evidence that histone demethylases play a significant role in pathological cardiac remodeling and function. Notably, this result suggests a vast network of novel therapeutic targets that have yet to be explored in CVD. To date, epigenetic targets in CVD primarily focus on the vast array of HDACs and DNA methylation.^{51, 54} However, use of insufficiently isoform-specific HDAC inhibitors results in a propensity for off-target effects that can complicate mechanistic studies. Interestingly, recent evidence shows a close cooperation between HDACs and LSD1.⁶⁷ In addition, LSD1 itself can produce oxidative stressors and damaging reactive aldehydes.⁸¹ Thus, we will show a new innovative strategy to treat CVD through modulation of LSD1.

Transgenic studies with LSD1 have proven difficult because LSD1 knockdown is embryonic lethal.¹³⁴ In addition, current LSD1 inhibitors are undesirable for their overt toxicity or off-target efficacy. Therefore, we pursued to successfully design and optimize a specific LSD1 inhibitor that could be used to pinpoint LSD1 involvement in cardiac IR injury. More importantly, we strove to

design a unique new chemotype that lacked the overt cytotoxicity seen with other known LSD1 inhibitors. Herein, we will disclose highly potent small molecule inhibitors of LSD1 that are the first published reversible, competitive inhibitors.¹³³ In addition, all compounds show utility in the treatment of epigenetically-based diseases where cell death is not a desired endpoint, such as CVD. Completion of the specific aims for this study will provide a mechanistic foundation for development of attractive cardiac drug candidates.

CHAPTER 2: Materials and Experimental Methods

I. CHEMISTRY REAGENTS AND REACTIONS

All reagents and dry solvents were purchased from Aldrich Chemical Co. (Milwaukee, WI), Sigma Chemical Co. (St. Louis, MO), VWR (Radnor, PA) or Fisher Scientific (Chicago, IL) and were used without further purification except as noted below. Pyridine was dried by passing it through an aluminum oxide column and then stored over KOH. Triethylamine was distilled from potassium hydroxide and stored in a nitrogen atmosphere. Methanol was distilled from magnesium and iodine under a nitrogen atmosphere and stored over molecular sieves. Methylene chloride was distilled from phosphorus pentoxide and chloroform was distilled from calcium sulfate. Tetrahydrofuran was purified by distillation from sodium and benzophenone. Dimethyl formamide was dried by distillation from anhydrous calcium sulfate and was stored under nitrogen. Microwave procedures were carried out on a Biotage Initiator 8 microwave synthesizer. Preparative scale chromatographic procedures were carried out on a Teledyne Isco Combi-Flash Rf200 using silica gel 60 cartridges, 230-440 mesh. Thin layer chromatography was conducted on Merck precoated silica gel 60 F-254. Compound **9** was purchased from Ryan Scientific (Mt. Pleasant, SC) and compounds **13-25** were purchased from Chembridge (San Diego, CA). TCP was purchased from Acros Organics (Pittsburgh, PA).

All ^1H - and ^{13}C -NMR spectra were recorded on a Varian Mercury 400 MHz spectrometer, and all chemical shifts are reported as δ values referenced to TMS or DSS. Splitting patterns are indicated as follows: s, singlet; d, doublet; t, triplet; q, quartet; p, pentuplet; m, multiplet; br, broad peak. In all cases, ^1H -NMR, ^{13}C -

NMR and MS spectra were consistent with assigned structures. Mass spectra were recorded by LC/MS on a Waters autopurification liquid chromatograph with a model 3100 mass spectrometer detector. All target molecules **26-44** were determined to be >95% pure by UPLC chromatography (95% H₂O/5% acetonitrile to 20% H₂O/80% acetonitrile over 10 minutes) using a Waters Acquity H-series ultrahigh-performance liquid chromatograph fitted with a C18 reversed-phase column (Acquity UPLC BEH C18 1.7 mM, 2.1 X 50 mm).

General procedure for the preparation of 2-chloro-6-phenoxy benzonitriles:

Synthesis of 2-chloro-6-phenoxybenzonitrile 23. To a 20 mL microwave vial containing a magnetic stir bar was added 0.78 g (5.0 mmol) of 2-fluoro-6-chlorobenzonitrile, 1.04 g (7.5 mmol) of K₂CO₃, 0.52 g (5.5mmol) of phenol and 12 mL of anhydrous DMSO. The vial was then sealed and stirred to distribute the contents evenly. The mixture was then microwaved at 190°C for 6 min at high absorption to insure even heating. The reaction mixture was then poured into a beaker containing 100 mL of crushed ice to precipitate the product. The aqueous layer was extracted with three 50 mL portions of diethyl ether, and the ether layer was washed with 25 mL of saturated NaCl, dried over anhydrous Na₂SO₄, filtered, and the ether was removed in vacuo to yield 1.11 g of the desired diaryl ether 23 (97% yield). The crude product 23 was pure enough (95%) to be used in the next reaction without further purification.

General procedure for the preparation of 2-chloro-6-phenoxy benzylamines:

Synthesis of 2-chloro-6-phenoxybenzylamine **45**. A 1.11 g portion of **44** (4.8 mmol) was dissolved in 50 mL of anhydrous diethyl ether, cooled to 0°C in an ice bath and stirred while bubbling dry argon into the reaction mixture for 10 min. A 14.49 mL portion of 1.0 M LiAlH₄ in THF (14.49 mmol) was then added dropwise with stirring over 20 min. The resulting reaction mixture was allowed to stir for 2hrs at 0°C, and then warmed to room temperature and allowed to stir overnight. The mixture was cooled to 0°C, and the reaction was quenched by the slow addition of Na₂SO₄•10 H₂O. When the evolution of gas subsided, the reaction was stirred for 30 min at room temperature, and the mixture was filtered through a Celite pad. The filtrate was concentrated to dryness to yield crude 2-chloro-6-benzoybenzylamine **45**.

General procedure for the preparation of target molecules 27-45:

Synthesis of *N*³-(2-chloro-6-phenoxybenzyl)-4*H*-1,2,4-triazole-3,5-diamine **9**. A 0.935 g portion of benzylamine **45** (4.0 mmol) was dissolved in 12 mL of diethyl ether and added to a 20 mL microwave vial equipped with a magnetic stir bar. A 0.702 g portion of dimethyl cyanodithioiminocarbonate **46** (4.8 mmol) was added and the vial was sealed. The contents were microwaved at 45°C for 5 min, cooled to room temperature, and the ether was removed *in vacuo* to yield the intermediate **47** as a white to pale yellow solid. A 0.192 g portion of hydrazine hydrate (6.0 mmol) in 12 mL of dry ethanol was then injected, the vial was stirred to break up the solid intermediate, and the resulting mixture was

microwaved at 90°C for 10 min at high absorption. The ethanol was removed *in vacuo* to yield crude **9**, which was purified on silica (9% MeOH in CH₂Cl₂) to afford 1.07 g of pure **9** (85%) as an off-white, amorphous solid. ¹H-NMR (400MHz, CD₃OD/TMS) δ 4.21 (s, 2H), 6.77-6.80 (dd, 1H), 6.99-7.01 (d, 2H), 7.11-7.15 (t, 1H), 7.20-7.27 (m, 2H), 7.33-7.38 (t, 2H). UPLC retention time: 12.1 min. MS calculated 315.09, found 316.33 ([M+1]⁺).

*N*³-(2-chloro-6-(4-(trifluoromethoxy)phenoxy)benzyl)-4H-1,2,4-triazole-3,5-diamine **26**. Compound **26** was synthesized exactly as described above in 86% yield as a white solid. ¹H-NMR (400MHz, CD₃OD/TMS) δ 4.31 (s, 2H), 6.72 (s, 1H), 6.85-6.87 (dd, 2H), 7.04-7.08 (d, 1H), 7.26-7.33 (m, 2H), 7.49 (s, 1H). UPLC retention time: 15.5 min. MS calculated 399.07, found 400.27 ([M+1]⁺).

*N*³-(2-chloro-6-(*p*-tolylloxy)benzyl)-4H-1,2,4-triazole-3,5-diamine **27**. Compound **27** was synthesized exactly as described above in 82% yield as a white solid. ¹H-NMR (400MHz, CD₃OD/TMS) δ 2.17 (s, 3H), 4.39 (s, 2H), 6.71-6.78 (m, 3H), 7.19 (d, 1H), 7.37-7.45 (m, 2H). UPLC retention time 14.4 min. MS calculated 329.79, found 330.36 ([M+1]⁺).

*N*³-(2-chloro-6-(2-isopropyl-5-methylphenoxy)benzyl)-4H-1,2,4-triazole-3,5-diamine **28**. Compound **28** was synthesized exactly as described above in 78% yield as a white solid. ¹H-NMR (400MHz, CD₃OD/TMS) δ 1.15-1.21 (d, 6H), 2.26 (s, 3H), 3.09-3.15 (m, 1H), 4.07 (s, 2H), 6.56-6.58 (dd, 1H), 6.97-7.00 (1H), 7.13-

7.25 (m, 3H), 7.51 (s, 1H). UPLC retention time 16.0 min. MS calculated 371.15, found 372.37 ($[M+1]^+$).

*N*³-(2-chloro-6-(3-methoxyphenoxy)benzyl)-4H-1,2,4-triazole-3,5-diamine **29**.

Compound **29** was synthesized exactly as described above in 81% yield as a white solid. ¹H-NMR (400MHz, CD₃OD/TMS) δ 3.80 (s, 3H), 4.29 (s, 2H), 6.56-6.59 (dd, 1H), 6.60-6.61 (t, 1H), 6.72-6.75 (dd, 1H), 6.85-6.88 (dd, 1H), 7.25-7.32 (m, 3H). UPLC retention time 15.5 min. MS calculated 345.10, found 346.30 ($[M+1]^+$).

*N*³-(2-(4-(tert-butyl)phenoxy)-6-chlorobenzyl)-4H-1,2,4-triazole-3,5-diamine **30**.

Compound **30** was synthesized exactly as described above in 81% yield as a white solid. ¹H-NMR (400MHz, CD₃OD/TMS) δ 1.35 (s, 9H), 4.02 (s, 2H), 6.78-6.81 (dd, 1H), 6.95-6.98 (dt, 2H), 7.21-7.28 (m, 2H), 7.42-7.45 (dt, 2H). UPLC retention time 16.1 min. MS calculated 371.15, found 372.37 ($[M+1]^+$).

*N*³-(2-chloro-6-(3,5-dimethylphenoxy)benzyl)-4H-1,2,4-triazole-3,5-diamine **31**.

Compound **31** was synthesized exactly as described above in 74% yield as a white solid. ¹H-NMR (400MHz, CD₃OD/TMS) δ 2.30 (s, 6H), 4.41 (s, 2H), 6.64 (s, 2H), 6.81 (s, 2H), 7.21-7.29 (m, 2H). UPLC retention time 14.5 min. MS calculated 343.82, found 344.33 ($[M+1]^+$).

*N*³-(2-(3,5-bis(trifluoromethyl)phenoxy)-6-chlorobenzyl)-4H-1,2,4-triazole-3,5-diamine **32**. Compound **32** was synthesized exactly as described above in 77% yield as a white solid. ¹H-NMR (400MHz, CD₃OD/TMS) δ 4.01 (s, 2H), 7.14 (s, 1H), 7.25 (s, 2H), 7.33 (s, 1H), 7.49 (s, 1H), 7.57 (s, 1H). UPLC retention time 15.4 min. MS calculated 451.76, found 452.63 ([M+1]⁺).

*N*³-(2-chloro-6-(4-((trifluoromethyl)thio)phenoxy)benzyl)-4H-1,2,4-triazole-3,5-diamine **33**. Compound **33** was synthesized exactly as described above in 79% yield as a white solid. ¹H-NMR (400MHz, CD₃OD/TMS) δ 4.22 (s, 2H), 7.14 (d, 1H), 7.28-7.39 (m, 5H), 7.40 (d, 1H). UPLC retention time 14.0 min. MS calculated 415.05, found 416.24 ([M+1]⁺).

*N*³-(2-(4-bromo-2-(trifluoromethyl)phenoxy)-6-chlorobenzyl)-4H-1,2,4-triazole-3,5-diamine **34**. Compound **34** was synthesized exactly as described above in 61% yield as a white solid. ¹H-NMR (400MHz, CD₃OD/TMS) δ 4.28 (s, 2H), 7.04 (d, 1H), 7.22 (d, 1H), 7.27 (dd, 1H), 7.44 (d, 1H), 7.55 (d, 1H), 7.71 (s, 1H). UPLC retention time 15.4 min. MS calculated 460.99, found 462.18 ([M+1]⁺).

*N*³-(2-chloro-6-(4-((methyl)thio)phenoxy)benzyl)-4H-1,2,4-triazole-3,5-diamine **35**. ¹H-NMR (400MHz, CD₃OD/TMS) δ 2.32 (s, 3H), 4.07 (s, 2H), 7.14 (d, 1H), 7.31 (m, 2H), 7.39-7.47 (m, 2H), 7.55 (d, 1H). UPLC retention time 14.6 min. MS calculated 361.08, found 362.23 ([M+1]⁺).

*N*³-(2-chloro-6-(2-methoxy-4-methylphenoxy)benzyl)-4H-1,2,4-triazole-3,5-diamine **36**. Compound **36** was synthesized exactly as described above in 40% yield as a white solid. ¹H-NMR (400MHz, CD₃OD/TMS) δ 2.40 (s, 3H), 3.75 (s, 3H), 6.54-6.57 (m, 3H), 6.83-6.88 (d, 1H), 7.06-7.18 (m, 2H). UPLC retention time 14.7 min. MS calculated 359.11, found 360.29 ([M+1]⁺).

*N*³-(2-chloro-6-(3,5-dimethoxyphenoxy)benzyl)-4H-1,2,4-triazole-3,5-diamine **37**. Compound **37** was synthesized exactly as described above in 76% yield as a white solid. ¹H-NMR (400MHz, CD₃OD/TMS) δ 3.75 (s, 6H), 6.14 (s, 1H), 6.22 (s, 2H), 6.90 (d, 1H), 7.26-7.33 (m, 2H). UPLC retention time 14.1 min. MS calculated 375.11, found 376.29 ([M+1]⁺).

*N*³-(2-chloro-6-(2,3-dimethylphenoxy)benzyl)-4H-1,2,4-triazole-3,5-diamine **38**. Compound **38** was synthesized exactly as described above in 43% yield as a white solid. ¹H-NMR (400MHz, CD₃OD/TMS) δ 2.14-2.21 (m, 3H), 2.35-2.37 (m, 3H), 6.52 (d, 1H), 6.73-6.79 (m, 3H), 7.01-7.20 (m, 2H). UPLC retention time 15.0 min. MS calculated 343.12, found 344.33 ([M+1]⁺).

*N*³-(2-(benzo[d][1,3]dioxol-5-yloxy)-6-chlorobenzyl)-4H-1,2,4-triazole-3,5-diamine **39**. Compound **39** was synthesized exactly as described above in 80% yield as a white solid. ¹H-NMR (400MHz, CD₃OD/TMS) δ 4.41 (s, 2H), 5.51 (s, 2H), 6.00 (s, 1H), 6.99-7.11 (m, 3H), 7.33-7.39 (m, 2H). UPLC retention time 13.7 min. MS calculated 359.08, found 360.25 ([M+1]⁺).

*N*³-(2-chloro-6-(phenylthio)benzyl)-4H-1,2,4-triazole-3,5-diamine **40**. Compound **40** was synthesized exactly as described above in 91% yield as a white solid. ¹H-NMR (400MHz, CD₃OD/TMS) δ 4.31 (s, 2H), 7.19 (m, 1H), 7.36-7.44 (m, 6H), 7.61 (d, 1H). UPLC retention time 14.2 min. MS calculated 331.07, found 332.28 ([M+1]⁺).

*N*³-(2-chloro-6-((3,4-dimethoxyphenyl)thio)benzyl)-4H-1,2,4-triazole-3,5-diamine **41**. Compound **41** was synthesized exactly as described above in 82% yield as a white solid. ¹H-NMR (400MHz, CD₃OD/TMS) δ 3.67 (s, 6H), 4.40 (s, 2H), 6.56 (m, 2H), 7.04 (m, 2H), 7.39 (d, 1H), 7.49 (d, 1H). UPLC retention time 13.7 min. MS calculated 391.09, found 392.29 ([M+1]⁺).

*N*³,*N*⁵-bis(2-methoxybenzyl)-1H-1,2,4-triazole-3,5-diamine (commercial compound **10**). Compound **10** was purchased from Chembridge (San Diego, CA) as a white solid. ¹H-NMR (400MHz, CD₃OD/TMS) δ 3.64 (s, 6H), 4.17 (s, 2H), 6.86-6.90 (t, 2H), 6.94-6.96 (m, 4H), 7.21-7.27 (m, 2H). UPLC retention time 13.7 min. MS calculated 339.17, found 340.28 ([M+1]⁺).

II. IN VITRO DRUG CHARACTERIZATION AND ENZYME ASSAYS

Cell culture and reagents:

Calu-6 cells (human lung adenocarcinoma ATCC-HTB-56) were purchased from ATCC, and cultured in EMEM growth medium containing 10%

(v/v) fetal bovine serum and 5% penicillin and streptomycin. Cultures were grown at 37°C in a humidified environment containing 5% CO₂. For each experiment, cells were seeded at a starting density of 400,000 cells per T25 flask.

Determination of cell viability:

For the (3-(4,5-dimethylthiazol-2-yl)-5-(3-carboxymethoxyphenyl)-2-(4-sulfophenyl)-2H-tetrazolium) (MTS) reduction assay, 4000 cells/well were seeded in 100 µl medium in a 96-well plate and the cells were allowed to attach at 37°C in 5% CO₂ for one day. The medium was aspirated and cells were treated with 100 µl of fresh medium containing appropriate concentrations of each test compound. The cells were incubated for 4 days at 37°C in 5% CO₂. After 4 days 20 µL of the MTS reagent solution (Promega CellTiter 96 Aqueous One Solution Cell Proliferation Assay) was added to the medium. The cells were incubated for another 2 hours at 37°C under 5% CO₂ environment. Absorbance was measured at 490 nm on a microplate reader equipped with SOFTmax PRO 4.0 software to determine the cell viability. Cell counts were confirmed by counting DAPI stained nuclei as previously mentioned. Absorbance was measured at 490 nm on a microplate reader equipped with SOFTmax PRO 4.0 software to determine the cell viability.

In vitro LSD1 demethylation assay and kinetics:

Inhibition assays and kinetics were performed using LSD1 Inhibitor Screening Assay Kit (Cayman Chemical, #700120). The substrate and all

compounds were incubated in assay buffer from 30 min up to 4 hr at 37°C as described in the commercial protocol. The volume of each reaction well was 50 μ l, containing 5 ml of a 200 mM solution of substrate peptide and 20 ml of a 15ng/ml enzyme solution. All compounds were diluted in 1% DMSO with assay buffer to a final concentration of 50 mM. Fluorescence was measured at the recommended wavelengths of λ_{ex} =530 nm, λ_{em} -590 nm. IC₅₀ determinations were performed using serial dilutions at 10, 5, 2.5, 1.25, 0.625, 0.3125 and 0.156 mM)..

In silico molecular modeling:

LSD1 active site (PDB #3ZMT, LSD1-CoREST in complex with PRSFLV peptide) was defined as a sphere enclosing residues within 10Å around the crystallographic peptide ligand. Prior to energy minimization, LSD1 was protonated and the PH was set to 7.4. The 3D structure of inhibitors was energy minimized using MM94x force field for 1000 iterations and a convergence value of 0.001 kcal/mol/Å as the termination criterion. Initial docking results yielded 60 poses of each structure bound the active site of LSD1. The top 5 poses that yielded the lowest E-score were chosen for further analysis. The best fit for binding was analyzed for interacting residues. Key interactions with compound **9** include two hydrogen bonds with aspartate 555 and another hydrogen bond with the carbonyl of alanine 539. In addition, the compound participates in pi-stacking with the flavin ring of the FAD cofactor within 2.98Å. Thus, compound **9** shows close association with the active site and effectively prohibits substrate binding.

Nanoisothermal calorimetry (ITC):

Experiment was performed on Nano-ITC Low Volume (TA Instruments). Initial setup protocols were run with 55.6M H₂O/H₂O titrations and run to remove any background heat release upon injection. Using 50mM PBS, buffer was added to the system with 20 injections to remove any buffer background. Compound **9** was then diluted to 1 μ M with <1% DMSO, and injected into the system to eliminate ligand background peaks. After equilibrating the system, LSD1 was diluted to 500 nM, added to the cell, and titrated in with 10 injections of compound **9**.

Monoamine oxidase A and B activity assay:

MAO/A/B activity was measured with the luminescent MAO-Glo assay kit (Promega, #V1452) according to the manufacturer's instructions. In brief, total MAO activity was assayed by incubation of compounds with MAO/A or MAO/B enzyme solution containing MAO substrate according to the suppliers directions. Reconstituted luciferin detection reagent was added, and the resulting luminescent signal was detected with 0.5 integration time after 20 mins.

Immunofluorescence staining of global methylation:

Cells were seeded at 1x10³ cells/well and were then stained for Immunofluorescence (IF) imaging using fluorescently labeled secondary antibodies. Cells were fixed and permeabilized as mentioned above, and then blocked with 10% Normal Donkey Serum (NDS) for 1hr, washed with PBS, and

incubated overnight at 4°C with the H3K4me2 antibody (Cell Signaling, #2139S). Fluorescent secondary antibodies were added to corresponding wells at 1:500 dilutions in 1% NDS for 2 hours. Cells were washed, left in 1X PBS and imaged using Hermes WiScan (IDEA Biomedical). The imaging system is able to view 10-40x pictures as well as quantify average intensity on a per-cell basis, eliminating any bias towards IF staining. Quantification of H3K4me2 marks was presented as a frequency distribution of the cell count population.

Cell viability/Cytotoxicity assay:

For the (3-(4,5-dimethylthiazol-2-yl)-5-(3-carboxymethoxyphenyl)-2-(4-sulfophenyl)-2H-tetrazolium) (MTS) reduction assay, 3×10^3 cells/well were seeded in 100µl medium in a 96-well plate and allowed to attach at 37°C in 5% CO₂ for one day. The medium was aspirated and cells were treated with 100µl of fresh medium containing appropriate dose-response concentrations of each test compound. The cells were incubated from 48-72hrs at 37°C in 5% CO₂. After, 20µL of the MTS reagent solution (Promega CellTiter 96 Aqueous One Solution Cell Proliferation Assay) was added to the medium. The cells were incubated for another 2 hours at 37°C. Absorbance was measured at 490 nm on a microplate reader equipped with SOFTmax PRO 4.0 software to determine the cell viability. Cell counts were confirmed by counting DAPI stained nuclei as previously mentioned.

Preparation of cell lysates:

Following treatment, cells were washed twice in sterile filtered cold 1× PBS. Cells were then lysed in 200 µl of lysis buffer (20 mM Tris, 150 mM NaCl, 1 mM EDTA, 1 mM EGTA, 1 mM β-glycerol, 2.5 mM sodium pyrophosphate, and 1% Triton X-100) Protease and phosphatase inhibitors were added to these buffers (1:100 dilutions of phosphatase inhibitor cocktail I and II and protease inhibitor cocktail; Sigma). The cells were then incubated on ice for 15 min, and insoluble material was pelleted by centrifugation at 4°C.

Western blot analysis:

Protein concentrations were determined by Pierce BCA protein assay kit (Thermo Sci, Product #23225). Cell lysates were subjected to SDS-PAGE, and Western blot analysis was performed with the appropriate antibodies. Primary antibodies against H3K4me2, H3K4me1, LSD1, GAPDH, p-p38, p-Akt and catalase were from Cell Signaling; Histone H3 primary antibody was from Millipore. Proteins were visualized by enhanced chemiluminescence (ECL).

Primary rat cardiomyocytes isolation:

Primary male Sprague-Dawley rat cardiomyocytes were isolated via a hanging heart preparation using enzymatic digestion, as previously described.¹³⁵⁻

¹³⁶ In brief, rats were euthanized with 5% isoflurane vaporized in 100% O₂. The heart was retrogradely perfused with collagenase. The cardiomyocytes were plated on 6-well culture trays that were coated with laminin at an initial plating

density of 1.5×10^5 cells/well. After overnight incubation, the cardiomyocytes were rinsed and maintained in serum-free medium.

Co-immunoprecipitation:

Primary rat cardiomyocytes were isolated as described earlier and treated with varying concentrations of test compounds. Cells were lysed and scraped with IP Lysis Buffer (20mM Tris-Cl, 150mM NaCl, 1mM EDTA, 1mM EGTA, 1mM β -glycerol, 2.5mM Na pyrophosphate). Dynabeads (Life Biosciences) were added 1:10 beads:lysate (v/v) and incubated at 4°C for 1-hour to pre-clear. Mixture was centrifuged (5000rpm) and the supernatant was saved. An antibody (2-5 μ g) for the protein of interest was added and rocked overnight in cold room. Dynabeads (20 μ L) were added and incubated at room temp for 1-hour. Centrifuge mixture for 1-minute at 5000rpm. The supernatant was decanted and the pellet washed 3X with IP Lysis Buffer with 0.1% Triton X-100. Samples were then analyzed by SDS-PAGE and immunoblotted.

III. PRECLINICAL TESTING – EX VIVO AND IN VIVO MODELS

Langendorff ex vivo retrograde perfusion isolated hanging heart model:

Male Sprague-Dawley rats (250-300g) were pretreated with test compound at an appropriate dosage determined from Specific Aim 2. For reference, *in vivo* literature on triazole compounds indicates 10mg/kg, *i.p.*, *QD*^{21,23} Hearts were isolated by Langendorff preparation (**Figure 2.1**). Rats were anesthetized with ketamine/xylazine (85/15mg/kg, *i.p.*). The trachea was

cannulated with a 16-gauge angiocatheter attached to a rodent ventilator. A midsternal thoracotomy was then performed to remove the heart. The aorta was cannulated *in situ* and perfused at a constant 75mmHg using Krebs-Henseleit buffer (1.25mM CaCl₂, 11mM glucose, 112mM NaCl, 25mM NaHCO₃, 5mM KCl, 1.2mM MgSO₄, 1mM K₂PO₄, and 0.2mM octanoic acid, bubbled with 95% O₂/5% CO₂, pH 7.4). Hearts were then perfused with buffer for 15min prior to 30-mins of global ischemia. Reperfusion was induced for 60min. A saline-filled balloon fixed to a pressure transducer inflated to 5-10mmHg in the LV measured contractile function. Pain and suffering was minimized in these models via use of anesthesia and analgesia. Anesthetic depth was monitored by loss of blink reflex and loss of response to pain by toe-pinch.

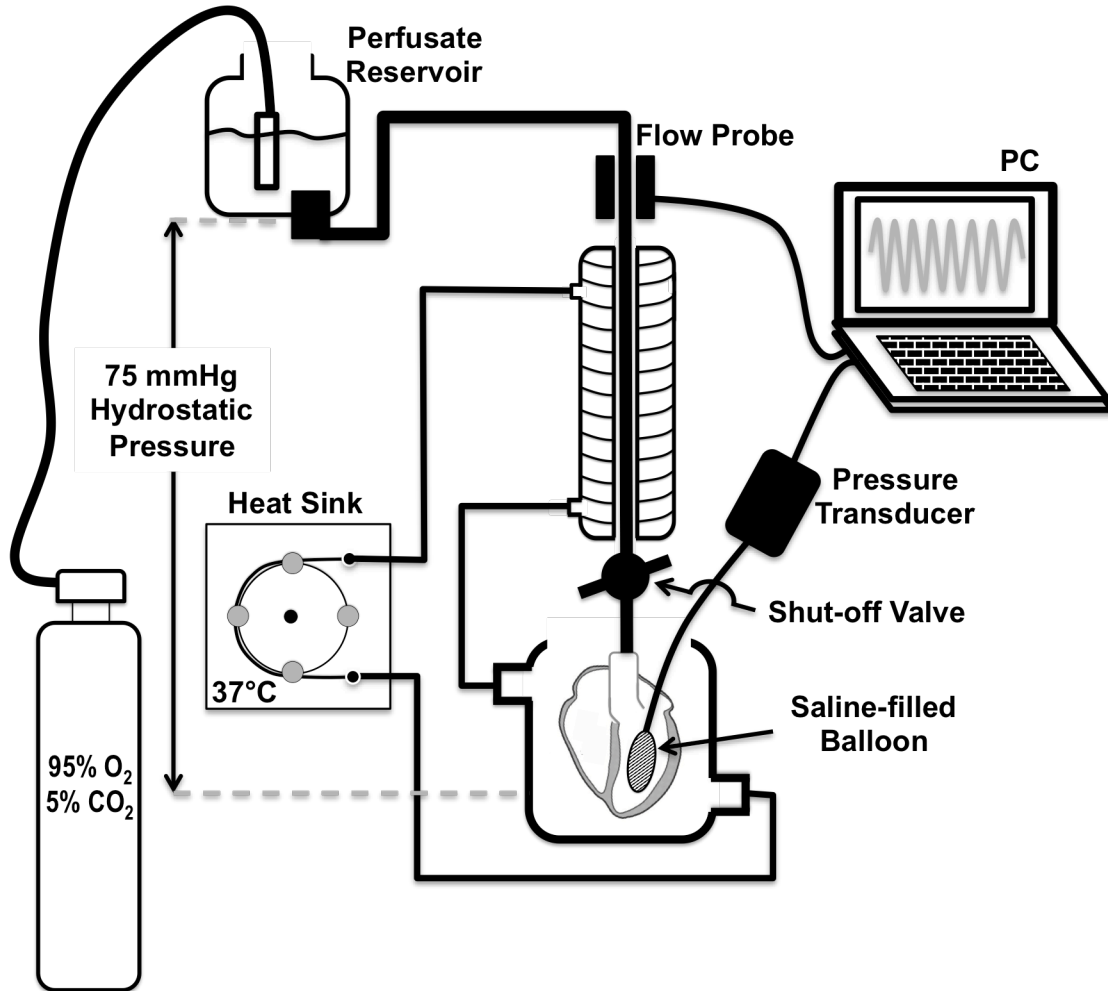


Figure 2.1. Langendorff *ex vivo* isolated heart retrograde perfusion apparatus. Male Sprague-Dawley rats were cared for in accordance to the guidelines of the Institutional Animal Care and Use Committee. They were anesthetized with (in mg per kg) 85 ketamine/15 xylazine. Tracheal ventilation was followed by translateral thoracotomy to expose the aorta, which will be cannulated *in situ*. The heart was rapidly excised to external perfusion with modified Krebs-Henseleit buffer heated to 37.4 °C and bubbled with (in %) 95/5 oxygen/carbon dioxide. Coronary flow was measured using a Doppler-type flow meter (Transonic Systems Inc., Ithaca, NY) and left ventricular contractile function was monitored via insertion of a saline-filled balloon connected to a pressure transducer (AD Instruments, Colorado Springs, CO). Hearts were perfused with buffer for 15 min before induction of global ischemia through complete cessation of perfusion for 30 min. Reperfusion was then induced for 60 min through restoration of normal perfusion with oxygenated buffer at 75 mm Hg perfusion pressure.

Infarct area staining by 2,3,5-triphenyltetrazolium chloride (TTC):

After Langendorff preparation, hearts were frozen at -80°C. A transverse sectioned into 2-mm slices was performed and incubated in 1% 2,3,5-triphenyltetrazolium chloride (TTC) at 37 °C for 10 min. Quantification of infarct area will be performed using ImageJ software (National Institutes of Health, USA, <http://imagej.nih.gov/ij>). Infarct size was reported as a percent of the total left ventricular area.

Left anterior descending coronary ligation-reperfusion *in vivo* IR:

Male CD1 mice (25-35g) underwent *in vivo* left anterior descending (LAD) coronary artery ligation-reperfusion as previously performed and described.¹³⁷ In short, the LAD was ligated with 6-0 silk suture and PE-10 tubing for 40-min prior to reperfusion. Compound **9** (3 mg/kg) or GSK-LSD1 (0.5 mg/kg) was injected intraperitoneal immediately following ligation and again once daily for 7-days. Echocardiographic determinations of LV volumes and ejection fractions was performed with a 15-MHz transducer (Sonos 5500; Agilent Technologies, Andover, MA, USA) placed on the hemithorax. Briefly, the parasternal long-axis view of the LV was recorded. LV volumes were determined by planimetry of the LV endocardial border at end diastole (frame with R wave) and end systole (smallest LV area in the cardiac cycle) and application of a variant of Simpson's algorithm (i.e. "method of disks"). The thoracic area was shaved and the heart removed via a midline sternotomy. Euthanasia occurred via exsanguination. All animals were placed under full surgical anesthesia for heart harvesting. Mice

were cared for in accordance to the guidelines of the Institutional Animal Care and Use Committee. Male CD1 mice were anesthetized by 3% isoflurane vaporized in 100% O₂. The experiment was repeated using the positive control, GSK-LSD1 (0.5 mg/kg, *i.p.*).

IV. DATA ANALYSIS AND STATISTICS. Power analyses was performed using a one-way analysis of variance model to determine sample size for each experiment in this application. All data was presented as mean \pm SEM. Significant differences within group comparison between baseline and terminal studies in any parameter were tested using unpaired t-test corrected for multiple comparisons using the Bonferroni method. Unless stated otherwise, $\alpha = 0.05$ and $\beta = 0.80$. The sample sizes for each experiment was listed under individual figure legends.

V. ETHICAL ASPECTS OF RESEARCH AND ANIMAL CARE

The ethical aspects of this research are limited to animal models. All of the animal work performed for this research was performed under approved animal protocols at the Medical University of South Carolina and the Ralph H. Johnson VA Medical Center. All experimental protocols conformed to the Guide for the Care and Use of Laboratory Animals published by the US NIH.

Rats were housed and cared for by the Division of Laboratory Animal Resources under the direction of Alison C. Smith, D.V.M., a diplomate of ACLAM. An assurance statement is on file with OPRR/DHHS detailing the

program for animal care at this institution, which has full accreditation from AAALAC effective 11/5/87. Trained AALAS-certified technicians cared and fed the animals including monitoring the health of animals on a routine basis. Several veterinarian consultants were available for animal care. All procedures involving rats were done in accordance with the *NIH Guide for the Care and Use of Laboratory Animals*.

Pain and suffering was minimized in these models via use of anesthesia and analgesia. Rats were anesthetized via ketamine/ xylazine (85/15 mg/kg). Anesthetic depth was monitored by loss of blink reflex and loss of response to pain by toe-pinch. The thoracic area was shaved and the heart removed via a midline sternotomy. Euthanasia occurred via exsanguination. All animals were placed under full surgical anesthesia for heart harvesting.

All rats were humanely euthanized in accordance with accepted IACUC protocol. Euthanasia was accomplished via exsanguination following removal of the heart. This procedure was performed under full surgical anesthesia. This method is consistent with the recommendations of the American Veterinary Medical Association Guidelines on Euthanasia.

CHAPTER 3: Structure-based discovery of small molecule LSD1 inhibitors

I. INTRODUCTION

To date, effective LSD1 inhibitors include tranylcypromine-based analogues¹³⁸⁻¹⁴¹ such as **2**, oligoamines such as verlindamycin **5**,¹⁴² related isosteric ureas and thioureas,¹⁴³⁻¹⁴⁴ and peptide based LSD1 inhibitors such as **6**.¹⁴⁵⁻¹⁴⁶ However, it is the tranylcypromine related analogues that have garnered the most attention. The tranylcypromine scaffolds are the most advanced chemical class with respect to drug development, and the first clinical trial for a tranylcypromine-based LSD1 inhibitor for treatment of acute myeloid leukemia began earlier this year.¹⁴⁷ TCP is a moderately potent, irreversible inhibitor of LSD1. However, it is challenging to design a TCP-based LSD1 inhibitor for clinical use that is specific, has low toxicity, and is devoid of the many biological responses to TCP itself. Thus, these analogues have the potential to produce off-target effects mediated through other flavin-dependent amine oxidase enzymes.¹⁴⁸ In addition, covalent compounds, such as these, are less desirable as clinical therapeutics than reversible ones. As such, there is a continuing need to identify novel small-molecule scaffolds for inhibitors of LSD1 that can be used to design highly specific, reversible LSD1 inhibitors. This chapter focuses on *de novo* identification, screening, synthesis, and *in vitro* characterization of novel small molecule LSD1 inhibitors. Herein, we describe a novel scaffold for a new series of reversible, competitive inhibitors of LSD1 using a 3,5-diamino-1,2,4-triazole scaffold.

Potential new scaffolds for small molecule LSD1 inhibitors were identified through a virtual screen of the Maybridge Hitfinder 5 compound library. This

virtual library consists of 50,000 compounds with high chemical diversity for rapid lead identification. Based on the lowest energy conformers to the crystal structure of LSD1/CoREST (PDB 2V1D), we were able to identify 10 potential leads. From this short list, we selected our initial parent compound based on chemical moieties and ease of synthesis. After screening 15-analogous compounds for LSD1 inhibition at 10 μ M, we selected compounds **9** and **10** for further evaluation. In addition, a synthesis for a small chemical library of 3,5-diamino-1,2,4-triazolamine structures was performed by an aminolysis of dimethyl-N-cyanodithiocarbamate followed by cyclization of the obtained N-cyano-S-methylisothiurea with hydrazine.

The results in this chapter disclose one of the first small molecule, reversible, competitive LSD1 inhibitors that is active at low micromolar concentrations. Therefore, the compounds covered show significant characteristics desirable as clinical therapeutics. **Figure 3.1** shows a workflow diagram of results covered in this chapter.

Goals of Chapter 3:

- 1.) *Perform computational, structure-based virtual screen to identify high affinity ligands*
- 2.) *High-throughput screening for lead identification*
- 3.) *Synthesis of small, focused chemical library*
- 4.) *Evaluate in vitro efficacy against LSD1*

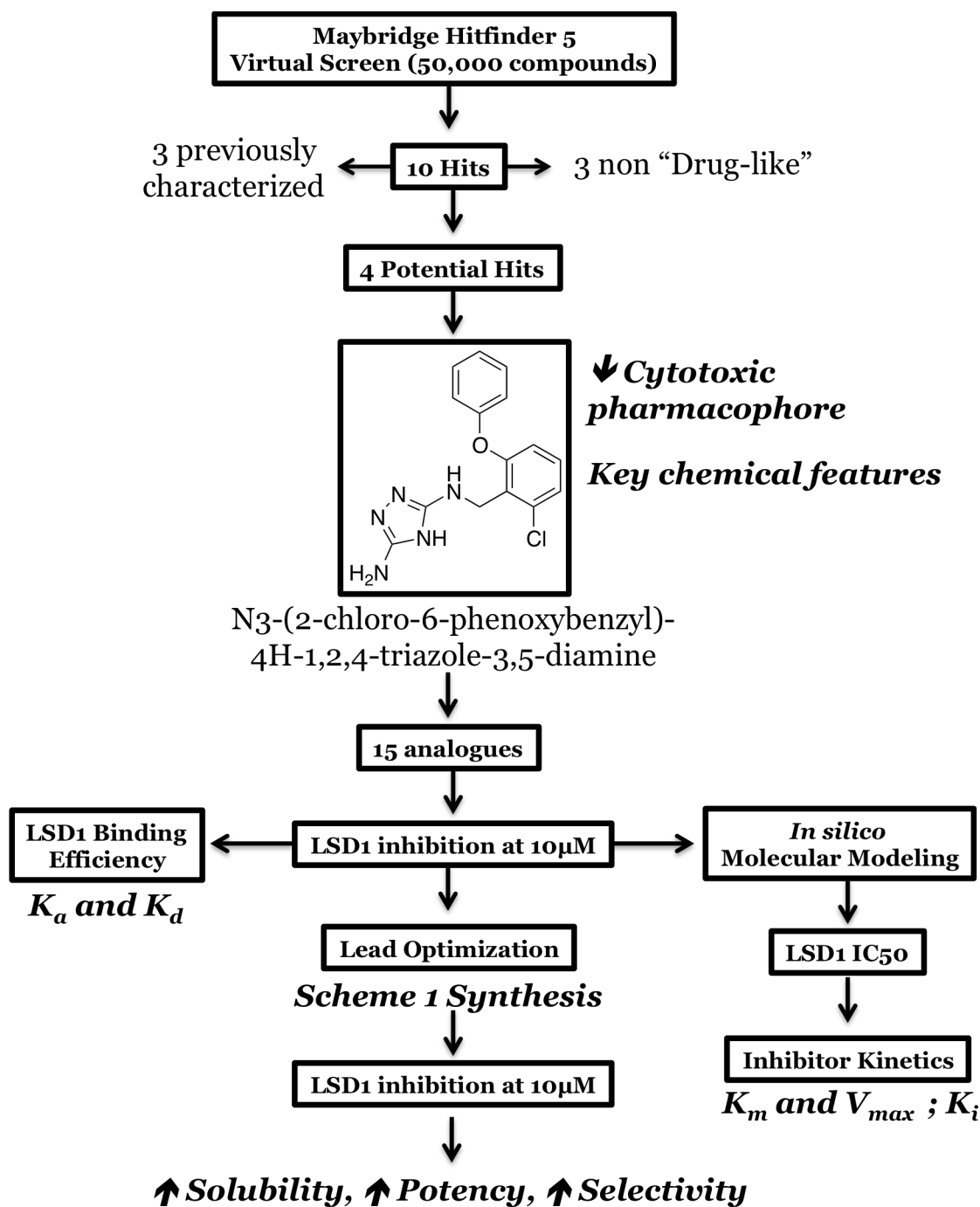


Figure 3.1. Chapter 3 workflow chart and structure-based drug design of novel LSD1 inhibitors. Early de novo drug design from a virtual screen to drug synthesis to lead optimization.

II. RESULTS

Virtual screen for novel LSD1 inhibitors:

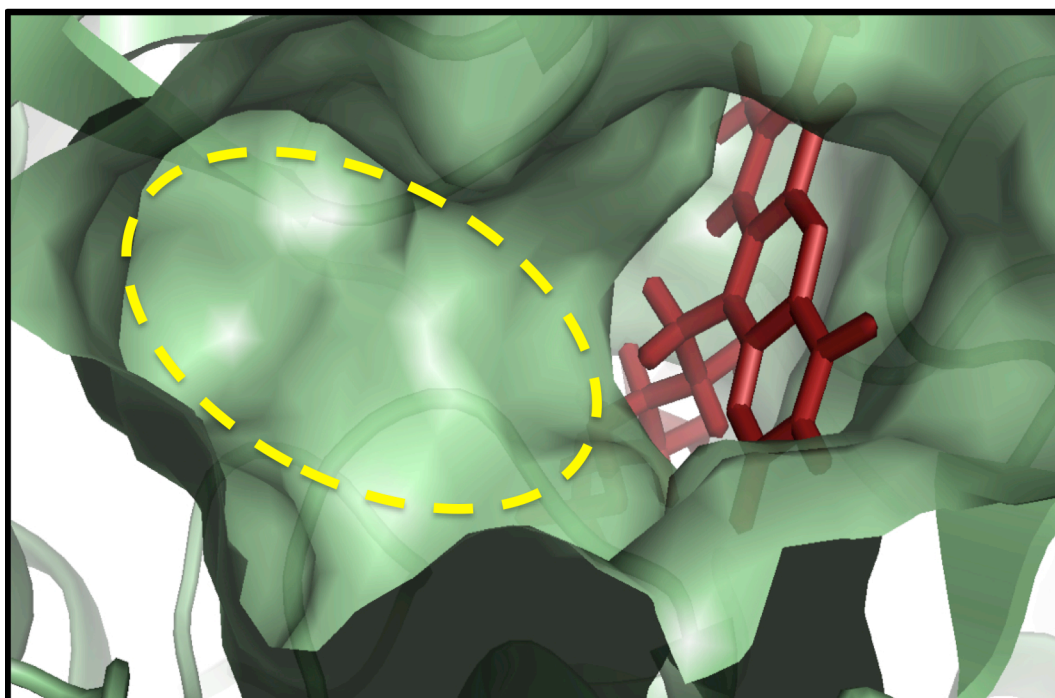
Potential new scaffolds for small-molecule LSD1 inhibitors were identified through a virtual screen of the Maybridge Hitfinder 5 compound library, as previously described. The crystal structure of LSD1/CoREST (PDB 2V1D) was prepared using PrepWizard, and SiteMap was then used to assess efficient binding within the LSD1 histone-binding pocket (**Figure 3.2**). The active site features a hydrophilic pocket near an FAD cofactor, with a large hydrophobic region nearby. Lowest energy conformers of 3D compounds were determined and docked in the LSD1 active site using Glide. A total of 10 hits were identified with Glide scores lower than -7.5 kcal/mol (compounds not shown). The synthesis and biological evaluation of other lead compounds identified in this screen have been previously published.¹⁴⁹ The 3,5-diamino-1,2,4-triazole **9** was chosen as a potential high affinity ligand for LSD1 efficacy because it featured an appropriately positioned hydrophobic aromatic ring and significant H-bonding donors and acceptors within the triazole ring.

A.

Lipinski Rule	Maybridge Compound Collection
< 5 H-bond Donors	99.7% are less than 5
<10 H-bond Acceptors	99.8% are less than 10
cLog P <5	mean cLogP = 3.23 (-0.11 to 6.3)
Molecular Weight <500	mean MW = 325, 95% range 150-500

Adapted from Maybridge HitFinder Collection website

B.



Hydrophobic Pocket

FAD Cofactor

Figure 3.2. Virtual screen of Maybridge HitFinder library against LSD1/CoREST (PDB 2V1D). (A) Maybridge HitFinder was used because their virtual library contains a very high percentage of “druggable” compounds that conform to Lipinski’s guidelines for successful therapeutic agents. (B) The LSD1 active site (green) contains a large hydrophobic pocket (dotted yellow) in close proximity to the FAD cofactor (red).

In silico molecular docking and predicted catalytic binding affinity:

Compounds that bind in close proximity to the FAD cofactor within the active site of LSD1 typically show greater potency towards the enzyme. Therefore, *in silico* molecular modeling (GOLD software package, version 5.1, Cambridge Crystallographic Data Center, Cambridge, UK) was performed to predict key residues interacting with **9** (**Figure 3.3**) and **10** (data not shown). The LSD1 active site (PDB #3ZMT, LSD1-CoREST in complex with a peptide with the sequence PRSFLV) was defined as a sphere enclosing residues within 10Å around the bound peptide ligand. Prior to energy minimization, protein residues were protonated and the pH was adjusted to 7.4. Initial screens focused on using the PRSFLV peptide for defining potential key interaction sites. The 3D inhibitor structures were energy minimized using the MM94x force field using 1000 iterations and a convergence value of 0.001 kcal/mol/Å as the termination criteria. Initial docking results yielded 60 poses of each structure bound in the active site of LSD1. The top 5 poses that yielded the lowest E-score were chosen for further analysis. The best fit for binding was analyzed for interacting residues. Key interactions with **9** include two hydrogen bonds with aspartate 555 and another hydrogen bond with the carbonyl of alanine 539. In addition, the compound participates in pi-stacking with the flavin ring of the FAD cofactor within 2.98Å. Thus, **9** shows close association with the active site and effectively prohibits substrate binding. A 2-dimensional rendition of the binding of **9** to LSD1/CoREST is also shown in **Figure 3.3**.

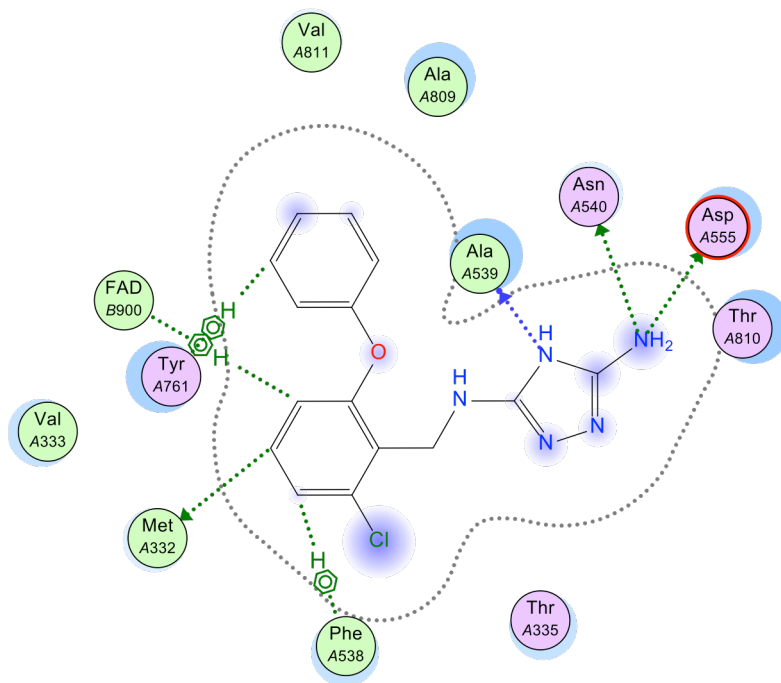
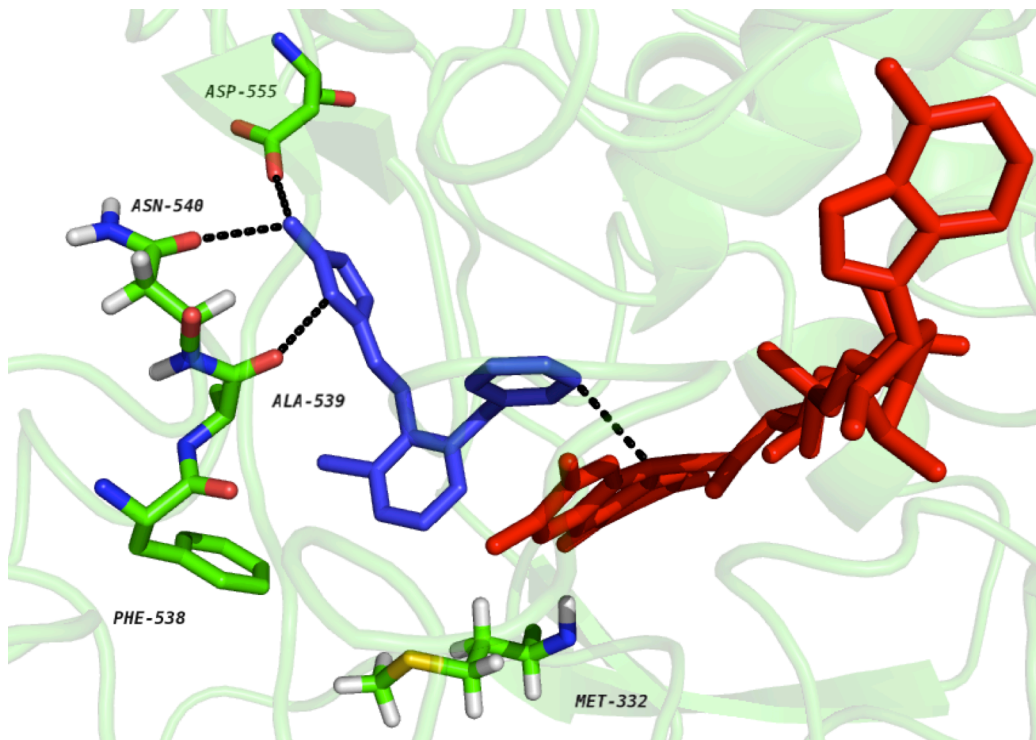


Figure 3.3. Molecular docking of compound 9. *In silico* analysis in the LSD1/CoREST catalytic site (PDB file 3ZMT). The aromatic portion of the o-phenoxy substituent lies 2.98Å from the FAD cofactor.

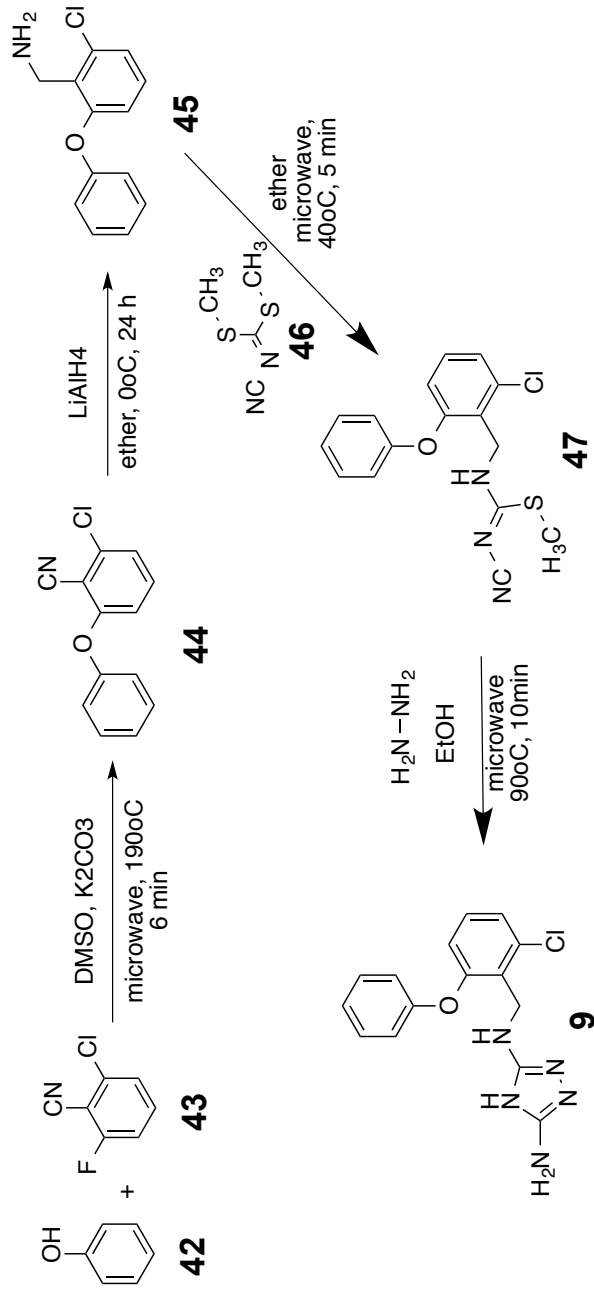
In vitro activity against recombinant LSD1/CoREST:

In the present study, one hit from the virtual screen, **9**, was identified, and this compound, as well as related analogues **10** and **13-25**, were purchased and evaluated (**Table 3.1**). The ability of compounds **9-25** to inhibit purified recombinant LSD1 was measured using a commercially available fluorescence-based assay kit (Cayman Chemicals #700120). Initially, all compounds were tested at a concentration of 10 μ M in phosphate-buffered saline (PBS) containing <1% DMSO (**Figure 3.4A**). The screen was performed as suggested by the supplier and modified as previously described.^{143, 149} Compounds **9** and **10** were the most effective inhibitors of LSD1 (%LSD1 activity remaining 15.1 ± 4.7 and 25.1 ± 1.9 , respectively). For comparison, tranilcypromine (**2**) and **5** reduced LSD1 activity to 72.6 and 15.8%, respectively. Compounds **9** and **10** were then subjected to titration analysis to determine the *in vitro* IC₅₀ of each compound against LSD1 (**Figure 3.4 B** and **C**). Compound **9** possessed an IC₅₀ value of 1.19 μ M while compound **10** had an IC₅₀ value of 2.22 μ M.

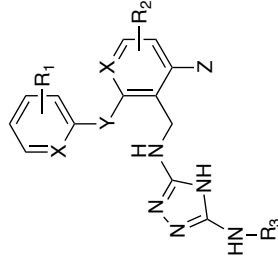
Synthesis of 3,5- diaminotriazole analogues:

In order to produce additional analogues in the 3,5-diaminotriazole library, a synthesis of **9** was developed as shown in **Scheme 1**. Condensation of phenol **42** and 2-cyano-3-chlorofluorobenzene **43** (K_2CO_3 , microwave, $190^\circ C$, 6 min) resulted in the phenoxyphenyl intermediate **44**. The cyano group in compound **44** was then reduced ($LiAlH_4$) to afford primary amine **45**, which was reacted with **46** (microwave, $40^\circ C$, 5 min) to yield **47**. Intermediate **48** was then treated with hydrazine (microwave, $90^\circ C$, 10 min) to produce the desired 3,5-diaminotriazole **9**. This route was used to synthesize the previously unreported 3,5-diaminotriazoles of **general structure 1**, compounds **26-41** (**Table 3.2**). Each compound was evaluated as an inhibitor of recombinant LSD1 as described above at a concentration of $10\ \mu M$ (**Figure 3.5**). Seven compounds (**9, 10, 31, 34, 36, 37** and **38**) were more effective LSD1 inhibitors at $10\ \mu M$ than the known LSD1 inhibitor **5**, while 11 of the 16 compounds measured inhibited LSD1 by 50% or more. Compounds **36** and **38**, which have LSD1 inhibitory activity comparable to **9**, demonstrate additional functional groups that will drive future chemical manipulation (see "**IV. Limitations and Future Directions**").

Scheme 1



General Structure 1



R_1, R_2 and $R_3 = \text{H, alkyl, aralkyl, alkyloxy, aralkyloxy, aralkyl, aralkyloxy, aryl, aralkyloxy}$

$X, Y = \text{C, N, S, O}$

$Z = \text{H, halogen, alkyl, aralkyl, alkyloxy, aralkyloxy, aralkyl, aralkyloxy, aryl, aralkyloxy}$

Table 3.1. Structures, cLogP and LSD1 inhibitory activity for 3,5-diaminotriazoles **9-25**. Activity mean \pm SEM (n=3)

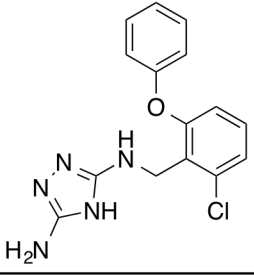
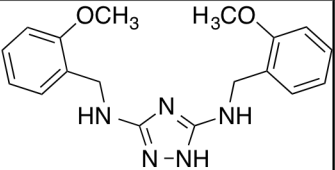
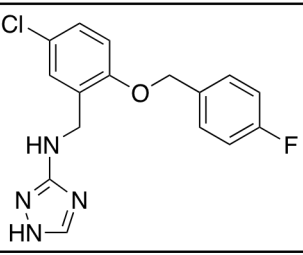
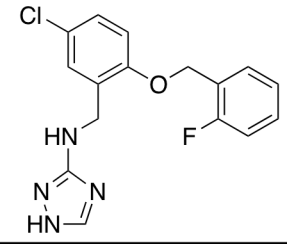
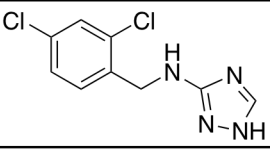
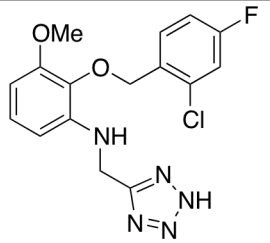
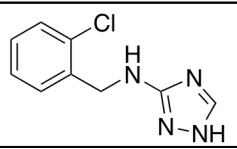
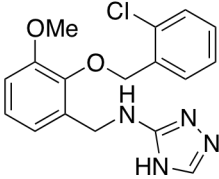
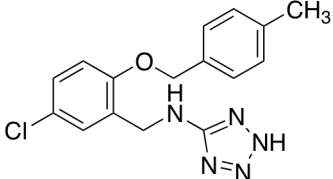
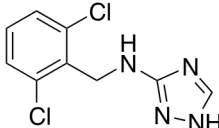
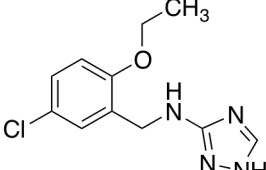
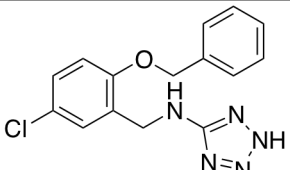
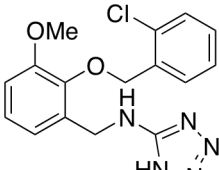
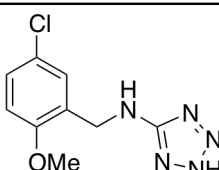
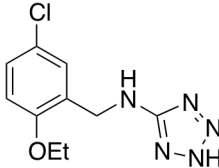
Structure	Compound	MW	cLogP	% Activity LSD1 at 10 μ M
	9	315.76	4.44	15.1 \pm 4.7
	10	339.39	3.58	25.1 \pm 1.9
	13	332.76	4.46	72.3 \pm 9.0
	14	332.76	4.46	69.4 \pm 6.4
	15	243.09	3.21	97.8 \pm 6.9
	16	363.77	2.90	103.1 \pm 7.8
	17	208.65	2.49	95.4 \pm 6.9

Table 3.1 (continued). Structures, cLogP and LSD1 inhibitory activity for 3,5-diaminotriazoles **9-25**. Activity mean \pm SEM (n=3)

Structure	Compound	MW	cLogP	% Activity LSD1 at 10 μ M
	18	344.80	3.648	81.9 \pm 8.2
	19	329.78	3.53	93.1 \pm 7.5
	20	243.09	3.21	69.1 \pm 7.7
	21	252.70	3.08	103 \pm 12.7
	22	315.76	3.03	80.1 \pm 8.4
	23	345.78	2.62	77.9 \pm 7.3
	24	239.66	1.27	69.2 \pm 5.7
	25	253.69	1.795	79.2 \pm 5.0

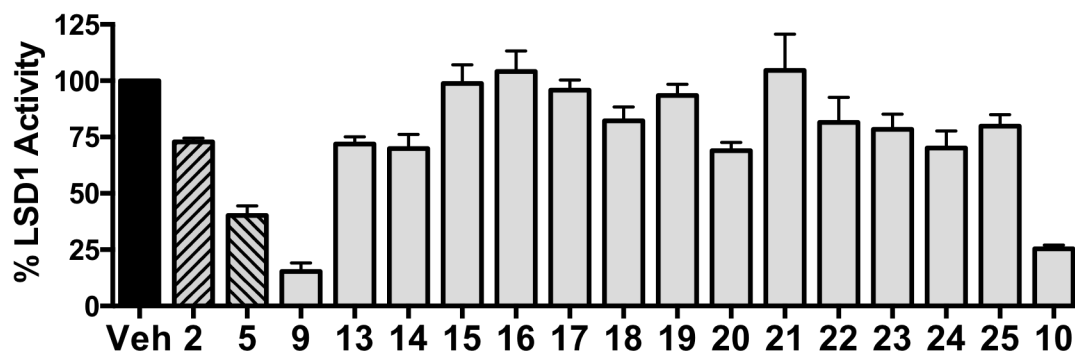
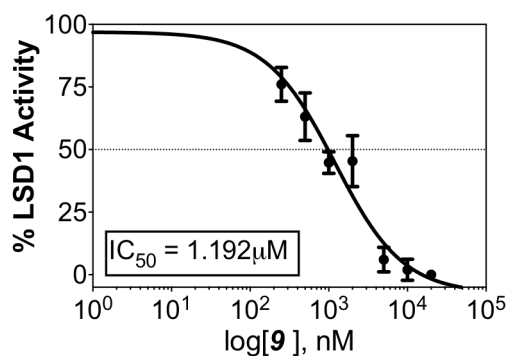
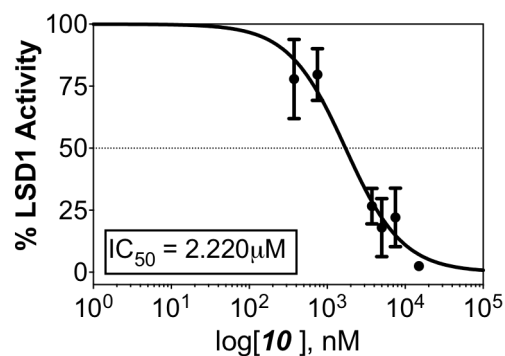
A.**Screen of Novel LSD1 Inhibition****B.****C.**

Figure 3.4. Initial LSD1 inhibition assay. (A) Percent LSD1 activity remaining after 10 μM treatment with 3,5-diamino-1,2,4-triazolamine **9** and chemically similar **10-25**. Positive control compounds verlindamycin, **5**, and tranlycypromine, **2**, showed similar inhibition at 10 μM as previously described. Dose-response of LSD1 following treatment with compounds **9** (B) and **10** (C). Compound **9** $\text{IC}_{50} = 1.19 \mu\text{M}$; compound **10** $\text{IC}_{50} = 2.22 \mu\text{M}$.

Table 3.2. Structures and LSD1 activity of compounds from Scheme 1

Compound	X	R ₁	R ₂	R ₃	R ₄	Residual % LSD1 Activity ([I] 10 μ M)
2	-	-	-	-	-	64.2 \pm 6.1
5	-	-	-	-	-	33.9 \pm 6.7
9	O	H	H	H	H	15.1 \pm 4.7
10	-	-	-	-	-	25.1 \pm 1.9
26	O	H	H	-OCF ₃	H	61.4 \pm 5.6
27	O	H	H	-CH ₃	H	40.7 \pm 6.1
28	O	-CH(CH ₃) ₂	H	H	-CH ₃	43.7 \pm 3.2
29	O	H	-OCH ₃	H	H	55.4 \pm 5.1
30	O	H	H	-C(CH ₃) ₃	H	41.8 \pm 8.8
31	O	H	-CH ₃	H	-CH ₃	32.1 \pm 8.8
32	O	H	-CF ₃	H	-CF ₃	55.1 \pm 4.6
33	O	H	H	-SCF ₃	H	Insoluble
34	O	-CF ₃	H	-Br	H	32.2 \pm 5.4
35	O	H	H	-SCH ₃	H	Insoluble
36	O	-OCH ₃	H	-CH ₃	H	15.3 \pm 3.2
37	O	H	-OCH ₃	H	-OCH ₃	36.7 \pm 8.6
38	O	-CH ₃	-CH ₃	H	H	19.4 \pm 1.9
39	O	H	Methylene dioxy	H	H	34.2 \pm 6.4
40	S	H	H	H	H	39.2 \pm 7.9
41	S	H	-OCH ₃	-OCH ₃	H	46.8 \pm 7.4

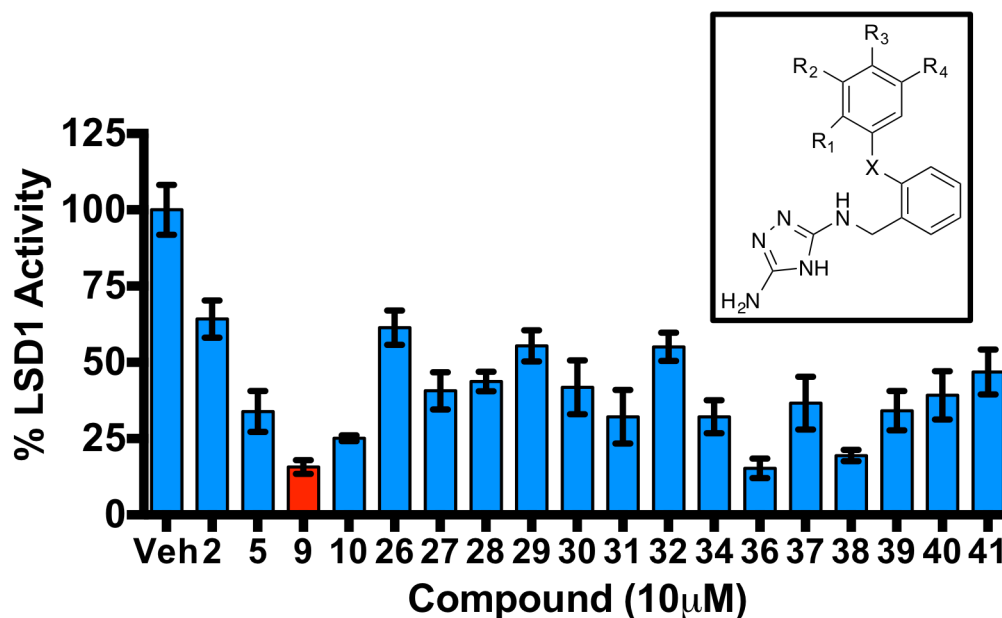
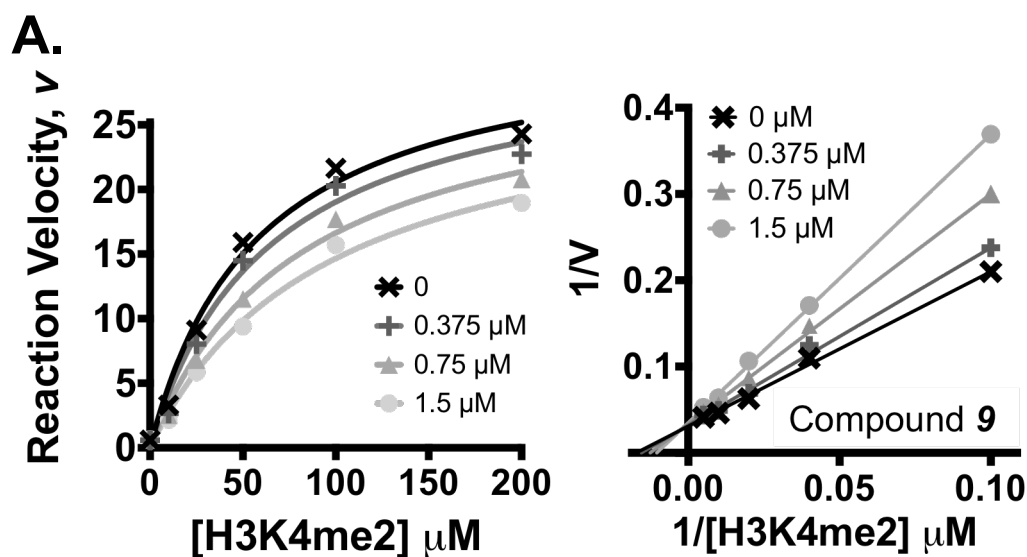


Figure 3.5. LSD1 inhibition assay of synthesized compounds. Residual LSD1 activity remaining after treatment with 3,5-diamino-1,2,4-triazoles derivatives 6, 10, 26-41 at 10 μ M. Positive control compounds verindamycin, 5, and tranlycypromine, 2. Each data point is the average of 3 determinations \pm SEM (see above Table 3.2).

Compound 9 is a reversible, competitive inhibitor of LSD1

The fluorescence-based assay method described above was then used to determine Michaelis-Menten kinetics for **9**, as shown in **Figure 3.6A**. In brief, compound **9** was incubated at 0, 0.375, 0.75 and 1.0 μM for 30 mins with 15 ng/ μL of LSD1 at 37 $^{\circ}\text{C}$ prior to addition of increasing amounts of the H3K4me2 peptide substrate (concentrations between 0 and 100 μM). Initial rates were determined by linear least-squares fit, and K_m and V_{max} values were determined using the GraphPad Prism 6 software package. The V_{max} remained constant (30.62 ± 0.8 unit/min) indicating competitive inhibition, and the K_i for **9** was determined to be 2.20 μM (**Figure 3.6B**).

To assure that 3,5-diaminotriazoles were bound to LSD1 with 1:1 stoichiometry, nanoisothermal titration calorimetry (TA Instruments Nano ITC) was performed (**Figure 3.7**) using **9** and purified LSD1 (Enzo Life Sciences, #BML-SE544-0050). The isotherm was generated by titrating 2 μL injections of a 1 μM solution of **9** into a 500 nM solution of recombinant LSD1 at 25 $^{\circ}\text{C}$. Titration of **9** to LSD1 resulted in an independent binding isotherm signifying significant heat release on binding of **9** to LSD1. The R^2 of heat released and the molar ratio was found to be 0.96. The resulting isotherm clearly shows that **9** and LSD1 bind with a 1:1 stoichiometry with a $K_a = 48.89 \text{ nM}^{-1}$ and 0.02nM K_d (calculated by the ITC system software).



B.

Substrate [S], μM	V_{max}	K_m
0	32.54 ± 2.6	58.34 ± 11.7
0.375	31.29 ± 2.9	64.42 ± 14.8
0.75	29.87 ± 2.3	79.61 ± 13.8
1.5	28.76 ± 2.5	96.22 ± 17.9

Figure 3.6. LSD1 enzyme kinetics show compound 9 as a competitive inhibitors. A fluorometric assay was used to evaluate kinetics. (A) Competitive enzyme inhibition kinetics for LSD1 treated with compound 9 at 0, 0.375, 0.75, and 1 μM concentrations over a range of substrate concentrations between 0 and 100 mM; K_i for 9 = 2.2 μM . (B) Table showing the values of V_{max} and K_m for enzyme kinetics.

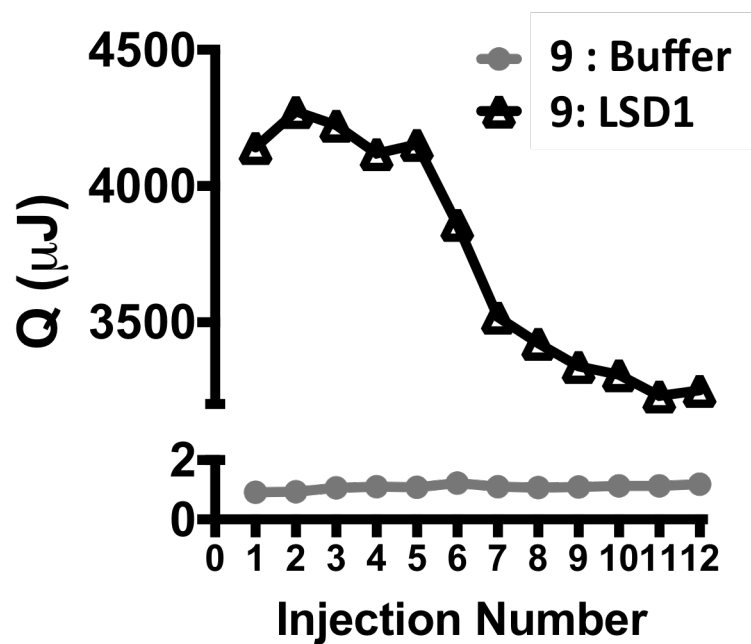


Figure 3.7. Thermal biomolecular binding of compound 9 to LSD1. Isothermal calorimetry (ITC) was performed using a Nano-ITC (TA Instruments). The thermal trace for LSD1 showed a exothermic release of heat upon titration with compound 9. $K_a = 48.89 \text{ nM}$, $R^2=0.96$.

III. DISCUSSION

Newly identified roles for epigenetic modulation mediated by LSD1 continue to emerge, both in cancer and in other disease states. Thus, LSD1 has become a promising target for therapeutic intervention. While the design of irreversible LSD1 inhibitors has been fundamental in the biological evaluation of LSD1, reversible inhibitor development has been less successful. The tranylcypromine-based irreversible inhibitors are the most advanced chemical class with respect to drug development and many successful LSD1 inhibitors are derived from tranylcypromine scaffolds. However, these irreversible inhibitors all require activation and/or covalent attachment to the FAD cofactor for inhibition of LSD1. Therefore, it is challenging to design selective LSD1 inhibitors that do not show off-target effects mediated through other flavin-dependent enzymes.¹⁴⁸ As such, there is a continuing need to identify novel small-molecule scaffolds for inhibitors of LSD1 that can be used to design highly specific LSD1 inhibitors. The 3,5-diamino-1,2,4-triazole motif described in this chapter could be used as such a scaffold, and the results described above support the contention that potent, non-toxic LSD1-specific inhibitors can be designed in this chemical class.

We successfully identified a new 3,5-diamino-1,2,4-triazole scaffold using computational chemistry. A virtual screen was performed with the Maybridge HitFinder 50,000 compound library, which revealed structurally distinct drug-like compounds as potential leads. Interestingly, compounds with primary amines, hydrophobic electron withdrawing groups, and heterocycloalkyl groups were well represented in our computational analysis. Of the 10 identified through selection

criteria discussed earlier, 1 compound (and 14 chemically similar compounds) were procured and screened in a recombinant LSD1/CoREST biochemical assay. Two novel compounds, **9** and **10**, were active with $IC_{50}(\text{LSD1}) < 2 \mu\text{M}$. The docking interactions of **9** include two hydrogen bonds with aspartate 555 and another hydrogen bond with the carbonyl of alanine 539. In addition, the compound participates in pi-stacking with the flavin ring of the FAD cofactor within 2.98Å (**Figure 3.3**). Thus, **9** shows close association with the active site and effectively prohibits substrate binding. This binding was confirmed by isothermal calorimetry. We then used enzyme kinetics to investigate the mechanism of action of compound **9** inhibition. Our calculated $K_m = 53.4 \pm 7 \mu\text{M}$ of the peptide was significantly higher than previously reported for a 21-mer H3K4me2 synthetic peptide. This may be attributed to the higher salt content in our reaction buffer, which is known to decrease affinity of the histone tail.¹⁵⁰

A synthetic route to produce analogues of **9** was developed, as shown in **Scheme 1**. Each newly synthesized compound was evaluated as an inhibitor of recombinant LSD1/CoREST as described above at a concentration of 10 μM (**Figure 3.5**). Six compounds (**9**, **10**, **31**, **34**, **36** and **38**) were more effective LSD1 inhibitors than the known LSD1 inhibitor **5**, while 11 of the 16 compounds measured inhibited LSD1 by 50% or more. Therefore, these results indicate a limited chemical library of **9** derivatives can be synthesized that is expected to contain multiple active compounds. We are continuing to synthesize analogues in this series for the purpose of refining a structure/activity model for 3,5-diamino-1,2,4-triazole-based LSD1 inhibitors.

IV. LIMITATIONS AND FUTURE DIRECTIONS

The LSD1 inhibitor screening assay is a fluorescence-based method for determining enzyme activity. During the first oxidative phase of demethylation, the reduced cofactor FAD reoxidizes to its functional form by molecular oxygen and releases H₂O₂ as a byproduct. The H₂O₂ reacts with 10-acetyl-3,7-dihydroxyphenoxazine (Amplex Red) to produce the highly fluorescent compound resorufin (Cayman Chemical, #700120). Therefore, our readout is an indirect measure of enzyme activity and may create variability in drug screens. An *in vitro* antibody-based assay with bulk histones and recombinant LSD1 can be used as an alternative, as previously described.¹⁵¹⁻¹⁵² In addition, kinetic Isothermal Titration Calorimetry (*kinITC*) can be used to obtain kinetics information, as well as k_{on} and k_{off} for experimental compounds.¹⁵³

Recently, using a similar synthesis to **Scheme 1**, we synthesized a series of new compounds with unique hydrophobic electron withdrawing groups. Two regioisomer derivatives, **M1** and **M2**, contain naphthalene-substituted phenols, and show very low nanomolar range IC₅₀ values for recombinant LSD1/CoREST (**Figure 3.8**). Thus, further biochemical evaluation of these highly potent LSD1 inhibitors is warranted. In addition, analogues containing functional groups designed to increase aqueous solubility are being synthesized.

Finally, a synthesis to generate compound **10** derivatives is also being generated, utilizing azide-alkyne cycloaddition click chemistry. Appropriate acetylenes and azides can be readily coupled using click chemistry in a single step (**Scheme 2**). Points for the introduction of chemically diverse substituents

where Z, R₁ and R₂ are any halogen, electron withdrawing group, alkyl group, aralkyl group, heteroalkyl or other substitution, and X and Z are carbon or heteroatoms such as S, N, O.

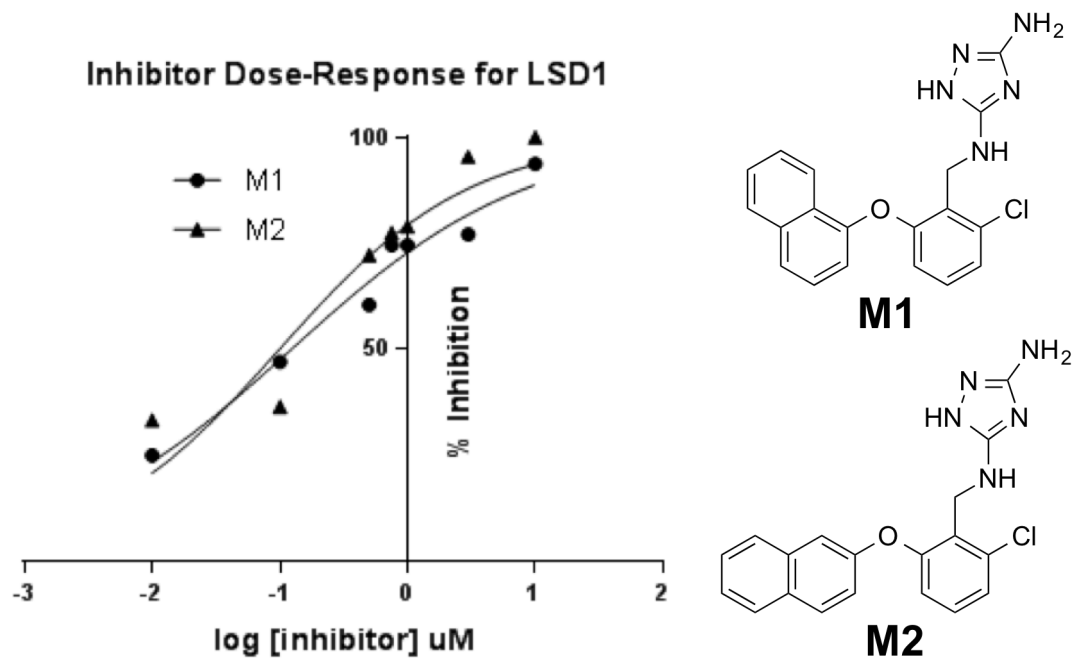
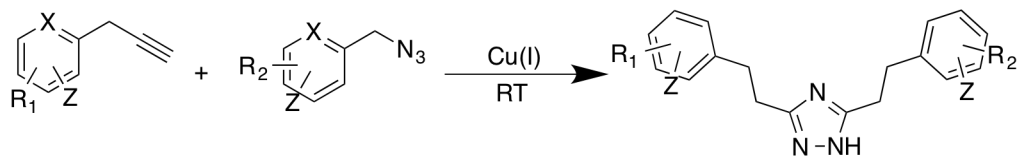


Figure 3.8. Lead optimization of compound 9 derivatives unveil novel compounds with improved potency. IC₅₀ values of new compounds show M1 (123 nM) and M2 (99 nM). Data credited to Mark Johnson, PhD.

Scheme 2.



Chapter 4: Assessment of selectivity, toxicity, and target validation of 3,5-diamino-1,2,4-triazoles.

I. INTRODUCTION

The amine oxidase family shows close sequence homology within their active sites and their catalytic mechanism. For this reason, selective inhibition of individual amine oxidases remains difficult. Many of the most successful inhibitors within the family show efficacy for other members and have been utilized as scaffolds for drug development. For instance, the most abundant class of effective LSD1 inhibitors is structurally based a nonspecific MAO inhibitor.¹⁵⁴ Therefore, this increases the potential for off-target effects mediated by other amine oxidases. More importantly, LSD1 inhibitors are being developed as antitumor agents, with the intent of cancer cell cytotoxicity. Because LSD1 biological function is better characterized within carcinogenesis and metastasis, the need for explicit toxic drugs has been a main focus in currently available compounds. In recent years, this paradigm has shifted with the emerging role of LSD1 in diseases other than cancer¹⁵⁵⁻¹⁵⁹, and as such, there is a need for potent epigenetic modulators that do not cause overt cytotoxicity.

Many LSD1 inhibitors show poor selectivity and *in vivo* toxicity, making it difficult to study the effects of specifically inhibiting LSD1.¹⁵⁴ Of the most potent and selective LSD1 inhibitors identified, the majority are based on the clinically used antidepressant tranylcypromine and were designed as cancer chemotoxicants.¹⁶⁰ Unfortunately, many tranylcypromine-based LSD1 inhibitors rely on covalent, irreversible adduct formation with FAD to inactivate the enzyme. For these reasons, current LSD1 inhibitors are undesirable as drug candidates for cardiovascular disease, where overt cytotoxicity and cell death is not a

desired endpoint. Thus, we have decided to pursue a new chemotype of reversible LSD1 inhibitors with increased potency, higher specificity, and reduced toxicity that are attractive drug candidates for cardiovascular disease.

This chapter focuses on the *in vitro* characterization of newly synthesized 3,5-diamino-1,2,4-triazole, **9** and **10**, for LSD1 selectivity, cellular cytotoxicity, and biological efficacy. First, the two lead compounds were screened against MAO-A, MAO-B, and spermine oxidase. Both **9** and **10** showed a selectivity index >100 for MAO-A and MAO-B. However, both 3,5-diamino-1,2,4-triazole derivatives showed significant potency for recombinant spermine oxidase (IC_{50} = 40-150 nM). Therefore, in our future cardiovascular studies using these compounds, we needed to dissect the individual roles of LSD1 and SMO. Thus, we screened a current SMO inhibitor, MDL 72527 (**11**), and a recent commercially available LSD1 inhibitor (**3**), for potency against both enzymes. Secondly, we screened our lead compounds for cytotoxicity in various cell lines and *in vivo* administration. In particular, we found that both **9** and **10** showed limited toxicity. Finally, both compounds were evaluated for their ability to increase histone methylation of H3K4, a known substrate of LSD1, and disrupt the LSD1/CoREST/HDAC corepressor complex in primary rat cardiomyocytes. **Figure 4.1** shows a workflow diagram of results covered in this chapter.

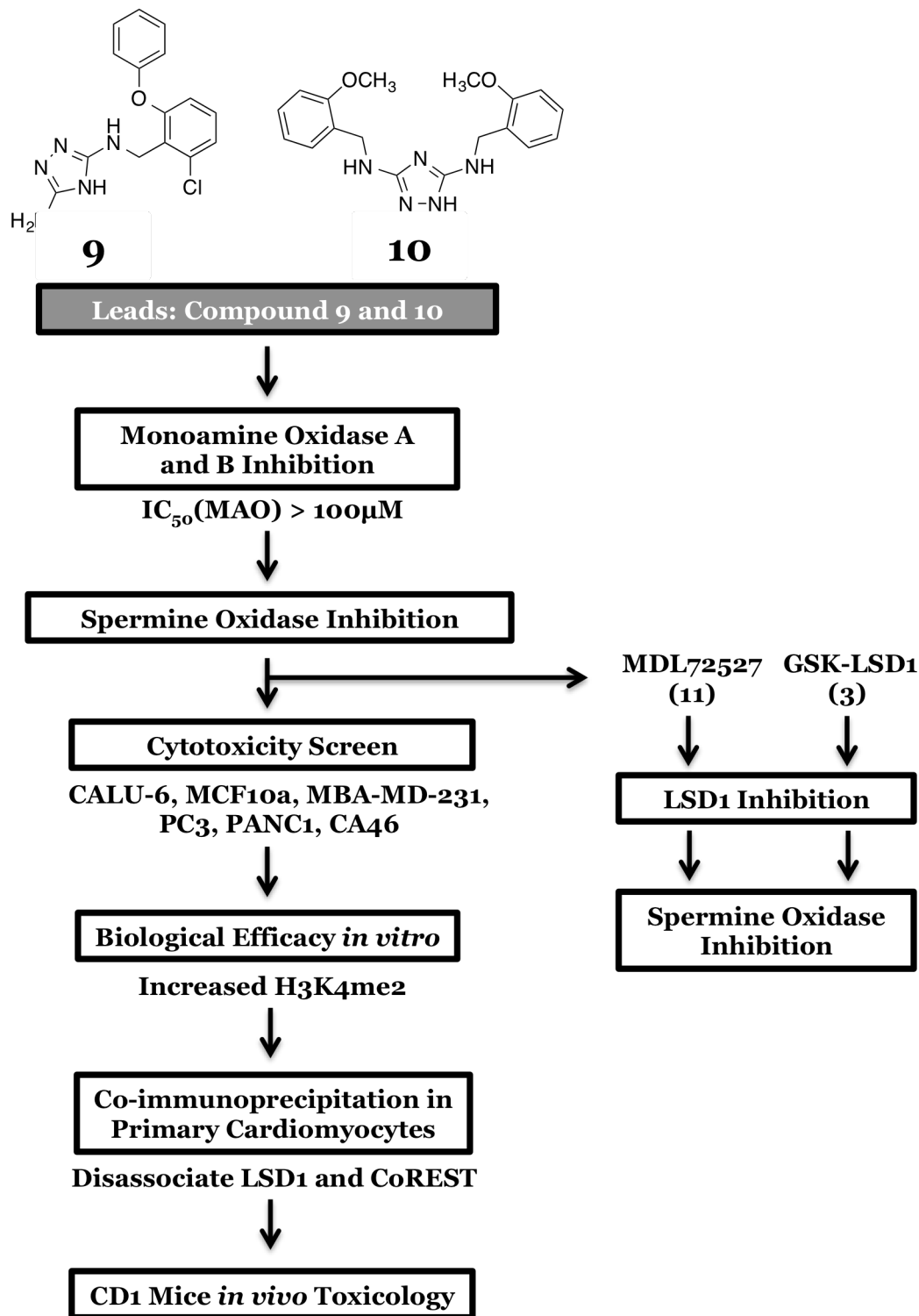


Figure 4.1. Chapter 4 workflow chart and *in vitro* characterization of two lead LSD1 inhibitors, 9 and 10. LSD1 selectivity, cytotoxicity, and biological efficacy will be evaluated.

GOALS FOR CHAPTER 4:

- 1.) *Determine MAO-A, MAO-B, and SMO IC₅₀ for both lead compounds*
- 2.) *Screen compounds **9** and **10** in six different cell lines and quantify toxicity IC₅₀*
- 3.) *Demonstrate compounds enter the cell and increase LSD1 substrate (H3K4me2)*
- 4.) *Show disruption of LSD1:CoREST:HDAC corepressor complex by inhibition of LSD1 in cardiomyocytes*
- 5.) *Perform an in vivo toxicology screen*

II. RESULTS

Selectivity of 3,5-diaminotriazoles – Monoamine Oxidases:

LSD1 and other amine oxidases, such as the monoamine oxidases (MAO), use the cofactor FAD to reoxidize molecular oxygen to produce H₂O₂. Tranylcypromine and derivatives often show significant off-target efficacy against MAO-A and MAO-B, and thus, are undesirable as clinical compounds. Therefore, it is crucial in the design of new LSD1 inhibitors to screen for efficacy against MAO-A and MAO-B. A commercial recombinant luminescent assay (Promega Corporation, #V1401) was performed as described by the manufacturer to assess the ability of 3,5-diaminotriazole **9** and **10** to inhibit MAO A and B isoforms. In short, Compounds **9** and **10** were titrated in 1% DMSO and incubated with MAO enzyme with a luminogenic MAO substrate and MAO-Glo™

reagent. MAO activity converts MAO-Glo™ to luciferin, which reacts with luciferase, and can be quantified by spectrophotometer. The amount of light produced is directly proportional to MAO activity. Compounds **9** and **10** both exhibited IC₅₀ values greater than 100 μM against both MAO isoforms, while tranylcypromine inhibited MAO A and B with IC₅₀ values of 4.2 μM and 5.8 μM, respectively (**Figure 4.2**).

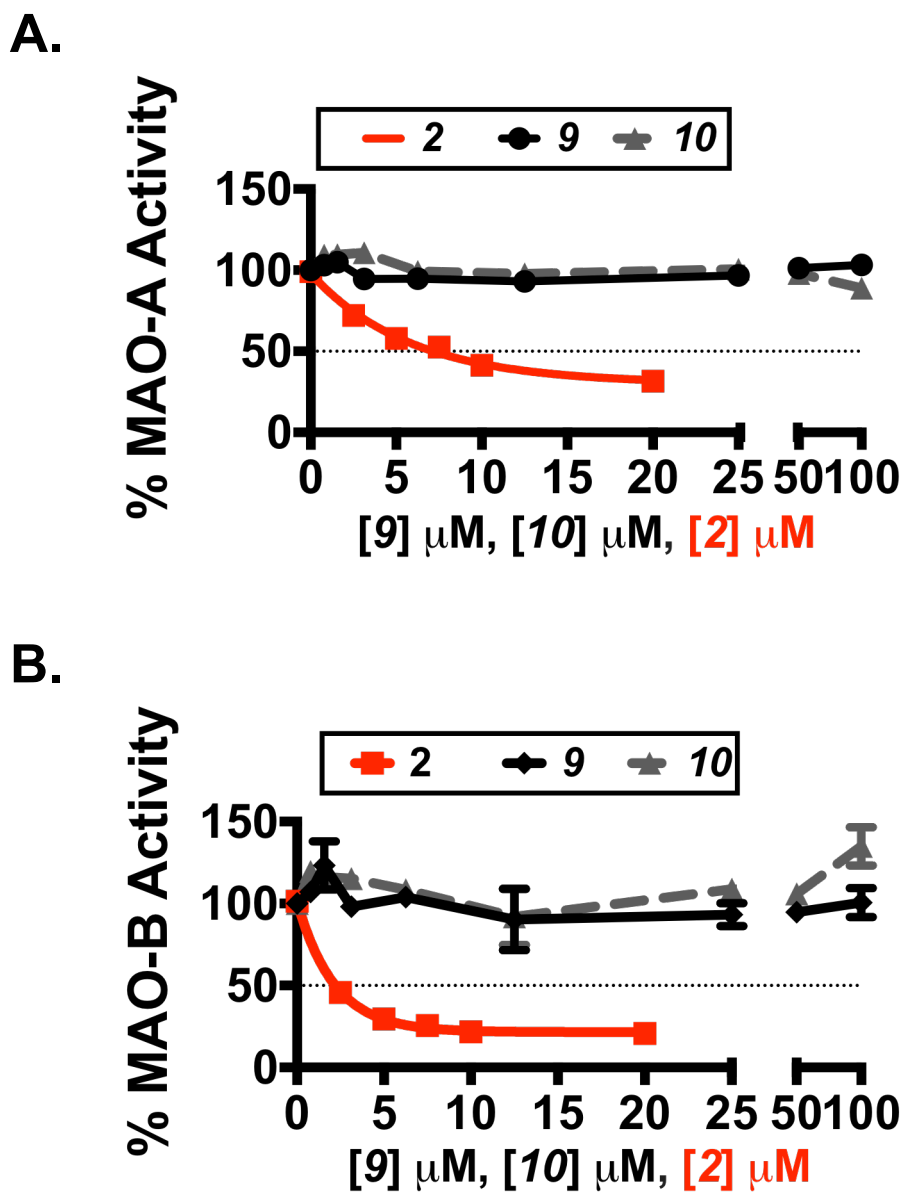
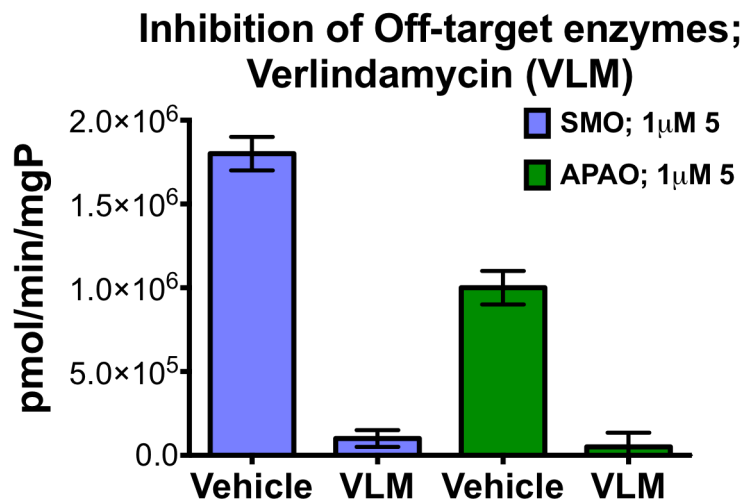


Figure 4.2. Monoamine oxidase A and B activity. MAO A and MAO B enzyme activity for 3,5-diaminotriazoles **9** and **10** compared to the known MAO inhibitor tranylcypromine (TCP). TCP IC_{50} = 4.2 μ M and 5.8 μ M for MAO A and MAO B, respectively). Compounds **9** and **10** exhibited IC_{50} values > 100 μ M for both MAO A and B. Graphs are representative of 3 separate experiments, with n=4-6 wells per treatment. Mean \pm SEM.

Selectivity of 3,5-diaminotriazoles – Spermine Oxidases:

Yet another amine oxidase with close homology to LSD1 is the polyamine enzyme, spermine oxidase (SMO). In fact, the initial discovery of LSD1 can be attributed to work with SMO.¹⁶¹ Despite this close relationship, many studies of LSD1 inhibitors fail to consider SMO in their off-target screening. However, we included SMO in our study because of previously reported roles for SMO and polyamines in kidney and liver ischemia-reperfusion.¹⁶² For example, the oligoamine LSD1 inhibitor, verlindamycin (**5**), showed significant potency in reduction of SMO and N-acetyl polyamine oxidase (APAO) activity at 10 μ M (**Figure 4.3A**). To screen our compounds, we performed a simple chemiluminescent assay using recombinant SMO, as previously described.¹⁶³ In short, the stoichiometric production of H₂O₂ was quantified using luminol and horseradish peroxidase. In addition, we used MDL72527 (Compound **11**), as a positive control (IC₅₀SMO < 10 μ M).¹⁶⁴ We showed that both compound **9** and **10** showed significant SMO potency, with an IC₅₀ = 40 nM and 180 nM, respectively (**Figure 4.3B**). Interestingly, this is the most potent small molecule inhibitor of SMO described yet. Therefore, future exploration into derivatives of the 3,5-diamino-1,2,4-triazole may be warranted as potent SMO inhibitors.

A.



B.

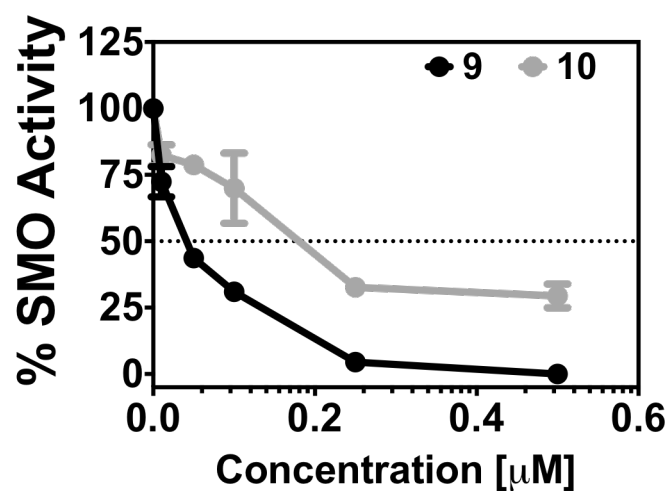


Figure 4.3. LSD1 inhibitors exhibit potency against SMO. A chemiluminescent assay was used to screen LSD1 inhibitors. (A) Recombinant SMO and APAO was treated with 1 μ M verlindamycin. (B) Titration analysis of compound **9** and **10** indicated $IC_{50} = 40$ nM and 180 nM, respectively. Data indicates replicates of three separate experiments with n=4-6 wells per treatment. Mean \pm SEM.

SMO inhibitor MDL72527 does not inhibit LSD1:

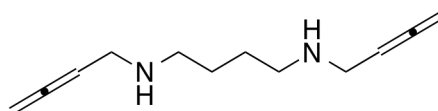
Our 3,5-diamino-1,2,4-triazole compounds showed significant efficacy for two enzymes – LSD1 and SMO. Therefore, we aimed to characterize the selectivity of known inhibitors of these individual enzymes. The selective, enzyme-activated irreversible SMO inhibitor, MDL72527, is a potent micromolar inhibitor of SMO (**Figure 4.4A-B**). However, no studies have shown whether or not this compound showed additional efficacy for LSD1. We performed an LSD1 inhibition assay, as previously described¹⁶⁵, and titrated MDL72527 up to 100 μ M. MDL72527 lacked any inhibition of LSD1, and thus, demonstrated it as a SMO selective inhibitor (**Figure 4.4C**).

LSD1 inhibitor GSK-LSD1 does not inhibit SMO:

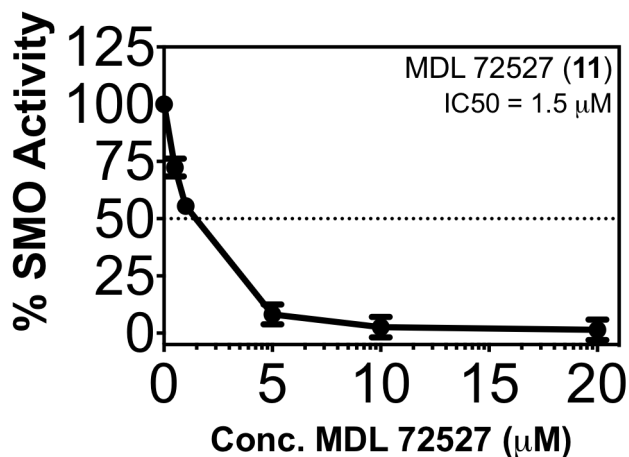
Similarly, we aimed to establish the potency of a known selective LSD1 inhibitor against SMO. GSK-LSD1 (**Figure 4.5A**) has a selectivity index of >1000 for MAO-A, MAO-B, and LSD2.¹⁶⁶ However, no studies have been performed with SMO. We performed a standard SMO inhibition assay, as previously described.¹⁶³ GSK-LSD1 did not show any significant inhibition of SMO (**Figure 4.5B**). Therefore, GSK-LSD1 is a highly selective for LSD1.

A.

MDL 72527



B.



C.

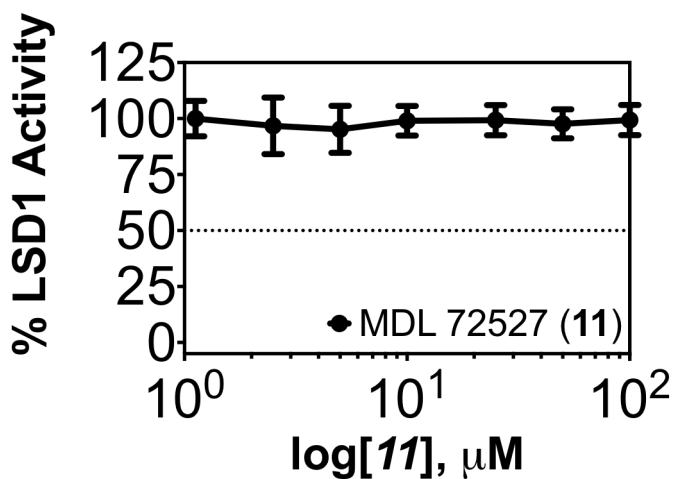


Figure 4.4. SMO inhibitor MDL72527 selectivity. (A) MDL72527 structure. (B) Recombinant SMO assay shows $\text{IC}_{50}(\text{SMO}) = 1.5 \mu\text{M}$ (C) Recombinant LSD1/CoREST assay. Data indicates replicates of three separate experiments with $n=4-6$ wells per treatment. Mean \pm SEM.

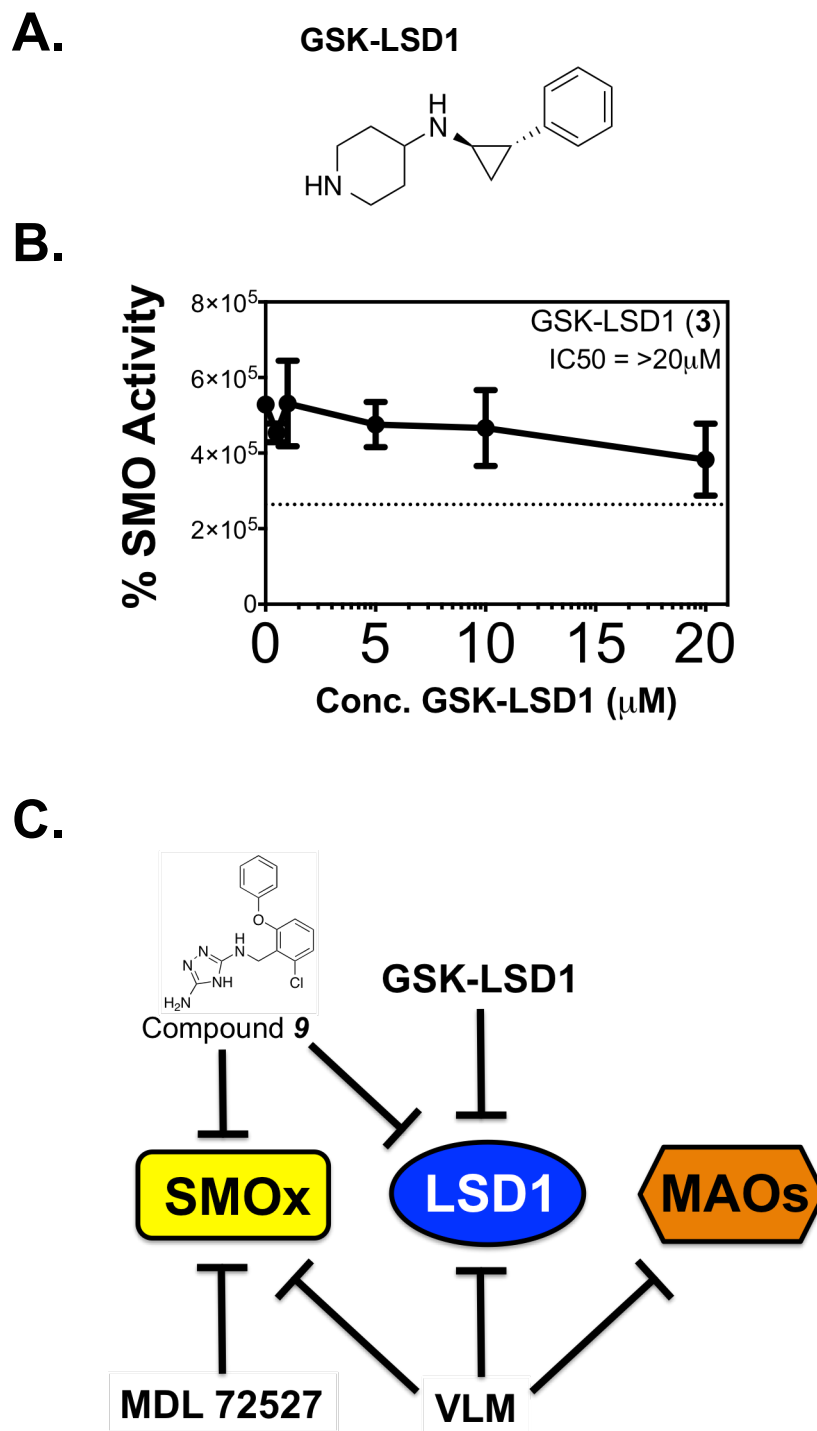


Figure 4.5. LSD1 inhibitor GSK-LSD1 selectivity. (A) GSK-LSD1 structure. (B) Recombinant SMO assay shows $IC_{50}(SMO) > 100 \mu M$. (C) Summary of amine oxidase inhibitors' selectivity. Data indicates replicates of three separate experiments with $n=4-6$ wells per treatment.

Differential inhibitors of LSD1, SMO, and MAO:

In summary, our recombinant enzyme screens of 3,5-diamino-1,2,4-triazoles, MDL72527, GSK-LSD1, and verlindamycin demonstrated distinct uses for each compound to dissect individual enzyme roles within cardiopathology (**Figure 4.5C**). Verlindamycin is the least selective, showing efficacy for all four amine oxidases tested (**Table 4.1**), making it a pan-amine oxidase inhibitor. Our newly designed 3,5-diamino-1,2,4-triazoles both showed significant potency for LSD1 and SMO. Interestingly, compound **9** favored SMO with almost 30-fold more potency. Therefore, 3,5-diamino-1,2,4-triazoles are dual inhibitors of LSD1 and SMO. Finally, we confirmed the selectivity of both MDL72527 and GSK-LSD1 for SMO and LSD1, respectively.

Table 4.1. Amine oxidase inhibitor classes and selectivity for LSD1, MAOs, and SMO.

#	Compound	Classification	MW (g/mol)	cLogP	IC ₅₀ (Enzyme; μ M)			
					LSD1	MAO-A	MAO-B	SMOX
2	Tranylcypromine	Suicide Inhibitor	133.2	1.585	20.7 **	4.2	5.8	Unkn.
3	GSK-LSD1	Tranylcypromine derivative	216.16	1.236	0.016 #	>10 #	>10 #	>20
5	Verlindamycin	Polyamine-analog	1020	9.463	7.3	36.5	9.9	0.05-0.1
9	Compound 9	3,5-diaminotriazole	315.8	4.443	1.19	>100	>100	0.04
10	Compound 10	3,5-diaminotriazole	339.4	1.818	2.22	>100	>100	0.18
11	MDL 72527	3,5-diaminotriazole	339.4	1.818	>100	>100	>100	10

** Schmidt DM, McCafferty DG. *trans-2-Phenylcyclopropylamine* is a mechanism-based inactivator of the histone demethylase LSD1. *Biochemistry*. 2007 Apr 10;46(14): 4408-16.

As reported by GSK and its distributors

3,5-diaminotriazoles show limited cytotoxicity :

The field of LSD1 drug development primarily focuses on compounds highly efficacious at cancer cell killing. However, LSD1 has emerged as a drug target in diseases other than cancer. As such, there is a need for epigenetic inhibitors that preclude overt cytotoxicity. Therefore, cellular characterization of these compounds focused on identifying compounds with decreased cytotoxicity in multiple cell lines.

In order to identify hits that showed a reduction in cytotoxicity, compounds exhibiting *in vitro* IC₅₀ < 5 μM were screened by a standard MTS reduction assay and verified by simple nuclei staining quantification. Multiple cell lines were screened, including CALU-6, MCF7, MCF-10a, MDA-MB-231, CA46, PC3, and PANC1. **Table 4.2** shows a brief description of each of these cell lines. Cultures were grown in appropriate media as per ATCC instructions at 37°C in a humidified environment containing 5% CO₂. The cells were plated and maintained in a clear bottom, 96 well plate and seeded at 1,000 cells/ well. After attachment, compounds were titrated from 500 nM-100 μM for 48 hrs. The cells were exposed to DMSO concentrations of less than 1%, and 1% DMSO was used as a negative control for cell growth. The known LSD1 inhibitor verlindamycin **5** was used as a positive control. A tetrazolium salt [3-(4,5-dimethylthiazol-2-yl)-5-(3-carboxymethoxyphenyl)-2-(4-sulfophenyl)-2H-tetrazolium, inner salt; MTS] is added and cleaved by intracellular esterases to form a colorimetric solution and quantified by spectrophotometry. In addition, cells were fixed with 4% PFA, permeabilized with 1% Triton-X100 and stained

with DAPI at 1:1000 with in PBS. Nuclei were then counted by high throughput immunofluorescence microscopy.

CALU-6 human lung adenocarcinoma cells express high endogenous levels of LSD1, and thus, are responsive to LSD1 compound treatments. Compound **9** and **10** were not cytotoxic to cultured CALU-6 cells ($IC_{50} > 100 \mu M$), while the internal standard verlindamycin (**5**) was cytotoxic with an $IC_{50} = 5 \mu M$ (**Figure 4.6A**). The negative control tranilcypromine, a known low toxicity compound, was cytotoxic at $IC_{50} \sim 1 \text{ mM}$ (**Figure 4.6B**).

The cytotoxicity of **9** and **10** was examined in five additional cell lines including CA46 Burkitt's lymphoma, the PC3 human prostate cancer cell line, the PANC1 human pancreatic cell line, the MDA-MB-231 estrogen receptor-negative cell line and the MCF-10A human breast epithelial cell line. LSD1 has been shown to be overexpressed in the PC3, PANC1 and MDA-MB-231 cell lines. Compounds **9** and **10** produced no significant cytotoxicity in the CA46 and MCF-10A lines, although **9** had an IC_{50} of 52 mM in the MCF-10A line (**Figure 4.7A-C**). In the PC3 line, both **9** and **10** exhibited IC_{50} values near 74 mM, compared to the internal standard **5**, which produced 85% growth inhibition at 8 mM (**Figure 4.8A**). In the PANC1 and MDA-MB-231 lines, **10** was not an effective growth inhibitor, with IC_{50} values of 80 and 55 mM, respectively. Interestingly, compound **10** was an effective growth inhibitor in the PANC1 and MDA-MB-231 cell lines, exhibiting IC_{50} values of 19 and 12 mM (**Figure 4.8**). The mechanism underlying this activity remains to be determined; however, it can be generally stated that **9** and **10** produce little cytotoxicity in multiple cell lines in vitro.

Table 4.2. Human immortalized cell lines and descriptions.

Cell Line	Organism	Tissue	Morphology	Description
<i>Carcinogenic</i>				
MCF7	Human	Breast	Epithelial	Metastatic adenocarcinoma
PANC1	Human	Pancreas/duct	Epithelial	Epithelioid carcinoma
MDA-MB-231	Human	Breast	Epithelial	Metastatic adenocarcinoma
CA46	Human	B-lymphocyte	Lymphoblast	Burkitt's lymphoma
PC-3	Human	Prostate	Epithelial	Metastatic, grade IV adenocarcinoma
CALU-6	Human	Lung	Epithelial	Anaplastic carcinoma; High endogenous LSD1
<i>Non-Carcinogenic</i>				
MCF10a	Human	Breast	Epithelial	Non-cancerous, fibrotic

Note: All cell lines were purchased from ATCC

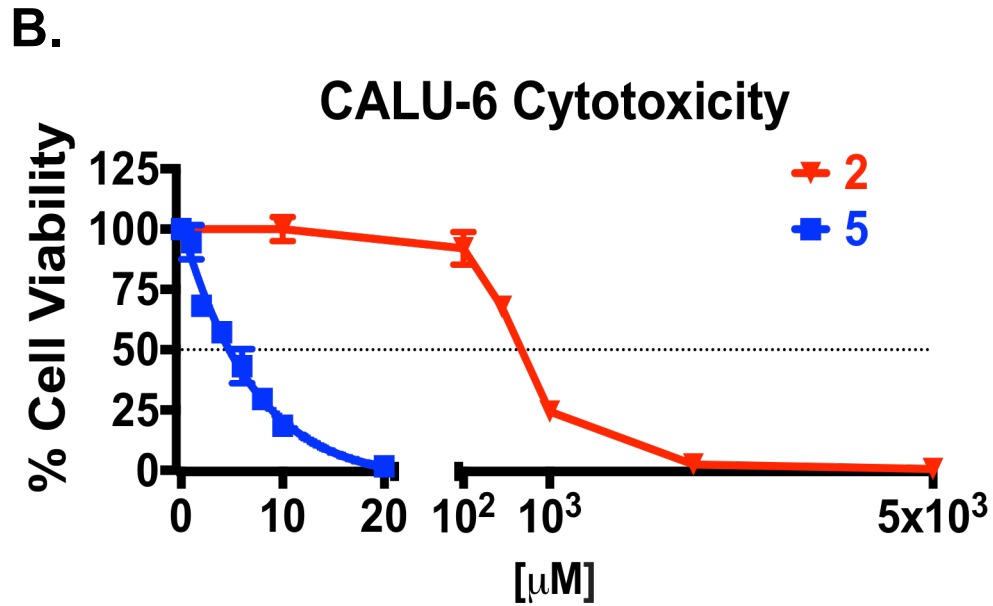
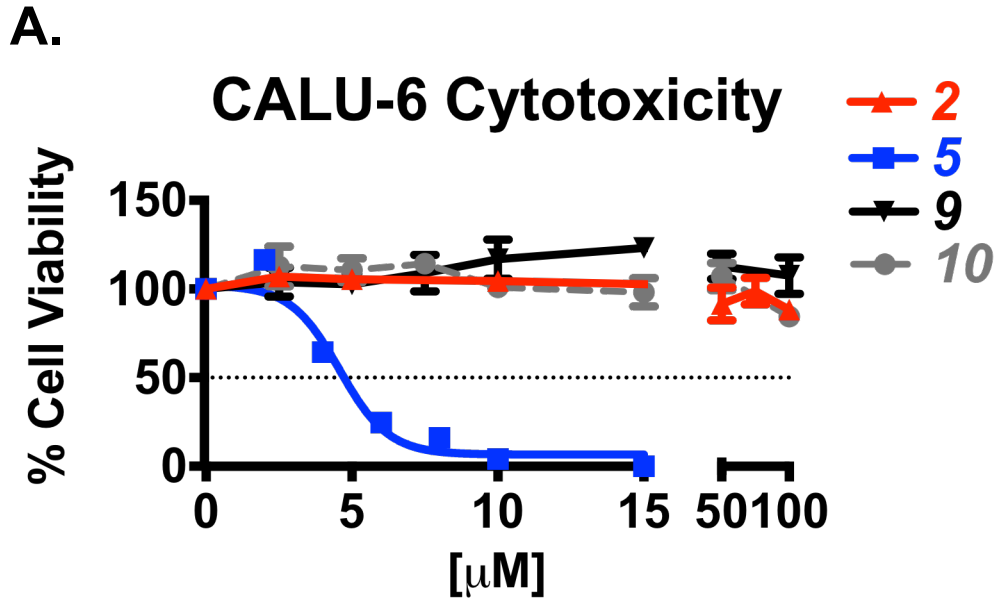
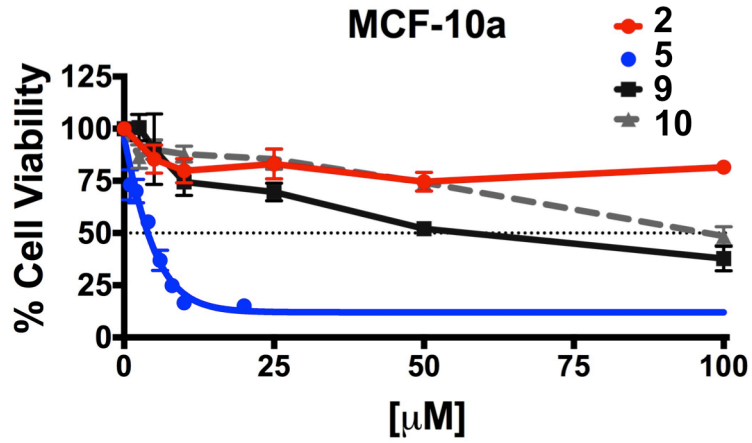
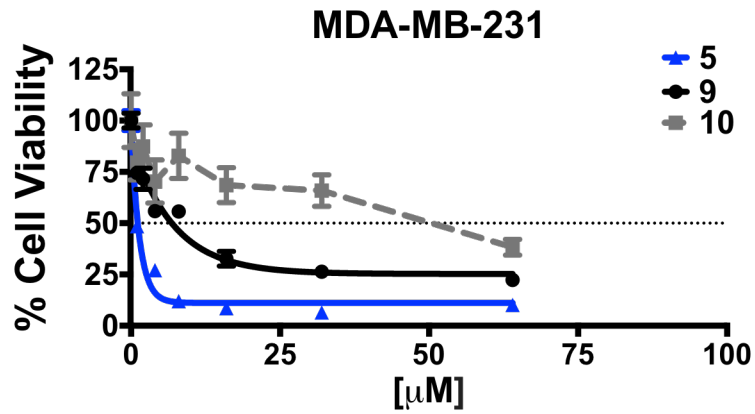


Figure 4.6. Cell viability and compound cytotoxicity in Calu-6. Cells were seeded at 3×10^3 cells/well and treated 48-72 hrs with increasing concentrations of 2, 5, 9, and 10. Cell viability was determined by colorimetric CellTiter 96 Aqueous MTS (Promega, #G3580). Data indicates replicates of three separate experiments with $n=4$ wells per treatment. Mean \pm SEM.

A.



B.



C.

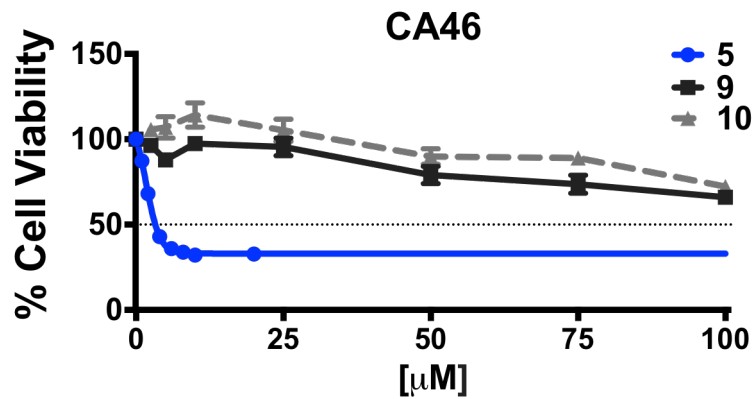


Figure 4.7. Cell viability in MCF-10a (A), MDA-MB-231 (B), and CA46 (C). Cells were treated 48-72hrs with increasing concentrations of 5, 9, and 10. Cell viability was determined by colormetric CellTiter MTS (Promega, #G3580). n=4 wells per experiment run in triplicate. Mean \pm SEM.

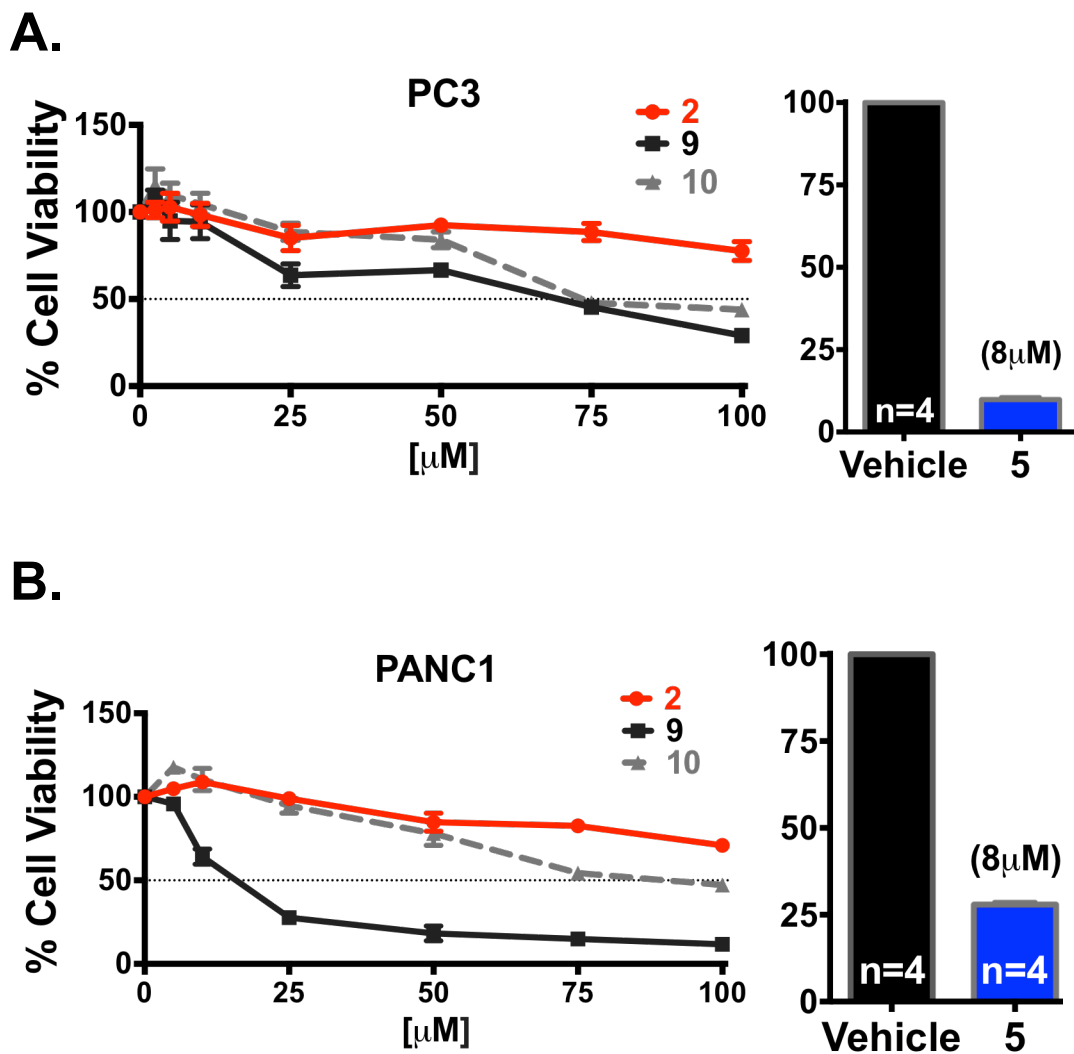


Figure 4.8. Cell viability and compound cytotoxicity in PC3 (A) and PANC1 (B). Cells were treated 48-72 hrs with increasing concentrations of 2, 9, and 10. Compound 5 was used at a fixed 8 μM concentration as an internal control. Cell viability was determined by colormetric CellTiter 96 Aqueous MTS (Promega, #G3580). Data indicates replicates of three separate experiments with $n=4$ wells per treatment. Mean \pm SEM.

Cellular phenotype and histone methylation changes of 3,5-diaminotriazoles:

To measure the cellular effects of **9** and **10**, treated cells from the cytotoxicity assay above were stained for immunofluorescence imaging using the appropriate fluorescently labelled secondary antibodies. In a 96-well plate, 5% BSA was added to specific wells and the plate was allowed to stand for 2 hours. The plate was then incubated at 4°C overnight with the primary antibody for H3K4me2. Fluorescent secondary antibodies were then added to each well at 1:500 dilutions in 1% BSA for 2 hours. Cells were washed, suspended in PBS and viewed for intensity of signal per cell (Hermes WiScan, Idea Biomedical). The imaging system is able to generate 10-40x images as well as quantify average intensity on a per-well basis, eliminating any bias towards fluorescent staining. Compounds **9** and **10** at both 1 and 10 µM developed green fluorescence in the nucleus at 48 hours that was comparable to the fluorescence promoted by 30 µM tranylcypramine, indicating a significant increase in H3K4me2 levels (**Figure 4.9A**). The H3K4me2 levels were quantified and graphed as cell count vs. average intensity (RFU) as shown in the histogram (**Figure 4.9B**). The mean population intensity (MPI) ± SEM for the vehicle was $1.44 \times 10^4 \pm 71$ RFU. In comparison, the MPI for 30mM TCP was $1.86 \times 10^4 \pm 136$ RFU (1.3-fold increase), for 10 mM compound **9** $1.82 \times 10^4 \pm 105$ RFU (1.26-fold increase), and for 10mM compound **10** $1.91 \times 10^4 \pm 124$ RFU (1.33-fold increase). Thus, **9** and **10** 1µM were as effective as 30mM TCP at increasing H3K4me2 *in vitro*. Western blot analysis of cell lysates were also performed to show a dose response increase in global methylation (**Figure 4.9C**).

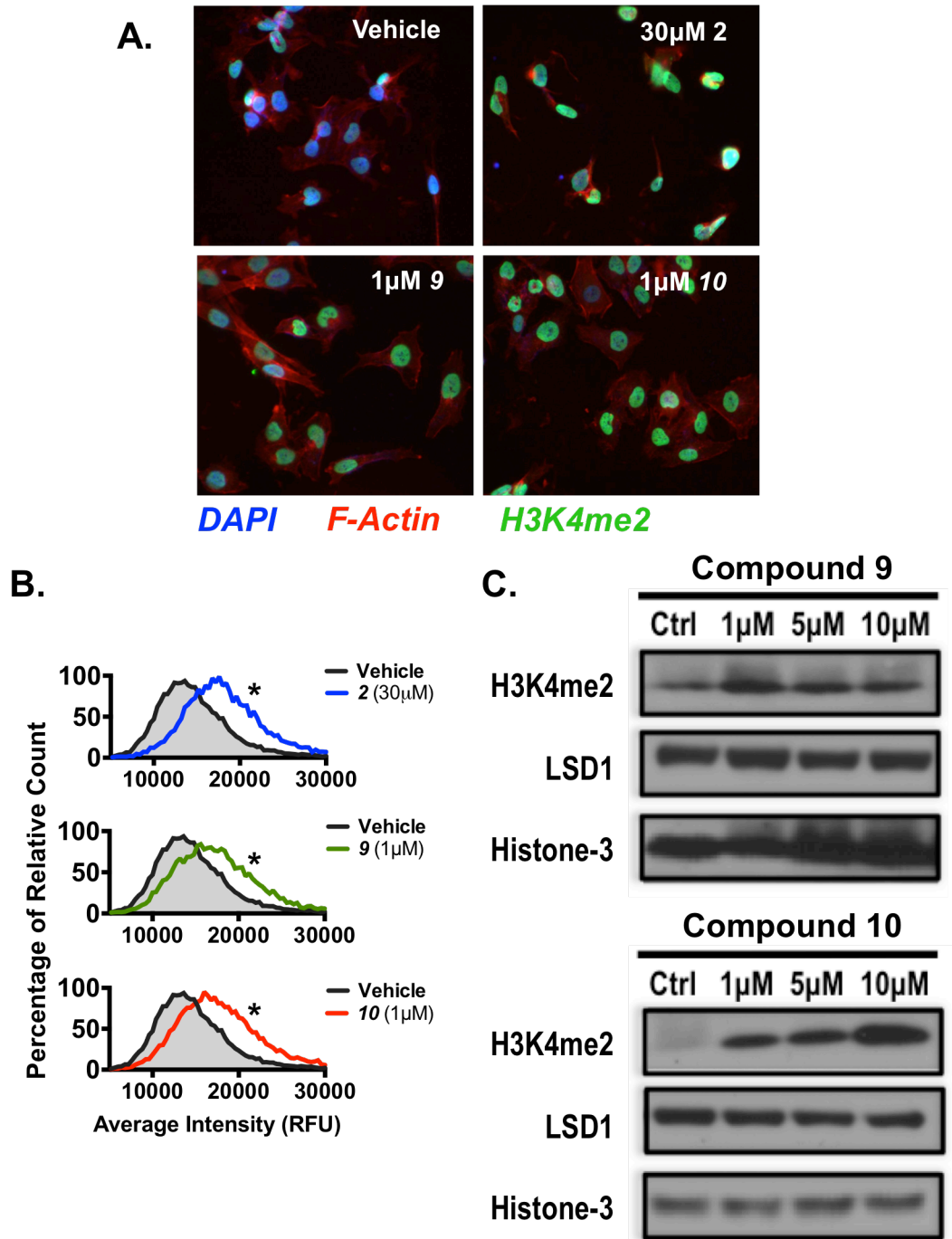


Figure 4.9. Global methylation changes. (A) CALU-6 cells were treated with 30µM TCP (2), 1µM 9, or 1µM 10 for 48hrs. Cells were stained for nucleus (DAPI), F-actin (Alexa Fluor 594 Phalloidin), and dimethyl-H3K4 (Alexa Fluor 488 Secondary Antibody). (B) Fluorescent intensity on cell-by-cell basis was obtained by Hermes WiScan (IDEA Biomedical) and graphed as a frequency distribution histogram of relative cell count at specific intensities. (C) Western blots of histone methylation. Two-way ANOVA; * P-value < 0.001, representative of 3 experiments with n=4 wells.

Disruption of Epigenetic Complexes in Primary Cardiomyocytes:

LSD1 activity at chromatin promoters is facilitated through binding in large epigenetic complexes. LSD1 is found in the CoREST/REST/HDAC corepressor complex and extensive crosstalk takes place amongst each enzyme. Therefore, we hypothesized that since HDAC inhibition within these complexes have shown cardioprotection, LSD1 inhibition could show similar results. In fact, we wanted to explore if LSD1 inhibition was sufficient to disrupt the CoREST:LSD1 interaction. Primary rat cardiomyocytes were isolated by hanging heart method as previously described.¹⁶⁷ Cardiomyocytes were treated at concentrations equivalent to their IC₅₀-values for 3-hours. Cell lysates were pulled-down with LSD1 and immunoblotted for CoREST. **Figure 4.10** shows that compound **9** considerably disrupted the LSD1:CoREST interaction. Interestingly, neither verlindamycin nor compound **10** were able to replicate this phenomenon so acutely. HDAC1 and total protein lysate were used as loading controls.

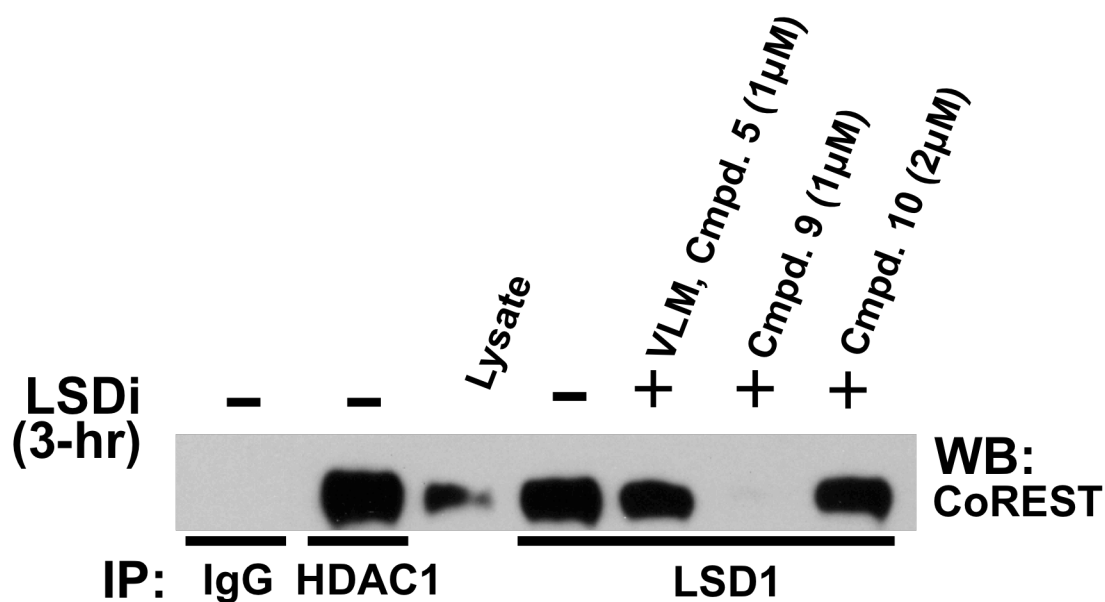


Figure 4.10. Primary rat cardiomyocytes provide preliminary data on 3,5-diamino-1,2,4-triazoles efficacy *in vitro* to disrupt co-repressor complexes. Co-immunoprecipitation analysis for LSD1:CoREST complex following treatment with 5 μM VLM, 1 μM **9**, 2 μM **10**. Lysates pulled down with LSD1 antibody and immunoblotted for CoREST. Data representative of three separate experiments.

Toxicology screen of Compound 9 in CD1 mice:

A pilot toxicology study in four CD1 mice was performed in collaboration with the MUSC Veterinary Services. In short, a 3 mg/kg, intraperitoneal injection of compound 9 was administered daily for 1-week. After the drug course, mice were evaluated by the MUSC veterinarian. A complete blood panel, liver enzymes, and kidney functional labs were obtained, followed by histological evaluation of various organs (i.e. heart, lung, liver, spleen, and kidney). A comprehensive report on histological damage was obtained by a veterinary pathologist. In addition, a consultation with an MUSC Hematology Resident and Nephrologist were also performed.

Upon gross examination, all four mice showed no abnormalities or contraindications from drug treatments. The blood panel and liver enzymes had no outstanding findings and were within normal range. However, blood urea nitrogen (BUN) was elevated, creatinine was low, and blood glucose was elevated (**Table 4.3**). Thus, the BUN:Creatinine ratio was higher than reported normal values. In addition, the CBC showed minor thrombocytopenia.

Histological evaluation by hemotoxylin and eosin staining of various organs revealed very minimal to minor pathological changes. Of note, the kidney showed minor ectatic cortical tubules with attenuated epithelium (**Figure 4.11A**). In addition, the heart showed minor vacuolation of cardiomyocytes without any interstitial immune infiltration (**Figure 4.11B**). There was also negligible multifocal hepatic inflammation and necrosis (**Figure 4.11C**). Finally, the spleen showed no outstanding lesions (not shown).

Table 4.3. Clinical laboratory values (mean ± SEM)

Blood Diagnostic Tests			
	Normal Range #	Compound 9 ¥	
ALT	45.08 ± 2 u/L	42.75 ± 5.0	
AST	80.55 ± 8.3 u/L	165.25 ± 17.8	
ALP	14-118 u/L	66.67 ± 21.5	
CREATININE	0.3-0.4 mg/dL	0.15 ± 0.03	L
BUN	14.68 ± 0.5 mg/dL	22 ± 1.5	H
GLU	164.89 ± 3.5 mg/dL	263.5 ± 19.5	H
<i>Leukocytes</i>			
WBC	8.79 ± 0.3 (k/µL)	5.3 ± 0.9	
NE	1.5 ± 0.1 (k/µL)	1.1 ± 0.1	
LY	6.59 ± 0.3 (k/µL)	4.0 ± 0.8	
MO	0.49 ± 0.03 (k/µL)	0.13 ± 0.03	L
EO	0.17 ± 0.02 (k/µL)	0.07 ± 0.02	
BA	0.04 ± 0.01 (k/µL)	0.01 ± 0.01	
NE%	6.6-38.9%	20.5 ± 2.1	
LY%	55.8-91.6%	75.3 ± 2.6	
MO%	0-7.5%	2.5 ± 0.6	
EO%	0-3.9%	1.4 ± 0.5	
BA%	0-2%	0.31 ± 0.2	
<i>Erythrocytes</i>			
RBC	8.93 ± 0.2 (M/µL)	10.3 ± 0.9	
Hb	14.67 ± 0.3 (g/dL)	15.6 ± 1.4	
HCT	49.97 ± 1.1 (%)	54.4 ± 5.3	
MCV	56.1 ± 0.6 (fL)	52.8 ± 1.8	
MCH	16.45 ± 0.6 (pg)	15.2 ± 0.3	
MCHC	29.5 ± 0.4 (g/dL)	28.9 ± 1.0	
RDW	16.79 ± 0.1 (%)	16.4 ± 0.4	
<i>Thrombocytes</i>			
PLT	1529 ± 53 (K/µL)	836.5 ± 324	L
MPV	5.1 ± 0.06 (%)	5.1 ± 0.1	

Normal clinical laboratory values as reported by Charles River Laboratories, CD1 mouse supplier

¥ 3mg/kg, i.p. QDx7days; n=4 CD1 mice

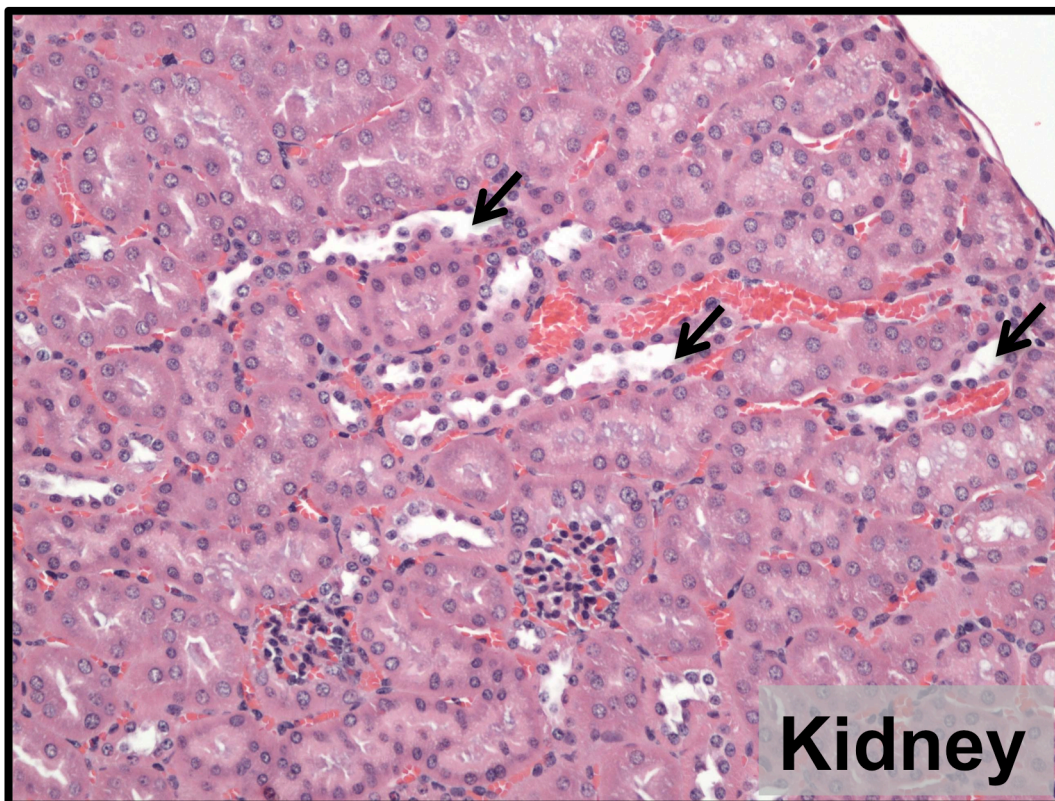


Figure 4.11A. Kidney histology of Compound 9 treated CD1 male mice (3mg/kg, *i.p.*, QD 7 days). Hemotoxylin and eosin staining of cortical kidney. Mild multifocal ectatic tubules with attenuated epithelium (Arrow). Limited tubular hyperplasia and regeneration. (Reported in 2 of 4 animals).

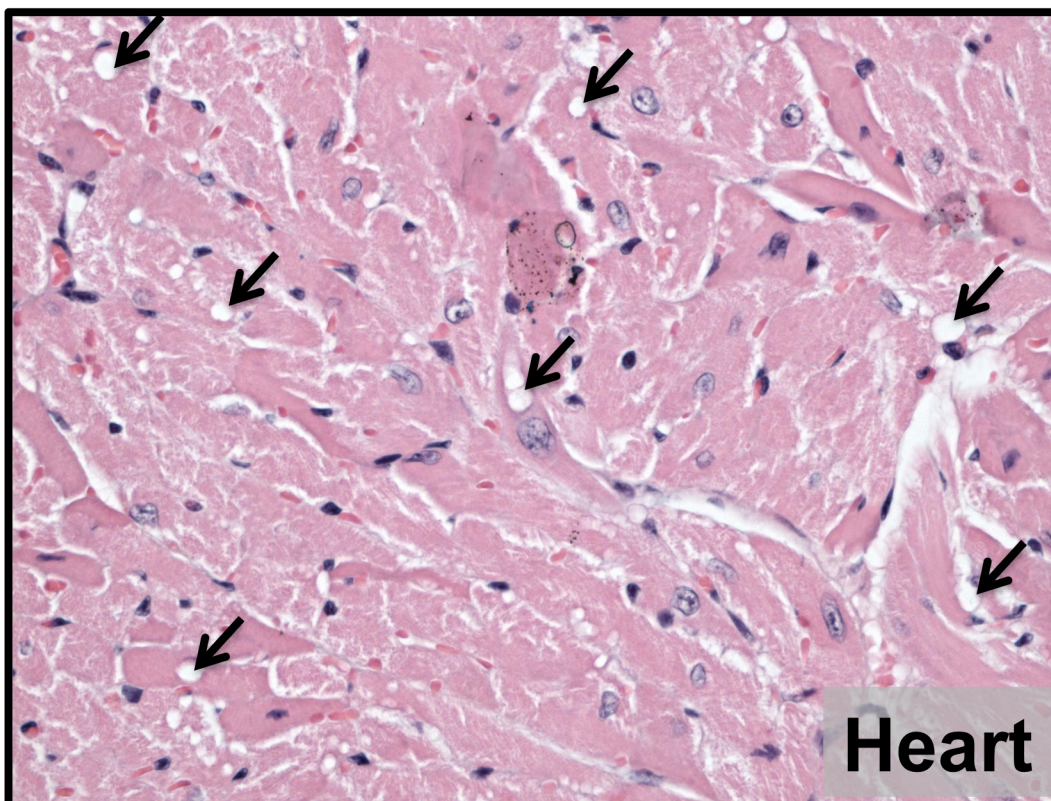


Figure 4.11B. Heart histology of Compound 9 treated male CD1 mice (3mg/kg, *i.p.*, QD 7 days). Hemotoxylin and eosin staining of left ventricular free wall. Mild diffuse cardiomyocyte intrasarcoplasmic vacuolation without interstitial infiltrate. (Reported in 2 of 4 animals)

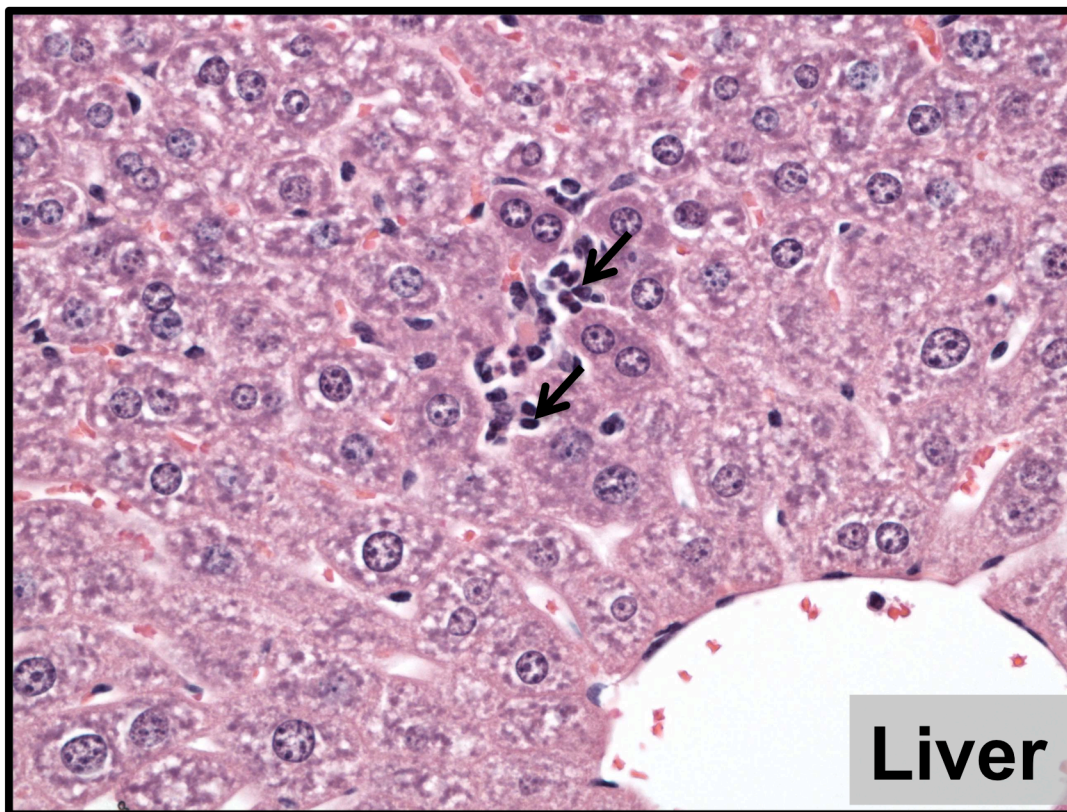


Figure 4.11C. Liver histology of Compound 9 treated male CD1 mice (3mg/kg, *i.p.*, QD 7 days). Hemotoxylin and eosin staining of left lobe. Mild multifocal hepatic inflammation and necrosis can be found, as indicated by the arrows. (Reported in 3 of 4 animals)

III. DISCUSSION

Current inhibitors of amine oxidases show significant undesirable potency towards other members of the family. This is due to, in part, because of the high sequence homology within the active sites. As such, we began to test newly designed LSD1 inhibitors for efficacy against other amine oxidases, including MAO-A, MAO-B, and SMO. In addition, the vast majority of LSD1 inhibitors were designed as antitumor agents, with the explicit goal of cancer cell toxicity. Recently, however, increasing evidence demonstrates a focus for epigenetic manipulation outside the realm of carcinogenesis.¹⁵⁵⁻¹⁵⁹ In particular, we were interested in the role of LSD1 in CVD, and thus, intended to manipulate epigenetic enzymes without causing drug-driven cellular damage. Therefore, we evaluated our compounds for cytotoxicity in multiple cell lines and during a small toxicology study. Finally, we performed a coimmunoprecipitation assay of the CoREST:LSD1:HDAC corepressor complex to determine whether LSD1 inhibition in cardiomyocytes disrupted this epigenetic complex.

Our initial evaluations of the selectivity of compounds **9** and **10** place them among the first reversible small molecule compounds that possess selectivity for LSD1 over MAO A and B. However, they also observe considerable inhibition against SMO. Therefore, the 3,5-diamino-1,2,4-triazole scaffold is, in fact, a dual inhibitor per say. In other words, these compounds can be utilized as agents to target both LSD1 and SMO. Interestingly, both enzymes may be playing a detrimental role in IR remodeling¹⁶² and inhibition of both amine oxidases could prove beneficial as a treatment strategy.

The dual selectivity of compound **9** and **10** for LSD1 and SMO, although potentially useful as a therapy, severely limits their utilization as a tool to unveil LSD1 as a key new therapeutic target. Therefore, we evaluated current LSD1 and SMO inhibitors for cross-reactivity. In particular, we aimed to find compounds that could inhibit one enzyme, but not the other. A few months prior to this dissertation, a highly selective irreversible LSD1 inhibitor was made commercially available.¹⁶⁶ This compound, **3**, did not show any inhibition of SMO. Likewise, we were able to find an irreversible SMO inhibitor, MDL72527, that did not affect LSD1 activity.¹⁶⁴ These compounds will be utilized in future cardiovascular experiments to dissect the individual contributions of each enzyme in 3,5-diamino-1,2,4-triazole mediated cardioprotection (see **Chapter 5**).

Compounds **9** and **10** also produce the desired epigenetic effect, namely a significant increase in H3K4me2 levels, indicating that they enter mammalian cells and are active within the cell nucleus. This was confirmed by our coimmunoprecipitation results in primary rat cardiomyocytes. In particular, these results implied that compounds **9** and **10** could reduce LSD1 activity and indirectly influence the activity of HDACs. In addition, the low level of toxicity to mammalian cells produced by **9** and **10** demonstrate that the 1,2,4-triazole scaffold can be used to produce LSD1 inhibitors that can be used in non-cancer disease states.

Preliminary results in a pilot study (discussed further in **Chapter 5**) indicated that an LSD1 inhibitor could protect the heart against IR injury. Therefore, to continue our preclinical evaluation of the 3,5-diamino-1,2,4-triazoles

scaffolds as potential cardiac candidates, we began to evaluate the *in vivo* toxicity using CD1 mice. With the assistance of the MUSC Veterinary Services, an MUSC hematology resident, and a nephrologist, we were able to evaluate any damage caused by intraperitoneal injections of 3 mg/kg compound **9**. We demonstrated that the compound showed minimal to mild histological damage to the kidney, liver, and heart. Of most interest, there was mild vacuolation of the sarcomeres within cardiomyocytes. This can be a precursor to cardiotoxic changes such as degeneration, or an age-related incidental finding. In short-term toxicology studies, treatment-related myocardial degeneration was characterized by multifocal myocardial and interstitial vacuolation, often associated with diffuse interstitial cellular infiltration consisting of macrophages and neutrophils.¹⁶⁸ These small to large vacuoles seen within sarcoplasm presumably represent degenerate myofibrils. Yet, in some drug studies, cellular infiltration was the sole insult seen. As such, minor multifocal sarcoplasmic vacuolation without accompanying cellular infiltration can be a relatively frequent event in control mice. Therefore, within the scope of this small, pilot toxicology study, we cannot rule-in or rule-out this finding as compound-induced toxicity.

In addition to the histology, we saw that the BUN:Creatinine ratio and blood glucose were elevated. A simple explanation for this could be that the mice were dehydrated, although no definitive laboratory test is available for this. Dehydration would cause decreased blood volume to be filtered to the kidneys, and as such, cause elevated BUN:Creatinine ratio. In addition, dehydration can lead to elevated blood glucose (i.e. vasopressin is produced by the kidneys to

compensate for dehydration, leading to gluconeogenesis in the liver). In order to rule out prerenal azotemia (i.e. elevated nitrogen-containing compounds), additional laboratory tests need to be performed, such as albumin.

In summary, we successfully identified compound **9** and **10** as dual inhibitors of LSD1 and SMO, with limited efficacy against MAOs. In addition, we confirmed these compounds successfully traversed the cell membrane and produced prolific epigenetic changes. Compounds **9** and **10** are also the first designed reversible inhibitors of LSD1 and potent SMO dual inhibitors to date. Augmented by their low toxicity, these compounds show promise as cardiac drug candidates.

IV. LIMITATIONS AND FUTURE DIRECTIONS

Compounds **9** and **10** did not show efficacy against MAO-A or B. Therefore, we do not expect to see many of our 3,5-diaminotriazole derivatives inhibit MAO-A or B as well. However, newer –azole family of fungicides incorporate the 1,2,4-triazole moiety and are potent CYP450 enzyme inhibitors.¹⁶⁹⁻¹⁷⁰ For instance, posaconazole is an extended spectrum antifungal with clinical concerns because of its CYP3A4 potency.¹⁷¹ Therefore, our new compounds may show concern with drug-drug interactions. Finally, triazole drugs have been shown to be extensively first-pass metabolized by CYP2C19.¹⁷² One primary concern is the population polymorphisms that exist with CYP2C19 and needs to be considered as preclinical work continues with these compounds.

Despite successful previous work in CALU-6 cells that express high endogenous LSD1, LSD1 still makes up just one of a vast multitude of histone demethylases in the cell, some of which have similar substrates.¹⁷³ Thus, LSD1 inhibition or removal may not be detectable on a *global* histone level. For instance, LSD1 knockout HCT116 cells failed to show any changes in global histone methylation.¹⁷⁴ LSD1 occupies approximately 2% of genomic promoters in corepressor complexes in stem cells.¹⁷⁵ Thus, LSD1 inhibition can alter gene transcription on a local level, without showing global changes. Therefore, a chromatin immunoprecipitation (ChIP) at known LSD1-regulated promoters may need to be done to verify target inhibition. Also, a recently published manuscript on using CD86 cell surface receptor as an LSD1 biomarker could also be evaluated.¹⁷⁶

The dual inhibition of SMO and LSD1 make future drug development intriguing. For instance, compound **9** and **10** demonstrate for the first time, a reversible, competitive small molecule inhibitor of LSD1. Yet, they also present the most potent SMO inhibitors to date. Therefore, extensive lead optimization of these compounds in both settings, SMO and LSD1, need to be explored. Early hit-to-lead studies suggest that we are able to identify more potent analogues. In addition, not all LSD1 inhibitors are effective against SMO, and vice versa. Therefore, it is not unreasonable to think that future evaluation of related analogues can diverge this dual inhibition. However, in the setting of cardiac ischemia-reperfusion injury, a dual inhibitor, such as **9**, may be beneficial because of the roles SMO and LSD1 both play in cardiopathology.

Furthermore, additional studies need to measure the interactions of these compounds with cytochrome P450 enzymes to eliminate undesirable side-effects early in drug development. As stated earlier, 1,2,4-triazole structures are first-pass metabolized by CYPs within the liver. In addition, Sorna *et al.* published LSD1 inhibitors with moderate CYP450 interactions of their benzohydrazide series. Therefore, these compounds will be screened for activity against relevant CYP450 enzymes utilizing the Vivid SelectScreen CYP450 Screening kits (Invitrogen).

Finally, our pilot toxicology study was severely limited by our low sample size and lack of controls. We performed this study as a snapshot of toxicity and compared our values to well-established laboratory values and histology of health CD1 mice. However, many of the lesions we saw within tissues were inconclusive because of these limitations. When further testing is performed, it will be important to look at increased numbers of animals, multiple doses of compounds, and both sexes.

CHAPTER 5: LSD1 as a novel therapeutic target to mitigate post-IR contractile dysfunction and infarction

I. INTRODUCTION

Current clinical therapies to achieve whole organ recovery following cardiac ischemia remain insufficient and are limited to reestablishing flow by primary percutaneous coronary intervention shortly after ischemic insult. However, reperfusion itself is detrimental at the cellular level and can lead to arrhythmias, mechanical dysfunction, and cell death.¹⁷⁷ We strove to unveil a previously unidentified enzyme target to improve recovery after an AMI by limiting reperfusion injury. In short, we aim to modulate pro-survival signaling and preconditioning responses through pharmacological manipulation of the epigenetic enzyme, LSD1.

Ischemia-reperfusion (IR) is a multifaceted pathological condition involving changes in inflammatory signaling, Ca^{2+} balance, and transcriptional reprogramming.¹⁷⁸ Formation of oxyradicals during IR leads to lipid peroxidation and sulfhydryl oxidation, resulting in membrane leak and intracellular protein denaturing.¹⁷⁷ An effective method to reduce the damage caused by IR is by the phenomenon of ischemic preconditioning.¹⁷⁹ However, the underlying mechanism as to how a tissue becomes “ischemia tolerant” remains obscure. One explanation is the activation of the reperfusion injury survival kinase (RISK) signaling cascade, and thus, favoring pro-survival kinases during anoxia.¹⁸⁰ Another is the upregulation of oxidant scavenging enzymes superoxide dismutase (SOD2) and catalase by preconditioning.¹⁸¹ This reduces the overall milieu of reactive oxygen species capable of causing oxidative stress.

In recent years, increasing evidence indicates that chromatin-remodeling processes such as histone demethylation and deacetylation play crucial roles in gene regulation during pathological cardiac events (e.g. IR injury) and cardiac preconditioning. To date, HDAC inhibitors, such as suberoylanilide hydroxamic acid (SAHA), have been beneficial in maintaining cardiac contractility and reducing infarct area post-IR injury.¹⁸² For instance, when administered before and at the time of reperfusion, SAHA partially rescued systolic function.¹⁸³ Increasing evidence indicates that class I HDACs crosstalk and act in tandem with LSD1 within the CoREST/LSD1/HDAC corepressor complex at similar promoters.¹⁸⁴ As such, previous studies have shown how class I HDAC inhibitors can increase histone methylation as well.¹⁸⁴ Therefore, we hypothesized that LSD1 inhibitors could also be applied as cardioprotective agents. This study is the first known attempt at utilizing this innovative strategy in CVD.

The ensuing chapter focuses on the identification of LSD1 as a novel therapeutic target in CVD by utilizing amine oxidase-specific inhibitors. Also, we will illustrate preclinical testing of our novel 3,5-diamino-1,2,4-triazole, **9**, as a potential cardiac drug candidate. As discussed in **Chapter 4**, compound **9** exhibits many characteristics of a successful cardiac clinical compound, such as its fairly nontoxic nature *in vitro* and *in vivo*. However, our understanding of the mechanism of action and importance of LSD1 is limited by the dual inhibition of **9**. In particular it shows efficacy against two enzymes, LSD1 and SMO. Therefore, in order to isolate LSD1 as a causative target during IR damage, we employed other selective compounds as tools to determine the mechanism of

action of **9**. We will use a well-documented SMO-specific inhibitor (i.e. MDL72527) and a highly potent LSD1-specific compound (i.e. GSK-LSD1).

We will test our hypothesis using two murine models of IR injury. First, we will test the effectiveness of test compounds in an *ex vivo* isolated heart model. This model is an effective tool in early drug discovery because it is highly reproducible and can accurately control drug concentrations. Most importantly, it provides a specific method of action by a compound at the tissue level that precludes any systemic, immune, and circulating stress factors. However, excising a whole organ from an animal moves our results farther from clinical resemblance, and thus, an additional model was considered. Therefore, in order to confirm our *ex vivo* results, we performed an *in vivo* coronary ligation and reperfusion model as well. It provides a more clinically relevant IR injury and allows observation of myocardial recovery at longer time points.

Figure 5.1 demonstrates the workflow progression utilized in this chapter.

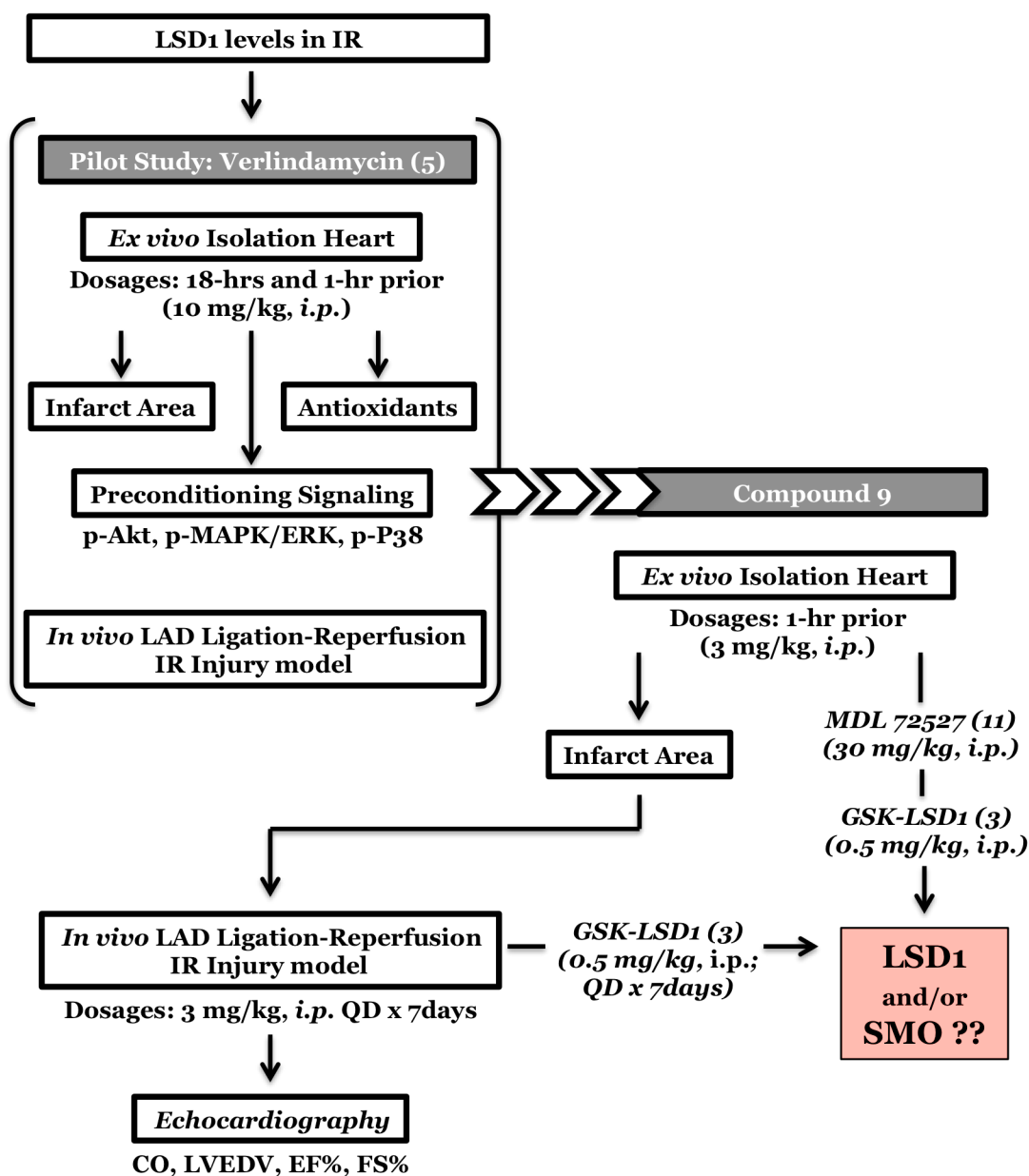


Figure 5.1. Chapter 4 workflow chart and preclinical testing of compound 9. A pilot study was performed with a known LSD1 inhibitor, verlindamycin (5). From this, preclinical testing of lead compound 9 was performed using two murine models of IR injury. Additional studies were performed with MDL72527 (compound 11), an SMO-specific inhibitor, and GSK-LSD1 (compound 3), an LSD1-specific inhibitor. IR = ischemia-reperfusion, LAD = left anterior descending coronary artery, QD = per day, *i.p.* = intraperitoneal, CO = cardiac output, LVEDV = left ventricular end diastolic volume, EF% = ejection fraction, FS = fractional shortening, SMO = spermine oxidase

Goals of Chapter 5:

- 1.) *Assess the levels of LSD1 during IR injury and its correlation to severity of cardiac dysfunction.*
- 2.) *Pilot study: Determine if the pan-amine oxidase inhibitor, verlindamycin, protect the heart from IR damage.*
 - a. *Does verlindamycin reduce infarction?*
 - b. *If so, is this preconditioning through the RISK pro-survival signaling pathway?*
 - c. *Does LSD1 inhibition increase antioxidants, such as catalase?*
- 3.) *Determine the efficacy of novel 3,5-diamino-1,2,4-triazole (9) to sustain cardiac function and structure, similar to the results found in our pilot study.*
- 4.) *Use SMO and LSD1-specific irreversible inhibitors to reveal the mechanism of action of compound 9 and identify LSD1 as a novel therapeutic target in CVD.*
- 5.) *Observe chronic cardiac remodeling in a more clinically relevant model of IR injury.*

II. RESULTS

LSD1 protein is increased within infarcted tissue following IR injury and levels of protein expression correlate to severity of cardiac contractile dysfunction:

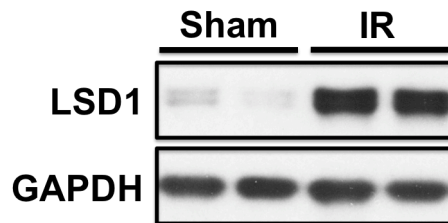
The induction of LSD1 activity by hypoxia has previously been shown in carcinogenesis¹⁸⁵ and DNA mismatch repair silencing by CoREST/HDAC/LSD1 corepressor complexes.¹⁸⁶ Interestingly, Zhang *et al.* were the first to show that LSD1 expression itself was responsive to transient global cerebral ischemia.¹⁸⁷ They demonstrated that LSD1 spatially and temporally increased in response to IR in the brain.¹⁸⁷ Therefore, we aimed to evaluate the expression status of LSD1 in response to IR injury.

The left anterior descending coronary artery (LAD) in CD1 mice was surgically ligated for 40-mins as described earlier. (**Chapter 2, “Left anterior descending coronary ligation-reperfusion *in vivo* IR”**). After 7-days post IR surgery, the infarcted tissue distal to the LAD ligation was homogenized and immunoblotted for LSD1. Similar to the induction of LSD1 previously reported by cerebral IR¹⁸⁷, we saw a significant increase in LSD1 protein (**Figure 5.2A**).

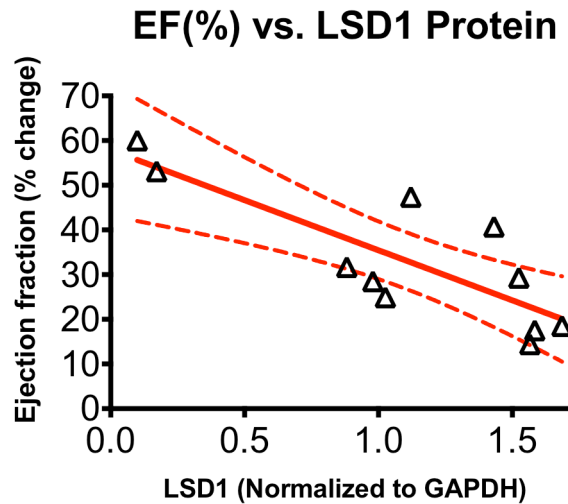
We also were interested in the correlation between LSD1 protein expression and cardiac function. In order to determine any correlation between the two, we analyzed infarcted tissue from mice after 5-days, 7-days, and 14-days post LAD ligation. Echocardiograph data of ejection fraction and LV end diastolic volume were observed and compared to individual LSD1 protein levels. A scatterplot of cardiac function vs. LSD1 protein was graphed (**Figure 5.2B-C**). In hearts demonstrating more detrimental cardiac function (i.e. reduced ejection

fraction and increased LV dilation), more abundant LSD1 protein was present. A nonparametric Spearman correlation analysis was performed (GraphPad Prism6). In comparison to LSD1 protein expression, ejection fraction and LV end diastolic volume demonstrated Spearman correlation coefficients of -0.7636 (95% confidence interval -0.9377 to -0.2835, p-value 0.0098) and 0.7909 (95% confidence interval 0.3456 to 0.9455, p-value 0.0055), respectively. A linear regression of the correlation study successfully showed a significant deviation of the slope from zero (p-value=0.0024 and 0.0067, respectively). Therefore, these results indicate that an increased expression of LSD1 is correlated with larger LV dilation and lower EF.

A.



B.



C.

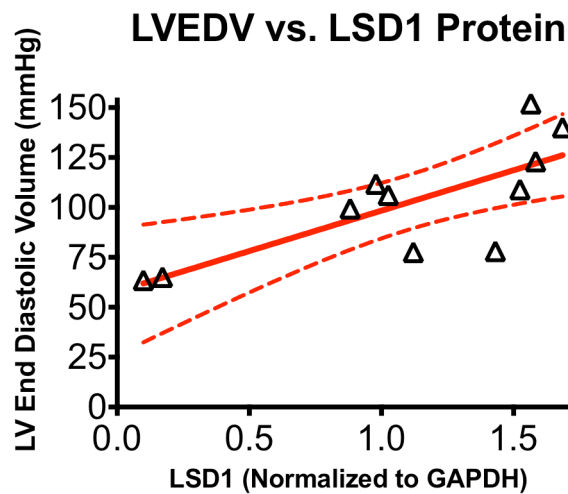


Figure 5.2. LSD1 increases within the infarction following IR. (A) LSD1 in 7-day lysates following LAD ligation-reperfusion. (B) Correlation of ejection fraction vs. LSD1 protein (C) LV end diastolic volume vs. LSD1 protein. Each data point represents one mouse. Spearman $r = -0.7636$ (EF vs. LSD1); $r = 0.7909$ (LVEDV vs. LSD1)

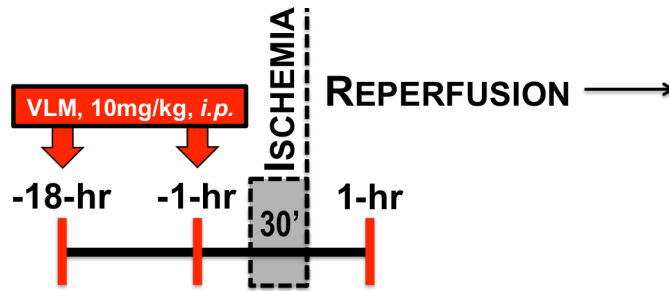
Pilot study – Verlindamycin sustains cardiac function and reduces infarct area following IR injury:

In order to determine whether LSD1 inhibition could blunt myocardial IR injury, we conducted a pilot study using a known LSD1 inhibitor. Our lab published the design of a noncompetitive, (bis)biguanide oligoamine derivative (Verlindamycin, VLM; **Chapter 1, Figure 1.12, Compound 5**) as a potent inhibitor of LSD1, which causes significant increases in global histone methylation.¹⁸⁸ To test our hypothesis, we used an *ex vivo* isolated heart model of cardiac ischemia-reperfusion injury (**Chapter 2; Langendorff *ex vivo* retrograde perfusion isolated hanging heart model**). This model was beneficial because it is highly reproducible and within self-sustaining cardiac tissue. Male Sprague-Dawley rats were treated with VLM (10mg/kg, *i.p.*) at 18- and again at 1-hr prior to excision of the heart onto the retrograde perfusion apparatus as previously described. A saline-filled balloon attached to a pressure transducer was inserted into the left ventricle (LV) and cardiac pressure traces were obtained. Following 10-minutes of baseline function, transient global ischemia was performed for 30-minutes, followed by reestablishment of retrograde flow for 1-hour (**Figure 5.3A**). Hearts treated with verlindamycin maintained left ventricular developed pressure (LVDP) due to its improvement of end diastolic pressure (LVEDP, **Figure 5.3B**). LV end systolic pressure did not change between treatment groups. This experimental observation was reproduced with tranilcypromine (**2**), a less potent LSD1 inhibitor. Therefore,

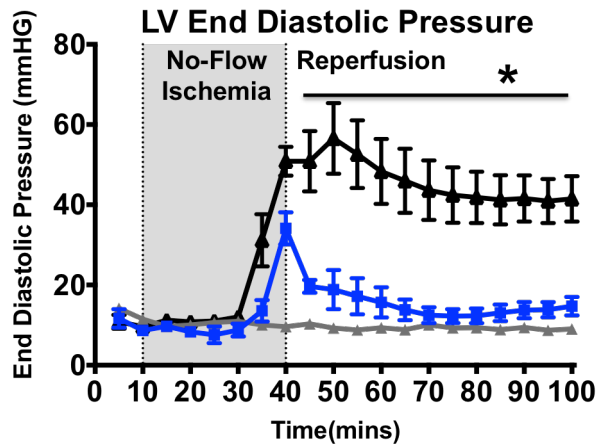
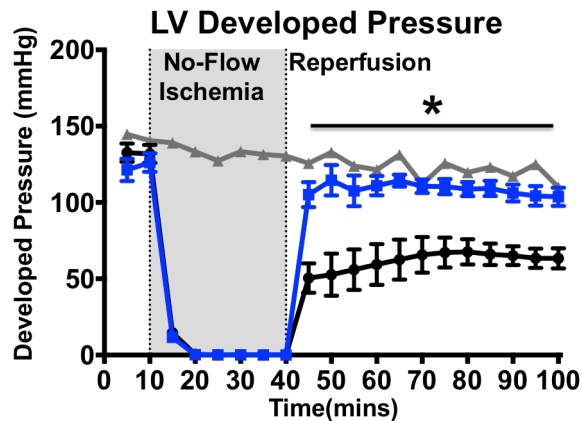
two LSD1 inhibitors with different mechanisms of action produced an acute functional protection in the isolated heart model.

In addition, we also demonstrated that both LSD1 inhibitors decreased infarct area when the hearts were transverse sectioned into 2-mm slices and incubated in 1% 2,3,5-triphenyltetrazolium chloride (TTC) for damaged tissue (**Figure 5.4**). In brief, TTC is enzymatically reduced in metabolically active cell dehydrogenases, forming a visible red dye. Therefore, tissue that shows white areas are considered necrotic or infarcted tissue. VLM and tranilcypromine both showed significantly less infarcted tissue than vehicle-controlled hearts.

A.



B.



▲ No IR (n=2) ● Vehicle (n=6) ■ VLM (n=6)

Figure 5.3. Verlindamycin; contractile recovery upon reperfusion in isolated male rat hearts after 30mins ischemia. (A) Timeline VLM treatments prior to heart isolation. (B) A saline-filled balloon fixed to a pressure transducer attached in the LV measured contractile function. Experimental groups (n=6) were injected 18hrs and 1hr prior to ischemia with 10 mg/kg, *i.p.* VLM or DMSO Vehicle. * $p < 0.001$. Mean \pm SEM.

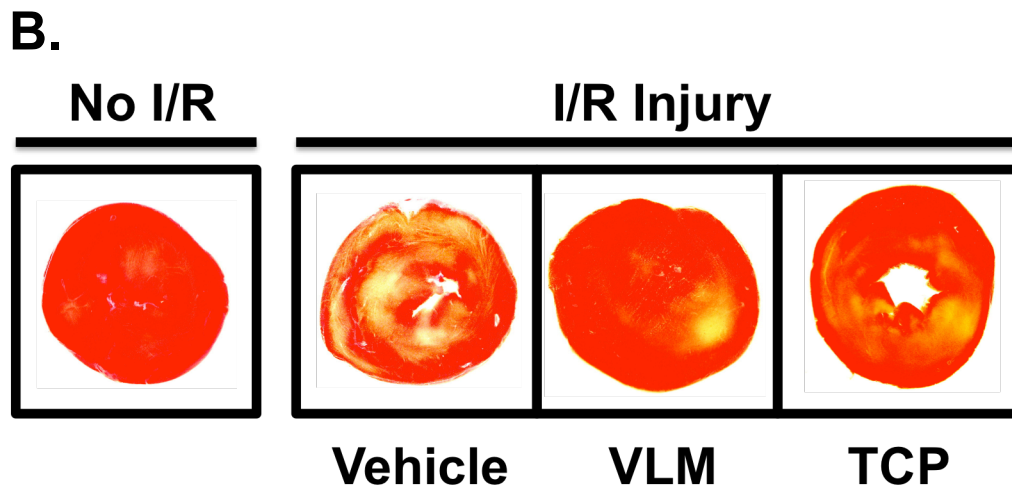
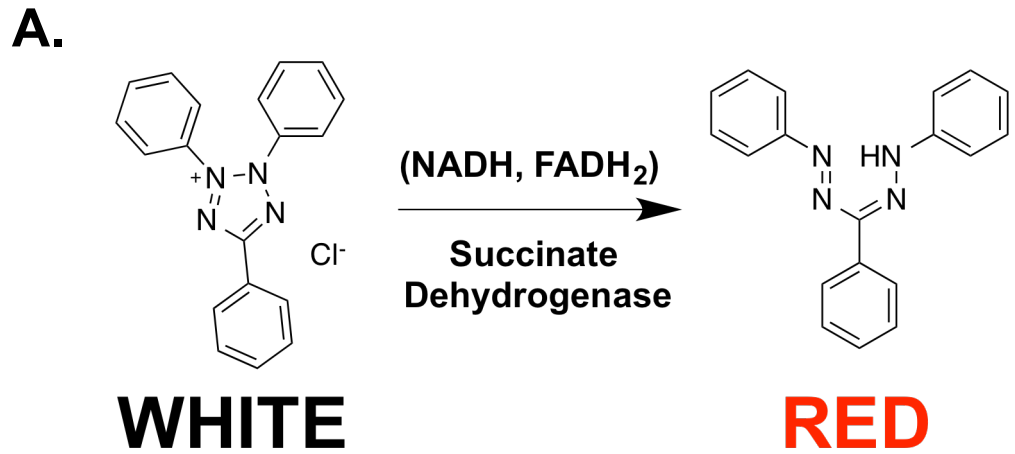


Figure 5.4. Infarct area in isolated rat hearts treated with LSD1 inhibitors. (A) Triphenyltetrazolium chloride (TTC) is a soluble redox indicator dye that is enzymatically converted by metabolically active, or live, cells to a red dye. Lack of staining (i.e. white) indicates infarction. (B) Following IR, rat hearts were sliced in 2-mm sections and incubated with 1% TTC at 37°C for 15mins and then fixed in formalin prior to photomicrography.

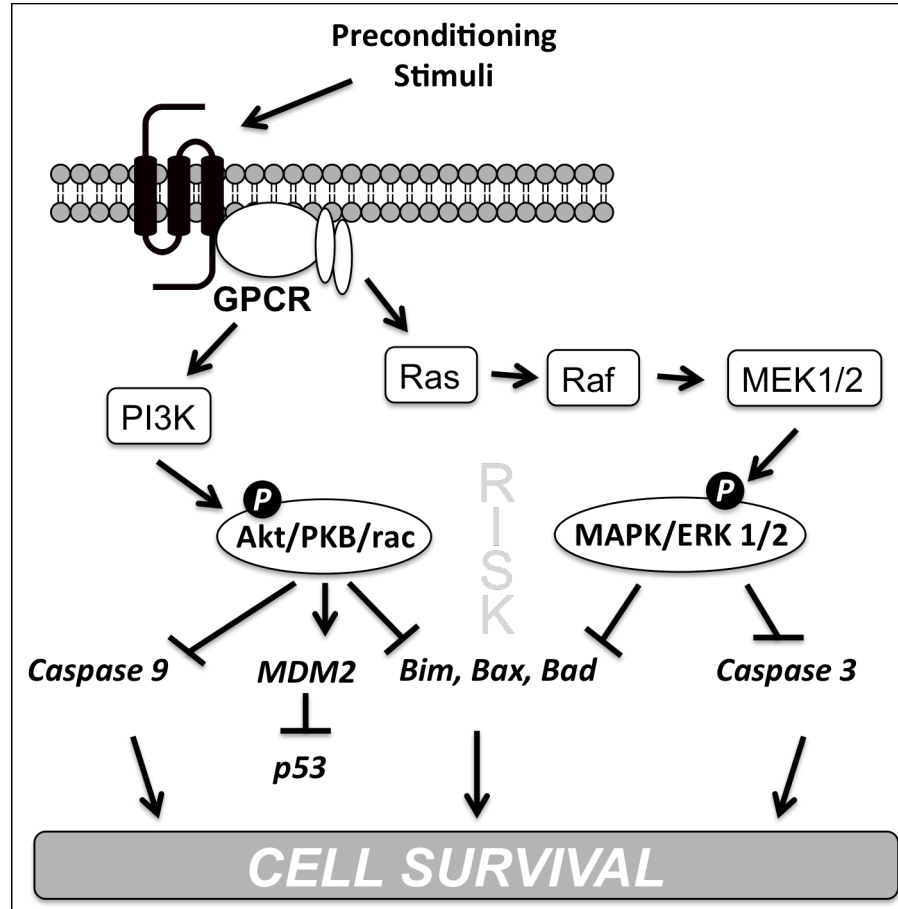
Pilot study – Verlindamycin treatment preconditioning of the heart was not achieved via the canonical RISK signaling pathway:

Verlindamycin (VLM) sustained cardiac function and reduced infarction in pretreated rats. This led us to hypothesize that LSD1 may be upregulating by traditional survival preconditioning signaling in cardiomyocytes. This includes activation of PI3K and its downstream targets Akt, p70S6K, and ERK1/2. These kinases are deemed the Reperfusion Injury Survival Kinase (RISK) pathway.¹⁷⁹

Following the 1-hour of reperfusion, the Langendorff hearts were homogenized for protein analysis and immunoblotted for activation of key kinases in the RISK pathway. All of the kinases downstream of PI3K signaling are activated through dual phosphorylation of serine and/or threonine residues. Therefore, we aimed to see if preconditioning by VLM caused increases in phosphorylation. Interestingly, p-Akt and p-MAPK/ERK were not changed in VLM-treated hearts when normalized to the loading control GAPDH (**Figure 5.5**).

Another focus in ischemic preconditioning has been on p38 MAPK signaling. However, its role still remains controversial because of the differential biological functions of various isoforms. The two primary isoforms found in the heart are p38 α and p38 β (**Figure 5.6A**). P38 α is thought to mediate apoptosis, whereas p38 β activation can lead to cardioprotection and anti-hypertrophic.¹⁸⁹ We found that VLM increased phosphorylation at threonine-180 and tyrosine-182 of p38 β by 6-fold as compared to non-treated IR hearts (**Figure 5.6B**).

A.



B.

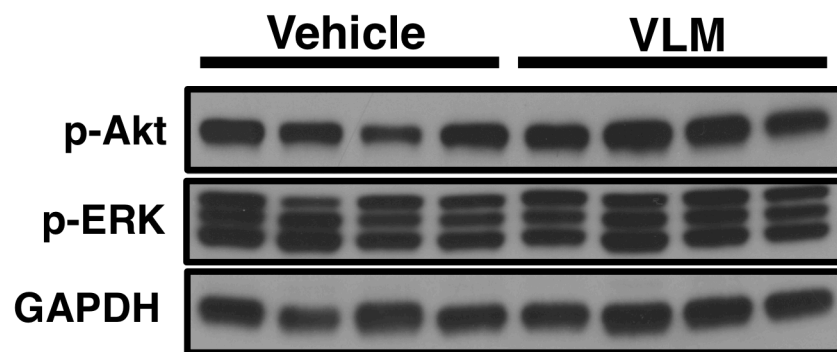
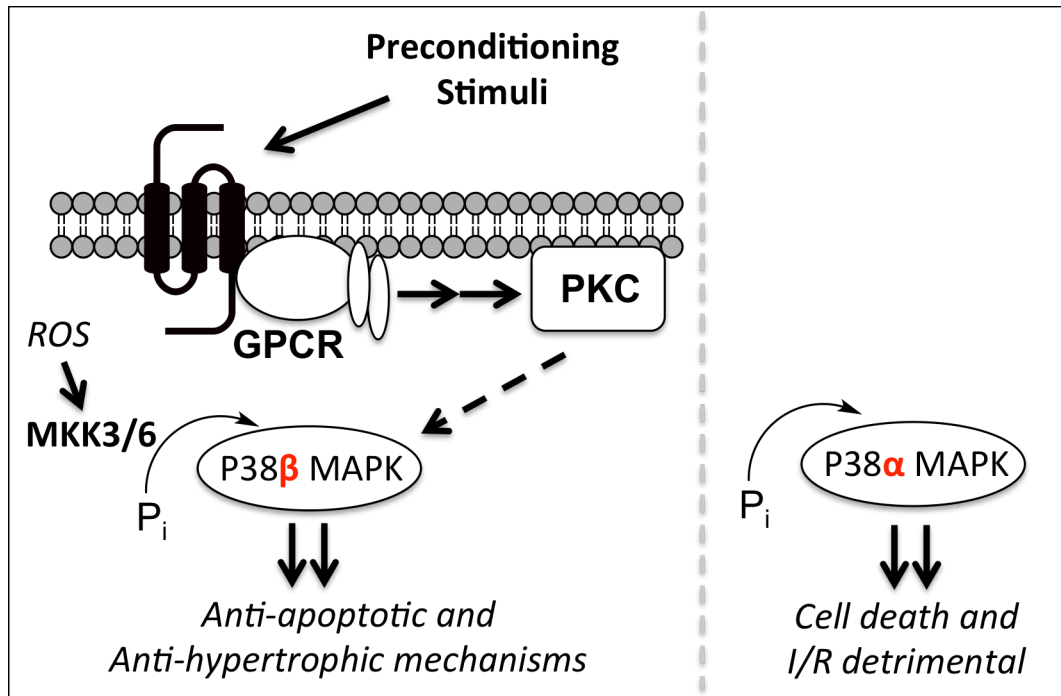


Figure 5.5. RISK survival signaling during IR injury. (A) RISK signaling. (B) Western blot of phosphorylation of Akt and ERK, both activating modifications in RISK signaling. Densitometry showed no significant differences between wells.

A.



B.

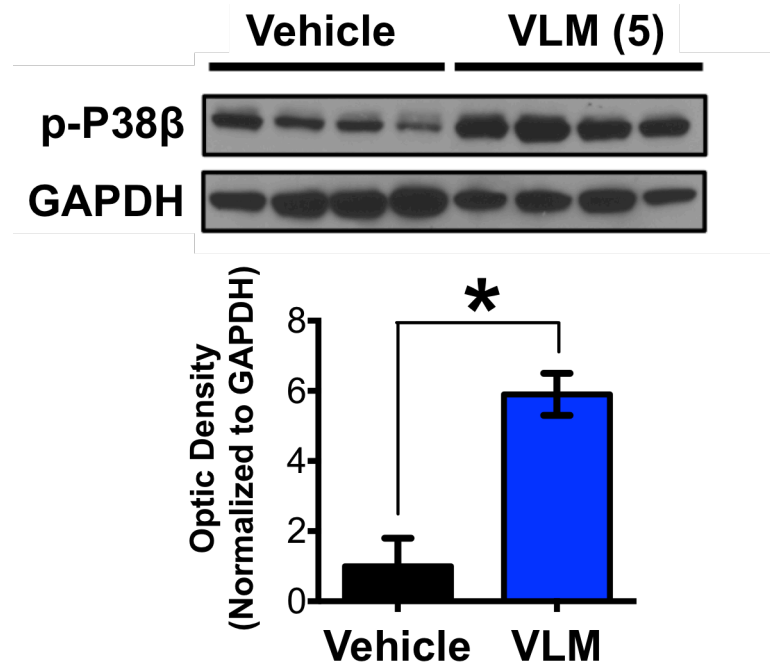


Figure 5.6. Isoform-specific roles of p38 during IR injury. (A) p38 signaling (B) Western blot of phosphorylation of p38 β . Densitometry showed a 6-fold increase in p-P38 in drug treated. N=4, * p-value < 0.05

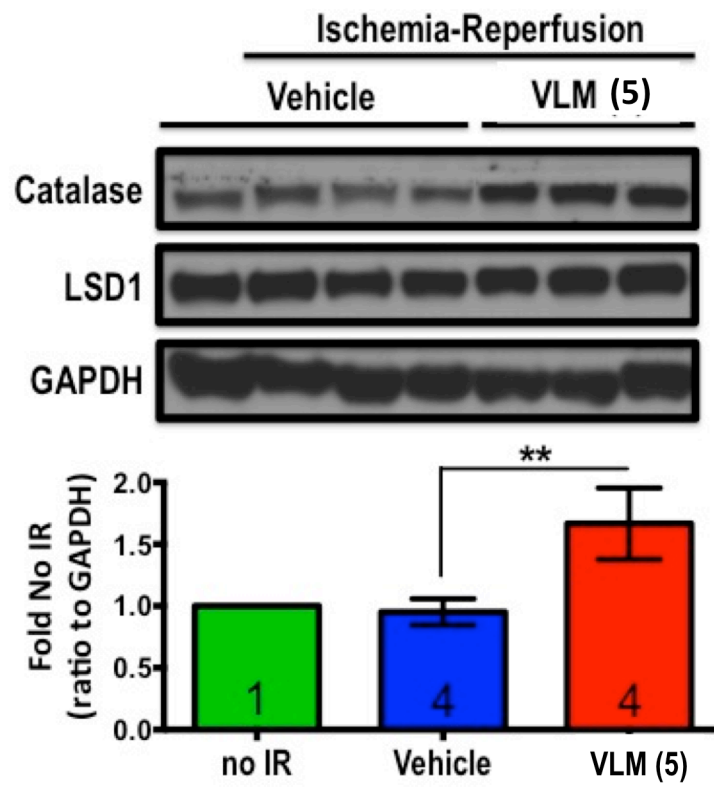
Pilot study – Pretreatment with verlindamycin increased endogenous antioxidants:

Since a high influx of reactive oxygen species, including H₂O₂, takes place during IR injury, increasing the general antioxidant milieu, in theory, should limit the amount of oxidative damage caused during IR injury. One such antioxidant enzyme, catalase, reduces hydrogen peroxide (H₂O₂) to water and molecular oxygen. In order to determine any changes in catalase levels, rat hearts from our pilot study were homogenized and resolved by Western blotting (**Figure 5.7A**). VLM increases endogenous catalase protein during IR injury by nearly 80%.

Pilot study – Evaluate histone methylation changes by verlindamycin:

In vitro studies in cancer have shown a dose-dependent global increase in histone methylation (i.e. H3K4me₂) with VLM.¹⁸⁸ However, these studies were performed in cells that are highly responsive to LSD1 inhibition. We aimed to evaluate whether global changes in histone methylation could be observed in our pilot study. In particular, because VLM treatment caused an increase in endogenous catalase, we hypothesized that this phenomenon was due to inhibition of LSD1/CoREST/HDAC1 corepressors, resulting in increased catalase expression. Contrary to this, western blot analysis of histone modifications indicated that globally, no change in H3K4me₂ was resolved (**Figure 5.7B**).

A.



B.

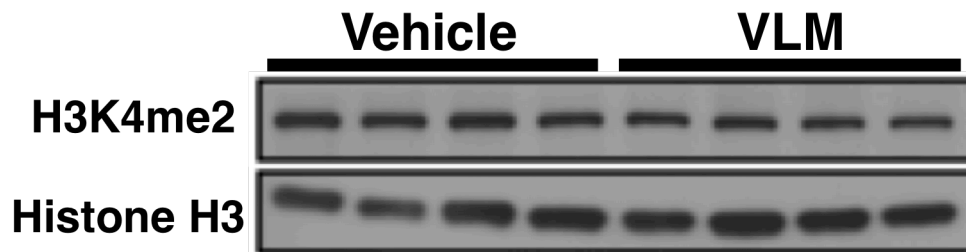
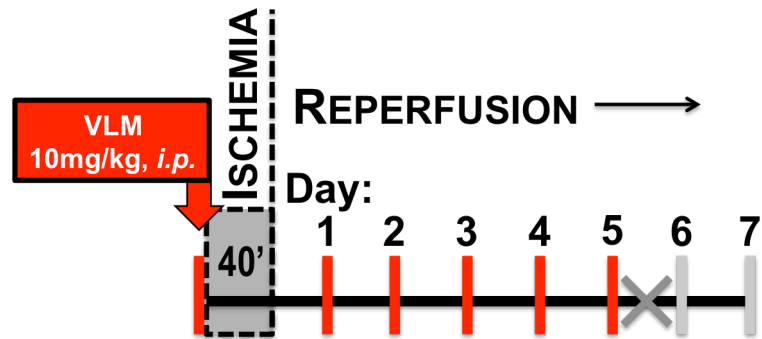


Figure 5.7. Antioxidant quantity and global histone methylation. (A) Western blot of endogenous catalase protein quantity and associated densitometry with ImageJ. (B) Western blot of global histone 3, dimethyl lysine 4 residue. N=4, ** p-value < 0.01. Mean \pm SEM.

Pilot study – in vivo analysis of long-term cardiac function with VLM treatment:

Since a significant improvement of cardiac function and infarction took place with pretreated mice, our next study looked at more chronic outcomes of VLM treatment. Because of the limitations in the isolated heart model, we designed an experiment using an *in vivo* IR model, as described earlier (**Chapter 2, “Left anterior descending coronary ligation-reperfusion *in vivo* IR”**). CD1 mice were treated with 10mg/kg, *i.p.* VLM at onset of ischemia and then daily (**Figure 5.8A**). The injections were planned for 1-week to allow for significant cardiac remodeling, fibrosis, and eccentric hypertrophy to take place. However, after 5-days, the mice experienced abdominal distension from a hypogastric exudate. Thus, due to the apparent toxic adverse events of the compound, the study was terminated two days early. An echocardiogram was still performed to assess cardiac function. Our data failed to show any significance in VLM-treated versus vehicle controls, but were trending towards a recovery of cardiac function (**Figure 5.8B**). Only a sample size of 2-3 mice per experimental group was performed in this pilot study.

A.



B.

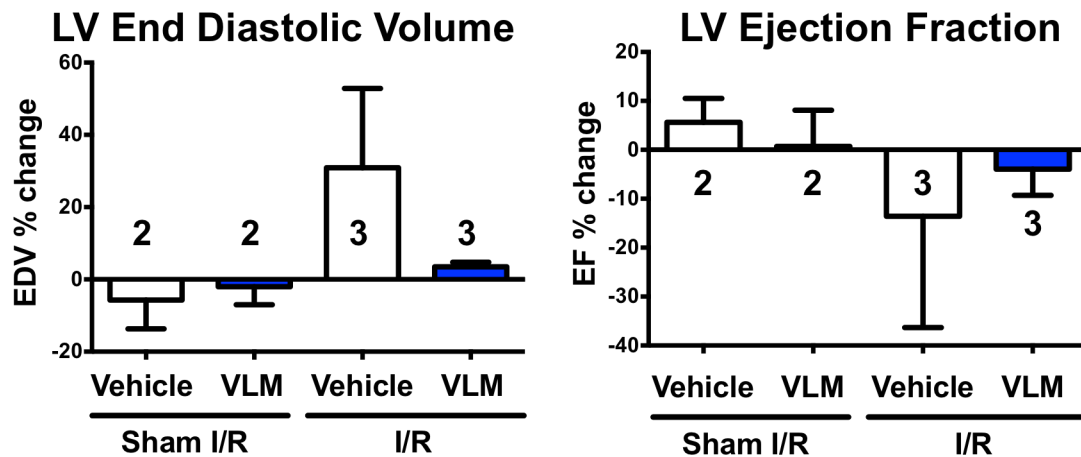


Figure 5.8. Verlindamycin (VLM) in chronic *in vivo* IR injury. (A) Timeline of drug treatments. VLM (3 mg/kg, *i.p.*) was injected independently at onset of ischemia and daily for 5 days. The experiment was cut short to 5-days instead of the planned 7-days due to toxicity of the compound. (B) Male CD1 mice were anesthetized by 3% isoflurane vaporized in 100% O₂. The left anterior descending coronary artery was ligated with 6-0 silk suture and PE-10 tubing for 40-min prior to reperfusion. Functional analysis of the heart was performed by echocardiograph. Heart function analysis was performed by long-axis and short-axis views using a modified Simpsons method. All p-values were <0.05 and thus not significant. Mean ± SEM.

Pilot Study – VLM facilitates cardioprotection by early-onset acute mechanisms:

Our initial experiments with VLM were performed with two intraperitoneal injections (10mg/kg), at 18-hours and 1-hour prior to heart isolation (**Figure 5.3A**). Thus, VLM treatments covered both early and late preconditioning mechanisms. As such, VLM-mediated cardioprotection could be via canonical LSD1 transcriptional regulation or acute post-translational modification (PTM) of signaling cascades. In order to investigate which mechanism (i.e. acute PTM or transcriptional) was being modulated, we performed additional experiments with VLM administered at only 1-hour prior to Langendorff preparation. Interestingly, these results were very comparable to our pilot study that involved two injections, indicating acute LSD1 inhibition could sustain cardiac function (**Figure 5.9**). Therefore, this result suggests LSD1 modulation of immediate-early genes by PTMs in signal transduction cascades may be facilitating the acute cardioprotection in our *ex vivo* model.

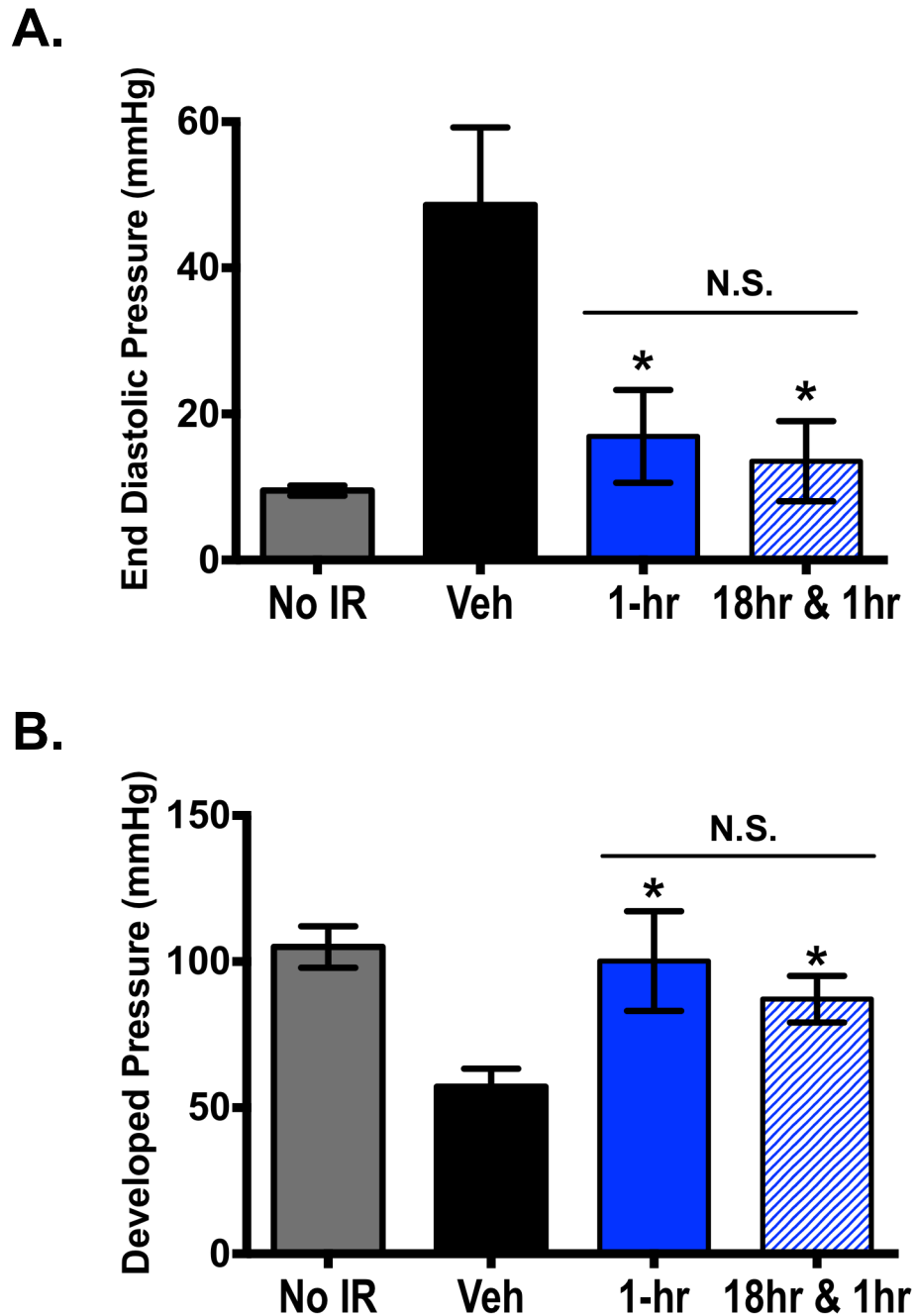


Figure 5.9. Verlindamycin (VLM) treatments at 1-hr are comparable to 18hr/1hr treatments. Contractile recovery upon reperfusion in isolated male rat hearts after 30mins ischemia. (A) End diastolic pressure and (B) LV developed pressure were measured. Experimental groups (n=3-6) were injected either 1.) 1hr prior to ischemia with 10 mg/kg, *i.p.* with compound VLM or 2.) twice at time points 18-hrs and 1-hr prior to heart excision. *p<0.001. Mean ± SEM.

The utility of VLM as a cardiac drug and to study LSD1 was limited by its cytotoxicity and off-target effects. To sufficiently evaluate the role of LSD1 in IR, we dedicated the remainder of our physiologic studies to a more attractive cardiac drug candidate, N³-(2-chloro-6-phenoxybenzyl)-4H-1,2,4-triazole-3,5-diamine.

Novel 3,5-diamino-1,2,4-triazole compound 9 improves acute cardiac function:

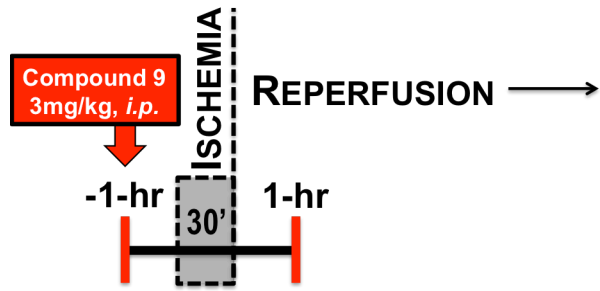
Our preliminary *ex vivo* data with VLM showed substantial promise for an LSD1 inhibitor as a cardioprotective agent. However, because of the extensive off-target effects of VLM (**Chapter 4, Table 4.1**), the exact mechanism of protection by VLM could not be ascertained. In addition, VLM caused extensive toxicity after 5-days of treatment. Because of these limitations, we aimed to utilize a more selective, more potent and less cytotoxic compound as a tool to understand the role of LSD1 in IR injury.

We began our evaluation using the reversible inhibitor, **9**, in the *ex vivo* IR model (**Figure 5.10A**). In particular, **9** shows improved selectivity for LSD1 at lower doses and precludes the off-target effects on monoamine oxidases (**Chapter 4, Table 4.1**). Because we did not know the toxicity of **9** at the time (i.e. prior to the toxicology results shown in **Chapter 4**), we chose an acute IR model where **9** was administered 1-hour before heart isolation (**Figure 5.10A**). A dose-response curve was generated to determine the dosage of **9** (not shown). We found that 3mg/kg treatment was sufficient to maintain LVEDP ($87.14 \pm 4.6\text{mmHg}$ vs. $57.16 \pm 2.8\text{mmHg}$ in vehicle treated) and LVDP ($26.70 \pm 3.9\text{mmHg}$

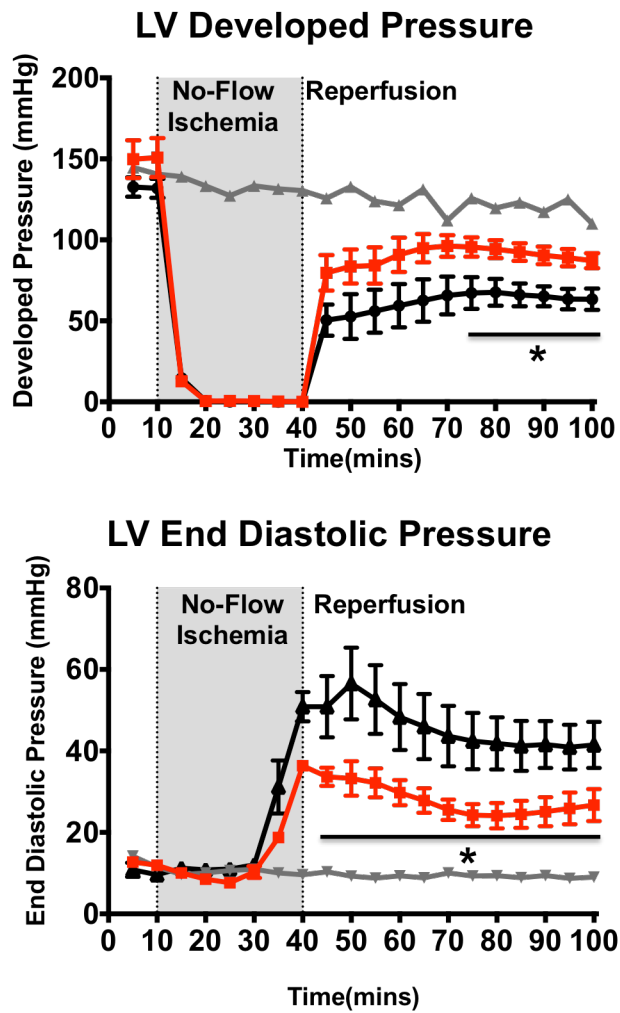
vs. 48.6 ± 5.3 mmHg in vehicle treated) after 60-minutes reperfusion following transient global IR (**Figure 5.10B**). Interestingly, when the pressure traces of **9** treated rats were examined closer during the anoxia phase, there was a significant delay in the onset of ischemic rigor contracture (**Figure 5.11**). The EDP after 30-min of ischemia was 39.17 ± 2.5 mmHg in **9** treated rats, a significant reduction from 52.31 ± 2.5 mmHg in vehicle treated. As projected by a nonlinear regression (GraphPad Prism6, sigmoid curve, variable slope), the delay in onset of peak rigor-contraction is approximately 10-minutes. This result indicates the acute energetics and/or Ca^{2+} -balance in the cardiomyocytes were improved and thus, suggests that LSD1 inhibition may be influencing their response to anoxia.

Finally, Infarct area was also assessed, as previously performed with our VLM pilot study. We stained 2-mm transverse sectioned hearts with 1% TTC. Compound **9** significantly reduced the infarct area and was equivalent to the results seen with VLM (**Figure 5.12**).

A.



B.



— No IR (n=2) — Vehicle (n=6) — Compound 9 (n=4)

Figure 5.10. Compound 9; contractile recovery upon reperfusion in isolated male rat hearts after 30mins ischemia. Contractile function measurements in the LV. Experimental group (n=4) were injected 1hr prior to ischemia with 3 mg/kg, *i.p.* with compound 9. * $p < 0.001$. Mean \pm SEM.

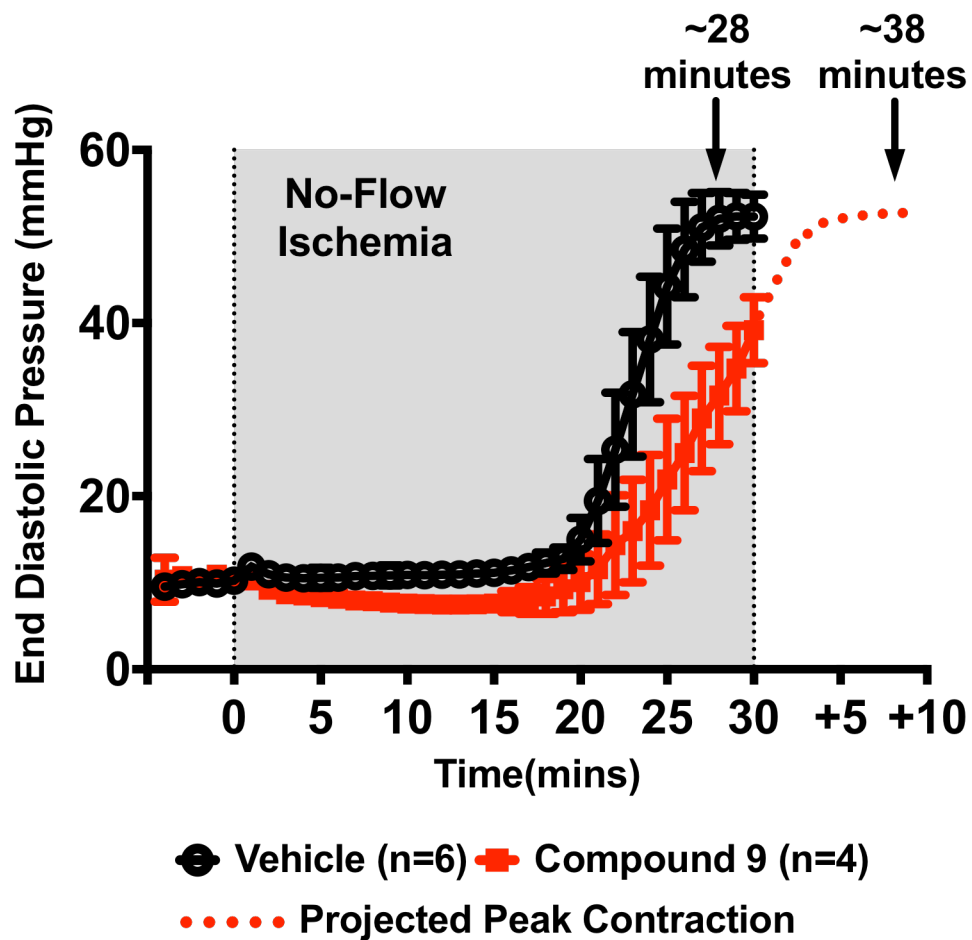


Figure 5.11. Compound 9; Hypoxia-induced rigor contracture. Pressure trace of end diastolic pressure in compound 9 treated rats. The dotted red shows a projected peak rigor-contraction delayed by compound 9. Experimental group (n=4) were injected 1hr prior to ischemia with 3 mg/kg, *i.p.* with N3-(2-chloro-6-phenoxybenzyl)-4H-1,2,4-triazole-3,5-diamine. Vehicles (n=6) were injected with DMSO. * $p < 0.001$. Mean \pm SEM.

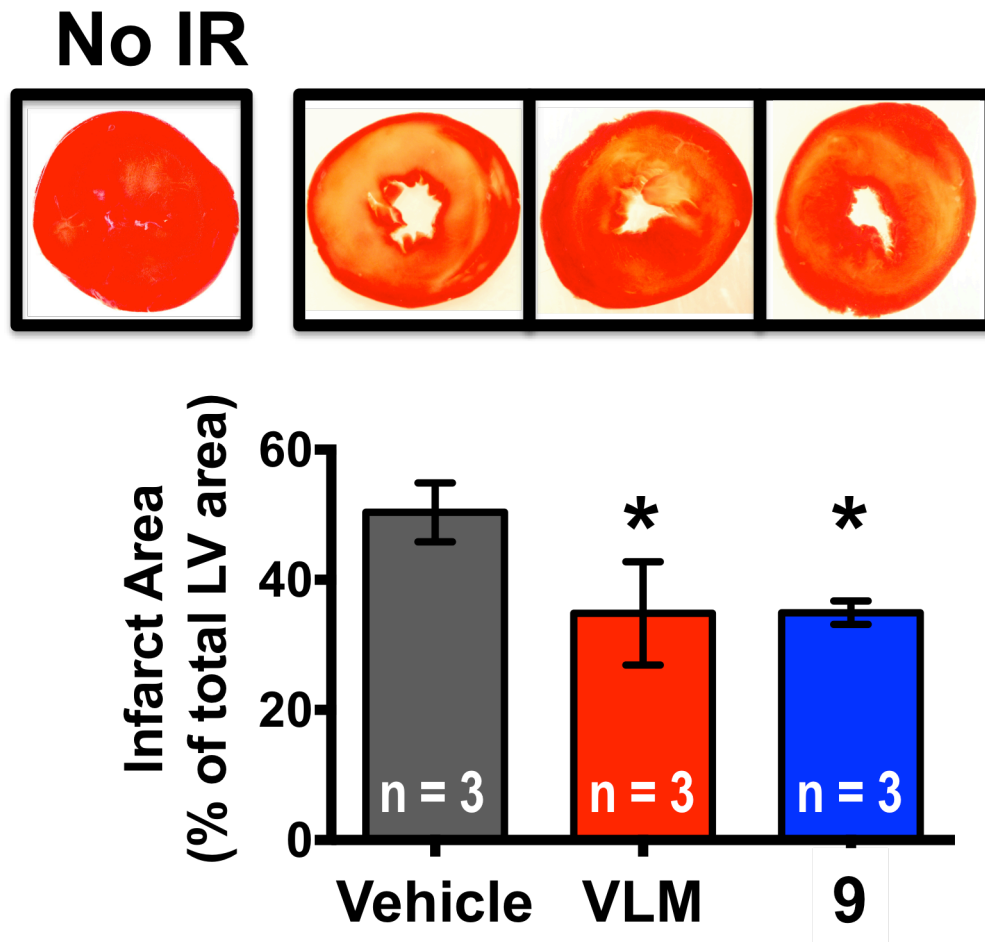


Figure 5.12. Infarct area in isolated rat hearts treated with LSD1 inhibitors. Following IR, rat hearts were sliced in 2-mm sections and incubated with 1% Triphenyltetrazolium chloride (TTC) at 37°C for 15mins and then fixed in formalin prior to photomicrography. The white area indicates zones of infarction. * p-value < 0.05, n=3. Mean ± SEM.

Dual inhibition of LSD1 and SMOx show cardioprotection from IR injury:

In vitro screening demonstrated that **9** inhibited both LSD1 and SMO activity (see **Chapter 4, Table 4.1**). Thus, it is difficult to dissect the individual roles of each enzyme in the protection afforded by **9**. We performed additional *ex vivo* Langendorff isolated heart experiments with compounds selective for each individual enzyme. For instance, MDL 72527 (compound **11**) is an SMO-specific inhibitor and does not inhibit LSD1 activity. Contrary, GSK-LSD1 (**3**) is a highly selective LSD1 inhibitor. Using each compound individually, we aimed to distinguish the importance of LSD1 versus SMO in **9**-mediated cardioprotection.

Sprague-Dawley rats were pretreated 1-hour prior to heart removal with GSK-LSD1 (0.5 mg/kg, *i.p.*). GSK-LSD1 is an irreversible inhibitor with a fast association constant. Therefore, it provided an effective method for confirmation of LSD1 in preconditioning. GSK-LSD1 pressure traces substantiated our results from **9** because they showed a significant recovery of LVEDP and LVDP (**Figure 5.13**). Interestingly, at a concentration nearly 6-fold less (i.e. 0.5 mg/kg vs. 3mg/kg), GSK-LSD1 had a profound effect on pressure values following transient global ischemia, with nearly a full recovery of function.

The results with GSK-LSD1, VLM, and **9** strongly suggested LSD1 was a viable target to improve cardiac function following IR. However, to eliminate doubt in the results seen by **9**, we performed a negative control with an SMO-specific inhibitor. MDL 72527 was injected (30 mg/kg, *i.p.*) 1-hour prior to excision of the heart. To our surprise, SMO inhibition had an overwhelming benefit in the isolated heart (**Figure 5.14**). Immediately following reperfusion, the

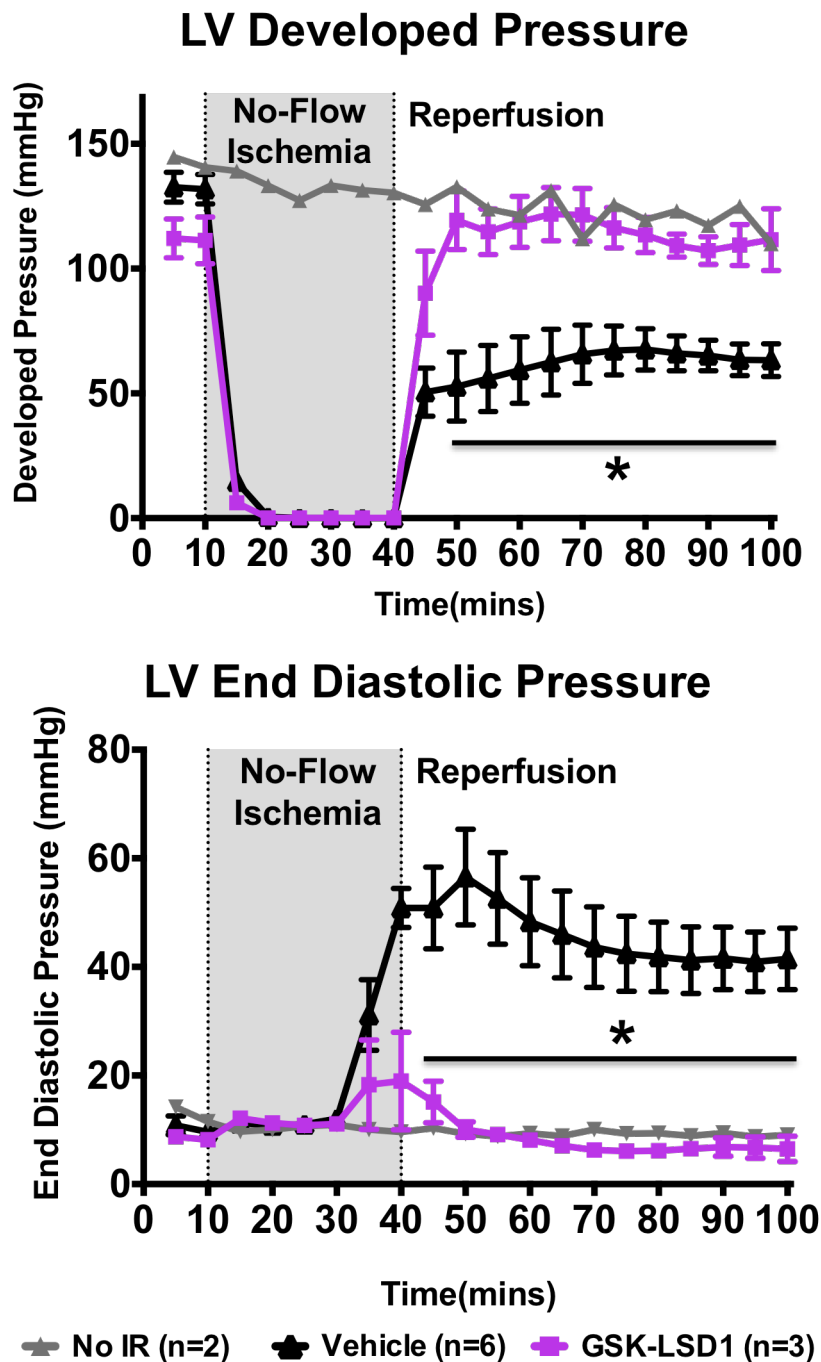


Figure 5.13. GSK-LSD1 (Compound 3); contractile recovery upon reperfusion in isolated male rat hearts after 30mins ischemia. A saline-filled balloon fixed to a pressure transducer measured contractile function. Experimental group (n=3) were injected 1hr prior to ischemia with 0.5 mg/kg, *i.p.* with GSK-LSD1. * $p < 0.001$. Mean \pm SEM.

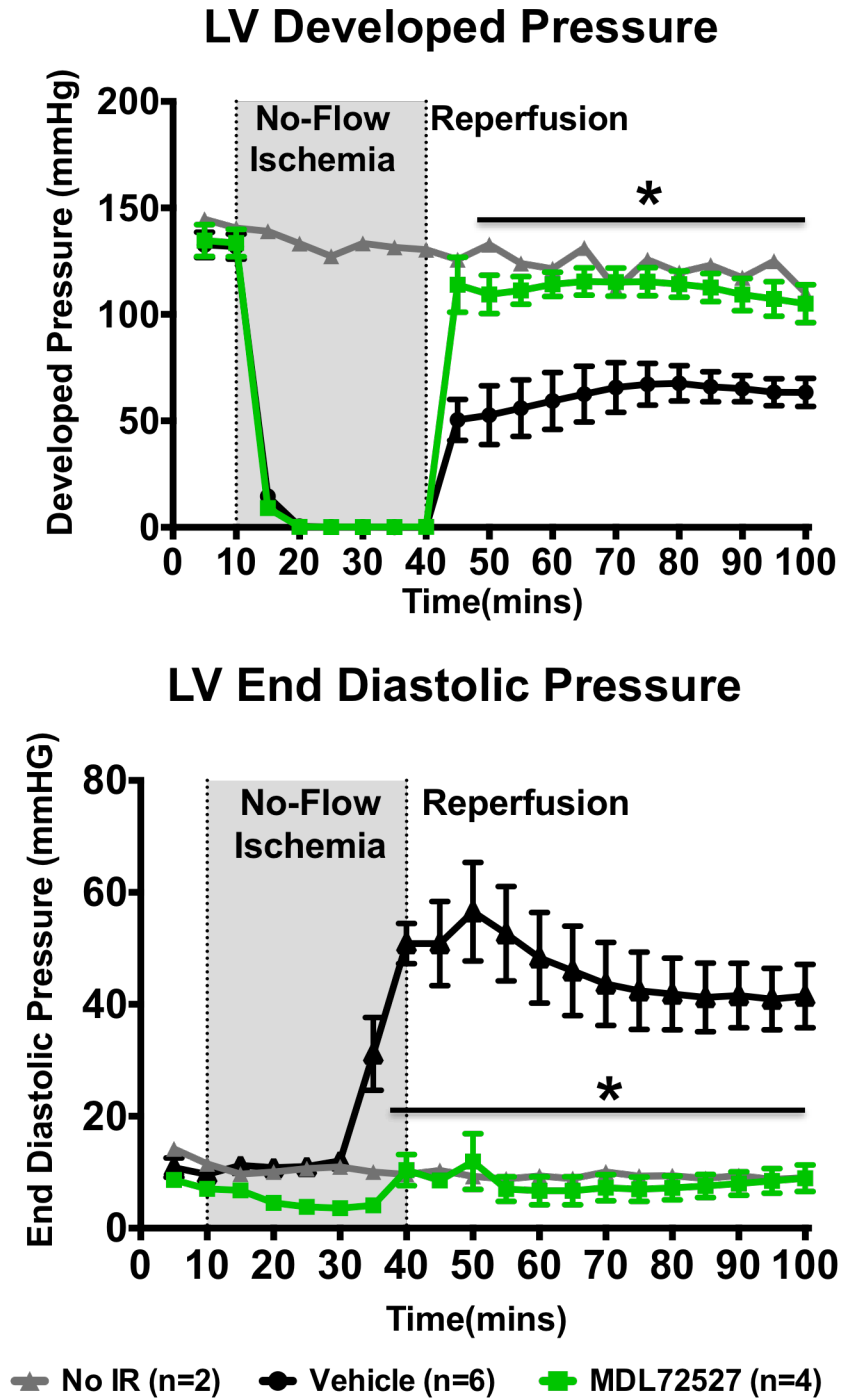


Figure 5.14. MDL 72527 (Compound 11); contractile recovery upon reperfusion in isolated male rat hearts after 30mins ischemia. A saline-filled balloon fixed to a pressure transducer measured contractile function. Experimental group (n=4) were injected 1hr prior to ischemia with 30 mg/kg, *i.p.* with MDL 72527. *p<0.001. Mean ± SEM.

heart pressure traces reflected values similar to our baseline measurements. Indeed, this implied that the **9** protective mechanisms might be through two separate pathways. Of particular interest, we observed similar delays in onset of peak rigor-contraction in both GSK-LSD1 and MDL72527 treatments. This suggests that the general catalytic mechanisms of the family of amine oxidases may be playing a collective role in acute energetics of cardiomyocytes. Therefore, further evaluation needs to be addressed to understand this phenomenon.

Despite the considerable improvement of functional pressure traces we observed with individually targeting LSD1 and SMO, our dual inhibitor compound **9** did not demonstrate a similar effect. In comparison, each inhibitor (i.e. compound **9**, MDL72527, GSK-LSD1, and VLM) improved LV developed pressure to 80-100 mmHg after 1-hour of reperfusion (**Figure 5.15**). In addition, they all sustained LV end diastolic pressure between 10-35 mmHg. Statistically, a one-way ANOVA with Tukey multiple comparisons for each experimental group showed no significant differences between each inhibitor.

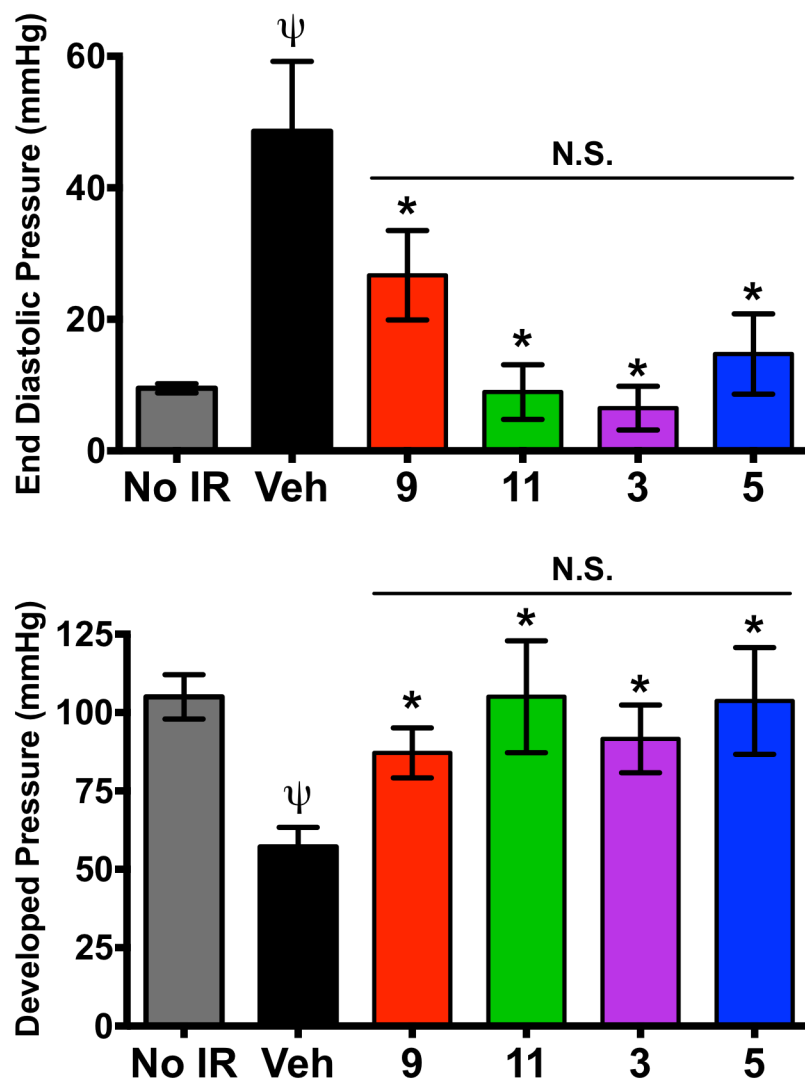


Figure 5.15. Left ventricle pressures of ischemic hearts following 60-minutes reperfusion. Experimental groups were injected 1-hour prior to heart removal for retrograde perfusion. Transient global ischemia was performed for 30-minutes. Compound **9** (3 mg/kg, *i.p.*); MDL72527, **11** (30 mg/kg, *i.p.*); GSK-LSD1, **3** (0.5 mg/kg, *i.p.*); Verindamycin, **5** (3 mg/kg, *i.p.*). ψ $p < 0.001$ Vehicle vs. No IR; * $p < 0.001$ Experimental Treatment vs. Vehicle; NS = no significance between experimental treatments. Mean \pm SEM.

LSD1 inhibition attenuates heart failure remodeling with reduced ejection fraction:

Chronic left ventricular remodeling takes place following reperfusion therapy following an AMI. In particular, fibrotic damage and eccentric hypertrophy lead to reduced ejection fraction and eventually heart failure (HFrEF). IR injury can potentiate heart failure with reduced ejection fraction. Therefore, we hypothesized that LSD1 inhibition could attenuate this effect.

CD1 mice underwent a surgical model of IR injury by reversible ligation of the left anterior descending (LAD) coronary artery. In short, the LAD was ligated with 6-0 silk suture and PE-10 tubing for 40-min prior to reperfusion. At onset of ischemia, compound **9** (3 mg/kg) or GSK-LSD1 (0.5 mg/kg) was injected intraperitoneal. The PE-10 tubing was removed to simulate reperfusion of the vasculature and the mouse was sutured for recovery. Two experimental groups of mice were injected daily with an LSD1 inhibitor, one set with compound **9** and the other with GSK-LSD1. A transthoracic echocardiogram was performed of heart function prior to surgery and following the 7-day course of treatments (**Figure 5.16**). Cardiac output, ejection fraction, fractional shortening, and LV end diastolic diameter were calculated as previously described. Interestingly, both LSD1 inhibitors better preserved the LV dilation expected from HFrEF (**Figure 5.17A**). In addition, a significant recovery in ejection fraction and cardiac output was observed (**Figure 5.17A and B**), as well as improved fractional shortening (**Figure 5.17B**). **Table 5.1** shows the absolute observed values 7-days after IR surgery. Overall, these results demonstrate a role for LSD1-targeted therapy in chronic heart failure remodeling.

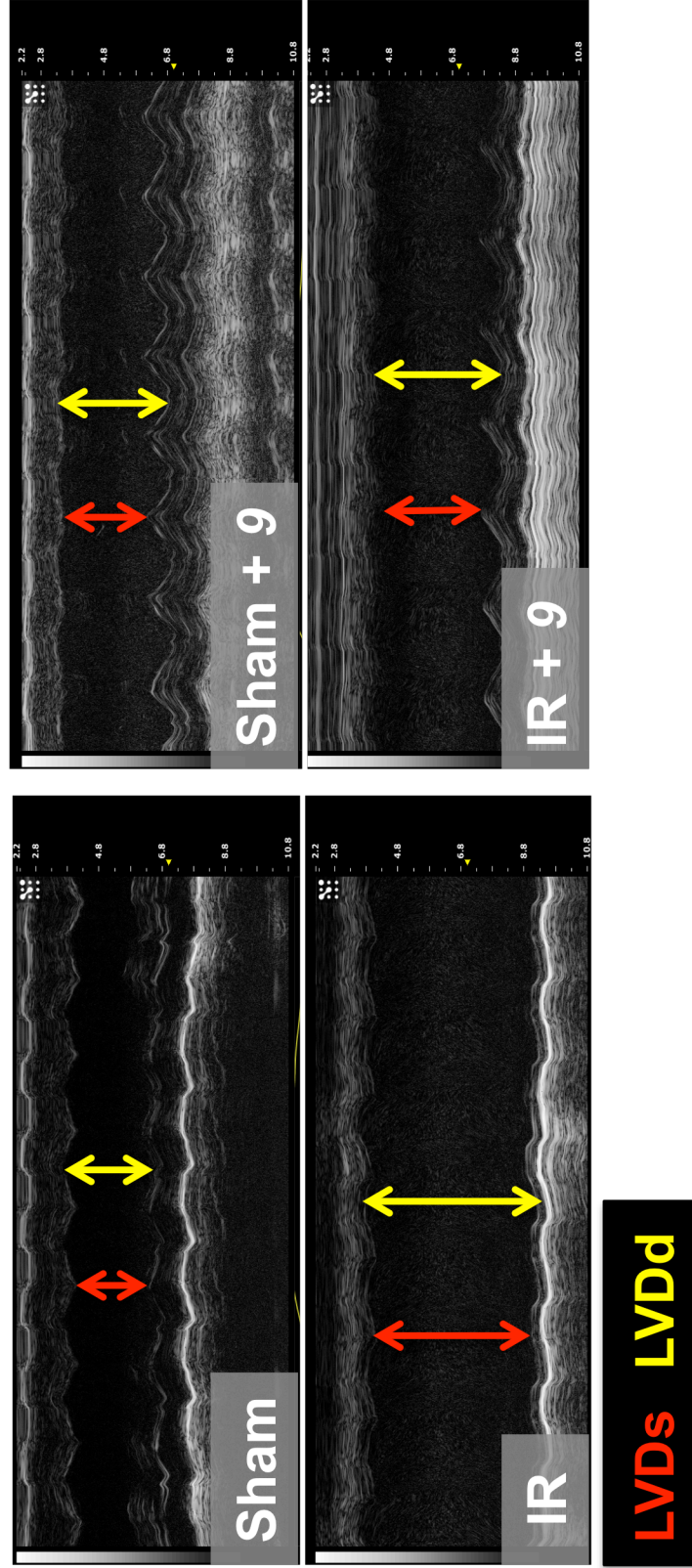


Figure 5.16. Transthoracic echocardiograms of 7-day IR study. The left anterior descending coronary artery was ligated for 40-min prior to reperfusion. Compound **9** (3 mg/kg; i.p.) was injected at onset of ischemia. Mice were injected daily with C1 for 1-week and analyzed by echocardiogram. Quantitative data for LVDs (red arrows) and LVDd (yellow arrows) are shown. Heart function analysis by long-axis and short-axis views using a modified Simpsons method before LAD ligation surgery and after 1- week post-surgery. Images represent echocardiograms. LVDs = Left Ventricular Diameter at Systole; LVDd = Left Ventricular Diameter at Diastole.

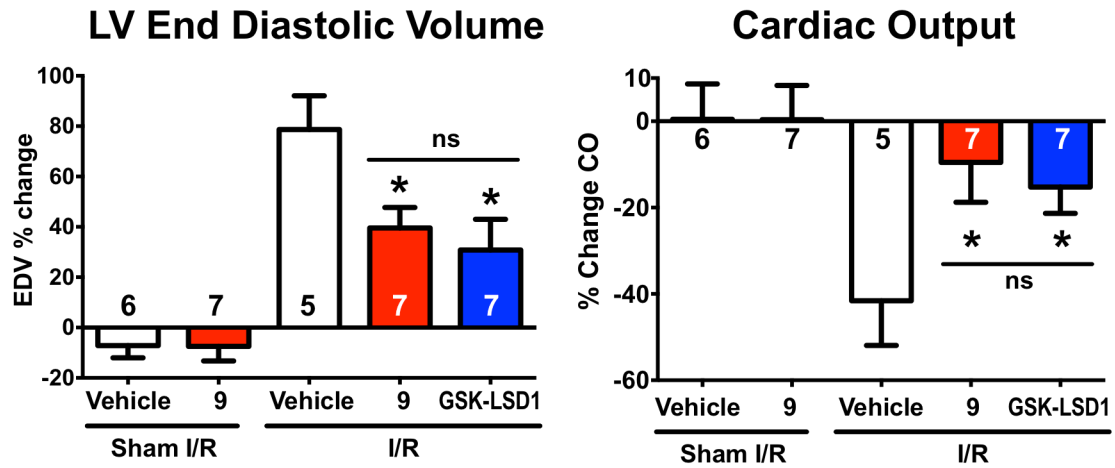
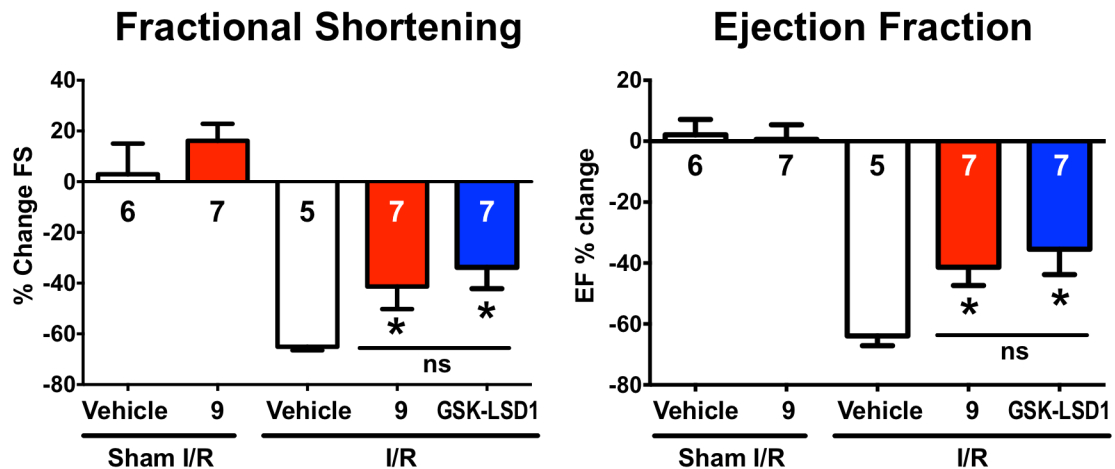
A.**B.**

Figure 5.17. Compound 9 and GSK-LSD1 reduction of chronic *in vivo* IR injury cardiac remodeling. Male CD1 mice were anesthetized by 3% isoflurane vaporized in 100% O₂. The left anterior descending coronary artery was ligated with 6-0 silk suture and PE-10 tubing for 40-min prior to reperfusion. Compound 9 (3 mg/kg; *i.p.*) and GSK-LSD1 (0.5 mg/kg, *i.p.*) were injected independently at onset of ischemia and daily for 7 days. Functional analysis of the heart was performed by echocardiograph. Heart function analysis was performed by long-axis and short-axis views using a modified Simpsons method. * P-value <0.05 vs. Vehicle Sham IR; ns = Compound 9 vs. GSK-LSD1. **Table 5.1.** shows the absolute values for these calculations. Percent change calculated by (Final value – Initial Value)/Initial Value x 100. Mean ± SEM.

Table 5.1. Absolute values 7days post-IR (mean ± SEM) of *in vivo* LAD ligation-reperfusion with LSD1 inhibitors.

	Baseline	Sham Surgery		Ischemia-Reperfusion Surgery	
		Vehicle	Compound 9	Vehicle	GSK-LSD1
	n=	6	7	5	7
LV End Diastolic Volume (mL)	72.35 ± 1.9	61.73 ± 2.5	62.54 ± 3.7	131.2 ± 6.2 *	103.3 ± 5.0 ¥
Cardiac Output (mL/min)	19.84 ± 0.8	19.98 ± 1.8	17.8 ± 0.7	12.14 ± 2.4 *	17.16 ± 0.7 ¥
Fractional Shortening (%)	25.53 ± 1.2	25.53 ± 1.8	29.44 ± 1.8	8.66 ± 1.3 *	12.11 ± 1.2 ¥
Ejection Fraction (%)	57.73 ± 0.9	60.32 ± 1.7	60.53 ± 2.2	19.24 ± 2.1 *	31.79 ± 2.2 ¥

mean ± SEM; ¥ p-value < 0.05 vs. IR vehicle; * p-value < 0.05 vs. Sham Vehicle

III. DISCUSSION

To date, no standard therapy exists that can mitigate the injury caused by reperfusing an occluded coronary artery after an AMI. In fact, up to 50% of total infarct damage is attributed to reperfusion injury.¹⁸⁰ Upon reperfusion, localized influx of oxidative stressors overwhelms the endogenous antioxidant systems and leads to contractile dysfunction and arrhythmias. Eccentric hypertrophy is a common outcome following an AMI.¹⁸⁰ In particular, diffuse dilation of the LV with reduced ejection fraction and cardiac output takes place following percutaneous coronary intervention after an AMI. Current therapies (e.g. ACE inhibitors, beta blockers, etc.) aim to prevent this chronic remodeling. In recent years, increasing evidence indicates that epigenetic enzymes such as the histone demethylases and deacetylases play crucial roles during CVD. One such enzyme, LSD1, is hypoxia-inducible¹⁸⁵ and regulates oxidative balance through epigenetic silencing of oxidative scavenging enzymes and production of hydrogen peroxide.¹⁹⁰ Yet, the role LSD1 and other demethylase enzymes play in cardiac IR has yet to be explored. Our goal was to identify LSD1 as a novel target to alleviate oxidative damage and cardiac remodeling during cardiac IR injury. In particular, we utilized our newly designed 3,5-diamino-1,2,4-triazolamine lead compound, **9**, and other amine oxidase-selective compounds to evaluate LSD1 in cardiac IR injury. The results presented in this chapter show supporting evidence that reveals a histone demethylase as a contributing factor to detrimental cardiac remodeling.

LSD1 and HDACs have been well characterized as cooperative enzymes.¹⁹¹ In fact, catalytic activity of one can improve the binding efficiency of

the other to its particular substrate. Forneris *et al.* showed that a synthetic 21-mer peptidomimic of H3 N-terminus with acetyl-lysine increased the K_m of LSD1 by 6-fold.¹⁹² In addition, many studies in cancer have shown *in vitro* changes in histone acetylation by an LSD1 inhibitor (or vice versa with methylation) or the sensitization of HDAC inhibition by means of LSD1 modulation.^{184-185, 193-194} Because there is a clear crosstalk between LSD1 and HDAC1/2, we were interested in the benefit seen by HDAC inhibitors in reducing myocardial IR damage^{182, 195} and the implications that LSD1 may also be contributory. Therefore, we aimed to test a well-characterized LSD1 inhibitor in two murine models of IR injury.

Our pilot study demonstrated that VLM, a noncompetitive inhibitor of LSD1 ($IC_{50} = 8 \mu M$), sustained cardiac function in an *ex vivo* isolated heart model (**Figure 5.3**). VLM showed a beneficial phenotype when injected intraperitoneal (3 mg/kg) at 1-hour prior to heart isolation. LV DP improved after reperfusion because of an attenuation of the rise in LV EDP. In addition, we demonstrated that total infarct area was reduced and that the preconditioning phenomenon was not by classical RISK pro-survival signaling (**Figure 5.4** and **Figure 5.5**). In fact, there was a significant increase in phosphorylated p38. P38 β has been shown to contribute to anti-hypertrophic and anti-apoptotic signaling in the capacity of IR injury¹⁸⁹ However, p38 activation as a cardioprotective target is controversial because it can also augment infarction.¹⁸⁹ Although the exact mechanism remains unclear, the timing of p38 activation and the isoform may play a role. For instance, SB203580, a potent p38/MAPK inhibitor, shows both improvement

when given prior to preconditioning and detriment when given during anoxia.¹⁹⁶ Therefore, further testing needs to be performed to elucidate the possible role of increased p-p38 β .

One strategy to prevent the detrimental increases in H₂O₂ and O²⁻ during reperfusion is by enhancing the endogenous antioxidant enzymes catalase and SOD2. One potential regulator of antioxidant expression is LSD1. For instance, chromatin immunoprecipitation in diabetic retinopathy showed recruitment of LSD1 to the SOD2 promoter, leading to changes in histone methylation and modulation of SOD2 levels.¹⁸⁶ Therefore, we observed whether targeting could increase endogenous antioxidants (i.e. catalase and SOD2) in cardiac IR. In animals pretreated with VLM, the protein levels of catalase significantly increased post-IR (**Figure 5.7A**). Similar results were seen with class I specific inhibitors of HDAC (HDAC1/2)¹⁸², a close functional counterpart to LSD1 within the CoREST/REST co-repressor complex.

Despite the favorable results in our pilot study, our over-arching goal is to develop compounds with attractive clinical potential and identify LSD1 as a therapeutic target. Previous work with verlindamycin demonstrates a very low therapeutic index (effective dose = 3mg/kg; lethal dose = 20mg/kg) and unabated potency for other amine oxidases. Therefore, its utilization as a therapeutic in a disease-state where cell death is not the desired endpoint is limited. Also, the non-selectivity limits its usefulness as a tool to study LSD1.

As described in earlier chapters (**Chapter 3** and **4**), we've designed a small molecule inhibitor (**9**) that demonstrates limited toxicity and is a more

favorable cardiac drug candidate. Like VLM, compound **9** improved similar hemodynamic parameters and reduced total infarction in the *ex vivo* IR model (**Figure 5.10** and **5.12**). Interestingly, we also observed a significant delay in onset of peak rigor-contraction during anoxia (**Figure 5.11**). Rigor-contraction is illustrated by a rise in end diastolic pressure with no developed pressure approximately 15-20mins after total anoxia of the tissue. It is caused by the insufficient supply of ATP to relinquish myosin heavy chains from actin filaments and overload of Ca²⁺-bound troponin. Often, a delay in onset of rigor-contraction is attributed to increased available high-energy phosphates or reduction in Ca²⁺-overload.¹⁹⁷ Therefore, this result indicates an ischemic protection versus a reperfusion event, and thus, further testing needs to be performed (discussed below).

Compound **9** also facilitated a significant mitigation of chronic systolic dysfunction associated with an *in vivo* IR model when treated when given daily for 7-days (**Figure 5.16** and **5.17**). In particular, the LV dilation that occurs from eccentric hypertrophy leading to chronic HFrEF was significantly reduced. Of note, the primary treatment with **9** was given immediately after the onset of ischemia, and thus, exhibits a more clinically relevant scenario for patient therapy. In other words, a patient with a new onset AMI can be treated post-coronary occlusion to assist with initial insult and chronic cardiac remodeling.

Aside from the physiologic benefit of **9**, our goal was to identify LSD1 as the causative target. However, as discussed in **Chapter 4**, compound **9** is a dual inhibitor of LSD1 and SMO. Therefore, we utilized enzyme selective

inhibitors of each enzyme individually to dissect the mechanism of action of **9**. Interestingly, we demonstrated that *both* LSD1 and SMO inhibition in an acute *ex vivo* experiment improved cardiac hemodynamic parameters (**Figure 5.13** and **5.14**). In addition, GSK-LSD1, the LSD1-selective inhibitor, also showed analogous results to **9** in chronic improvement of systolic dysfunction (**Figure 5.17**). Of particular note, both GSK-LSD1 and MDL72527 demonstrated robust delay in rigor-contraction (**Figures 5.13** and **5.14**). In fact, both inhibitors were more effective in preventing the ischemic rise in EDP associated with rigor-contraction than **9**. Clearly, further evaluation into the acute energetics of cardiomyocytes needs to be addressed in future experiments to understand how the amine oxidase family is improving the heart's hypoxic response.

The individual roles LSD1 and SMO play during IR are still unclear. However, we show three separate LSD1 inhibitors, including a highly potent and selective LSD1 inhibitor, are protective in cardiac IR injury (**Figure 5.15**). Therefore, our results suggest LSD1 is a viable therapeutic target to prevent IR damage. The exact mechanisms behind this protective phenomenon are still unclear.

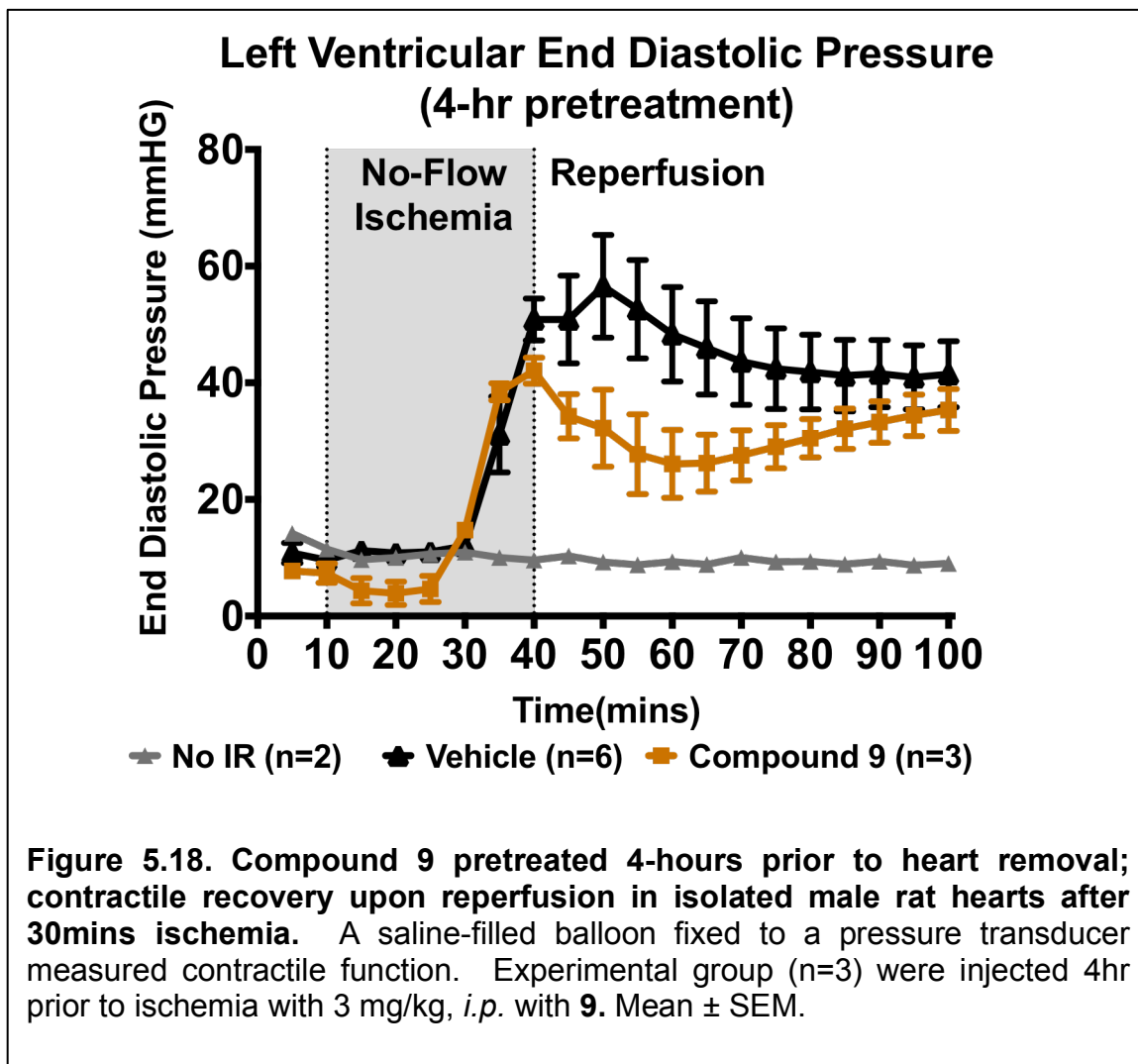
IV. LIMITATIONS AND FUTURE DIRECTIONS

Despite the beneficial changes in the *ex vivo* isolated heart experiments with LSD1 and SMO inhibitors, the acute administration of the drugs and lack of global histone H3K4me2 changes (**Figure 5.7B**) suggest that the protective effects of these compound were, in fact, a non-transcriptional event. Although

less common, LSD1 has been shown to demethylate non-histone proteins.¹⁹⁸ Also, there was a significant delay in onset of rigor contracture, advocating an anoxic phenomenon versus the hypothesized reperfusion injury. Therefore, future experiments will focus on the quantification of ATP/ADP and Ca²⁺-transients during no-flow ischemia in the isolated heart. ATP/ADP can be measured by a simple colorimetric assay (Abcam #ab83355) and Ca²⁺-transients can be detected by whole cell voltage patch clamp in primary cardiomyocytes. Not dissimilar, whole organ live imaging of voltage potential and calcium wave propagation can be performed in the Langendorff preparation through spatiotemporal optical mapping.¹⁹⁹ Finally, if this phenomenon is an anoxia-triggered protection, a one-time bolus of compound given at ischemia (or just prior to it) using the *in vivo* LAD ligation-reperfusion model should give similar cardioprotective results 7-days after surgery.

As shown in **Figure 5.15**, inhibitors of LSD1 and SMO showed substantial improvement in hemodynamic parameters. However, despite compound **9** being efficacious against both enzymes, the effect seen was less pronounced, albeit not statistically different from the other treatments. Compound **9** was the only reversible, competitive inhibitor out of the four used in this assay. In particular, MDL 72527 and GSK-LSD1 are covalent, “suicide” mechanism inhibitors. Thus, it is highly possible that the diminished effect seen by **9** is simply due to enzyme kinetics. In fact, an experimental group with compound **9** was injected at the same dose as previously described, but at 4-hours prior to heart isolation

(instead of 1-hour). **Figure 5.18** demonstrates that a gradual loss in function occurs during the period of reperfusion. We hypothesize that based on this



outcome, compound 9 may have a fast K_{off} rate or a very short-term effect. Contrary, the irreversible inhibitors demonstrated no difference between 4- and 1-hour treatments (data not shown). One explanation for this is that irreversibly inhibiting LSD1 with a highly potent inhibitor is sufficient enough in acute treatments to noticeably ablate LSD1 activity. Thus, the only way the cells can

recover is through expression turnover of the enzyme, which may be limited by the isolated heart model. In short, the exact pharmacodynamics of compound **9** is unknown and as such, the tissue bioavailability is unclear. Future experiments should be performed at various time points (i.e. 1-, 2-, and 3-hours prior to heart isolation). Another strategy to address this issue is through a comprehensive pharmacokinetic/pharmacodynamics screen. However, we are reserving this study for future lead optimized compound **9** derivatives.

LSD1 makes up just one of a vast multitude of histone demethylases in the cell, some of which have similar substrates.²⁰⁰ Thus, LSD1 inhibition or removal may not be detectable on a global histone level. In fact, many highly potent LSD1 inhibitors fail to detect global methylation in certain cell lines on a global scale. For instance, LSD1 knockout HCT116 cells failed to show any changes in global histone methylation.²⁰¹ **Figure 5.7B** corroborated this finding, showing no changes in global methylation in homogenized whole isolated rat hearts. LSD1 occupies approximately 2% of genomic promoters in corepressor complexes in stem cells.²⁰² LSD1 inhibition can alter gene transcription on a local level, without showing global changes. Therefore, a chromatin immunoprecipitation (ChIP) of histone marks or key promoters may need to be performed.

Chapter 6: Overall Summary and Discussion

Current treatments strategies for AMI continue to be palliative and aim to prevent chronic remodeling through administration of post-insult ACE inhibitors and beta-blockers. This strategy lowers total mortality and hospitalizations by nearly 30% and hastens LV dysfunction.²⁰³ More importantly, prevention of long-term damage is best treated by fast restoration of flow to the occluded coronary artery, often through thrombolytic therapy or primary percutaneous coronary intervention.²⁰⁴ However, despite an improvement in outcomes with reperfusion therapy, no standard pharmacological therapy exists that can mitigate the unintentional damage caused by reperfusion injury. Recently, epigenetic enzymes have become popular targets to limit IR damage and hypertrophic remodeling.²⁰⁵ This dissertation identified a previously unexplored cardiac target, the Lysine Specific Demethylase-1, as a completely new strategy to prevent IR damage and chronic cardiac dysfunction. As such, we utilized structure-based drug design as a tool to selectively target LSD1 and generated potent, nontoxic LSD1-specific inhibitors with significant characteristics desirable as clinical therapeutics.

LSD1 is overexpressed in a number of human cancers such as acute myeloid leukemia, neuroblastoma, retinoblastoma, prostate cancer, breast cancer, lung cancer and bladder cancer.²⁰⁶⁻²⁰⁹ Thus, the protein is traditionally an important target for antitumor agents.²¹⁰ However, new emerging roles for LSD1 in disease pathogenesis other than cancer are being reported.²¹¹⁻²¹⁵ Thus, LSD1 has become a promising target for therapeutic intervention. The tranylcypromine-based irreversible inhibitors (such as **2** and **3**) are the most

advanced chemical class with respect to drug development, and many successful LSD1 inhibitors are derived from tranylcypromine scaffolds. However, they rely on activation and/or covalent attachment to the FAD cofactor of LSD1. Therefore, it is challenging to design selective LSD1 inhibitors that do not show off-target effects mediated through other flavin-dependent enzymes.²¹⁶ The 3,5-diamino-1,2,4-triazole motif described in this dissertation is the first presented scaffold of its kind and supports the contention that potent, non-toxic LSD1-specific inhibitors can be designed in this chemical class. To date, the structurally diverse analogues utilizing this scaffold present the first reversible, competitive inhibitors of LSD1.

Design of first reversible, competitive LSD1 inhibitors and their limited toxicity:

Chapter 3 and **Chapter 4** describes the early process of hit-to-lead optimization for compounds based on a 3,5-diamino-1,2,4-triazole scaffold. To start, we applied a virtual screen of the Maybridge HitFinder 50,000 compound library, which revealed structurally distinct drug-like compounds as potential leads. Interestingly, compounds with primary amines, hydrophobic electron withdrawing groups, and heterocycloalkyl groups were well represented in our computational analysis. Two novel compounds, **9** and **10**, were active with $IC_{50}(\text{LSD1}) < 2 \mu\text{M}$ (**Figure 3.4**) and demonstrated favourable proximity interactions within 2.98Å of the FAD cofactor in the LSD1 active site (**Figure 3.3**). These lead compounds were selected for future lead optimization and biochemical characterization. A successful synthetic route to produce chemically

diverse compounds was presented (**Scheme 1**) and a number of compounds measured significant LSD1 inhibition (**Table 3.2**). Therefore, these results indicate a limited chemical library of **9** derivatives can be effectively synthesized and is expected to contain multiple active compounds. We are continuing to synthesize analogues in this series for the purpose of refining a structure/activity model for 3,5-diamino-1,2,4-triazole-based LSD1 inhibitors. Also, analogues containing functional groups designed to increase aqueous solubility are being synthesized.

Of particular interest, we aimed to optimize compounds that showed greater selectivity towards LSD1 and also demonstrated limited cytotoxicity, making them ideal for studying LSD1 in the heart. Current inhibitors of amine oxidases show significant undesirable potency towards other members of the family. This is due, in part, because of the high sequence homology within the active sites. Our initial evaluations of the selectivity of compounds **9** and **10** verified they possessed selectivity for LSD1 over MAO A and B (Selectivity Index >100) (**Figure 4.2**). Also, compound **9** revealed competitive enzyme kinetics (**Figure 3.6**), establishing it as the first small molecule scaffold of a reversible, competitive LSD1 inhibitor.

Many current LSD1 inhibitors have been designed as antitumor agents and demonstrate significant toxicity to cells. We were interested in the role of LSD1 in CVD, and thus, intended to manipulate epigenetic enzymes without causing drug-driven cellular damage. In **Chapter 4**, we presented evidence that 3,5-diamino-1,2,4-triazoles showed limited *in vitro* and *in vivo* toxicity. In

particular, a short 7-day toxicology study revealed minimal to mild histological damage to the kidney, liver, and heart. The low level of toxicity to mammalian cells and CD1 mice demonstrate that the 1,2,4-triazole scaffold can be utilized to produce LSD1 inhibitors for diseases without desirable cell death.

Selective compounds reveal LSD1 as a novel cardiac therapeutic target:

The induction of LSD1 activity and expression during hypoxia has been previously explored in cancer²¹⁷, DNA mismatch repair mechanisms²¹⁸, and global cerebral ischemia.²¹⁹ Thus, we explored the responsiveness of LSD1 within hypoxic tissue distal to an occluded coronary artery. Our results showed a significant increase in LSD1 protein (**Figure 5.2A**) and notably, the expression of LSD1 correlated to cardiac systolic function (**Figure 5.2B and C**). As such, we hypothesized that LSD1 could be a new responsive therapeutic for an AMI.

Evidence in the literature supported the notion that LSD1 could be a viable target in mitigation of cardiac damage after an ischemic event. Traditional mechanisms of action on histones involved discrete, individual activities of HDACs and LSD1 on lysine tails. However, increasing evidence is showing that residue modifications are dependent on interplay between the vast milieu of epigenetic enzymes. In fact, LSD1 and HDACs have been recently characterized as cooperative enzymes,²²⁰ where catalytic activity of one can improve the binding efficiency of the other to its particular substrate. Forneris *et al.* showed that a synthetic 21-mer peptidomimic of H3 N-terminus with acetyl-lysine increased the Km of LSD1 by 6-fold.²²¹ Because there is a clear crosstalk

between LSD1 and HDAC1/2, we were interested in the benefit seen by HDAC inhibitors in reducing myocardial IR damage²²²⁻²²³ and the implications that LSD1 may also be contributory.

Early experiments with a noncompetitive, nonselective LSD1 inhibitor (VLM, **Figure 5.3**) were successful in maintaining acute cardiac hemodynamic parameters following transient global IR. Using an *ex vivo* isolated heart model, we successfully reproduced these results with compound **9** and treated with a significantly less effective dose (**Figure 5.10**). With both compounds, we saw a significant improvement in LV developed pressure, LV end diastolic pressure, and a reduction in the total infarct cross-sectional area (**Figure 5.12**).

As discussed in **Chapter 4**, compound **9** is a dual inhibitor of LSD1 and SMO, and thus, it was difficult to draw conclusions for the mechanism of action of **9**. Therefore, we utilized enzyme selective inhibitors of each enzyme individually to dissect the mechanism of action of **9**. GSK-LSD1 is a recent commercially available, highly selective LSD1 irreversible inhibitor²²⁴ and MDL 72527 is a well characterized irreversible SMO inactivator.²²⁵ Interestingly, we demonstrated that *both* LSD1 and SMO inhibition in an acute *ex vivo* experiment improved cardiac function (**Figure 5.13** and **5.14**).

Of note, we observed a significant delay of onset in peak rigor-contraction during no-flow ischemia with all three compounds (**Figure 5.11**). Rigor-contraction is caused by the insufficient supply of ATP to relinquish myosin heavy chains from actin filaments and overload of Ca²⁺-bound troponin. Often, a delay in onset of rigor-contraction is attributed to increased available high-energy

phosphates or reduction in Ca^{2+} -overload.²²⁶ Therefore, this result indicates an ischemic protection versus a reperfusion event. Clearly, further evaluation into the acute energetics of cardiomyocytes needs to be addressed in future experiments to understand how the amine oxidase family is improving the heart's hypoxic response.

Our observations in the Langendorff isolated hearts was crucial in our understanding of acute management of IR injury. However, it failed to show long-term cardiac outcomes and cardiac remodeling. We implemented a more clinically relevant *in vivo* LAD ligation-reperfusion model of IR (see **Chapter 2 – “Left anterior descending coronary ligation-reperfusion in vivo IR”**). This model causes LV dilation and reduced ejection fraction similar to clinical manifestations from eccentric hypertrophy and chronic HFrEF. Compound **9** and GSK-LSD1 both facilitated a significant mitigation of chronic systolic dysfunction (**Figure 5.17**). Most importantly, primary treatment was given immediately after the onset of ischemia, and thus, exhibits a more clinically relevant scenario for patient therapy. In other words, a patient with a new onset AMI can be treated post-coronary occlusion to assist with initial insult and chronic cardiac remodeling.

Conclusions and final thoughts:

We successfully designed a novel scaffold of reversible, competitive LSD1 inhibitors that show limited cytotoxicity. One compound, **9**, was advanced into preclinical testing and was effective in sustaining cardiac structure and function. We presented evidence utilizing selective inhibitors for the two enzymes

modulated by **9** as tools to reveal LSD1 as a novel therapeutic target in CVD. More additional lead optimization studies are currently being performed that will lead to derivatives of **9** with improved pharmacodynamics/pharmacokinetic parameters and higher potency for LSD1.

Overall, LSD1 plays a previously unexplored role in cardiovascular disease. Although the exact mechanism is still unclear, continued experiments with LSD1 selective inhibitors, such as GSK-LSD1 or **9** derivatives, should reveal a highly coordinated effort by epigenetic complexes in tissue damage and remodeling.

LIST OF REFERENCES

- 1.) Go, A. S.; Mozaffarian, D.; Roger, V. L.; Benjamin, E. J.; Berry, J. D.; Blaha, M. J.; Dai, S.; Ford, E. S.; Fox, C. S.; Franco, S.; Fullerton, H. J.; Gillespie, C.; Hailpern, S. M.; Heit, J. A.; Howard, V. J.; Huffman, M. D.; Judd, S. E.; Kissela, B. M.; Kittner, S. J.; Lackland, D. T.; Lichtman, J. H.; Lisabeth, L. D.; Mackey, R. H.; Magid, D. J.; Marcus, G. M.; Marelli, A.; Matchar, D. B.; McGuire, D. K.; Mohler, E. R., 3rd; Moy, C. S.; Mussolino, M. E.; Neumar, R. W.; Nichol, G.; Pandey, D. K.; Paynter, N. P.; Reeves, M. J.; Sorlie, P. D.; Stein, J.; Towfighi, A.; Turan, T. N.; Virani, S. S.; Wong, N. D.; Woo, D.; Turner, M. B.; American Heart Association Statistics, C.; Stroke Statistics, S., Executive summary: heart disease and stroke statistics--2014 update: a report from the American Heart Association. *Circulation* **2014**, *129* (3), 399-410.
- 2.) Promotion, N. C. f. C. D. P. a. H., Heart Disease and Stroke Prevention: Addressing the Nation's Leading Killers. July 21, 2010 ed.; Center for Disease Control: 2011.
- 3.) Mozaffarian, D.; Benjamin, E. J.; Go, A. S.; Arnett, D. K.; Blaha, M. J.; Cushman, M.; de Ferranti, S.; Despres, J. P.; Fullerton, H. J.; Howard, V. J.; Huffman, M. D.; Judd, S. E.; Kissela, B. M.; Lackland, D. T.; Lichtman, J. H.; Lisabeth, L. D.; Liu, S.; Mackey, R. H.; Matchar, D. B.; McGuire, D. K.; Mohler, E. R., 3rd; Moy, C. S.; Muntner, P.; Mussolino, M. E.; Nasir, K.; Neumar, R. W.; Nichol, G.; Palaniappan, L.; Pandey, D. K.; Reeves, M. J.; Rodriguez, C. J.; Sorlie, P. D.; Stein, J.; Towfighi, A.; Turan, T. N.; Virani, S. S.; Willey, J. Z.; Woo, D.; Yeh, R. W.; Turner, M. B.; American Heart Association Statistics, C.; Stroke Statistics, S., Heart disease and stroke statistics--2015 update: a report from the American Heart Association. *Circulation* **2015**, *131* (4), e29-322.
- 4.) Tarride, J. E.; Lim, M.; DesMeules, M.; Luo, W.; Burke, N.; O'Reilly, D.; Bowen, J.; Goeree, R., A review of the cost of cardiovascular disease. *The Canadian journal of cardiology* **2009**, *25* (6), e195-202.
- 5.) Association, A. H., Cost to treat heart disease in United States will triple by 2030. American Heart Association Policy Statement: 2011.
- 6.) Health, N. I. o., Clinicaltrials.gov. 2014 ed.; NIH: 2014.
- 7.) Health, N. I. o., Clinical trials - heart attack, cardiovascular disease, drugs. ClinicalTrials.gov, 2015.
- 8.) Klabunde, R. E., *Cardiovascular physiology concepts*. 2nd ed.; Lippincott Williams & Wilkins/Wolters Kluwer: Philadelphia, PA, 2012; p xi, 243 p.
- 9.) Boyle, A. J., *Chapter 8. Acute Myocardial Infarction*. McGraw-Hill: New York, NY, 2014.
- 10.) Keeley, E. C.; Boura, J. A.; Grines, C. L., Primary angioplasty versus intravenous thrombolytic therapy for acute myocardial infarction: a quantitative review of 23 randomised trials. *Lancet* **2003**, *361* (9351), 13-20.
- 11.) McKay, R. G.; Pfeffer, M. A.; Pasternak, R. C.; Markis, J. E.; Come, P. C.; Nakao, S.; Alderman, J. D.; Ferguson, J. J.; Safian, R. D.; Grossman, W., Left ventricular remodeling after myocardial infarction: a corollary to infarct expansion. *Circulation* **1986**, *74* (4), 693-702.

- 12.)** Konstam, M. A.; Kramer, D. G.; Patel, A. R.; Maron, M. S.; Udelson, J. E., Left ventricular remodeling in heart failure: current concepts in clinical significance and assessment. *JACC. Cardiovascular imaging* **2011**, *4* (1), 98-108.
- 13.)** Solomon, S. D.; Glynn, R. J.; Greaves, S.; Ajani, U.; Rouleau, J. L.; Menapace, F.; Arnold, J. M.; Hennekens, C.; Pfeffer, M. A., Recovery of ventricular function after myocardial infarction in the reperfusion era: the healing and early afterload reducing therapy study. *Ann Intern Med* **2001**, *134* (6), 451-8.
- 14.)** Iwano, H.; Little, W. C., Heart failure: what does ejection fraction have to do with it? *Journal of cardiology* **2013**, *62* (1), 1-3.
- 15.)** Verma, A.; Meris, A.; Skali, H.; Ghali, J. K.; Arnold, J. M.; Bourgoun, M.; Velazquez, E. J.; McMurray, J. J.; Kober, L.; Pfeffer, M. A.; Califf, R. M.; Solomon, S. D., Prognostic implications of left ventricular mass and geometry following myocardial infarction: the VALIANT (VALsartan In Acute myocardial iNfarcTion) Echocardiographic Study. *JACC. Cardiovascular imaging* **2008**, *1* (5), 582-91.
- 16.)** Jessup, M.; Abraham, W. T.; Casey, D. E.; Feldman, A. M.; Francis, G. S.; Ganiats, T. G.; Konstam, M. A.; Mancini, D. M.; Rahko, P. S.; Silver, M. A.; Stevenson, L. W.; Yancy, C. W., 2009 focused update: ACCF/AHA Guidelines for the Diagnosis and Management of Heart Failure in Adults: a report of the American College of Cardiology Foundation/American Heart Association Task Force on Practice Guidelines: developed in collaboration with the International Society for Heart and Lung Transplantation. *Circulation* **2009**, *119* (14), 1977-2016.
- 17.)** Brouwers, F. P.; de Boer, R. A.; van der Harst, P.; Voors, A. A.; Gansevoort, R. T.; Bakker, S. J.; Hillege, H. L.; van Veldhuisen, D. J.; van Gilst, W. H., Incidence and epidemiology of new onset heart failure with preserved vs. reduced ejection fraction in a community-based cohort: 11-year follow-up of PREVEND. *European heart journal* **2013**, *34* (19), 1424-31.
- 18.)** Eltzschig, H. K.; Eckle, T., Ischemia and reperfusion--from mechanism to translation. *Nature medicine* **2011**, *17* (11), 1391-401.
- 19.)** Granger, A.; Abdullah, I.; Huebner, F.; Stout, A.; Wang, T.; Huebner, T.; Epstein, J. A.; Gruber, P. J., Histone deacetylase inhibition reduces myocardial ischemia-reperfusion injury in mice. *FASEB journal : official publication of the Federation of American Societies for Experimental Biology* **2008**, *22* (10), 3549-60.
- 20.)** Frank, A.; Bonney, M.; Bonney, S.; Weitzel, L.; Koeppen, M.; Eckle, T., Myocardial ischemia reperfusion injury: from basic science to clinical bedside. *Seminars in cardiothoracic and vascular anesthesia* **2012**, *16* (3), 123-32.
- 21.)** Ventura-Clapier, R.; Veksler, V., Myocardial ischemic contracture. Metabolites affect rigor tension development and stiffness. *Circ Res* **1994**, *74* (5), 920-9.
- 22.)** Grover, G. J.; Atwal, K. S.; Sleph, P. G.; Wang, F. L.; Monshizadegan, H.; Monticello, T.; Green, D. W., Excessive ATP hydrolysis in ischemic myocardium by mitochondrial F1F0-ATPase: effect of selective pharmacological inhibition of

mitochondrial ATPase hydrolase activity. *American journal of physiology. Heart and circulatory physiology* **2004**, 287 (4), H1747-55.

23.) Dhalla, N. S.; Elmoselhi, A. B.; Hata, T.; Makino, N., Status of myocardial antioxidants in ischemia-reperfusion injury. *Cardiovascular research* **2000**, 47 (3), 446-56.

24.) Kerr, J. F.; Wyllie, A. H.; Currie, A. R., Apoptosis: a basic biological phenomenon with wide-ranging implications in tissue kinetics. *Br J Cancer* **1972**, 26 (4), 239-57.

25.) Alberts, B., *Molecular biology of the cell*. 4th ed.; Garland Science: New York, 2002; p xxxiv, 1548 p.

26.) Hochhauser, E.; Kivity, S.; Offen, D.; Maulik, N.; Otani, H.; Barhum, Y.; Pannet, H.; Shneyvays, V.; Shainberg, A.; Goldshtaub, V.; Tobar, A.; Vidne, B. A., Bax ablation protects against myocardial ischemia-reperfusion injury in transgenic mice. *American journal of physiology. Heart and circulatory physiology* **2003**, 284 (6), H2351-9.

27.) Chen, Z.; Chua, C. C.; Ho, Y. S.; Hamdy, R. C.; Chua, B. H., Overexpression of Bcl-2 attenuates apoptosis and protects against myocardial I/R injury in transgenic mice. *American journal of physiology. Heart and circulatory physiology* **2001**, 280 (5), H2313-20.

28.) Zhang, Y.; Ren, J., Targeting autophagy for the therapeutic application of histone deacetylase inhibitors in ischemia/reperfusion heart injury. *Circulation* **2014**, 129 (10), 1088-91.

29.) Xie, M.; Kong, Y.; Tan, W.; May, H.; Battiprolu, P. K.; Pedrozo, Z.; Wang, Z. V.; Morales, C.; Luo, X.; Cho, G.; Jiang, N.; Jessen, M. E.; Warner, J. J.; Lavandero, S.; Gillette, T. G.; Turer, A. T.; Hill, J. A., Histone deacetylase inhibition blunts ischemia/reperfusion injury by inducing cardiomyocyte autophagy. *Circulation* **2014**, 129 (10), 1139-51.

30.) Matsui, Y.; Takagi, H.; Qu, X.; Abdellatif, M.; Sakoda, H.; Asano, T.; Levine, B.; Sadoshima, J., Distinct roles of autophagy in the heart during ischemia and reperfusion: roles of AMP-activated protein kinase and Beclin 1 in mediating autophagy. *Circ Res* **2007**, 100 (6), 914-22.

31.) Valentim, L.; Laurence, K. M.; Townsend, P. A.; Carroll, C. J.; Soond, S.; Scarabelli, T. M.; Knight, R. A.; Latchman, D. S.; Stephanou, A., Urocortin inhibits Beclin1-mediated autophagic cell death in cardiac myocytes exposed to ischaemia/reperfusion injury. *Journal of molecular and cellular cardiology* **2006**, 40 (6), 846-52.

32.) Koike, M.; Shibata, M.; Tadakoshi, M.; Gotoh, K.; Komatsu, M.; Waguri, S.; Kawahara, N.; Kuida, K.; Nagata, S.; Kominami, E.; Tanaka, K.; Uchiyama, Y., Inhibition of autophagy prevents hippocampal pyramidal neuron death after hypoxic-ischemic injury. *Am J Pathol* **2008**, 172 (2), 454-69.

33.) Zhao, T. C.; Cheng, G.; Zhang, L. X.; Tseng, Y. T.; Padbury, J. F., Inhibition of histone deacetylases triggers pharmacologic preconditioning effects against myocardial ischemic injury. *Cardiovascular research* **2007**, 76 (3), 473-81.

- 34.) Chen, J. K.; Chow, S. E., Antioxidants and myocardial ischemia: reperfusion injuries. *Chang Gung medical journal* **2005**, *28* (6), 369-77.
- 35.) Eckle, T.; Grenz, A.; Kohler, D.; Redel, A.; Falk, M.; Rolaufts, B.; Osswald, H.; Kehl, F.; Eltzhig, H. K., Systematic evaluation of a novel model for cardiac ischemic preconditioning in mice. *American journal of physiology. Heart and circulatory physiology* **2006**, *291* (5), H2533-40.
- 36.) Thornton, J.; Striplin, S.; Liu, G. S.; Swafford, A.; Stanley, A. W.; Van Winkle, D. M.; Downey, J. M., Inhibition of protein synthesis does not block myocardial protection afforded by preconditioning. *The American journal of physiology* **1990**, *259* (6 Pt 2), H1822-5.
- 37.) Murphy, E.; Steenbergen, C., Mechanisms underlying acute protection from cardiac ischemia-reperfusion injury. *Physiol Rev* **2008**, *88* (2), 581-609.
- 38.) Hausenloy, D. J.; Yellon, D. M., New directions for protecting the heart against ischaemia-reperfusion injury: targeting the Reperfusion Injury Salvage Kinase (RISK)-pathway. *Cardiovascular research* **2004**, *61* (3), 448-60.
- 39.) Bolli, R., Cardioprotective function of inducible nitric oxide synthase and role of nitric oxide in myocardial ischemia and preconditioning: an overview of a decade of research. *Journal of molecular and cellular cardiology* **2001**, *33* (11), 1897-918.
- 40.) Tong, H.; Imahashi, K.; Steenbergen, C.; Murphy, E., Phosphorylation of glycogen synthase kinase-3beta during preconditioning through a phosphatidylinositol-3-kinase--dependent pathway is cardioprotective. *Circ Res* **2002**, *90* (4), 377-9.
- 41.) Bodalia, A.; Li, H.; Jackson, M. F., Loss of endoplasmic reticulum Ca²⁺ homeostasis: contribution to neuronal cell death during cerebral ischemia. *Acta pharmacologica Sinica* **2013**, *34* (1), 49-59.
- 42.) Kim, H. S.; Cho, J. E.; Hong, S. W.; Kim, S. O.; Shim, J. K.; Kwak, Y. L., Remifentanil protects myocardium through activation of anti-apoptotic pathways of survival in ischemia-reperfused rat heart. *Physiol Res* **2010**, *59* (3), 347-56.
- 43.) Chen, B.; Caballero, S.; Seo, S.; Grant, M. B.; Lewin, A. S., Delivery of antioxidant enzyme genes to protect against ischemia/reperfusion-induced injury to retinal microvasculature. *Investigative ophthalmology & visual science* **2009**, *50* (12), 5587-95.
- 44.) Cai, Z.; Luo, W.; Zhan, H.; Semenza, G. L., Hypoxia-inducible factor 1 is required for remote ischemic preconditioning of the heart. *Proceedings of the National Academy of Sciences of the United States of America* **2013**, *110* (43), 17462-7.
- 45.) Stein, A. B.; Tang, X. L.; Guo, Y.; Xuan, Y. T.; Dawn, B.; Bolli, R., Delayed adaptation of the heart to stress: late preconditioning. *Stroke; a journal of cerebral circulation* **2004**, *35* (11 Suppl 1), 2676-9.
- 46.) Jaenisch, R.; Bird, A., Epigenetic regulation of gene expression: how the genome integrates intrinsic and environmental signals. *Nat Genet* **2003**, *33* Suppl, 245-54.

- 47.) Andreoli, F.; Del Rio, A., Physicochemical modifications of histones and their impact on epigenomics. *Drug discovery today* **2014**, doi: 10.1016/j.drudis.2014.05.005. [Epub ahead of print].
- 48.) Elder, S. J.; Lichtenstein, A. H.; Pittas, A. G.; Roberts, S. B.; Fuss, P. J.; Greenberg, A. S.; McCrory, M. A.; Bouchard, T. J., Jr.; Saltzman, E.; Neale, M. C., Genetic and environmental influences on factors associated with cardiovascular disease and the metabolic syndrome. *J Lipid Res* **2009**, *50* (9), 1917-26.
- 49.) Fraga, M. F.; Ballestar, E.; Paz, M. F.; Ropero, S.; Setien, F.; Ballestar, M. L.; Heine-Suner, D.; Cigudosa, J. C.; Urioste, M.; Benitez, J.; Boix-Chornet, M.; Sanchez-Aguilera, A.; Ling, C.; Carlsson, E.; Poulsen, P.; Vaag, A.; Stephan, Z.; Spector, T. D.; Wu, Y. Z.; Plass, C.; Esteller, M., Epigenetic differences arise during the lifetime of monozygotic twins. *Proceedings of the National Academy of Sciences of the United States of America* **2005**, *102* (30), 10604-9.
- 50.) Handy, D. E.; Castro, R.; Loscalzo, J., Epigenetic modifications: basic mechanisms and role in cardiovascular disease. *Circulation* **2011**, *123* (19), 2145-56.
- 51.) Aune, S. E.; Herr, D. J.; Mani, S. K.; Menick, D. R., Selective inhibition of class I but not class IIb histone deacetylases exerts cardiac protection from ischemia reperfusion. *Journal of molecular and cellular cardiology* **2014**, *72*, 138-45.
- 52.) Zhong, Q.; Kowluru, R. A., Epigenetic modification of Sod2 in the development of diabetic retinopathy and in the metabolic memory: role of histone methylation. *Investigative ophthalmology & visual science* **2013**, *54* (1), 244-50.
- 53.) Yan, M. S.; Matouk, C. C.; Marsden, P. A., Epigenetics of the vascular endothelium. *Journal of applied physiology* **2010**, *109* (3), 916-26.
- 54.) Webster, A. L.; Yan, M. S.; Marsden, P. A., Epigenetics and cardiovascular disease. *The Canadian journal of cardiology* **2013**, *29* (1), 46-57.
- 55.) Shi, Y.; Lan, F.; Matson, C.; Mulligan, P.; Whetstone, J. R.; Cole, P. A.; Casero, R. A.; Shi, Y., Histone demethylation mediated by the nuclear amine oxidase homolog LSD1. *Cell* **2004**, *119* (7), 941-53.
- 56.) Suzuki, T.; Miyata, N., Lysine demethylases inhibitors. *Journal of medicinal chemistry* **2011**, *54* (24), 8236-50.
- 57.) Varier, R. A.; Timmers, H. T., Histone lysine methylation and demethylation pathways in cancer. *Biochimica et biophysica acta* **2011**, *1815* (1), 75-89.
- 58.) Nicholson, T. B.; Chen, T., LSD1 demethylates histone and non-histone proteins. *Epigenetics* **2009**, *4*, 129-132.
- 59.) Huang, J.; Sengupta, R.; Espejo, A. B.; Lee, M. G.; Dorsey, J. A.; Richter, M.; Opravil, S.; Shiekhhattar, R.; Bedford, M. T.; Jenuwein, T.; Berger, S. L., p53 is regulated by the lysine demethylase LSD1. *Nature* **2007**, *449* (7158), 105-8.
- 60.) Wang, J.; Hevi, S.; Kurash, J. K.; Lei, H.; Gay, F.; Bajko, J.; Su, H.; Sun, W.; Chang, H.; Xu, G.; Gaudet, F.; Li, E.; Chen, T., The lysine demethylase LSD1 (KDM1) is required for maintenance of global DNA methylation. *Nat Genet* **2009**, *41* (1), 125-9.

- 61.)** Kong, X.; Ouyang, S.; Liang, Z.; Lu, J.; Chen, L.; Shen, B.; Li, D.; Zheng, M.; Li, K. K.; Luo, C.; Jiang, H., Catalytic mechanism investigation of lysine-specific demethylase 1 (LSD1): a computational study. *PloS one* **2011**, *6* (9), e25444.
- 62.)** Forneris, F.; Binda, C.; Battaglioli, E.; Mattevi, A., LSD1: oxidative chemistry for multifaceted functions in chromatin regulation. *Trends Biochem Sci* **2008**, *33* (4), 181-9.
- 63.)** Forneris, F.; Binda, C.; Adamo, A.; Battaglioli, E.; Mattevi, A., Structural basis of LSD1-CoREST selectivity in histone H3 recognition. *The Journal of biological chemistry* **2007**, *282* (28), 20070-4.
- 64.)** Da, G.; Lenkart, J.; Zhao, K.; Shiekhattar, R.; Cairns, B. R.; Marmorstein, R., Structure and function of the SWIRM domain, a conserved protein module found in chromatin regulatory complexes. *Proceedings of the National Academy of Sciences of the United States of America* **2006**, *103* (7), 2057-62.
- 65.)** Forneris, F.; Binda, C.; Vanoni, M. A.; Battaglioli, E.; Mattevi, A., Human histone demethylase LSD1 reads the histone code. *The Journal of biological chemistry* **2005**, *280* (50), 41360-5.
- 66.)** Zhang, K.; Siino, J. S.; Jones, P. R.; Yau, P. M.; Bradbury, E. M., A mass spectrometric "Western blot" to evaluate the correlations between histone methylation and histone acetylation. *Proteomics* **2004**, *4* (12), 3765-75.
- 67.)** Vasilatos, S. N.; Katz, T. A.; Oesterreich, S.; Wan, Y.; Davidson, N. E.; Huang, Y., Crosstalk between lysine-specific demethylase 1 (LSD1) and histone deacetylases mediates antineoplastic efficacy of HDAC inhibitors in human breast cancer cells. *Carcinogenesis* **2013**, *34* (6), 1196-207.
- 68.)** Hayami, S.; Kelly, J. D.; Cho, H. S.; Yoshimatsu, M.; Unoki, M.; Tsunoda, T.; Field, H. I.; Neal, D. E.; Yamaue, H.; Ponder, B. A.; Nakamura, Y.; Hamamoto, R., Overexpression of LSD1 contributes to human carcinogenesis through chromatin regulation in various cancers. *International Journal of Cancer* **2011**, *128* (3), 574-586.
- 69.)** Lim, S.; Janzer, A.; Becker, A.; Zimmer, A.; Schule, R.; Buettner, R.; Kirfel, J., Lysine-specific demethylase 1 (LSD1) is highly expressed in ER-negative breast cancers and a biomarker predicting aggressive biology. *Carcinogenesis* **2010**, *31* (3), 512-520.
- 70.)** Rotili, D.; Mai, A., Targeting Histone Demethylases: A New Avenue for the Fight against Cancer. *Genes & cancer* **2011**, *2* (6), 663-79.
- 71.)** Schulte, J. H.; Lim, S.; Schramm, A.; Friedrichs, N.; Koster, J.; Versteeg, R.; Ora, I.; Pajtler, K.; Klein-Hitpass, L.; Kuhfittig-Kulle, S.; Metzger, E.; Schule, R.; Eggert, A.; Buettner, R.; Kirfel, J., Lysine-specific demethylase 1 is strongly expressed in poorly differentiated neuroblastoma: implications for therapy. *Cancer research* **2009**, *69* (5), 2065-71.
- 72.)** Stavropoulos, P.; Hoelz, A., Lysine-specific demethylase 1 as a potential therapeutic target. *Expert Opin Ther Targets* **2007**, *11* (6), 809-20.
- 73.)** Gottesfeld, J. M.; Pandolfo, M., Development of histone deacetylase inhibitors as therapeutics for neurological disease. *Future Neurol* **2009**, *4* (6), 775-784.

- 74.) Lakowski, B.; Roelens, I.; Jacob, S., CoREST-like complexes regulate chromatin modification and neuronal gene expression. *J Mol Neurosci* **2006**, *29* (3), 227-39.
- 75.) Shi, L.; Cui, S.; Engel, J. D.; Tanabe, O., Lysine-specific demethylase 1 is a therapeutic target for fetal hemoglobin induction. *Nat Med* **2013**, *19* (3), 291-4.
- 76.) Ginder, G. D., Epigenetic regulation of fetal globin gene expression in adult erythroid cells. *Translational research : the journal of laboratory and clinical medicine* **2014**.
- 77.) Yang, I. V.; Schwartz, D. A., Epigenetics of idiopathic pulmonary fibrosis. *Translational research : the journal of laboratory and clinical medicine* **2014**.
- 78.) Mosammamarast, N.; Kim, H.; Laurent, B.; Zhao, Y.; Lim, H. J.; Majid, M. C.; Dango, S.; Luo, Y.; Hempel, K.; Sowa, M. E.; Gygi, S. P.; Steen, H.; Harper, J. W.; Yankner, B.; Shi, Y., The histone demethylase LSD1/KDM1A promotes the DNA damage response. *J Cell Biol* **2013**, *203* (3), 457-70.
- 79.) Perillo, B.; Di Santi, A.; Cenera, G.; Ombra, M. N.; Castoria, G.; Migliaccio, A., Nuclear receptor-induced transcription is driven by spatially and timely restricted waves of ROS. The role of Akt, IKKalpha, and DNA damage repair enzymes. *Nucleus* **2014**, *5* (5), 482-91.
- 80.) Zhang, Q. J.; Chen, H. Z.; Wang, L.; Liu, D. P.; Hill, J. A.; Liu, Z. P., The histone trimethyllysine demethylase JMJD2A promotes cardiac hypertrophy in response to hypertrophic stimuli in mice. *The Journal of clinical investigation* **2011**, *121* (6), 2447-56.
- 81.) Williams, J. S.; Chamarthi, B.; Goodarzi, M. O.; Pojoga, L. H.; Sun, B.; Garza, A. E.; Raby, B. A.; Adler, G. K.; Hopkins, P. N.; Brown, N. J.; Jeunemaitre, X.; Ferri, C.; Fang, R.; Leonor, T.; Cui, J.; Guo, X.; Taylor, K. D.; Ida Chen, Y. D.; Xiang, A.; Raffel, L. J.; Buchanan, T. A.; Rotter, J. I.; Williams, G. H.; Shi, Y., Lysine-specific demethylase 1: an epigenetic regulator of salt-sensitive hypertension. *American journal of hypertension* **2012**, *25* (7), 812-7.
- 82.) Zhang, Y. Z.; Zhang, Q. H.; Ye, H.; Zhang, Y.; Luo, Y. M.; Ji, X. M.; Su, Y. Y., Distribution of lysine-specific demethylase 1 in the brain of rat and its response in transient global cerebral ischemia. *Neuroscience research* **2010**, *68* (1), 66-72.
- 83.) Lu, Y.; Chu, A.; Turker, M. S.; Glazer, P. M., Hypoxia-induced epigenetic regulation and silencing of the BRCA1 promoter. *Molecular and cellular biology* **2011**, *31* (16), 3339-50.
- 84.) Bertrand, P., Inside HDAC with HDAC inhibitors. *Eur J Med Chem* **2010**, *45* (6), 2095-116.
- 85.) McKinsey, T. A., Therapeutic potential for HDAC inhibitors in the heart. *Annu Rev Pharmacol Toxicol* **2012**, *52*, 303-19.
- 86.) Barrios, A. P.; Gomez, A. V.; Saez, J. E.; Ciossani, G.; Toffolo, E.; Battaglioli, E.; Mattevi, A.; Andres, M. E., Differential properties of transcriptional complexes formed by the CoREST family. *Molecular and cellular biology* **2014**.
- 87.) Laird, P. W., Cancer epigenetics. *Hum Mol Genet* **2005**, *14 Spec No 1*, R65-76.

- 88.) Trievel, R. C., Structure and function of histone methyltransferases. *Critical reviews in eukaryotic gene expression* **2004**, 14 (3), 147-69.
- 89.) Cao, Y.; Lu, L.; Liu, M.; Li, X. C.; Sun, R. R.; Zheng, Y.; Zhang, P. Y., Impact of epigenetics in the management of cardiovascular disease: a review. *European review for medical and pharmacological sciences* **2014**, 18 (20), 3097-104.
- 90.) Yu, L.; Yang, G.; Weng, X.; Liang, P.; Li, L.; Li, J.; Fan, Z.; Tian, W.; Wu, X.; Xu, H.; Fang, M.; Ji, Y.; Li, Y.; Chen, Q.; Xu, Y., Histone Methyltransferase SET1 Mediates Angiotensin II-Induced Endothelin-1 Transcription and Cardiac Hypertrophy in Mice. *Arterioscler Thromb Vasc Biol* **2015**.
- 91.) Binda, C.; Mattevi, A.; Edmondson, D. E., Structure-function relationships in flavoenzyme-dependent amine oxidations: a comparison of polyamine oxidase and monoamine oxidase. *The Journal of biological chemistry* **2002**, 277 (27), 23973-6.
- 92.) Marton, L. J.; Pegg, A. E.; Morris, D. R., Directions for polyamine research. *J Cell Biochem* **1991**, 45 (1), 7-8.
- 93.) Wallace, H. M.; Fraser, A. V.; Hughes, A., A perspective of polyamine metabolism. *The Biochemical journal* **2003**, 376 (Pt 1), 1-14.
- 94.) Lovaas, E.; Carlin, G., Spermine: an anti-oxidant and anti-inflammatory agent. *Free radical biology & medicine* **1991**, 11 (5), 455-61.
- 95.) Schuber, F., Influence of polyamines on membrane functions. *The Biochemical journal* **1989**, 260 (1), 1-10.
- 96.) Pegg, A. E., Recent advances in the biochemistry of polyamines in eukaryotes. *The Biochemical journal* **1986**, 234 (2), 249-62.
- 97.) Oyanagui, Y., Anti-inflammatory effects of polyamines in serotonin and carrageenan paw edemata - possible mechanism to increase vascular permeability inhibitory protein level which is regulated by glucocorticoids and superoxide radical. *Agents Actions* **1984**, 14 (2), 228-37.
- 98.) Wallace, H. M., The physiological role of the polyamines. *Eur J Clin Invest* **2000**, 30 (1), 1-3.
- 99.) Barone, S.; Okaya, T.; Rudich, S.; Petrovic, S.; Tenrani, K.; Wang, Z.; Zahedi, K.; Casero, R. A.; Lentsch, A. B.; Soleimani, M., Distinct and sequential upregulation of genes regulating cell growth and cell cycle progression during hepatic ischemia-reperfusion injury. *Am J Physiol Cell Physiol* **2005**, 289 (4), C826-35.
- 100.) Zahedi, K.; Lentsch, A. B.; Okaya, T.; Barone, S.; Sakai, N.; Witte, D. P.; Arend, L. J.; Alhonen, L.; Jell, J.; Janne, J.; Porter, C. W.; Soleimani, M., Spermidine/spermine-N1-acetyltransferase ablation protects against liver and kidney ischemia-reperfusion injury in mice. *Am J Physiol Gastrointest Liver Physiol* **2009**, 296 (4), G899-909.
- 101.) Han, L.; Xu, C.; Guo, Y.; Li, H.; Jiang, C.; Zhao, Y., Polyamine metabolism in rat myocardial ischemia-reperfusion injury. *International journal of cardiology* **2009**, 132 (1), 142-4.
- 102.) Zhao, Y. J.; Xu, C. Q.; Zhang, W. H.; Zhang, L.; Bian, S. L.; Huang, Q.; Sun, H. L.; Li, Q. F.; Zhang, Y. Q.; Tian, Y.; Wang, R.; Yang, B. F.; Li, W. M.,

Role of polyamines in myocardial ischemia/reperfusion injury and their interactions with nitric oxide. *Eur J Pharmacol* **2007**, *562* (3), 236-46.

103.) Moghe, A.; Ghare, S.; Lamoreau, B.; Mohammad, M.; Barve, S.; McClain, C.; Joshi-Barve, S., Molecular mechanisms of acrolein toxicity: relevance to human disease. *Toxicol Sci* **2015**, *143* (2), 242-55.

104.) Bianchi, P.; Kunduzova, O.; Masini, E.; Cambon, C.; Bani, D.; Raimondi, L.; Seguelas, M. H.; Nistri, S.; Colucci, W.; Leducq, N.; Parini, A., Oxidative stress by monoamine oxidase mediates receptor-independent cardiomyocyte apoptosis by serotonin and postischemic myocardial injury. *Circulation* **2005**, *112* (21), 3297-305.

105.) Kaludercic, N.; Carpi, A.; Menabo, R.; Di Lisa, F.; Paolocci, N., Monoamine oxidases (MAO) in the pathogenesis of heart failure and ischemia/reperfusion injury. *Biochimica et biophysica acta* **2011**, *1813* (7), 1323-32.

106.) Bianchi, P.; Seguelas, M. H.; Parini, A.; Cambon, C., Activation of pro-apoptotic cascade by dopamine in renal epithelial cells is fully dependent on hydrogen peroxide generation by monoamine oxidases. *Journal of the American Society of Nephrology : JASN* **2003**, *14* (4), 855-62.

107.) Kaludercic, N.; Mialet-Perez, J.; Paolocci, N.; Parini, A.; Di Lisa, F., Monoamine oxidases as sources of oxidants in the heart. *Journal of molecular and cellular cardiology* **2014**, *73C*, 34-42.

108.) Chahine, R.; Nadeau, R.; Lamontagne, D.; Yamaguchi, N.; de Champlain, J., Norepinephrine and dihydroxyphenylglycol effluxes from sympathetic nerve endings during hypoxia and reoxygenation in the isolated rat heart. *Canadian journal of physiology and pharmacology* **1994**, *72* (6), 595-601.

109.) Rochette, L.; Lorin, J.; Zeller, M.; Guillard, J. C.; Lorgis, L.; Cottin, Y.; Vergely, C., Nitric oxide synthase inhibition and oxidative stress in cardiovascular diseases: possible therapeutic targets? *Pharmacol Ther* **2013**, *140* (3), 239-57.

110.) Lee, M. G.; Wynder, C.; Schmidt, D. M.; McCafferty, D. G.; Shiekhattar, R., Histone H3 lysine 4 demethylation is a target of nonselective antidepressive medications. *Chem Biol* **2006**, *13* (6), 563-7.

111.) Schmidt, D. M.; McCafferty, D. G., trans-2-Phenylcyclopropylamine is a mechanism-based inactivator of the histone demethylase LSD1. *Biochemistry* **2007**, *46* (14), 4408-16.

112.) Yang, M.; Culhane, J. C.; Szewczuk, L. M.; Jalili, P.; Ball, H. L.; Machius, M.; Cole, P. A.; Yu, H., Structural basis for the inhibition of the LSD1 histone demethylase by the antidepressant trans-2-phenylcyclopropylamine. *Biochemistry* **2007**, *46* (27), 8058-65.

113.) Mimasu, S.; Umezawa, N.; Sato, S.; Higuchi, T.; Umehara, T.; Yokoyama, S., Structurally designed trans-2-phenylcyclopropylamine derivatives potently inhibit histone demethylase LSD1/KDM1. *Biochemistry* **2010**, *49* (30), 6494-503.

114.) GlaxoSmithKline, A Phase I Dose Escalation Study for GSK2879552 in Subjects With Acute Myeloid Leukemia (AML). ClinicalTrials.gov, 2015.

115.) Zou, Y.; Wu, Z.; Sirisoma, N.; Woster, P. M.; Casero, R. A., Jr.; Weiss, L. M.; Rattendi, D.; Lane, S.; Bacchi, C. J., Novel alkylpolyamine analogues that

possess both antitrypanosomal and antimicrosporidial activity. *Bioorganic & medicinal chemistry letters* **2001**, *11* (12), 1613-7.

116.) Zhu, Q.; Huang, Y.; Marton, L. J.; Woster, P. M.; Davidson, N. E.; Casero, R. A., Jr., Polyamine analogs modulate gene expression by inhibiting lysine-specific demethylase 1 (LSD1) and altering chromatin structure in human breast cancer cells. *Amino acids* **2011**.

117.) Sharma, S. K.; Wu, Y.; Steinbergs, N.; Crowley, M. L.; Hanson, A. S.; Casero, R. A.; Woster, P. M., (Bis)urea and (bis)thiourea inhibitors of lysine-specific demethylase 1 as epigenetic modulators. *Journal of medicinal chemistry* **2010**, *53* (14), 5197-212.

118.) Huang, Y.; Greene, E.; Murray Stewart, T.; Goodwin, A. C.; Baylin, S. B.; Woster, P. M.; Casero, R. A., Jr., Inhibition of lysine-specific demethylase 1 by polyamine analogues results in reexpression of aberrantly silenced genes. *Proceedings of the National Academy of Sciences of the United States of America* **2007**, *104* (19), 8023-8.

119.) Nowotarski, S. L.; Pachaiyappan, B.; Holshouser, S. L.; Kutz, C. J.; Li, Y.; Huang, Y.; Sharma, S. K.; Casero, R. A., Jr.; Woster, P. M., Structure-activity study for (bis)ureidopropyl- and (bis)thioureidopropyldiamine LSD1 inhibitors with 3-5-3 and 3-6-3 carbon backbone architectures. *Bioorganic & medicinal chemistry* **2015**, *23* (7), 1601-12.

120.) Dulla, B.; Kirla, K. T.; Rathore, V.; Deora, G. S.; Kavela, S.; Maddika, S.; Chatti, K.; Reiser, O.; Iqbal, J.; Pal, M., Synthesis and evaluation of 3-amino/guanidine substituted phenyl oxazoles as a novel class of LSD1 inhibitors with anti-proliferative properties. *Organic & biomolecular chemistry* **2013**, *11* (19), 3103-7.

121.) Forneris, F.; Binda, C.; Adamo, A.; Battaglioli, E.; Mattevi, A., Structural basis of LSD1-CoREST selectivity in histone H3 recognition. *The Journal of biological chemistry* **2007**, *282* (28), 20070-20074.

122.) Kumarasinghe, I. R.; Woster, P. M., Synthesis and Evaluation of Novel Cyclic Peptide Inhibitors of Lysine-Specific Demethylase 1. *ACS Med. Chem. Lett.* **2014**, *5* (1), 29-33.

123.) Kumarasinghe, I. R.; Woster, P. M., Synthesis and evaluation of novel cyclic Peptide inhibitors of lysine-specific demethylase 1. *ACS medicinal chemistry letters* **2014**, *5* (1), 29-33.

124.) Willmann, D.; Lim, S.; Wetzel, S.; Metzger, E.; Jandausch, A.; Wilk, W.; Jung, M.; Forne, I.; Imhof, A.; Janzer, A.; Kirfel, J.; Waldmann, H.; Schule, R.; Buettner, R., Impairment of prostate cancer cell growth by a selective and reversible lysine-specific demethylase 1 inhibitor. *Int J Cancer* **2012**, *131* (11), 2704-9.

125.) Tortorici, M.; Borrello, M. T.; Tardugno, M.; Chiarelli, L. R.; Pilotto, S.; Ciossani, G.; Vellore, N. A.; Bailey, S. G.; Cowan, J.; O'Connell, M.; Crabb, S. J.; Packham, G.; Mai, A.; Baron, R.; Ganesan, A.; Mattevi, A., Protein recognition by short peptide reversible inhibitors of the chromatin-modifying LSD1/CoREST lysine demethylase. *ACS chemical biology* **2013**, *8* (8), 1677-82.

- 126.)** Sorna, V.; Theisen, E. R.; Stephens, B.; Warner, S. L.; Bearss, D. J.; Vankayalapati, H.; Sharma, S., High-throughput virtual screening identifies novel N'-(1-phenylethylidene)-benzohydrazides as potent, specific, and reversible LSD1 inhibitors. *Journal of medicinal chemistry* **2013**, *56* (23), 9496-508.
- 127.)** Baell, J. B.; Holloway, G. A., New substructure filters for removal of pan assay interference compounds (PAINS) from screening libraries and for their exclusion in bioassays. *Journal of medicinal chemistry* **2010**, *53* (7), 2719-40.
- 128.)** Bey, P.; Bolkenius, F. N.; Seiler, N.; Casara, P., N-2,3-Butadienyl-1,4-butanediamine derivatives: potent irreversible inactivators of mammalian polyamine oxidase. *Journal of medicinal chemistry* **1985**, *28* (1), 1-2.
- 129.)** Bellelli, A.; Cavallo, S.; Nicolini, L.; Cervelli, M.; Bianchi, M.; Mariottini, P.; Zelli, M.; Federico, R., Mouse spermine oxidase: a model of the catalytic cycle and its inhibition by N,N1-bis(2,3-butadienyl)-1,4-butanediamine. *Biochemical and biophysical research communications* **2004**, *322* (1), 1-8.
- 130.)** Wang, Y.; Hacker, A.; Murray-Stewart, T.; Frydman, B.; Valasinas, A.; Fraser, A. V.; Woster, P. M.; Casero, R. A., Jr., Properties of recombinant human N1-acetylpolyamine oxidase (hPAO): potential role in determining drug sensitivity. *Cancer chemotherapy and pharmacology* **2005**, *56* (1), 83-90.
- 131.)** Wang, Y.; Murray-Stewart, T.; Devereux, W.; Hacker, A.; Frydman, B.; Woster, P. M.; Casero, R. A., Jr., Properties of purified recombinant human polyamine oxidase, PAOh1/SMO. *Biochemical and biophysical research communications* **2003**, *304* (4), 605-11.
- 132.)** Cona, A.; Manetti, F.; Leone, R.; Corelli, F.; Tavladoraki, P.; Polticelli, F.; Botta, M., Molecular basis for the binding of competitive inhibitors of maize polyamine oxidase. *Biochemistry* **2004**, *43* (12), 3426-35.
- 133.)** Kutz, C. J.; Holshouser, S. L.; Marrow, E. A.; Woster, P. M., 3,5-Diamino-1,2,4-triazoles as a novel scaffold for potent, reversible LSD1 (KDM1A) inhibitors. *MedChemComm* **2014**, *5* (12), 1863-1870.
- 134.)** Pojoga, L. H.; Williams, J. S.; Yao, T. M.; Kumar, A.; Raffetto, J. D.; do Nascimento, G. R.; Reslan, O. M.; Adler, G. K.; Williams, G. H.; Shi, Y.; Khalil, R. A., Histone demethylase LSD1 deficiency during high-salt diet is associated with enhanced vascular contraction, altered NO-cGMP relaxation pathway, and hypertension. *American journal of physiology. Heart and circulatory physiology* **2011**, *301* (5), H1862-71.
- 135.)** Xu, X.; Colecraft, H. M., Primary culture of adult rat heart myocytes. *Journal of visualized experiments : JoVE* **2009**, (28).
- 136.)** Chandrasekaran, S.; Peterson, R. E.; Mani, S. K.; Addy, B.; Buchholz, A. L.; Xu, L.; Thiyagarajan, T.; Kasiganesan, H.; Kern, C. B.; Menick, D. R., Histone deacetylases facilitate sodium/calcium exchanger up-regulation in adult cardiomyocytes. *FASEB journal : official publication of the Federation of American Societies for Experimental Biology* **2009**, *23* (11), 3851-64.
- 137.)** Mani, S. K.; Kern, C. B.; Kimbrough, D.; Addy, B.; Kasiganesan, H.; Rivers, W. T.; Patel, R. K.; Chou, J. C.; Spinale, F. G.; Mukherjee, R.; Menick, D. R., Inhibition of Class I Histone Deacetylase Activity Represses Matrix Metalloproteinase-2 and -9 Expression and Preserves LV Function Post

Myocardial Infarction. *American journal of physiology. Heart and circulatory physiology* **2015**, ajpheart 00390 2014.

138.) Suzuki, T.; Miyata, N., Lysine demethylases inhibitors. *Journal of medicinal chemistry* **2011**, *54* (24), 8236-50.

139.) Mimasu, S.; Umezawa, N.; Sato, S.; Higuchi, T.; Umehara, T.; Yokoyama, S., Structurally designed trans-2-phenylcyclopropylamine derivatives potently inhibit histone demethylase LSD1/KDM1. *Biochemistry* **2010**, *49* (30), 6494-503.

140.) Guibourt, N.; Ortega-Munoz, A.; Castro-Palomino Laria, J. Preparation of phenylcyclopropylamine derivatives as LSD1 selective and LSD1/MAO-B dual inhibitors in treating or preventing cancer. 2010.

141.) Ortega-Munoz, A.; Castro-Palomino Laria, J.; Fyfe, M. C. T. Lysine-specific demethylase 1 inhibitors and their use. 2011.

142.) Huang, Y.; Greene, E.; Murray Stewart, T.; Goodwin, A. C.; Baylin, S. B.; Woster, P. M.; Casero, R. A., Jr., Inhibition of lysine-specific demethylase 1 by polyamine analogues results in reexpression of aberrantly silenced genes. *Proceedings of the National Academy of Sciences of the United States of America* **2007**, *104* (19), 8023-8.

143.) Sharma, S.; Wu, Y.; Steinbergs, N.; Crowley, M.; Hanson, A.; Casero, R. A. J.; Woster, P., (Bis)urea and (bis)thiourea inhibitors of lysine-specific demethylase 1 as epigenetic modulators. *J. Med. Chem.* **2010**, *53* (14), 5197–5212.

144.) Sharma, S. K.; Hazeldine, S.; Crowley, M. L.; Hanson, A.; Beattie, R.; Varghese, S.; Sennanayake, T. M. D.; Hirata, A.; Hirata, F.; Huang, Y.; Wu, Y.; Steinbergs, N.; Murray-Stewart, T.; Bytheway, I.; Casero, J., R.A.; Woster, P. M., Polyamine-based small molecule epigenetic modulators. *MedChemComm* **2012**, *3*, 14-21.

145.) Forneris, F.; Binda, C.; Adamo, A.; Battaglioli, E.; Mattevi, A., Structural basis of LSD1-CoREST selectivity in histone H3 recognition. *The Journal of biological chemistry* **2007**, *282* (28), 20070-20074.

146.) Kumarasinghe, I. R.; Woster, P. M., Synthesis and evaluation of novel cyclic Peptide inhibitors of lysine-specific demethylase 1. *ACS medicinal chemistry letters* **2014**, *5* (1), 29-33.

147.) http://www.oryzon.com/files/NdP2014/PRESS_RELEASE_01-2014def.pdf.

148.) Khan, M. N.; Suzuki, T.; Miyata, N., An overview of phenylcyclopropylamine derivatives: biochemical and biological significance and recent developments. *Medicinal research reviews* **2013**, *33* (4), 873-910.

149.) Hazeldine, S.; Pachaiyappan, B.; Steinbergs, N.; Nowotarski, S.; Hanson, A. S.; Casero, R. A., Jr.; Woster, P. M., Low molecular weight amidoximes that act as potent inhibitors of lysine-specific demethylase 1. *Journal of medicinal chemistry* **2012**, *55* (17), 7378-91.

150.) Forneris, F.; Binda, C.; Vanoni, M. A.; Battaglioli, E.; Mattevi, A., Human histone demethylase LSD1 reads the histone code. *The Journal of biological chemistry* **2005**, *280* (50), 41360-5.

- 151.)** Shi, Y.; Lan, F.; Matson, C.; Mulligan, P.; Whetstone, J. R.; Cole, P. A.; Casero, R. A.; Shi, Y., Histone demethylation mediated by the nuclear amine oxidase homolog LSD1. *Cell* **2004**, *119* (7), 941-53.
- 152.)** Abdulla, A.; Zhao, X.; Yang, F., Natural Polyphenols Inhibit Lysine-Specific Demethylase-1. *Journal of biochemical and pharmacological research* **2013**, *1* (1), 56-63.
- 153.)** Burnouf, D.; Ennifar, E.; Guedich, S.; Puffer, B.; Hoffmann, G.; Bec, G.; Disdier, F.; Baltzinger, M.; Dumas, P., kinITC: a new method for obtaining joint thermodynamic and kinetic data by isothermal titration calorimetry. *J Am Chem Soc* **2012**, *134* (1), 559-65.
- 154.)** Suzuki, T.; Miyata, N., Lysine demethylases inhibitors. *Journal of medicinal chemistry* 2011, *54* (24), 8236-50.
- 155.)** Gottesfeld, J. M.; Pandolfo, M., Development of histone deacetylase inhibitors as therapeutics for neurological disease. *Future Neurol* 2009, *4* (6), 775-784.
- 156.)** Lakowski, B.; Roelens, I.; Jacob, S., CoREST-like complexes regulate chromatin modification and neuronal gene expression. *J Mol Neurosci* 2006, *29* (3), 227-39.
- 157.)** Shi, L.; Cui, S.; Engel, J. D.; Tanabe, O., Lysine-specific demethylase 1 is a therapeutic target for fetal hemoglobin induction. *Nat Med* 2013, *19* (3), 291-4.
- 158.)** Ginder, G. D., Epigenetic regulation of fetal globin gene expression in adult erythroid cells. *Translational research : the journal of laboratory and clinical medicine* 2014.
- 159.)** Yang, I. V.; Schwartz, D. A., Epigenetics of idiopathic pulmonary fibrosis. *Translational research : the journal of laboratory and clinical medicine* 2014.
- 160.)** Neelamegam, R.; Ricq, E. L.; Malvaez, M.; Patnaik, D.; Norton, S.; Carlin, S. M.; Hill, I. T.; Wood, M. A.; Haggarty, S. J.; Hooker, J. M., Brain-penetrant LSD1 inhibitors can block memory consolidation. *ACS chemical neuroscience* 2012, *3* (2), 120-128.
- 161.)** Shi, Y.; Lan, F.; Matson, C.; Mulligan, P.; Whetstone, J. R.; Cole, P. A.; Casero, R. A.; Shi, Y., Histone demethylation mediated by the nuclear amine oxidase homolog LSD1. *Cell* 2004, *119* (7), 941-53.
- 162.)** Zahedi, K.; Lentsch, A. B.; Okaya, T.; Barone, S.; Sakai, N.; Witte, D. P.; Arend, L. J.; Alhonen, L.; Jell, J.; Janne, J.; Porter, C. W.; Soleimani, M., Spermidine/spermine-N1-acetyltransferase ablation protects against liver and kidney ischemia-reperfusion injury in mice. *Am J Physiol Gastrointest Liver Physiol* 2009, *296* (4), G899-909.
- 163.)** Goodwin, A. C.; Murray-Stewart, T. R.; Casero, R. A., Jr., A simple assay for mammalian spermine oxidase: a polyamine catabolic enzyme implicated in drug response and disease. *Methods in molecular biology* 2011, *720*, 173-81.
- 164.)** Seiler, N.; Durantou, B.; Raul, F., The polyamine oxidase inactivator MDL 72527. *Prog Drug Res* 2002, *59*, 1-40.

- 165.)** Kutz, C. J.; Holshouser, S. L.; Marrow, E. A.; Woster, P. M., 3,5-Diamino-1,2,4-triazoles as a novel scaffold for potent, reversible LSD1 (KDM1A) inhibitors. *MedChemComm* 2014, 5 (12), 1863-1870.
- 166.)** Health, N. I. o., Clinicaltrials.gov. 2014 ed.; NIH: 2014.
- 167.)** Menick, D. R.; Li, M. S.; Chernysh, O.; Renaud, L.; Kimbrough, D.; Kasiganesan, H.; Mani, S. K., Transcriptional pathways and potential therapeutic targets in the regulation of Ncx1 expression in cardiac hypertrophy and failure. *Advances in experimental medicine and biology* 2013, 961, 125-35.
- 168.)** Jokinen, M. P.; Lieuallen, W. G.; Boyle, M. C.; Johnson, C. L.; Malarkey, D. E.; Nyska, A., Morphologic aspects of rodent cardiotoxicity in a retrospective evaluation of National Toxicology Program studies. *Toxicologic pathology* 2011, 39 (5), 850-60.
- 169.)** Conner, K. P.; Vennam, P.; Woods, C. M.; Krzyaniak, M. D.; Bowman, M. K.; Atkins, W. M., 1,2,3-Triazole-heme interactions in cytochrome P450: functionally competent triazole-water-heme complexes. *Biochemistry* 2012, 51 (32), 6441-57.
- 170.)** Herbrecht, R., Posaconazole: a potent, extended-spectrum triazole anti-fungal for the treatment of serious fungal infections. *International journal of clinical practice* 2004, 58 (6), 612-24.
- 171.)** Nagappan, V.; Deresinski, S., Reviews of anti-infective agents: posaconazole: a broad-spectrum triazole antifungal agent. *Clinical infectious diseases : an official publication of the Infectious Diseases Society of America* 2007, 45 (12), 1610-7.
- 172.)** Scholz, I.; Oberwittler, H.; Riedel, K. D.; Burhenne, J.; Weiss, J.; Haefeli, W. E.; Mikus, G., Pharmacokinetics, metabolism and bioavailability of the triazole antifungal agent voriconazole in relation to CYP2C19 genotype. *Br J Clin Pharmacol* 2009, 68 (6), 906-15.
- 173.)** Kampranis, S. C.; Tsiachlis, P. N., Histone demethylases and cancer. *Advances in cancer research* 2009, 102, 103-69.
- 174.)** Jin, L.; Hanigan, C. L.; Wu, Y.; Wang, W.; Park, B. H.; Woster, P. M.; Casero, R. A., Loss of LSD1 (lysine-specific demethylase 1) suppresses growth and alters gene expression of human colon cancer cells in a p53- and DNMT1(DNA methyltransferase 1)-independent manner. *The Biochemical journal* 2013, 449 (2), 459-68.
- 175.)** Whyte, W. A.; Bilodeau, S.; Orlando, D. A.; Hoke, H. A.; Frampton, G. M.; Foster, C. T.; Cowley, S. M.; Young, R. A., Enhancer decommissioning by LSD1 during embryonic stem cell differentiation. *Nature* 2012, 482 (7384), 221-5.
- 176.)** Lynch, J. T.; Cockerill, M. J.; Hitchin, J. R.; Wiseman, D. H.; Somervaille, T. C., CD86 expression as a surrogate cellular biomarker for pharmacological inhibition of the histone demethylase lysine-specific demethylase 1. *Anal Biochem* 2013, 442 (1), 104-6.
- 177.)** Dhalla, N. S.; Elmoselhi, A. B.; Hata, T.; Makino, N., Status of myocardial antioxidants in ischemia-reperfusion injury. *Cardiovascular research* 2000, 47 (3), 446-56.

- 178.)** Eltzschig, H. K.; Eckle, T., Ischemia and reperfusion--from mechanism to translation. *Nature medicine* 2011, 17 (11), 1391-401.
- 179.)** Hausenloy, D. J.; Yellon, D. M., New directions for protecting the heart against ischaemia-reperfusion injury: targeting the Reperfusion Injury Salvage Kinase (RISK)-pathway. *Cardiovascular research* 2004, 61 (3), 448-60.
- 180.)** Frank, A.; Bonney, M.; Bonney, S.; Weitzel, L.; Koeppen, M.; Eckle, T., Myocardial ischemia reperfusion injury: from basic science to clinical bedside. *Seminars in cardiothoracic and vascular anesthesia* 2012, 16 (3), 123-32.
- 181.)** Murphy, E.; Steenbergen, C., Mechanisms underlying acute protection from cardiac ischemia-reperfusion injury. *Physiol Rev* 2008, 88 (2), 581-609.
- 182.)** Aune, S. E.; Herr, D. J.; Mani, S. K.; Menick, D. R., Selective inhibition of class I but not class IIb histone deacetylases exerts cardiac protection from ischemia reperfusion. *Journal of molecular and cellular cardiology* 2014, 72, 138-45.
- 183.)** Xie, M.; Kong, Y.; Tan, W.; May, H.; Battiprolu, P. K.; Pedrozo, Z.; Wang, Z. V.; Morales, C.; Luo, X.; Cho, G.; Jiang, N.; Jessen, M. E.; Warner, J. J.; Lavandero, S.; Gillette, T. G.; Turer, A. T.; Hill, J. A., Histone deacetylase inhibition blunts ischemia/reperfusion injury by inducing cardiomyocyte autophagy. *Circulation* 2014, 129 (10), 1139-51.
- 184.)** Huang, Y.; Vasilatos, S. N.; Boric, L.; Shaw, P. G.; Davidson, N. E., Inhibitors of histone demethylation and histone deacetylation cooperate in regulating gene expression and inhibiting growth in human breast cancer cells. *Breast Cancer Res Treat* 2012, 131 (3), 777-89.
- 185.)** Lu, Y.; Chu, A.; Turker, M. S.; Glazer, P. M., Hypoxia-induced epigenetic regulation and silencing of the BRCA1 promoter. *Molecular and cellular biology* 2011, 31 (16), 3339-50.
- 186.)** Lu, Y.; Wajapeyee, N.; Turker, M. S.; Glazer, P. M., Silencing of the DNA mismatch repair gene MLH1 induced by hypoxic stress in a pathway dependent on the histone demethylase LSD1. *Cell reports* 2014, 8 (2), 501-13.
- 187.)** Zhang, Y. Z.; Zhang, Q. H.; Ye, H.; Zhang, Y.; Luo, Y. M.; Ji, X. M.; Su, Y. Y., Distribution of lysine-specific demethylase 1 in the brain of rat and its response in transient global cerebral ischemia. *Neuroscience research* 2010, 68 (1), 66-72.
- 188.)** Sharma, S. K.; Wu, Y.; Steinbergs, N.; Crowley, M. L.; Hanson, A. S.; Casero, R. A.; Woster, P. M., (Bis)urea and (bis)thiourea inhibitors of lysine-specific demethylase 1 as epigenetic modulators. *Journal of medicinal chemistry* 2010, 53 (14), 5197-212.
- 189.)** Ping, P.; Murphy, E., Role of p38 mitogen-activated protein kinases in preconditioning: a detrimental factor or a protective kinase? *Circ Res* 2000, 86 (9), 921-2.
- 190.)** Kowluru, R. A.; Santos, J. M.; Mishra, M., Epigenetic modifications and diabetic retinopathy. *BioMed research international* 2013, 2013, 635284.
- 191.)** Vasilatos, S. N.; Katz, T. A.; Oesterreich, S.; Wan, Y.; Davidson, N. E.; Huang, Y., Crosstalk between lysine-specific demethylase 1 (LSD1) and histone

deacetylases mediates antineoplastic efficacy of HDAC inhibitors in human breast cancer cells. *Carcinogenesis* 2013, 34 (6), 1196-207.

192.) Forneris, F.; Binda, C.; Vanoni, M. A.; Battaglioli, E.; Mattevi, A., Human histone demethylase LSD1 reads the histone code. *The Journal of biological chemistry* 2005, 280 (50), 41360-5.

193.) Gu, H.; Roizman, B., Engagement of the lysine-specific demethylase/HDAC1/CoREST/REST complex by herpes simplex virus 1. *J Virol* 2009, 83 (9), 4376-85.

194.) Hu, X.; Li, X.; Valverde, K.; Fu, X.; Noguchi, C.; Qiu, Y.; Huang, S., LSD1-mediated epigenetic modification is required for TAL1 function and hematopoiesis. *Proceedings of the National Academy of Sciences of the United States of America* 2009, 106 (25), 10141-6.

195.) Granger, A.; Abdullah, I.; Huebner, F.; Stout, A.; Wang, T.; Huebner, T.; Epstein, J. A.; Gruber, P. J., Histone deacetylase inhibition reduces myocardial ischemia-reperfusion injury in mice. *FASEB journal : official publication of the Federation of American Societies for Experimental Biology* 2008, 22 (10), 3549-60.

196.) Mocanu, M. M.; Baxter, G. F.; Yue, Y.; Critz, S. D.; Yellon, D. M., The p38 MAPK inhibitor, SB203580, abrogates ischaemic preconditioning in rat heart but timing of administration is critical. *Basic Res Cardiol* 2000, 95 (6), 472-8.

197.) Hayashi, H., Pathogenesis and the role of Ca²⁺ overload during myocardial ischemia/reperfusion. *Nagoya journal of medical science* 2000, 63 (3-4), 91-8.

198.) Huang, J.; Sengupta, R.; Espejo, A. B.; Lee, M. G.; Dorsey, J. A.; Richter, M.; Opravil, S.; Shiekhattar, R.; Bedford, M. T.; Jenuwein, T.; Berger, S. L., p53 is regulated by the lysine demethylase LSD1. *Nature* 2007, 449 (7158), 105-8.

199.) Lang, D.; Sulkin, M.; Lou, Q.; Efimov, I. R., Optical mapping of action potentials and calcium transients in the mouse heart. *Journal of visualized experiments : JoVE* 2011, (55).

200.) Kampranis, S. C.; Tsiachlis, P. N., Histone demethylases and cancer. *Advances in cancer research* 2009, 102, 103-69.

201.) Jin, L.; Hanigan, C. L.; Wu, Y.; Wang, W.; Park, B. H.; Woster, P. M.; Casero, R. A., Loss of LSD1 (lysine-specific demethylase 1) suppresses growth and alters gene expression of human colon cancer cells in a p53- and DNMT1(DNA methyltransferase 1)-independent manner. *The Biochemical journal* 2013, 449 (2), 459-68.

202.) Whyte, W. A.; Bilodeau, S.; Orlando, D. A.; Hoke, H. A.; Frampton, G. M.; Foster, C. T.; Cowley, S. M.; Young, R. A., Enhancer decommissioning by LSD1 during embryonic stem cell differentiation. *Nature* 2012, 482 (7384), 221-5.

203.) Foody, J. M.; Farrell, M. H.; Krumholz, H. M., beta-Blocker therapy in heart failure: scientific review. *JAMA : the journal of the American Medical Association* 2002, 287 (7), 883-9.

204.) Iwano, H.; Little, W. C., Heart failure: what does ejection fraction have to do with it? *Journal of cardiology* 2013, 62 (1), 1-3.

- 205.) Webster, A. L.; Yan, M. S.; Marsden, P. A., Epigenetics and cardiovascular disease. *The Canadian journal of cardiology* 2013, 29 (1), 46-57.
- 206.) Hayami, S.; Kelly, J. D.; Cho, H. S.; Yoshimatsu, M.; Unoki, M.; Tsunoda, T.; Field, H. I.; Neal, D. E.; Yamaue, H.; Ponder, B. A.; Nakamura, Y.; Hamamoto, R., Overexpression of LSD1 contributes to human carcinogenesis through chromatin regulation in various cancers. *International Journal of Cancer* 2011, 128 (3), 574-586.
- 207.) Lim, S.; Janzer, A.; Becker, A.; Zimmer, A.; Schule, R.; Buettner, R.; Kirfel, J., Lysine-specific demethylase 1 (LSD1) is highly expressed in ER-negative breast cancers and a biomarker predicting aggressive biology. *Carcinogenesis* 2010, 31 (3), 512-520.
- 208.) Rotili, D.; Mai, A., Targeting Histone Demethylases: A New Avenue for the Fight against Cancer. *Genes & cancer* 2011, 2 (6), 663-79.
- 209.) Schulte, J. H.; Lim, S.; Schramm, A.; Friedrichs, N.; Koster, J.; Versteeg, R.; Ora, I.; Pajtler, K.; Klein-Hitpass, L.; Kuhfittig-Kulle, S.; Metzger, E.; Schule, R.; Eggert, A.; Buettner, R.; Kirfel, J., Lysine-specific demethylase 1 is strongly expressed in poorly differentiated neuroblastoma: implications for therapy. *Cancer research* 2009, 69 (5), 2065-71.
- 210.) Stavropoulos, P.; Hoelz, A., Lysine-specific demethylase 1 as a potential therapeutic target. *Expert Opin Ther Targets* 2007, 11 (6), 809-20.
- 211.) Gottesfeld, J. M.; Pandolfo, M., Development of histone deacetylase inhibitors as therapeutics for neurological disease. *Future Neurol* 2009, 4 (6), 775-784.
- 212.) Lakowski, B.; Roelens, I.; Jacob, S., CoREST-like complexes regulate chromatin modification and neuronal gene expression. *J Mol Neurosci* 2006, 29 (3), 227-39.
- 213.) Shi, L.; Cui, S.; Engel, J. D.; Tanabe, O., Lysine-specific demethylase 1 is a therapeutic target for fetal hemoglobin induction. *Nat Med* 2013, 19 (3), 291-4.
- 214.) Ginder, G. D., Epigenetic regulation of fetal globin gene expression in adult erythroid cells. *Translational research : the journal of laboratory and clinical medicine* 2014.
- 215.) Yang, I. V.; Schwartz, D. A., Epigenetics of idiopathic pulmonary fibrosis. *Translational research : the journal of laboratory and clinical medicine* 2014.
- 216.) Khan, M. N.; Suzuki, T.; Miyata, N., An overview of phenylcyclopropylamine derivatives: biochemical and biological significance and recent developments. *Medicinal research reviews* 2013, 33 (4), 873-910.
- 217.) Lu, Y.; Chu, A.; Turker, M. S.; Glazer, P. M., Hypoxia-induced epigenetic regulation and silencing of the BRCA1 promoter. *Molecular and cellular biology* 2011, 31 (16), 3339-50.
- 218.) Lu, Y.; Wajapeyee, N.; Turker, M. S.; Glazer, P. M., Silencing of the DNA mismatch repair gene MLH1 induced by hypoxic stress in a pathway dependent on the histone demethylase LSD1. *Cell reports* 2014, 8 (2), 501-13.
- 219.) Zhang, Y. Z.; Zhang, Q. H.; Ye, H.; Zhang, Y.; Luo, Y. M.; Ji, X. M.; Su, Y. Y., Distribution of lysine-specific demethylase 1 in the brain of rat and its

- response in transient global cerebral ischemia. *Neuroscience research* 2010, 68 (1), 66-72.
- 220.)** Vasilatos, S. N.; Katz, T. A.; Oesterreich, S.; Wan, Y.; Davidson, N. E.; Huang, Y., Crosstalk between lysine-specific demethylase 1 (LSD1) and histone deacetylases mediates antineoplastic efficacy of HDAC inhibitors in human breast cancer cells. *Carcinogenesis* 2013, 34 (6), 1196-207.
- 221.)** Forneris, F.; Binda, C.; Vanoni, M. A.; Battaglioli, E.; Mattevi, A., Human histone demethylase LSD1 reads the histone code. *The Journal of biological chemistry* 2005, 280 (50), 41360-5.
- 222.)** Granger, A.; Abdullah, I.; Huebner, F.; Stout, A.; Wang, T.; Huebner, T.; Epstein, J. A.; Gruber, P. J., Histone deacetylase inhibition reduces myocardial ischemia-reperfusion injury in mice. *FASEB journal : official publication of the Federation of American Societies for Experimental Biology* 2008, 22 (10), 3549-60.
- 223.)** Aune, S. E.; Herr, D. J.; Mani, S. K.; Menick, D. R., Selective inhibition of class I but not class IIb histone deacetylases exerts cardiac protection from ischemia reperfusion. *Journal of molecular and cellular cardiology* 2014, 72, 138-45.
- 224.)** Health, N. I. o., Clinicaltrials.gov. 2014 ed.; NIH: 2014.
- 225.)** Seiler, N.; Durantou, B.; Raul, F., The polyamine oxidase inactivator MDL 72527. *Prog Drug Res* 2002, 59, 1-40.
- 226.)** Hayashi, H., Pathogenesis and the role of Ca²⁺ overload during myocardial ischemia/reperfusion. *Nagoya journal of medical science* 2000, 63 (3-4), 91-8.